The book presents a comprehensive study on the 2D and 3D boundary element analysis of thermomagnetoelectroelastic anisotropic solids. Several novelties are introduced, which allow derivation of the efficient boundary element approach. The main of them is the usage of new boundary integral equations of 2D and 3D anisotropic thermomagnetoelectroelasticity. These integral equations do not contain temperature volume integral terms, which is advantageous comparing to existing boundary element formulations for anisotropic thermoelastic solids. Thermal effects are accounted for through the boundary integrals containing temperature and heat flux functions (or discontinuity functions).

Iaroslav Pasternak, PhD, DSc, Professor, Head of Department of Applied Mathematics and Mechanics; Viktoriya Pasternak, PhD, Associated Professor, Department of Applied Mechanics; Nataliia Ilchuk, PhD, Associated Professor, Department of Construction and Civil Engineering. Lutsk National Technical University.

978-613-9-93599-4

BEM for defective multifield materials

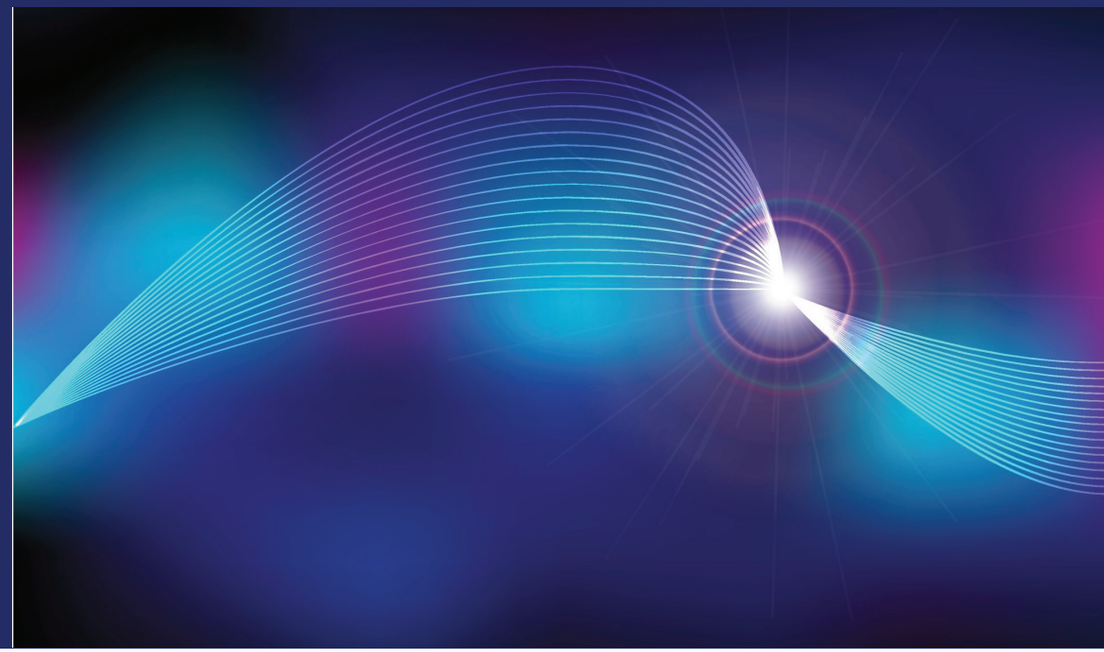

Iaroslav Pasternak
Viktoriya Pasternak
Nataliia Ilchuk

Boundary Element Method for Defective Multifield Materials

LAP LAMBERT Academic Publishing

Pasternak, Pasternak, Ilchuk

Iaroslav Pasternak
Viktoriya Pasternak
Nataliia Ilchuk

Boundary Element Method for Defective Multifield Materials

Iaroslav Pasternak
Viktoriya Pasternak
Nataliia Ilchuk

Boundary Element Method for Defective Multifield Materials

LAP LAMBERT Academic Publishing

Imprint
Any brand names and product names mentioned in this book are subject to trademark, brand or patent protection and are trademarks or registered trademarks of their respective holders. The use of brand names, product names, common names, trade names, product descriptions etc. even without a particular marking in this work is in no way to be construed to mean that such names may be regarded as unrestricted in respect of trademark and brand protection legislation and could thus be used by anyone.

Cover image: www.ingimage.com

Publisher:
LAP LAMBERT Academic Publishing
is a trademark of
International Book Market Service Ltd., member of OmniScriptum Publishing Group
17 Meldrum Street, Beau Bassin 71504, Mauritius

Printed at: see last page
ISBN: 978-613-9-93599-4

CONTENTS

INTRODUCTION

The book concerns a comprehensive study of 2D and 3D anisotropic thermomagnetoelectroelastic solids with cracks and thin inclusions. To study considered problems new boundary integral equations are obtained and new models are introduced for thin inclusions of arbitrary shape. These models can be also used for the analysis of solids with impermeable, permeable and semi-permeable cracks, and cracks with an imperfect thermal contact of their faces.

The book presents a modified boundary element method for the efficient solution of the formulated two-dimensional and three-dimensional problems. The interpolation quadratures with Chebyshev nodes along with the polynomial transformations are adopted for efficient numerical evaluation of singular and hypersingular integrals. New crack/inclusion front shape functions are introduced for high-precision evaluation of generalized intensity factors of physical and mechanical fields in the vicinity of tips of thin inhomogeneities.

Proposed boundary element method is based on a) novel extended Somigliana identities of heat conduction and thermoelectroelasticity for 2D and 3D space and bimaterial; b) coupling principle for continua of different dimension, which replaces a thin inclusion with a line of fields discontinuity; c) mathematical models of thin inclusions, which give relations between fields at the opposite sides of the inhomogeneity. A simple transform of a volume integral due to the temperature field to the boundary integral is proposed both for 2D and 3D, which allow efficient boundary element modeling of thermoelectroelastic solids without introduction of internal cells.

The authors would like to acknowledge the Reviewers of this book, Prof. Vasyl Shvabyuk, Prof. Volodymyr Maksymovych (Lutsk National Technical University), and Prof. Oleh Yasniy (Ternopil National State University), for their proposals and constructive discussions.

CHAPTER 1. Boundary element analysis of 2D defective thermomagnetoelectroelastic materials

1.1. Introduction

Modern high-tech devices often include parts produced from piezoelectric materials, which are used as sensor, precision positioning tools, transducers etc. The highest electromechanical coupling is possessed by ferroelectric materials, which in turn are pyroelectrics, i.e. materials, which polarize with a temperature change. The pyroelectric phenomenon is widely used, in particular, in infrared radiation sensors [1]. In addition, these effects are utilized in the design of modern smart materials. Due to the thermoelectric and thermomechanical effects, presence of cracks and inhomogeneities cause high concentration of stress and electric displacement at their tips. Thus, the pyroelectric phenomenon should be accounted for in the analysis of piezoelectric solids.

A wide range of publications in the scientific literature provides a study of thermal stress and electric displacement in thermoelectroelastic materials near inclusions, holes and cracks. In particular, Lu et al. [2] obtained a solution for an elliptic hole in piezoelectric medium under a uniform heat flux. Liu et al. [3] studied thermal stress and electric displacement at an elliptic inclusion or a hole in an infinite pyroelectric medium. Gao and Wang [4] and Gao et al. [5] determined stress and electric displacement intensity factors for periodic cracks in thermoelectroelastic and thermomagnetoelectroelastic media. Kaloerov and Khoroshev [6, 7] obtained Lekhnitskii type complex potentials of thermoelectroelasticity and solved a number of problems for solids with holes and cracks using the expansions of these complex potentials into power series, with unknown coefficients determined from the boundary conditions. Qin [8, 9] obtained Green's function for pyroelectric and thermomagnetoelectroelastic materials with holes and cracks. Hou [10] derived a 2D fundamental solution for orthotropic pyroelectric plane and half-plane. The majority of papers, which study infinite thermoelectroelastic media, use the assumption that the remote uniform steady-state heat flux does not cause stress and electric displacement in the unnotched pyroelectric medium. However, this assumption was not sufficiently proved, and in some cases of thermal load it can be invalid.

The abovementioned papers generally use analytical or semi-analytical approaches for studying of notched pyroelectric solids, which limits their application mainly to solids of a canonical shape. One can overcome these limitations using numerical methods, in particular, the boundary element method (BEM), which possesses high accuracy due to its semi-analytic nature and requires only boundary mesh. Qin [11, 12] and Qin et al. [13, 14] were the first, who obtained the BEM for anisotropic pyroelectric solids with thermally insulated cracks, holes and inclusions minimizing the related potential energy and using the Green's function approach. However, no integral equations were provided, since the latter approach used the boundary element representation of this potential energy.

Therefore, there are still a number of unsolved problems about the application of the BEM to the analysis of pyroelectric solids. In particular, there are no closed-form boundary integral equations developed, which allow studying insulated cracks and cracks with temperature boundary conditions set on their faces. In addition, the analysis of piezoelectric solids with cracks should account for the crack medium permittivity, because stress and electric displacement intensity factors obtained for permeable and impermeable cracks essentially differ [4]. Therefore, this article focuses on the development of the truly boundary integral equations for 2D thermoelectroelasticity using two different approaches based on the reciprocity relations and the complex variable analysis. Besides, the model of a thin inclusion [15] is extended to account for the thermal effects. This model also allows studying permeable, impermeable and semi-permeable cracks with perfect or imperfect thermal contact of their faces with the appropriate choice of a thickness and material properties of the crack medium.

1.2. Governing equations of thermoelectroelasticity. Extended Stroh formalism

In a fixed rectangular system of coordinates $Ox_1x_2x_3$ under the assumption that all fields depend only on in-plane coordinates x_1 and x_2 the balance equations for stress, electric displacement and heat flux, and constitutive laws can be written in the following compact form [11, 15–17]:

$$\tilde{\sigma}_{ij,j} + \tilde{f}_i = 0\,, \quad h_{i,i} - f_h = 0 \quad (i = 1,..,4;\ j = 1,2)\,; \tag{1}$$

$$\tilde{\sigma}_{ij} = \tilde{C}_{ijkm}\tilde{u}_{k,m} - \tilde{\beta}_{ij}\theta\,, \quad h_i = -k_{ij}\theta_{,j} \quad (i,k = 1,..,4;\ j,m = 1,2) \tag{2}$$

with

$$\begin{gathered} \tilde{u}_i = u_i,\ \tilde{u}_4 = \phi;\ \tilde{f}_i = f_i,\ \tilde{f}_4 = -q;\ \tilde{\sigma}_{ij} = \sigma_{ij},\ \tilde{\sigma}_{4j} = D_j;\ \tilde{\beta}_{ij} = \beta_{ij},\ \tilde{\beta}_{4j} = -\chi_j; \\ \tilde{C}_{ijkm} = C_{ijkm},\ \tilde{C}_{ij4m} = e_{mij},\ \tilde{C}_{4jkm} = e_{jkm},\ \tilde{C}_{4j4m} = -\kappa_{jm} \quad (i,k = 1,2,3;\ j,m = 1,2). \end{gathered} \tag{3}$$

Here σ_{ij} is a stress tensor; h_i is a heat flux; D_i is an electric displacement; f_i is a body force vector; q is a free charge volume density; f_h is a distributed heat source density; u_i is a displacement; ϕ is an electric potential; θ is a temperature change with respect to the reference temperature; C_{ijkm} are elastic moduli; k_{ij} are heat conduction coefficients; $\beta_{ij} = C_{ijkm}\alpha_{km} + e_{mij}\lambda_m\ (i,j,k,m = 1,..,3)$ are thermal moduli (thermal stress coefficients); α_{ij} are thermal expansion coefficients; e_{ijk} are piezoelectric constants; κ_{ij} are dielectric constants; $\chi_i = -e_{ikm}\alpha_{km} + \kappa_{ij}\lambda_j$ are pyroelectric coefficients; and λ_i are pyroelectric constants. Tensors C_{ijkm}, k_{ij}, κ_{ij} and β_{ij} are assumed to be symmetric. Here and further, the Einstein summation convention is used. A comma at subscript denotes differentiation with respect to a coordinate indexed after the comma, i.e. $u_{i,j} = \partial u_i / \partial x_j$.

If the temperature, electric potential and displacement depend only on in-plane coordinates x_1 and x_2, according to the extended Stroh formalism [11], the general

homogeneous (i.e. for $\tilde{f}_i \equiv 0$ and $f_h \equiv 0$) solution of Eqs. (1), (2) can be expressed in terms of complex analytic functions as follows

$$\theta = 2\,\mathrm{Re}\{g'(z_t)\},\quad \vartheta = 2k_t\,\mathrm{Im}\{g'(z_t)\},\quad h_1 = -\vartheta_{,2},\quad h_2 = \vartheta_{,1},\quad k_t = \sqrt{k_{11}k_{22} - k_{12}^{\,2}};$$
$$\tilde{\mathbf{u}} = 2\,\mathrm{Re}\{\mathbf{A}\mathbf{f}(z_*) + \mathbf{c}g(z_t)\},\quad \tilde{\boldsymbol{\varphi}} = 2\,\mathrm{Re}\{\mathbf{B}\mathbf{f}(z_*) + \mathbf{d}g(z_t)\};\quad \tilde{\sigma}_{i1} = -\tilde{\varphi}_{i,2},\quad \tilde{\sigma}_{i2} = \tilde{\varphi}_{i,1}; \tag{4}$$
$$z_t = x_1 + p_t x_2;\quad z_\alpha = x_1 + p_\alpha x_2;\quad \mathbf{f}(z_*) = \left[F_1(z_1), F_2(z_2), F_3(z_3), F_4(z_4)\right]^{\mathrm{T}},$$

where $g(z_t)$ and $F_\alpha(z_\alpha)$ are complex analytic functions with respect to their arguments; the complex constant p_t is a root (with a positive imaginary part) of the characteristic equation for heat conduction

$$k_{22}p_t^2 + 2k_{12}p_t + k_{11} = 0; \tag{5}$$

4x4 complex matrices $\mathbf{A} \equiv [A_{i\alpha}] = [\mathbf{a}_\alpha]$, $\mathbf{B} \equiv [B_{i\alpha}] = [\mathbf{b}_\alpha]$ and constants p_α $(\alpha = 1,..,4)$ are determined from the 8x8 Stroh eigenvalue problem [11, 16, 17]:

$$\mathbf{N} = \begin{bmatrix} \mathbf{N}_1 & \mathbf{N}_2 \\ \mathbf{N}_3 & \mathbf{N}_1^{\mathrm{T}} \end{bmatrix},\quad \begin{matrix} \mathbf{N}\boldsymbol{\xi} = p\boldsymbol{\xi}, \\ \mathbf{N}^{\mathrm{T}}\boldsymbol{\eta} = p\boldsymbol{\eta}, \end{matrix} \tag{6}$$

and vectors $\mathbf{c}$ and $\mathbf{d}$ satisfy the following matrix equation [16, 17]:

$$\mathbf{N}\boldsymbol{\zeta} = p_t\boldsymbol{\zeta} + \boldsymbol{\gamma},\quad \boldsymbol{\zeta} = \begin{bmatrix} \mathbf{c} \\ \mathbf{d} \end{bmatrix},\quad \boldsymbol{\gamma} = -\begin{bmatrix} \mathbf{0} & \mathbf{N}_2 \\ \mathbf{I} & \mathbf{N}_1^{\mathrm{T}} \end{bmatrix}\begin{bmatrix} \boldsymbol{\beta}_1 \\ \boldsymbol{\beta}_2 \end{bmatrix}. \tag{7}$$

Here $\mathbf{N}_1 = -\mathbf{T}^{-1}\mathbf{R}^{\mathrm{T}}$, $\mathbf{N}_2 = \mathbf{T}^{-1}$, $\mathbf{N}_3 = \mathbf{R}\mathbf{T}^{-1}\mathbf{R}^{\mathrm{T}} - \mathbf{Q}$; $\boldsymbol{\beta}_1 = \left[\tilde{\beta}_{i1}\right]$, $\boldsymbol{\beta}_2 = \left[\tilde{\beta}_{i2}\right]$; $\boldsymbol{\xi} = [\mathbf{a}, \mathbf{b}]^{\mathrm{T}}$ is a right eigenvector and $\boldsymbol{\eta} = [\mathbf{b}, \mathbf{a}]^{\mathrm{T}}$ is a left eigenvector of the fundamental electro-elasticity matrix $\mathbf{N}$; superscript "T" denotes matrix transpose. The components of 4x4 matrices $\mathbf{Q}$, $\mathbf{R}$ and $\mathbf{T}$ are defined as $Q_{ik} = \tilde{C}_{i1k1}$, $T_{ik} = \tilde{C}_{i2k2}$, $R_{ik} = \tilde{C}_{i1k2} = \tilde{C}_{k2i1}$. Matrices $\mathbf{Q}$ and $\mathbf{T}$ are symmetric due to the symmetry of the tensor $\tilde{C}_{ijkm}$ [15]: $\tilde{C}_{ijkm} = \tilde{C}_{kmij}$.

Since eigenvectors of the matrix $\mathbf{N}$ are unique up to an arbitrary multiplier, matrices $\mathbf{A}$ and $\mathbf{B}$ are normalized such that [11, 16, 17]:

$$\begin{bmatrix} \mathbf{B}^{\mathrm{T}} & \mathbf{A}^{\mathrm{T}} \\ \overline{\mathbf{B}}^{\mathrm{T}} & \overline{\mathbf{A}}^{\mathrm{T}} \end{bmatrix}\begin{bmatrix} \mathbf{A} & \overline{\mathbf{A}} \\ \mathbf{B} & \overline{\mathbf{B}} \end{bmatrix} = \begin{bmatrix} \mathbf{I} & \mathbf{0} \\ \mathbf{0} & \mathbf{I} \end{bmatrix}. \tag{8}$$

According to [18], based on Eqs. (6)–(8) one can obtain the following identity

$$\mathbf{P}\mathbf{B}^{\mathrm{T}}\,\mathrm{Im}\{\mathbf{c}\} + \mathbf{P}\mathbf{A}^{\mathrm{T}}\,\mathrm{Im}\{\mathbf{d}\} = \mathbf{B}^{\mathrm{T}}\,\mathrm{Im}\{p_t\mathbf{c}\} + \mathbf{A}^{\mathrm{T}}\,\mathrm{Im}\{p_t\mathbf{d}\},\quad \mathbf{P} = \mathrm{diag}[p_1, p_2, p_3, p_4], \tag{9}$$

which plays a key role in derivation of the boundary integral equations of anisotropic thermoelectroelasticity using the complex variable approach.

1.3. Derivation of the boundary integral equations of 2D thermoelectroelasticity

Since there are no truly boundary integral equations of anisotropic thermoelectroelasticity, this section presents two approaches for their derivation. The first one is the commonly used approach based on the reciprocity relations. However, it results in the extra domain integral, which accounts for the thermal effects. Here this domain integral is converted to the boundary one for the first time. The second approach is a novel one based on the Stroh formalism and Cauchy integral formula, recently applied to the analysis of 2D anisotropic thermoelasticity [18]. The latter

approach directly results in truly boundary integral equations. Both approaches produce the same boundary integral equations, which prove their validity.

1.3.1. Reciprocity based derivation of the boundary integral equations

In order to derive boundary integral equations of heat transfer and thermoelectroelasticity, first consider two arbitrary thermoelectroelastic states of a solid, denoted by superscripts "(1)" and "(2)" respectively. Due to the symmetry of heat conduction coefficients $k_{ij} = k_{ji}$ and electro-elastic constants $\tilde{C}_{ijkm} = \tilde{C}_{kmij}$ and according to the constitutive relations (2), the following reciprocity relations hold:

$$h_i^{(1)}\theta_{,i}^{(2)} = -k_{ij}\theta_{,j}^{(1)}\theta_{,i}^{(2)} = -k_{ji}\theta_{,i}^{(2)}\theta_{,j}^{(1)} = h_j^{(2)}\theta_{,j}^{(1)} = h_i^{(2)}\theta_{,i}^{(1)}, \tag{10}$$

$$\left(\tilde{\sigma}_{ij}^{(1)} + \tilde{\beta}_{ij}\theta^{(1)}\right)\tilde{u}_{i,j}^{(2)} = \tilde{C}_{ijkm}\tilde{u}_{k,m}^{(1)}\tilde{u}_{i,j}^{(2)} = \tilde{C}_{kmij}\tilde{u}_{i,j}^{(2)}\tilde{u}_{k,m}^{(1)} = \left(\tilde{\sigma}_{km}^{(2)} + \tilde{\beta}_{km}\theta^{(2)}\right)\tilde{u}_{k,m}^{(1)} = \left(\tilde{\sigma}_{ij}^{(2)} + \tilde{\beta}_{ij}\theta^{(2)}\right)\tilde{u}_{i,j}^{(1)}. \tag{11}$$

Consider a solid occupying a domain S. Integrating (10) and (11) over this domain and then applying Gauss divergence theorem one obtains

$$\begin{aligned}
\iint_S h_i^{(1)}\theta_{,i}^{(2)}dS &= \iint_S\left[\frac{\partial}{\partial x_i}\left(h_i^{(1)}\theta^{(2)}\right) - h_{i,i}^{(1)}\theta^{(2)}\right]dS \\
&= \int_{\partial S} h_i^{(1)}n_i\theta^{(2)}d\Gamma - \iint_S h_{i,i}^{(1)}\theta^{(2)}dS \\
&= \iint_S h_i^{(2)}\theta_{,i}^{(1)}dS = \int_{\partial S} h_i^{(2)}n_i\theta^{(1)}d\Gamma - \iint_S h_{i,i}^{(2)}\theta^{(1)}dS,
\end{aligned} \tag{12}$$

$$\begin{aligned}
\iint_S\left(\tilde{\sigma}_{ij}^{(1)} + \tilde{\beta}_{ij}\theta^{(1)}\right)\tilde{u}_{i,j}^{(2)}dS &= \iint_S\left[\frac{\partial}{\partial x_j}\left(\tilde{\sigma}_{ij}^{(1)}\tilde{u}_i^{(2)}\right) - \tilde{\sigma}_{ij,j}^{(1)}\tilde{u}_i^{(2)} + \tilde{\beta}_{ij}\theta^{(1)}\tilde{u}_{i,j}^{(2)}\right]dS \\
&= \int_{\partial S}\tilde{\sigma}_{ij}^{(1)}n_j\tilde{u}_i^{(2)}d\Gamma - \iint_S\tilde{\sigma}_{ij,j}^{(1)}\tilde{u}_i^{(2)}dS + \iint_S\tilde{\beta}_{ij}\theta^{(1)}\tilde{u}_{i,j}^{(2)}dS \\
&= \iint_S\left(\tilde{\sigma}_{ij}^{(2)} + \tilde{\beta}_{ij}\theta^{(2)}\right)\tilde{u}_{i,j}^{(1)}dS = \int_{\partial S}\tilde{\sigma}_{ij}^{(2)}n_j\tilde{u}_i^{(1)}d\Gamma - \iint_S\tilde{\sigma}_{ij,j}^{(2)}\tilde{u}_i^{(1)}dS + \iint_S\tilde{\beta}_{ij}\theta^{(2)}\tilde{u}_{i,j}^{(1)}dS.
\end{aligned} \tag{13}$$

Here n_i is a unit normal vector to the boundary $\Gamma = \partial S$ of the solid.

Denoting extended traction vector by $\tilde{t}_i = \tilde{\sigma}_{ij}n_j$ and surface heat flux by $h_n = h_i n_i$, and substituting balance equations (1) into Eqs. (12) and (13) the following Betti type reciprocity theorems are obtained for steady-state heat conduction and thermoelectroelasticity

$$\iint_S f_h^{(2)}\theta^{(1)}dS = -\int_{\partial S}\left[\theta^{(2)}h_n^{(1)} - h_n^{(2)}\theta^{(1)}\right]d\Gamma + \iint_S f_h^{(1)}\theta^{(2)}dS, \tag{14}$$

$$\iint_S\tilde{f}_i^{(2)}\tilde{u}_i^{(1)}dS = \int_{\partial S}\left[\tilde{u}_i^{(2)}\tilde{t}_i^{(1)} - \tilde{t}_i^{(2)}\tilde{u}_i^{(1)}\right]d\Gamma + \iint_S\tilde{f}_i^{(1)}\tilde{u}_i^{(2)}dS + \tilde{\beta}_{ij}\iint_S\left[\tilde{u}_{i,j}^{(2)}\theta^{(1)} - \theta^{(2)}\tilde{u}_{i,j}^{(1)}\right]dS. \tag{15}$$

Consider that the second thermal state of the solid S corresponds to the action of the unit heat source $f_h^{(2)} = \delta(\mathbf{x} - \boldsymbol{\xi})$ applied at the point $\boldsymbol{\xi} \in S(\boldsymbol{\xi} \notin \partial S)$ of an infinite medium. Then Eq. (14) results in the following Somigliana type identity

$$\theta(\boldsymbol{\xi}) = \int_{\partial S}\left[\Theta^*(\mathbf{x},\boldsymbol{\xi})h_n(\mathbf{x}) - H^*(\mathbf{x},\boldsymbol{\xi})\theta(\mathbf{x})\right]d\Gamma(\mathbf{x}) - \iint_S\Theta^*(\mathbf{x},\boldsymbol{\xi})f_h(\mathbf{x})dS(\mathbf{x}). \tag{16}$$

Here

$$\Theta^*(\mathbf{x},\mathbf{y})=\frac{1}{2\pi k_t}\ln\left|Z_t(\mathbf{x}-\mathbf{y})\right|,\quad H^*(\mathbf{x},\mathbf{y})=\frac{1}{2\pi}\mathrm{Im}\left\{\frac{n_2-p_t n_1}{Z_t(\mathbf{x}-\mathbf{y})}\right\} \tag{17}$$

are Green's functions for the infinite medium subjected to a point heat source [11]; $Z_t(\mathbf{x})=x_1+p_t x_2$ and $\delta(\mathbf{x})$ is a Dirac delta-function. Superscripts "(1)" and "(2)" are omitted, since the state "(2)" is given and the state "(1)" can be arbitrary.

Now consider that the second state of the solid S is caused by the action of unit concentrated forces $\tilde{f}_j^{(2,i)}=\delta_{ij}\delta(\mathbf{x}-\boldsymbol{\xi})$ at the point $\boldsymbol{\xi}\in S(\boldsymbol{\xi}\notin\partial S)$. Here δ_{ij} is a Kronecker delta. For this type of load, Eq. (15) results in the extended Somigliana identity for thermoelectroelasticity

$$\begin{aligned}\tilde{u}_i(\boldsymbol{\xi})=&\int_{\partial S}\left[U_{ij}(\mathbf{x},\boldsymbol{\xi})\tilde{t}_j(\mathbf{x})-T_{ij}(\mathbf{x},\boldsymbol{\xi})\tilde{u}_j(\mathbf{x})\right]d\Gamma(\mathbf{x})\\&+\iint_S U_{ij}(\mathbf{x},\boldsymbol{\xi})\tilde{f}_j(\mathbf{x})dS(\mathbf{x})+\tilde{\beta}_{jk}\iint_S U_{ij,k}(\mathbf{x},\boldsymbol{\xi})\theta(\mathbf{x})dS(\mathbf{x}),\end{aligned} \tag{18}$$

where the kernels are equal to corresponding Green's functions [11]

$$U_{ij}(\mathbf{x},\boldsymbol{\xi})=\frac{1}{\pi}\mathrm{Im}\left[A_{i\alpha}A_{j\alpha}\ln Z_\alpha(\mathbf{x}-\boldsymbol{\xi})\right],\quad T_{ij}(\mathbf{x},\boldsymbol{\xi})=\frac{1}{\pi}\mathrm{Im}\left[A_{i\alpha}B_{j\alpha}\frac{(n_2-n_1p_\alpha)}{Z_\alpha(\mathbf{x}-\boldsymbol{\xi})}\right], \tag{19}$$

and $Z_\alpha(\mathbf{x})=x_1+p_\alpha x_2$.

Even if body forces $\tilde{f}_i$ are absent, Eq. (18) still contains a domain integral. To this time the complicated approach for conversion of the domain integral to the boundary one in the mapped temperature domain is proposed only for the case of anisotropic thermoelasticity [19]. Therefore, this chapter is concerned with a general approach, which can be applied to the analysis of thermoelectroelastic problems.

Prior to conversion of the domain integral, it is useful to generalize Green's second identity. For this purpose consider the following differential identity, which is proved by direct differentiation,

$$\frac{\partial}{\partial x_p}\left(\phi k_{pq}\frac{\partial\psi}{\partial x_q}-\psi k_{pq}\frac{\partial\phi}{\partial x_q}\right)=\phi k_{pq}\frac{\partial^2\psi}{\partial x_p\partial x_q}-\psi k_{pq}\frac{\partial^2\phi}{\partial x_p\partial x_q}+k_{pq}\frac{\partial\phi}{\partial x_p}\cdot\frac{\partial\psi}{\partial x_q}-k_{pq}\frac{\partial\psi}{\partial x_p}\cdot\frac{\partial\phi}{\partial x_q}. \tag{20}$$

Here ϕ and ψ are arbitrary functions of the spatial coordinates, and k_{pq} is constant. When k_{pq} is symmetric, i.e. $k_{pq}=k_{qp}$, the sum of the last two terms in the right hand side of Eq. (20) is equal to zero, since

$$k_{pq}\frac{\partial\phi}{\partial x_p}\cdot\frac{\partial\psi}{\partial x_q}-k_{pq}\frac{\partial\psi}{\partial x_p}\cdot\frac{\partial\phi}{\partial x_p}=k_{pq}\frac{\partial\phi}{\partial x_p}\cdot\frac{\partial\psi}{\partial x_q}-k_{qp}\frac{\partial\phi}{\partial x_q}\cdot\frac{\partial\psi}{\partial x_p}=0. \tag{21}$$

Therefore, for symmetric k_{pq} Eq. (20) writes as

$$\frac{\partial}{\partial x_p}\left(\phi k_{pq}\frac{\partial\psi}{\partial x_q}-\psi k_{pq}\frac{\partial\phi}{\partial x_q}\right)=\phi k_{pq}\frac{\partial^2\psi}{\partial x_p\partial x_q}-\psi k_{pq}\frac{\partial^2\phi}{\partial x_p\partial x_q}. \tag{22}$$

Integrating both sided of Eq. (22) over the domain S and applying Gauss divergence theorem one can obtain

$$\iint_S \frac{\partial}{\partial x_p}\left(\phi k_{pq}\frac{\partial \psi}{\partial x_q}-\psi k_{pq}\frac{\partial \phi}{\partial x_q}\right)dS$$
$$=\int_{\partial S}\left(\phi k_{pq}\frac{\partial \psi}{\partial x_q}-\psi k_{pq}\frac{\partial \phi}{\partial x_q}\right)n_p d\Gamma=\iint_S\left[\phi k_{pq}\frac{\partial^2 \psi}{\partial x_p \partial x_q}-\psi k_{pq}\frac{\partial^2 \phi}{\partial x_p \partial x_q}\right]dS. \tag{23}$$

If one assumes that $k_{pq}=\delta_{pq}$, Eq. (23) reduces to Green's second identity.

Now consider the thermoelectroelastic domain integral. Denoting $\psi = V_i(\mathbf{x},\boldsymbol{\xi})$, $\phi=\theta(\mathbf{x})$, and hence, according to Eq. (2), $k_{pq}\theta_{,q}=-h_p$, and using these notations in Eq. (23) yields

$$\int_{\partial S}\left(\theta(\mathbf{x})k_{pq}\frac{\partial V_i(\mathbf{x},\boldsymbol{\xi})}{\partial x_q}n_p(\mathbf{x})+V_i(\mathbf{x},\boldsymbol{\xi})h_p(\mathbf{x})n_p(\mathbf{x})\right)d\Gamma(\mathbf{x})$$
$$=\iint_S\left[\theta(\mathbf{x})k_{pq}\frac{\partial^2 V_i(\mathbf{x},\boldsymbol{\xi})}{\partial x_p \partial x_q}+V_i(\mathbf{x},\boldsymbol{\xi})h_{p,p}(\mathbf{x})\right]dS(\mathbf{x}). \tag{24}$$

As stated in Eq. (1), $h_{p,p}=f_h$, thus, rearranging terms in Eq. (24) one obtains

$$\iint_S \theta(\mathbf{x})k_{pq}\frac{\partial^2 V_i(\mathbf{x},\boldsymbol{\xi})}{\partial x_p \partial x_q}dS$$
$$=\int_{\partial S}\left[R_i(\mathbf{x},\boldsymbol{\xi})\theta(\mathbf{x})+V_i(\mathbf{x},\boldsymbol{\xi})h_n(\mathbf{x})\right]d\Gamma(\mathbf{x})-\iint_S V_i(\mathbf{x},\boldsymbol{\xi})f_h(\mathbf{x})dS(\mathbf{x}). \tag{25}$$

Here

$$R_i(\mathbf{x},\boldsymbol{\xi})=k_{pq}\frac{\partial V_i(\mathbf{x},\boldsymbol{\xi})}{\partial x_q}n_p(\mathbf{x}). \tag{26}$$

If there exists such a function $V_i(\mathbf{x},\boldsymbol{\xi})$, which satisfies differential equation

$$k_{pq}\frac{\partial^2 V_i(\mathbf{x},\boldsymbol{\xi})}{\partial x_p \partial x_q}=\tilde{\beta}_{jk}\frac{\partial}{\partial x_k}U_{ij}(\mathbf{x},\boldsymbol{\xi}), \tag{27}$$

then the termoelectroelastic domain integral in Eq. (18) can be transformed to a boundary one through Eq. (25) as

$$\tilde{\beta}_{jk}\iint_S U_{ij,k}\theta dS=\iint_S \theta(\mathbf{x})k_{pq}\frac{\partial^2 V_i(\mathbf{x},\boldsymbol{\xi})}{\partial x_p \partial x_q}dS$$
$$=\int_{\partial S}\left[R_i(\mathbf{x},\boldsymbol{\xi})\theta(\mathbf{x})+V_i(\mathbf{x},\boldsymbol{\xi})h_n(\mathbf{x})\right]d\Gamma(\mathbf{x})-\iint_S V_i(\mathbf{x},\boldsymbol{\xi})f_h(\mathbf{x})dS(\mathbf{x}). \tag{28}$$

Finally, substitution of Eq. (28) into Eq. (18) yields the extended Somigliana identity for thermoelectroelasticity

$$\tilde{u}_i(\boldsymbol{\xi})=\int_{\partial S}\left[U_{ij}(\mathbf{x},\boldsymbol{\xi})\tilde{t}_j(\mathbf{x})-T_{ij}(\mathbf{x},\boldsymbol{\xi})\tilde{u}_j(\mathbf{x})\right]d\Gamma(\mathbf{x})$$
$$+\int_{\partial S}\left[R_i(\mathbf{x},\boldsymbol{\xi})\theta(\mathbf{x})+V_i(\mathbf{x},\boldsymbol{\xi})h_n(\mathbf{x})\right]d\Gamma(\mathbf{x})$$
$$+\iint_S U_{ij}(\mathbf{x},\boldsymbol{\xi})\tilde{f}_j(\mathbf{x})dS(\mathbf{x})-\iint_S V_i(\mathbf{x},\boldsymbol{\xi})f_h(\mathbf{x})dS(\mathbf{x}). \tag{29}$$

Heat flux, stress and electric displacement at the arbitrary point $\boldsymbol{\xi}\in S(\boldsymbol{\xi}\notin \partial S)$ of the solid can be evaluated by applying constitutive relations (2) to the integral identities (16) and (29):

$$
\begin{aligned}
h_i(\xi) &= -k_{ij}\frac{\partial}{\partial \xi_j}\theta(\xi) = \int_{\partial S}\Theta_i^{**}(\mathbf{x},\xi)\,h_n(\mathbf{x})\,d\Gamma(\mathbf{x}) \\
&\quad - \int_{\partial S} H_i^{**}(\mathbf{x},\xi)\,\theta(\mathbf{x})\,d\Gamma(\mathbf{x}) - \iint_S \Theta_i^{**}(\mathbf{x},\xi)\,f_h(\mathbf{x})\,dS(\mathbf{x}),
\end{aligned}
\tag{30}
$$

$$
\begin{aligned}
\tilde{\sigma}_{ij}(\xi) &= \tilde{C}_{ijkm}\frac{\partial}{\partial \xi_m}\tilde{u}_k(\xi) - \tilde{\beta}_{ij}\theta(\xi) = \\
&= \int_{\partial S} D_{ijk}(\mathbf{x},\xi)\,\tilde{t}_k(\mathbf{x})d\Gamma(\mathbf{x}) - \int_{\partial S} S_{ijk}(\mathbf{x},\xi)\,\tilde{u}_k(\mathbf{x})d\Gamma(\mathbf{x}) \\
&\quad + \int_{\partial S} Q_{ij}(\mathbf{x},\xi)\,\theta(\mathbf{x})\,d\Gamma(\mathbf{x}) + \int_{\partial S} W_{ij}(\mathbf{x},\xi)\,h_n(\mathbf{x})\,d\Gamma(\mathbf{x}) \\
&\quad + \iint_S D_{ijk}(\mathbf{x},\xi)\,\tilde{f}_k(\mathbf{x})dS(\mathbf{x}) - \iint_S W_{ij}(\mathbf{x},\xi)\,f_h(\mathbf{x})\,dS(\mathbf{x}),
\end{aligned}
\tag{31}
$$

where the kernels are defined as

$$
\Theta_i^{**}(\mathbf{x},\xi) = -k_{ij}\frac{\partial}{\partial \xi_j}\Theta^*(\mathbf{x},\xi), \quad H_i^{**}(\mathbf{x},\xi) = -k_{ij}\frac{\partial}{\partial \xi_j}H^*(\mathbf{x},\xi),
\tag{32}
$$

$$
\begin{aligned}
&D_{ijk}(\mathbf{x},\xi) = \tilde{C}_{ijmp}\frac{\partial}{\partial \xi_p}U_{mk}(\mathbf{x},\xi), \quad S_{ijk}(\mathbf{x},\xi) = \tilde{C}_{ijmp}\frac{\partial}{\partial \xi_p}T_{mk}(\mathbf{x},\xi), \\
&Q_{ij}(\mathbf{x},\xi) = \tilde{C}_{ijmp}\frac{\partial}{\partial \xi_p}R_m(\mathbf{x},\xi) + \tilde{\beta}_{ij}H^*(\mathbf{x},\xi), \quad W_{ij}(\mathbf{x},\xi) = \tilde{C}_{ijmp}\frac{\partial}{\partial \xi_p}V_m(\mathbf{x},\xi) - \tilde{\beta}_{ij}\Theta^*(\mathbf{x},\xi).
\end{aligned}
\tag{33}
$$

It is rather complicated to obtain an explicit expression for the kernel $V_i(\mathbf{x},\xi)$ using Eq. (27). However, another approach can be used, which is based on the physical interpretation of Eq. (29). Consider an infinite thermoelectroelastic medium loaded by a unit heat source at the point $\mathbf{x}^*$. Since the infinite medium is considered, all path integrals in Eq. (29) and also domain integral containing body forces $\tilde{f}_i$ should vanish. The only nonzero term remaining is

$$
\tilde{u}_i^*(\xi) = -\iint_S V_i(\mathbf{x},\xi)\,\delta(\mathbf{x}-\mathbf{x}^*)\,dS(\mathbf{x}) = -V_i(\mathbf{x}^*,\xi).
\tag{34}
$$

Therefore, according to Eq. (34), the kernel $V_i(\mathbf{x},\xi)$ corresponds to the displacements (with an opposite sign) at the point ξ produced by a point heat source of a unit magnitude (actually a line heat source, since plane strain is considered) applied at the point $\mathbf{x}$ of the infinite medium. Thus, $V_i(\mathbf{x},\xi)$ is a fundamental solution of thermoelectroelasticity, which can be obtained using the Stroh formalism (see Appendix A)

$$
\begin{aligned}
V_i(\mathbf{x},\xi) &= -\frac{1}{\pi k_t}\operatorname{Im}\Big[A_{i\alpha}f^*\big(Z_\alpha(\mathbf{x}-\xi)\big)\big(A_{j\alpha}\operatorname{Im}\{d_j\} + B_{j\alpha}\operatorname{Im}\{c_j\}\big)\Big] \\
&\quad - \frac{1}{2\pi k_t}\operatorname{Re}\Big[c_i f^*\big(Z_t(\mathbf{x}-\xi)\big)\Big],
\end{aligned}
\tag{35}
$$

where $f^*(z) = z(\ln z - 1)$ is an anti-derivative of the logarithmic function, and $Z_t(\mathbf{x}) = x_1 + p_t x_2$. One should note that Eq. (35) is not the same as Eq. (3.8) given in Ref. [11], since the latter does not consider stress and displacement continuity conditions, which is physically incorrect. For the case of orthotropic material Eq. (35) coincides with a fundamental solution obtained by Hou [10].

The proof of the theorem that Eq. (27) holds for the function $V_i(\mathbf{x},\boldsymbol{\xi})$ given by Eq. (35) is presented in Appendix B.

Approaching the internal point $\boldsymbol{\xi}$ in Eqs. (16) and (29) to the boundary point $\mathbf{y}\in\Gamma$, using the Sokhotskii-Plemelj formula [20, 21] and assuming that the boundary is smooth at $\mathbf{y}$ one obtains boundary integral equations of thermoelectroelasticity

$$\begin{aligned}\frac{1}{2}\theta(\mathbf{y}) &= \mathrm{RPV}\int_{\partial S}\Theta^*(\mathbf{x},\mathbf{y})h_n(\mathbf{x})d\Gamma(\mathbf{x}) - \mathrm{CPV}\int_{\partial S}H^*(\mathbf{x},\mathbf{y})\theta(\mathbf{x})d\Gamma(\mathbf{x})\\ &\quad - \iint_S \Theta^*(\mathbf{x},\mathbf{y})f_h(\mathbf{x})dS(\mathbf{x}),\end{aligned} \tag{36}$$

$$\begin{aligned}\frac{1}{2}\tilde{u}_i(\mathbf{y}) &= \mathrm{RPV}\int_{\partial S}U_{ij}(\mathbf{x},\mathbf{y})\tilde{t}_j(\mathbf{x})d\Gamma(\mathbf{x}) - \mathrm{CPV}\int_{\partial S}T_{ij}(\mathbf{x},\mathbf{y})\tilde{u}_j(\mathbf{x})d\Gamma(\mathbf{x})\\ &\quad + \mathrm{RPV}\int_{\partial S}R_i(\mathbf{x},\mathbf{y})\theta(\mathbf{x})d\Gamma(\mathbf{x}) + \int_{\partial S}V_i(\mathbf{x},\mathbf{y})h_n(\mathbf{x})d\Gamma(\mathbf{x})\\ &\quad + \iint_S U_{ij}(\mathbf{x},\mathbf{y})\tilde{f}_j(\mathbf{x})dS(\mathbf{x}) - \iint_S V_i(\mathbf{x},\mathbf{y})f_h(\mathbf{x})dS(\mathbf{x}),\end{aligned} \tag{37}$$

where RPV stands for the Riemann Principal Value (improper Riemann integral) and CPV for the Cauchy Principal Value of an integral.

Thus, to solve the thermoelectroelasticity problem for a given boundary conditions on ∂S one has first to solve heat conduction equation (36), and then displacement boundary integral equation (37) utilizing obtained boundary values of the temperature $\theta(\mathbf{x})$ and heat flux $h_n(\mathbf{x})$.

When extended body forces $\tilde{f}_i$ and distributed heat sources f_h are absent, i.e. $\tilde{f}_i \equiv 0$ and $f_h \equiv 0$, obtained integral equations (36) and (37) contain only boundary integrals, which is advantageous comparing to the existing integral equations, which are similar to Eq. (18).

To validate boundary integral equations obtained and physical assumptions made, another derivation procedure can be applied, which can strictly prove correctness of the obtained integral identities, equations and kernels of thermoelectroelasticity, and also gives explicit expressions for the kernels (32) and (33) through the complex constants $\mathbf{A}$, $\mathbf{B}$, $\mathbf{c}$ and $\mathbf{d}$ of the extended Stroh formalism used in Eq. (4).

1.3.2. Stroh formalism based derivation of the boundary integral equations

Recently Pasternak [18] used the complex variable approach and holomorphy theorems to derive the boundary integral equations and the boundary element method for 2D anisotropic thermoelasticity. This approach can be naturally extended on derivation of the integral equations of 2D thermoelectroelasticity. Here this approach is modified and starts from the Cauchy integral formula instead of the holomorphy theorems.

First, recall the Cauchy integral formula [20, 21], which states that a complex function $\phi(z)$ in a finite domain $z\in S, z\notin\partial S$ at the complex plane $z=x_1+ix_2$ is

completely determined by its values $\phi(\tau)$ on the boundary $\tau \in \partial S$ of the domain S with the following contour integral

$$\phi(z) = \frac{1}{2\pi i} \int_{\partial S} \frac{\phi(\tau)}{\tau - z} d\tau, \tag{38}$$

where $i = \sqrt{-1}$ is an imaginary unit.

Utilizing Cauchy integral formula one obtains that a holomorphic function $g'(z_t)$, which defines temperature field inside the solid S, can be determined using its boundary values as follows

$$g'(z_t) = \frac{1}{2\pi i} \int_{\partial S} \frac{g'(\tau_t)}{\tau_t - z_t} d\tau_t, \tag{39}$$

where τ_t is a boundary variable in the temperature domain $z_t = x_1 + p_t x_2$. According to Eq. (4),

$$g'(z_t) = \frac{1}{2}\left(\theta + i\frac{\vartheta}{k_t}\right), \tag{40}$$

therefore, Eq. (39) can be rewritten as

$$g'(z_t) = \frac{1}{4\pi i} \int_{\partial S} \frac{\theta(\tau_t)}{\tau_t - z_t} d\tau_t + \frac{1}{4\pi k_t} \int_{\partial S} \frac{\vartheta(\tau_t)}{\tau_t - z_t} d\tau_t. \tag{41}$$

The latter integral formula relates the function $g'(z_t)$ with the boundary values of the temperature change θ and the heat flux function ϑ. Since according to Eq. (4),

$$\frac{\partial \vartheta}{\partial s} = \frac{\partial \vartheta}{\partial x_1}\frac{\partial x_1}{\partial s} + \frac{\partial \vartheta}{\partial x_2}\frac{\partial x_2}{\partial s} = -h_2 n_2 - h_1 n_1 = -h_i n_i = -h_n, \tag{42}$$

the last term in Eq. (41) can be integrated by parts as

$$\int_{\partial S} \frac{\vartheta(\tau_t)}{\tau_t - z_t} d\tau_t = \vartheta(\tau_t) \ln(\tau_t - z_t)\Big|_a^b + \int_{\partial S} h_n(\mathbf{x}) \ln\left(Z_t(\mathbf{x}) - z_t\right) d\Gamma(\mathbf{x}), \tag{43}$$

where $Z_t(\mathbf{x}) = x_1 + p_t x_2$, $\mathbf{x}$ is a position vector of the boundary point τ_t; $d\Gamma(\mathbf{x}) \equiv ds(\mathbf{x})$ is a real differential of the arc $\Gamma = \partial S$; a and b are the starting and end points of the integration path ∂S. Due to the heat balance $\vartheta(a) = \vartheta(b) = 0$, and the first term in the right hand side of Eq. (43) is equal to zero. Substituting Eq. (43) into Eq. (41) and utilizing differential identity $dZ_t(\mathbf{x}) = dx_1 + p_t dx_2 = -(n_2 - p_t n_1) d\Gamma(\mathbf{x})$, one obtains

$$g'(z_t) = \frac{1}{4\pi k_t} \int_{\partial S} h_n(\mathbf{x}) \ln\left(Z_t(\mathbf{x}) - z_t\right) d\Gamma(\mathbf{x}) - \frac{1}{4\pi i} \int_{\partial S} \frac{(n_2 - p_t n_1)\theta(\mathbf{x})}{Z_t(\mathbf{x}) - z_t} d\Gamma(\mathbf{x}). \tag{44}$$

Substituting Eq. (44) into Eq. (4) one can easily obtain Eq. (16) as

$$\theta(\boldsymbol{\xi}) = 2\,\mathrm{Re}\left\{g'\left(Z_t(\boldsymbol{\xi})\right)\right\} = \int_{\partial S} \left[\Theta^*(\mathbf{x}, \boldsymbol{\xi}) h_n(\mathbf{x}) - H^*(\mathbf{x}, \boldsymbol{\xi}) \theta(\mathbf{x})\right] d\Gamma(\mathbf{x}). \tag{45}$$

It should be noted that distributed heat sources are not accounted for in Eq. (45) since Eq. (4), and hence Eq. (45), define only the homogeneous solution of Eqs. (1), (2). Due to the linearity of the problem particular solution corresponding to the distributed heat sources can be simply added to the right hand side of Eq. (45).

Integration of Eq. (44) over z_t yields the integral formula for the analytic function $g(z_t)$

$$g(z_t)=-\frac{1}{4\pi k_t}\int_{\partial S} f^*\left(Z_t(\mathbf{x})-z_t\right)h_n(\mathbf{x})d\Gamma(\mathbf{x}) \\ +\frac{1}{4\pi i}\int_{\partial S}(n_2-p_t n_1)\ln\left(Z_t(\mathbf{x})-z_t\right)\theta(\mathbf{x})d\Gamma(\mathbf{x}). \tag{46}$$

Derivation of the extended Somigliana identity of thermoelectroelasticity by means of the Stroh formalism is more complicated. It should be noted that Stroh complex functions $F_\alpha(z_\alpha)$ defined by the vector $\mathbf{f}(z_*)$ are holomorphic in different complex planes $z_\alpha=x_1+p_\alpha x_2$ $(\alpha=1,..,4)$. Therefore, it is more convenient to use real-valued position vectors $\boldsymbol{\xi}$ and $\mathbf{x}$ of the source and boundary points, respectively, instead of the complex variables $z_\alpha=Z_\alpha(\boldsymbol{\xi})$ and $\tau_\alpha=Z_\alpha(\mathbf{x})$. Utilizing these notations the Cauchy integral formula (38) for Stroh complex functions $F_\alpha(z_\alpha)$ writes as

$$F_\alpha(z_\alpha)=\frac{1}{2\pi i}\int_{\partial S}\frac{F_\alpha(\tau_\alpha)\,d\tau_\alpha}{\tau_\alpha-z_\alpha}=\frac{1}{2\pi i}\int_{\partial S}\frac{F_\alpha\left(Z_\alpha(\mathbf{x})\right)dZ_\alpha(\mathbf{x})}{Z_\alpha(\mathbf{x}-\boldsymbol{\xi})}, \tag{47}$$

or in a vector-matrix notation

$$\mathbf{f}\left(Z_*(\boldsymbol{\xi})\right)=\frac{1}{2\pi i}\int_{\partial S}\left\langle\frac{dZ_*(\mathbf{x})}{Z_*(\mathbf{x}-\boldsymbol{\xi})}\right\rangle\mathbf{f}\left(Z_*(\mathbf{x})\right), \tag{48}$$

where $\left\langle F(Z_*)\right\rangle=\operatorname{diag}\left[F_1(Z_1),F_2(Z_2),F_3(Z_3),F_4(Z_4)\right]$.

Using Eq. (4) and orthogonality relations (8) one can rewrite complex functions $\mathbf{f}(z_*)$ in the following way [18]

$$\mathbf{f}(z_*)=\mathbf{B}^{\mathrm{T}}\tilde{\mathbf{u}}+\mathbf{A}^{\mathrm{T}}\tilde{\boldsymbol{\varphi}}-\mathbf{B}^{\mathrm{T}}\tilde{\mathbf{u}}^t-\mathbf{A}^{\mathrm{T}}\tilde{\boldsymbol{\varphi}}^t,\quad \tilde{\mathbf{u}}^t=2\,\mathrm{Re}\left\{\mathbf{c}g(z_t)\right\},\quad \tilde{\boldsymbol{\varphi}}^t=2\,\mathrm{Re}\left\{\mathbf{d}g(z_t)\right\}. \tag{49}$$

Substituting Eq. (49) into Eq. (48) one obtains the integral formula relating Stroh complex function in the domain S with the extended displacement and stress function at the boundary ∂S

$$\mathbf{f}\left(Z_*(\boldsymbol{\xi})\right)=\frac{1}{2\pi i}\int_{\partial S}\left\langle\frac{dZ_*(\mathbf{x})}{Z_*(\mathbf{x}-\boldsymbol{\xi})}\right\rangle\left(\mathbf{A}^{\mathrm{T}}\tilde{\boldsymbol{\varphi}}(\mathbf{x})+\mathbf{B}^{\mathrm{T}}\tilde{\mathbf{u}}(\mathbf{x})\right) \\ -\frac{1}{2\pi i}\int_{\partial S}\left\langle\frac{dZ_*(\mathbf{x})}{Z_*(\mathbf{x}-\boldsymbol{\xi})}\right\rangle\left(\mathbf{A}^{\mathrm{T}}\tilde{\boldsymbol{\varphi}}^t(\mathbf{x})+\mathbf{B}^{\mathrm{T}}\tilde{\mathbf{u}}^t(\mathbf{x})\right). \tag{50}$$

Following [18] (see Appendix C for detailed derivation) Eq. (50) can be transformed to

$$\mathbf{f}\left(Z_*(\boldsymbol{\xi})\right)=\frac{1}{2\pi i}\int_{\partial S}\left\langle\ln Z_*(\mathbf{x}-\boldsymbol{\xi})\right\rangle\mathbf{A}^{\mathrm{T}}\tilde{\mathbf{t}}(\mathbf{x})d\Gamma(\mathbf{x}) \\ -\frac{1}{2\pi i}\int_{\partial S}\left\langle\frac{n_2-n_1p_*}{Z_*(\mathbf{x}-\boldsymbol{\xi})}\right\rangle\mathbf{B}^{\mathrm{T}}\tilde{\mathbf{u}}(\mathbf{x})d\Gamma(\mathbf{x}) \\ -\frac{1}{2\pi i}\int_{\partial S}\left\langle\ln Z_*(\mathbf{x}-\boldsymbol{\xi})\right\rangle\left(\mathbf{A}^{\mathrm{T}}\,\mathrm{Re}\left\{\mathbf{d}(n_2-n_1p_t)\right\}+\mathbf{B}^{\mathrm{T}}\,\mathrm{Re}\left\{\mathbf{c}(n_2-n_1p_t)\right\}\right)\theta(\mathbf{x})\,d\Gamma(\mathbf{x}) \\ -\frac{1}{2\pi ik_t}\int_{\partial S}\left\langle f^*\left(Z_*(\mathbf{x}-\boldsymbol{\xi})\right)\right\rangle\left(\mathbf{A}^{\mathrm{T}}\,\mathrm{Im}\{\mathbf{d}\}+\mathbf{B}^{\mathrm{T}}\,\mathrm{Im}\{\mathbf{c}\}\right)h_n(\mathbf{x})\,d\Gamma(\mathbf{x}). \tag{51}$$

Eq. (51) relates Stroh complex functions with the boundary values of extended tractions, displacements, temperature and heat flux at ∂S.

Now one can use Eqs. (4), (46) and (51) to obtain the extended Somigliana identity for anisotropic thermoelectroelasticity

$$\begin{aligned}\tilde{\mathbf{u}}(\xi) &= 2\,\mathrm{Re}\left\{\mathbf{A}\mathbf{f}\left(Z_*(\xi)\right) + \mathbf{c}g\left(Z_t(\xi)\right)\right\} \\ &= \int_{\partial S} \mathbf{U}(\mathbf{x},\xi)\tilde{\mathbf{t}}(\mathbf{x})d\Gamma(\mathbf{x}) - \int_{\partial S} \mathbf{T}(\mathbf{x},\xi)\tilde{\mathbf{u}}(\mathbf{x})d\Gamma(\mathbf{x}) \\ &+ \int_{\partial S} \mathbf{r}(\mathbf{x},\xi)\theta(\mathbf{x})\,d\Gamma(\mathbf{x}) + \int_{\partial S} \mathbf{v}(\mathbf{x},\xi)h_n(\mathbf{x})\,d\Gamma(\mathbf{x}),\end{aligned} \tag{52}$$

where the kernels $\mathbf{U} = \left[U_{ij}\right]$ and $\mathbf{T} = \left[T_{ij}\right]$ are defined by Eq. (19) and new kernels $\mathbf{r}(\mathbf{x},\xi)$ and $\mathbf{v}(\mathbf{x},\xi)$ are equal to

$$\begin{aligned}\mathbf{r}(\mathbf{x},\xi) &= -\frac{1}{\pi}\,\mathrm{Im}\left[\mathbf{A}\left\langle \ln Z_*(\mathbf{x}-\xi)\right\rangle\left(\mathbf{A}^{\mathrm{T}}\,\mathrm{Re}\left\{\mathbf{d}(n_2 - n_1 p_t)\right\} + \mathbf{B}^{\mathrm{T}}\,\mathrm{Re}\left\{\mathbf{c}(n_2 - n_1 p_t)\right\}\right)\right] \\ &+ \frac{1}{2\pi}\,\mathrm{Im}\left[\mathbf{c}(n_2 - n_1 p_t)\ln Z_t(\mathbf{x}-\xi)\right], \\ \mathbf{v}(\mathbf{x},\xi) &= -\frac{1}{\pi k_t}\,\mathrm{Im}\left[\mathbf{A}\left\langle f^*\left(Z_*(\mathbf{x}-\xi)\right)\right\rangle\left(\mathbf{A}^{\mathrm{T}}\,\mathrm{Im}\{\mathbf{d}\} + \mathbf{B}^{\mathrm{T}}\,\mathrm{Im}\{\mathbf{c}\}\right)\right] \\ &- \frac{1}{2\pi k_t}\,\mathrm{Re}\left[\mathbf{c}f^*\left(Z_t(\mathbf{x}-\xi)\right)\right].\end{aligned} \tag{53}$$

Eq. (52) does not account for extended body forces $\tilde{f}_i$ and distributed heat sources f_h, since the Stroh formalism seeks for the homogeneous solution ($\tilde{f}_i \equiv 0$, $f_h \equiv 0$) of Eqs. (1) and (2).

From Eqs. (35) and (53) it is readily observed that the kernel $V_i(\mathbf{x},\xi)$ in Eq. (29) is the same as the corresponding kernel $\mathbf{v}(\mathbf{x},\xi)$ in Eq. (52). This proves correctness of physical considerations used for obtaining of Eq. (29). The equality of the kernel $R_i(\mathbf{x},\xi)$ given by Eq. (26) and the kernel $\mathbf{r}(\mathbf{x},\xi)$ is proved based on Eqs. (1)–(5) and (9). Therefore, reciprocity approach and complex variable approach produce the same integral equations, which verify their validity. The reciprocity approach is more transparent, since it is based on the general mechanical and mathematical concepts. It also allows accounting for the body forces and distributed heat sources. In turn, the complex variable approach is straightforward, mathematically strict and directly results in closed-form expressions for the kernels.

The Stroh formalism also allows easy obtaining of integral formulae for heat flux and extended stress at the arbitrary internal point ξ of the solid S using Eqs. (4), (44) and (51) as

$$\begin{aligned}h_i(\xi) &= 2k_t\,\mathrm{Im}\left\{(\delta_{2i} - \delta_{1i}p_t)\,g''\left(Z_t(\xi)\right)\right\} \\ &= \int_{\partial S} \Theta_i^{**}(\mathbf{x},\xi)h_n(\mathbf{x})\,d\Gamma(\mathbf{x}) - \int_{\partial S} H_i^{**}(\mathbf{x},\xi)\theta(\mathbf{x})\,d\Gamma(\mathbf{x}),\end{aligned} \tag{54}$$

$$\begin{aligned}\tilde{\boldsymbol{\sigma}}_j(\xi) &= \left[\tilde{\sigma}_{ij}(\xi)\right] \\ &= 2\,\mathrm{Re}\left\{\mathbf{B}(\delta_{2j} - \delta_{1j}\mathbf{P})\mathbf{f}'\left(Z_*(\xi)\right) + \mathbf{d}(\delta_{2j} - \delta_{1j}p_t)\,g'\left(Z_t(\xi)\right)\right\} \\ &= \int_{\partial S} \mathbf{D}_j(\mathbf{x},\xi)\tilde{\mathbf{t}}(\mathbf{x})d\Gamma(\mathbf{x}) - \int_{\partial S} \mathbf{S}_j(\mathbf{x},\xi)\tilde{\mathbf{u}}(\mathbf{x})d\Gamma(\mathbf{x}) \\ &+ \int_{\partial S} \mathbf{q}_j(\mathbf{x},\xi)\theta(\mathbf{x})\,d\Gamma(\mathbf{x}) + \int_{\partial S} \mathbf{w}_j(\mathbf{x},\xi)h_n(\mathbf{x})\,d\Gamma(\mathbf{x}),\end{aligned} \tag{55}$$

where the kernels are defined as

$$\Theta_i^{**}(\mathbf{x},\mathbf{y}) = -\frac{1}{2\pi}\operatorname{Im}\left\{\frac{\delta_{i2}-p_t\delta_{i1}}{Z_t(\mathbf{x}-\mathbf{y})}\right\},\quad H_i^{**}(\mathbf{x},\mathbf{y}) = -\frac{k_t}{2\pi}\operatorname{Re}\left\{\frac{(\delta_{i2}-p_t\delta_{i1})(n_2-p_t n_1)}{\left[Z_t(\mathbf{x}-\mathbf{y})\right]^2}\right\}, \quad (56)$$

$$\mathbf{D}_j(\mathbf{x},\mathbf{y}) = -\frac{1}{\pi}\operatorname{Im}\left[\mathbf{B}\left\langle(\delta_{2j}-\delta_{1j}p_*)\left[Z_*(\mathbf{x}-\mathbf{y})\right]^{-1}\right\rangle\mathbf{A}^{\mathrm{T}}\right],$$

$$\mathbf{S}_j(\mathbf{x},\mathbf{y}) = \frac{1}{\pi}\operatorname{Im}\left[\mathbf{B}\left\langle\frac{(n_2-n_1p_*)(\delta_{2j}-\delta_{1j}p_*)}{\left[Z_*(\mathbf{x}-\mathbf{y})\right]^2}\right\rangle\mathbf{B}^{\mathrm{T}}\right],$$

$$\mathbf{q}_j(\mathbf{x},\mathbf{y}) = \frac{1}{\pi}\operatorname{Im}\left[\mathbf{B}\left\langle\frac{(\delta_{2j}-\delta_{1j}p_*)}{Z_*(\mathbf{x}-\mathbf{y})}\right\rangle\left(\mathbf{A}^{\mathrm{T}}\operatorname{Re}\{\mathbf{d}(n_2-n_1p_t)\}+\mathbf{B}^{\mathrm{T}}\operatorname{Re}\{\mathbf{c}(n_2-n_1p_t)\}\right)\right] \quad (57)$$

$$-\frac{1}{2\pi}\operatorname{Im}\left[\mathbf{d}(\delta_{2j}-\delta_{1j}p_t)\frac{n_2-n_1p_t}{Z_t(\mathbf{x}-\mathbf{y})}\right],$$

$$\mathbf{w}_j(\mathbf{x},\mathbf{y}) = \frac{1}{\pi k_t}\operatorname{Im}\left[\mathbf{B}\left\langle(\delta_{2j}-\delta_{1j}p_*)\ln Z_*(\mathbf{x}-\mathbf{y})\right\rangle\left(\mathbf{A}^{\mathrm{T}}\operatorname{Im}\{\mathbf{d}\}+\mathbf{B}^{\mathrm{T}}\operatorname{Im}\{\mathbf{c}\}\right)\right]$$

$$+\frac{1}{2\pi k_t}\operatorname{Re}\left[\mathbf{d}(\delta_{2j}-\delta_{1j}p_t)\ln Z_t(\mathbf{x}-\mathbf{y})\right].$$

Since the Stroh formalism is used, Eqs. (54) and (55) assume zero values of body forces and distributed heat. If body force or distributed heat exists, they can be accounted for using Eqs. (29) and (31). Based on the identities of the Stroh formalism [11] it can be proved that the kernels (56) and (57) are identical to the kernels defined by Eqs. (32) and (33).

1.3.3. Accounting for the remote load in the unbounded domains

In the engineering numerical analysis most problems for bulky solids are simplified, and infinite medium with holes and cracks is considered. Therefore it is useful to derive integral identities of thermoelectroelasticity, which account for the remote load. Complex variable approach allows easy derivation of such equations using the Cauchy integral formula for an infinite domain [20, 21]

$$\phi(z) = \frac{1}{2\pi i}\int_{\partial S}\frac{\phi(\tau)\,d\tau}{\tau-z} + \phi_\infty(z), \quad (58)$$

where $\phi_\infty(z) = A_0 + A_1 z + A_2 z^2 + \ldots$ is a principal part of the function $\phi(z)$ at the point $z=\infty$.

Since Eqs. (38) and (58) differ only in the term $\phi_\infty(z)$, entire derivation of the integral identity (52) is still valid, however, for infinite domains one should add to the right hand side of Eq. (52) a term corresponding to the principal parts of Stroh complex functions at the infinity. Therefore, for an infinite domain Eq. (52) writes as

$$\tilde{\mathbf{u}}(\xi) = \int_{\partial S} \mathbf{U}(\mathbf{x},\xi)\tilde{\mathbf{t}}(\mathbf{x})d\Gamma(\mathbf{x}) - \int_{\partial S} \mathbf{T}(\mathbf{x},\xi)\tilde{\mathbf{u}}(\mathbf{x})d\Gamma(\mathbf{x}) + \int_{\partial S} \mathbf{r}(\mathbf{x},\xi)\theta(\mathbf{x})d\Gamma(\mathbf{x}) + \int_{\partial S} \mathbf{v}(\mathbf{x},\xi)h_n(\mathbf{x})d\Gamma(\mathbf{x}) + 2\,\mathrm{Re}\left\{\mathbf{A}\mathbf{f}_\infty(Z_*(\xi)) + \mathbf{c}g_\infty(Z_t(\xi))\right\}, \tag{59}$$

where $\mathbf{f}_\infty(z_*)$ and $g_\infty(z_t)$ are principal parts of corresponding analytic functions.

When the medium is heated by the temperature θ_0 and the heat flux h_i^∞ flows steady and uniformly at the infinity, then according to [16, 18, 22], the function $g_\infty(z_t)$ is equal to

$$g_\infty(z_t) = \frac{1}{2}e_0 z_t^2 + \theta_0 z_t, \quad e_0 = -\frac{h_1^\infty + h_2^\infty \overline{p}_t}{2k_t \operatorname{Im} p_t}. \tag{60}$$

and complex functions $\mathbf{f}_\infty(z_*)$ write as

$$\mathbf{f}_\infty(z_*) = \frac{1}{2}\left\langle z_*^2 \right\rangle \left(\mathbf{A}^{\mathrm{T}}\mathbf{q}_a^h + \mathbf{B}^{\mathrm{T}}\mathbf{q}_b^h\right) + \left\langle z_* \right\rangle \left(\mathbf{A}^{\mathrm{T}}\mathbf{q}_a^\theta + \mathbf{B}^{\mathrm{T}}\mathbf{q}_b^\theta\right), \tag{61}$$

where four real vectors $\mathbf{q}_a^h$, $\mathbf{q}_b^h$, $\mathbf{q}_a^\theta$ and $\mathbf{q}_b^\theta$ satisfy the following equations

$$\begin{aligned} &\mathbf{q}_a^\theta = -2\,\mathrm{Re}\{\theta_0 \mathbf{d}\}, \quad \mathbf{N}_1^{\mathrm{T}}\mathbf{q}_a^\theta + \mathbf{N}_3\mathbf{q}_b^\theta + 2\,\mathrm{Re}\{\theta_0 p_t \mathbf{d}\} = 0; \\ &\mathbf{q}_a^h = -2\,\mathrm{Re}\{e_0 \mathbf{d}\}, \quad \mathbf{N}_1^{\mathrm{T}}\mathbf{q}_a^h + \mathbf{N}_3\mathbf{q}_b^h + 2\,\mathrm{Re}\{e_0 p_t \mathbf{d}\} = 0, \\ &\left(\mathbf{N}_3\mathbf{N}_2 + \mathbf{N}_1^{\mathrm{T}}\mathbf{N}_1^{\mathrm{T}}\right)\mathbf{q}_a^h + \left(\mathbf{N}_3\mathbf{N}_1 + \mathbf{N}_1^{\mathrm{T}}\mathbf{N}_3\right)\mathbf{q}_b^h + 2\,\mathrm{Re}\{e_0 p_t^2 \mathbf{d}\} = 0. \end{aligned} \tag{62}$$

Since the matrix $\mathbf{N}_3$ is singular [17], components of the vector $\mathbf{q}_b^\theta$ are defined to within a real constant, which equals to the rigid rotation of the medium. According to [17], the rigid rotation does not influence the stress/strain state of the medium, thus, this constant is assumed zero.

It should be mentioned that the vector $\mathbf{q}_b^h$ should satisfy simultaneously two last equalities in Eq. (62). The numerical analysis confirms that this is possible for transversely isotropic pyroelectrics, when the heat is flowing steady and uniformly along the polarization direction. In general, it is not always possible to determine the vector $\mathbf{q}_b^h$, as Eqs. (62) can be inconsistent. This indicates that the uniform heat flow can cause the nonzero values of stress and electric displacement in the unnotched pyroelectric medium, which is not observed in the anisotropic thermoelasticity. Physically this behavior can be explained by the *tertiary pyroelectric effect*, which is caused by the gradients of temperature field, which in turn are heat flows. Thus, in this case the stress and electric displacement boundedness condition

$$\lim_{z\to\infty} \tilde{\sigma}_{ij}(z) = 0 \tag{63}$$

is not always satisfied. The detailed analysis of this phenomenon is provided in the numerical examples section (see Subsections 5.1 and 5.2).

1.3.4. Boundary integral equations of thermoelectroelasticity for solids with internal cuts (or cracks)

To study thermoelectroelastic solids with cracks and thin inclusions one should account for the temperature, displacement and electric potential discontinuities. Based on the method of fictitious boundaries introduction and their further coupling

[21] for a solid S with an internal mathematical cut Γ_C one can use integral equations (16), (29), (30) and (31) (or identical equations (45), (52), (54) and (55) obtained by the complex variable approach) to obtain the following integral identities for temperature, heat flux, extended displacement and stress

$$\begin{aligned}\theta(\xi) &= \int_{\Gamma}\left[\Theta^*(\mathbf{x},\xi)h_n(\mathbf{x}) - H^*(\mathbf{x},\xi)\theta(\mathbf{x})\right]d\Gamma(\mathbf{x}) \\ &+ \int_{\Gamma_C}\left[\Theta^*(\mathbf{x},\xi)\Sigma h_n(\mathbf{x}) - H^*(\mathbf{x},\xi)\Delta\theta(\mathbf{x})\right]d\Gamma(\mathbf{x}) \\ &- \iint_S \Theta^*(\mathbf{x},\xi) f_h(\mathbf{x})\,dS(\mathbf{x}),\end{aligned} \tag{64}$$

$$\begin{aligned}h_i(\xi) &= \int_{\Gamma}\left[\Theta_i^{**}(\mathbf{x},\xi)h_n(\mathbf{x}) - H_i^{**}(\mathbf{x},\xi)\theta(\mathbf{x})\right]d\Gamma(\mathbf{x}) \\ &+ \int_{\Gamma_C}\left[\Theta_i^{**}(\mathbf{x},\xi)\Sigma h_n(\mathbf{x}) - H_i^{**}(\mathbf{x},\xi)\Delta\theta(\mathbf{x})\right]d\Gamma(\mathbf{x}) \\ &- \iint_S \Theta_i^{**}(\mathbf{x},\xi) f_h(\mathbf{x})\,dS(\mathbf{x}),\end{aligned} \tag{65}$$

$$\begin{aligned}\tilde{u}_i(\xi) &= \int_{\Gamma}\left[U_{ij}(\mathbf{x},\xi)\tilde{t}_j(\mathbf{x}) - T_{ij}(\mathbf{x},\xi)\tilde{u}_j(\mathbf{x})\right]d\Gamma(\mathbf{x}) \\ &+ \int_{\Gamma}\left[R_i(\mathbf{x},\xi)\theta(\mathbf{x}) + V_i(\mathbf{x},\xi)h_n(\mathbf{x})\right]d\Gamma(\mathbf{x}) \\ &+ \int_{\Gamma_C}\left[U_{ij}(\mathbf{x},\xi)\Sigma\tilde{t}_j(\mathbf{x}) - T_{ij}(\mathbf{x},\xi)\Delta\tilde{u}_j(\mathbf{x})\right]d\Gamma(\mathbf{x}) \\ &+ \int_{\Gamma_C}\left[R_i(\mathbf{x},\xi)\Delta\theta(\mathbf{x}) + V_i(\mathbf{x},\xi)\Sigma h_n(\mathbf{x})\right]d\Gamma(\mathbf{x}) \\ &+ \iint_S U_{ij}(\mathbf{x},\xi)\tilde{f}_j(\mathbf{x})\,dS(\mathbf{x}) - \iint_S V_i(\mathbf{x},\xi) f_h(\mathbf{x})\,dS(\mathbf{x}),\end{aligned} \tag{66}$$

$$\begin{aligned}\tilde{\sigma}_{ij}(\xi) &= \int_{\Gamma}\left[D_{ijk}(\mathbf{x},\xi)\tilde{t}_k(\mathbf{x}) - S_{ijk}(\mathbf{x},\xi)\tilde{u}_k(\mathbf{x})\right]d\Gamma(\mathbf{x}) \\ &+ \int_{\Gamma}\left[Q_{ij}(\mathbf{x},\xi)\theta(\mathbf{x}) + W_{ij}(\mathbf{x},\xi)h_n(\mathbf{x})\right]d\Gamma(\mathbf{x}) \\ &+ \int_{\Gamma_C}\left[D_{ijk}(\mathbf{x},\xi)\Sigma\tilde{t}_k(\mathbf{x}) - S_{ijk}(\mathbf{x},\xi)\Delta\tilde{u}_k(\mathbf{x})\right]d\Gamma(\mathbf{x}) \\ &+ \int_{\Gamma_C}\left[Q_{ij}(\mathbf{x},\xi)\Delta\theta(\mathbf{x}) + W_{ij}(\mathbf{x},\xi)\Sigma h_n(\mathbf{x})\right]d\Gamma(\mathbf{x}) \\ &+ \iint_S D_{ijk}(\mathbf{x},\xi)\tilde{f}_k(\mathbf{x})dS(\mathbf{x}) - \iint_S W_{ij}(\mathbf{x},\xi) f_h(\mathbf{x})\,dS(\mathbf{x}).\end{aligned} \tag{67}$$

Here Γ is a boundary of the domain S without internal cuts Γ_C; $\Sigma(\bullet) = (\bullet)^+ + (\bullet)^-$; $\Delta(\bullet) = (\bullet)^+ - (\bullet)^-$; signs "+" and "–" denote variables concerned with faces Γ_C^+ and Γ_C^- of the mathematical cut Γ_C.

It is well known [23] that displacement boundary integral equation (37) degenerate for problems with cuts, and in particular, for crack problems. Therefore, dual boundary integral equations are used. For thermoelectroelastic solids with cuts these equations can be derived from Eqs. (64)–(67) by approaching the internal source point ξ to the boundary points $\mathbf{y} \in \Gamma$ and $\mathbf{y}_C \in \Gamma_C$ and applying the Sokhotskii-

Plemelj formula [20, 21]. Consequently the following dual integral equations are obtained

1) for heat conduction

- when $\mathbf{y} \in \Gamma$ and Γ is smooth at $\mathbf{y}$

$$\begin{aligned}\frac{1}{2}\theta(\mathbf{y}) &= \mathrm{RPV}\int_{\Gamma}\Theta^{*}(\mathbf{x},\mathbf{y})h_n(\mathbf{x})d\Gamma(\mathbf{x}) - \mathrm{CPV}\int_{\Gamma}H^{*}(\mathbf{x},\mathbf{y})\theta(\mathbf{x})d\Gamma(\mathbf{x}) \\ &+ \int_{\Gamma_C}\left[\Theta^{*}(\mathbf{x},\mathbf{y})\Sigma h_n(\mathbf{x}) - H^{*}(\mathbf{x},\mathbf{y})\Delta\theta(\mathbf{x})\right]d\Gamma(\mathbf{x}) - \iint_{S}\Theta^{*}(\mathbf{x},\mathbf{y})f_h(\mathbf{x})dS(\mathbf{x}),\end{aligned} \tag{68}$$

- when $\mathbf{y}_C \in \Gamma_C$ and Γ_C is smooth at $\mathbf{y}_C$

$$\begin{aligned}&\frac{1}{2}\Sigma\theta(\mathbf{y}_C) = \mathrm{RPV}\int_{\Gamma_C}\Theta^{*}(\mathbf{x},\mathbf{y}_C)\Sigma h_n(\mathbf{x})d\Gamma(\mathbf{x}) - \mathrm{CPV}\int_{\Gamma_C}H^{*}(\mathbf{x},\mathbf{y}_C)\Delta\theta(\mathbf{x})d\Gamma(\mathbf{x}) \\ &+ \int_{\Gamma}\left[\Theta^{*}(\mathbf{x},\mathbf{y}_C)h_n(\mathbf{x}) - H^{*}(\mathbf{x},\mathbf{y}_C)\theta(\mathbf{x})\right]d\Gamma(\mathbf{x}) - \iint_{S}\Theta^{*}(\mathbf{x},\mathbf{y}_C)f_h(\mathbf{x})dS(\mathbf{x}), \\ &\frac{1}{2}\Delta h_n(\mathbf{y}_C) = n_i^{+}(\mathbf{y}_C)\Bigg[\mathrm{CPV}\int_{\Gamma_C}\Theta_i^{**}(\mathbf{x},\mathbf{y}_C)\Sigma h_n(\mathbf{x})d\Gamma(\mathbf{x}) - \mathrm{HPV}\int_{\Gamma_C}H_i^{**}(\mathbf{x},\mathbf{y}_C)\Delta\theta(\mathbf{x})d\Gamma(\mathbf{x}) \\ &+\int_{\Gamma}\left[\Theta_i^{**}(\mathbf{x},\mathbf{y}_C)h_n(\mathbf{x}) - H_i^{**}(\mathbf{x},\mathbf{y}_C)\theta(\mathbf{x})\right]d\Gamma(\mathbf{x}) - \iint_{S}\Theta_i^{**}(\mathbf{x},\mathbf{y}_C)f_h(\mathbf{x})dS(\mathbf{x})\Bigg],\end{aligned} \tag{69}$$

2) for thermoelectroelasticity

- when $\mathbf{y} \in \Gamma$ and Γ is smooth at $\mathbf{y}$

$$\begin{aligned}\frac{1}{2}\tilde{u}_i(\mathbf{y}) &= \mathrm{RPV}\int_{\Gamma}U_{ij}(\mathbf{x},\mathbf{y})\tilde{t}_j(\mathbf{x})d\Gamma(\mathbf{x}) - \mathrm{CPV}\int_{\Gamma}T_{ij}(\mathbf{x},\mathbf{y})\tilde{u}_j(\mathbf{x})d\Gamma(\mathbf{x}) \\ &+ \mathrm{RPV}\int_{\Gamma}R_i(\mathbf{x},\mathbf{y})\theta(\mathbf{x})d\Gamma(\mathbf{x}) + \int_{\Gamma}V_i(\mathbf{x},\mathbf{y})h_n(\mathbf{x})d\Gamma(\mathbf{x}) \\ &+ \int_{\Gamma_C}\left[U_{ij}(\mathbf{x},\mathbf{y})\Sigma\tilde{t}_j(\mathbf{x}) - T_{ij}(\mathbf{x},\mathbf{y})\Delta\tilde{u}_j(\mathbf{x}) + R_i(\mathbf{x},\mathbf{y})\Delta\theta(\mathbf{x}) + V_i(\mathbf{x},\mathbf{y})\Sigma h_n(\mathbf{x})\right]d\Gamma(\mathbf{x}) \\ &+ \iint_{S}U_{ij}(\mathbf{x},\mathbf{y})\tilde{f}_j(\mathbf{x})dS(\mathbf{x}) - \iint_{S}V_i(\mathbf{x},\mathbf{y})f_h(\mathbf{x})dS(\mathbf{x}),\end{aligned} \tag{70}$$

- when $\mathbf{y}_C \in \Gamma_C$ and Γ_C is smooth at $\mathbf{y}_C$

$$\frac{1}{2}\Sigma\tilde{u}_i(\mathbf{y}_C) = \mathrm{RPV}\int_{\Gamma_C} U_{ij}(\mathbf{x},\mathbf{y}_C)\Sigma\tilde{t}_j(\mathbf{x})d\Gamma(\mathbf{x}) - \mathrm{CPV}\int_{\Gamma_C} T_{ij}(\mathbf{x},\mathbf{y}_C)\Delta\tilde{u}_j(\mathbf{x})d\Gamma(\mathbf{x})$$
$$+\mathrm{RPV}\int_{\Gamma_C} R_i(\mathbf{x},\mathbf{y}_C)\Delta\theta(\mathbf{x})d\Gamma(\mathbf{x}) + \int_{\Gamma_C} V_i(\mathbf{x},\mathbf{y}_C)\Sigma h_n(\mathbf{x})d\Gamma(\mathbf{x})$$
$$+\int_{\Gamma}\left[U_{ij}(\mathbf{x},\mathbf{y}_C)\tilde{t}_j(\mathbf{x}) - T_{ij}(\mathbf{x},\mathbf{y}_C)\tilde{u}_j(\mathbf{x}) + R_i(\mathbf{x},\mathbf{y}_C)\theta(\mathbf{x}) + V_i(\mathbf{x},\mathbf{y}_C)h_n(\mathbf{x})\right]d\Gamma(\mathbf{x})$$
$$+\iint_S U_{ij}(\mathbf{x},\mathbf{y}_C)\tilde{f}_j(\mathbf{x})dS(\mathbf{x}) - \iint_S V_i(\mathbf{x},\mathbf{y}_C)f_h(\mathbf{x})dS(\mathbf{x}),$$

$$\frac{1}{2}\Delta\tilde{t}_i(\mathbf{y}_C) = n_j^+(\mathbf{y}_C)\left[\mathrm{CPV}\int_{\Gamma_C} D_{ijk}(\mathbf{x},\mathbf{y}_C)\Sigma\tilde{t}_k(\mathbf{x})d\Gamma(\mathbf{x}) - \mathrm{HPV}\int_{\Gamma_C} S_{ijk}(\mathbf{x},\mathbf{y}_C)\Delta\tilde{u}_k(\mathbf{x})d\Gamma(\mathbf{x})\right.$$
$$+\mathrm{CPV}\int_{\Gamma_C} Q_{ij}(\mathbf{x},\mathbf{y}_C)\Delta\theta(\mathbf{x})d\Gamma(\mathbf{x}) + \mathrm{RPV}\int_{\Gamma_C} W_{ij}(\mathbf{x},\mathbf{y}_C)\Sigma h_n(\mathbf{x})d\Gamma(\mathbf{x})$$
$$+\int_{\Gamma}\left[D_{ijk}(\mathbf{x},\mathbf{y}_C)\tilde{t}_k(\mathbf{x}) - S_{ijk}(\mathbf{x},\mathbf{y}_C)\tilde{u}_k(\mathbf{x}) + Q_{ij}(\mathbf{x},\mathbf{y}_C)\theta(\mathbf{x}) + W_{ij}(\mathbf{x},\mathbf{y}_C)h_n(\mathbf{x})\right]d\Gamma(\mathbf{x})$$
$$\left.+\iint_S D_{ijk}(\mathbf{x},\mathbf{y}_C)\tilde{f}_k(\mathbf{x})dS(\mathbf{x}) - \iint_S W_{ij}(\mathbf{x},\mathbf{y}_C)f_h(\mathbf{x})dS(\mathbf{x})\right]. \qquad (71)$$

Here RPV stands for the Riemann Principal Value, CPV for the Cauchy Principal Value and HPV for the Hadamard Principal Value (finite part) of an integral.

Accompanied with the thermal and mechanical boundary conditions at Γ and Γ_C boundary integral equations (68)–(71) allow determining all boundary functions θ, h_n, $\tilde{u}_i$ and $\tilde{t}_i$. Consequent application of the integral identities (64)–(67) allow determining of the thermo-electro-elastic state of the solid with internal cuts at an arbitrary internal point.

1.4. A model of a thin thermoelectroelastic inclusion

Modeling of cracks in a pyroelectric medium is more complicated as the thermoelastic cracks modeling, since one should account for the electric permeability of a crack medium. Pasternak [15] used the linear model of a thin piezoelectric inclusion to study permeable, impermeable and semi-permeable cracks in piezoelectric solids. To study the pyroelectric solids, this model can be extended to account for the thermal effects. For self-consistency this section contains general considerations and the principles used in modeling of thin inclusions, and also the detailed derivation of the model of a thin pyroelectric inclusion.

For modeling of solids with thin inhomogeneities, a coupling principle for continua of different dimension is often used (e.g. see [15, 24, 25]). This principle involves the replacement of a thin inclusion with a surface of a field discontinuity for stress, electric displacement, displacement, electric potential, temperature, and heat flux (Fig. 1). Frequently a median surface of a thin inhomogeneity is chosen as the discontinuity surface. The inclusion is thus removed from consideration as a geometrical object, and it is assumed that the thermal, electric and mechanical influence of the inclusion is reduced to the influence of the above-mentioned discontinuity surface (a line for 2D problems). Thus, according to a discontinuity

function method [24], the study of a stress state of a solid (*an exterior problem*) is reduced to the study of the influence of unknown discontinuity functions and is considered without account of the inclusion's material properties. It is clear that the thermoelectroelastic state of the solid depends on these discontinuity functions, material properties of the solid, the geometrical features of the problem, the contact conditions at the thin inhomogeneity interface, and the external load.

On the other hand, due to a small thickness of the inclusion, the extended tractions and displacements, temperature and heat flux at the faces of the inclusion are related with each other. Corresponding relations, which include thermo-electro-mechanical properties of the inclusion and its thickness, are called the mathematical model of a thin inclusion. This model does not depend on the solid's properties, and it can be considered as *an interior problem*. There are only three basic requirements for the mathematical model of a thin inclusion [24]: (a) the number of equations should equal to the number of the unknown discontinuity functions; (b) the model should be simple for further solution of the obtained system of equations; and (c) the model should simulate essential features of thermoelectroelastic behavior of the inclusion.

Since the coupling principle and a discontinuity function method consider exterior and interior problems independently, several inclusion models, which simulate different features of the inhomogeneity, can be developed for the same exterior problem, and using the same inclusion model one can solve different exterior problems.

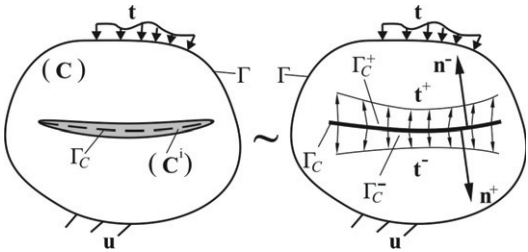

Fig. 1. Coupling principle applied to modeling of a solid with a thin inclusion

Using the philosophy of the discontinuity function method and the coupling principle (Fig. 1) for the development of a line inclusion model, one withdraws the inclusion from consideration as a geometrical object, and transfers the contact tractions, displacements, surface charges, electric potential, temperature, and heat flux onto its median surface Γ_C (accordingly onto the faces Γ_C^+ and Γ_C^-, Fig. 1). Thus, the present problem is reduced to the determination of the thermoelectroelastic state of a solid with the line Γ_C of thermo-electro-mechanical field discontinuities. After development of the interaction conditions for a thin inhomogeneity along with the integral equations (68)–(71) concerning abovementioned field discontinuities for a solid, the thermoelectroelastic state of the latter can be determined.

Consider the thermoelectroelastic state of a certain cross-section $\mathbf{y}$ of a thin pyroelectric inclusion. Assume that the Ox_1' axis of a local coordinate system $Ox_1'x_2'x_3$

is directed along the normal vector $\mathbf{n}^{+}(\mathbf{y})$ of the surface Γ_C^{+} at the point $\mathbf{y}$. All vectors in the local coordinate system are related with those of the global one by the relations $\tilde{t}_i' = \Omega_{ij}\tilde{t}_j$, $\tilde{t}_i = \Omega_{ji}\tilde{t}_j'$, where $\mathbf{\Omega}$ is a rotation matrix. The origin of the local coordinate system is placed at the median surface of the thin inclusion. Thus, $\tilde{f}(-h) = \tilde{f}^{+}$ and $\tilde{f}(h) = \tilde{f}^{-}$, where $\tilde{f}$ is one of the scalars θ, h_n or vectors $\tilde{u}_i$, $\tilde{t}_i$; $2h = 2h(\mathbf{y})$ is the thickness of the inclusion at $\mathbf{y}$. With the account of the identity $\mathbf{n}^{\pm} = -\mathbf{n}^{\mathrm{i}\pm}$, the conditions of a perfect thermal, mechanical and electric contact of the inclusion and the solid are $\theta^{\pm} = \theta^{\mathrm{i}\pm}$, $h_n^{\pm} = -h_n^{\mathrm{i}\pm}$, $\tilde{u}_i^{\pm} = \tilde{u}_i^{\mathrm{i}\pm}$, $\tilde{t}_i^{\pm} = -\tilde{t}_i^{\mathrm{i}\pm}$. Here the non-italic superscript "i" denotes values concerned with the inclusion.

According to Eq. (2), a heat flux, stress and electric displacement inside the inclusion within the notations (7) equal

$$\begin{aligned} &h_1' = -k_{11}'^{\mathrm{i}}\theta_{,1}' - k_{12}'^{\mathrm{i}}\theta_{,2}', \quad h_2' = -k_{12}'^{\mathrm{i}}\theta_{,1}' - k_{22}'^{\mathrm{i}}\theta_{,2}'; \\ &\tilde{\sigma}_{i1}' = Q_{ik}'^{\mathrm{i}}\tilde{u}_{k,1}' + R_{ik}'^{\mathrm{i}}\tilde{u}_{k,2}' - \tilde{\beta}_{i1}'^{\mathrm{i}}\theta, \quad \tilde{\sigma}_{i2}' = R_{ki}'^{\mathrm{i}}\tilde{u}_{k,1}' + T_{ik}'^{\mathrm{i}}\tilde{u}_{k,2}' - \tilde{\beta}_{i2}'^{\mathrm{i}}\theta. \end{aligned} \tag{72}$$

Integrating Eq. (72) over the thickness of the inclusion one can obtain

$$\begin{aligned} &\int_{-h}^{h} h_1' dx_1' = -k_{11}'^{\mathrm{i}}\left[\theta(h) - \theta(-h)\right] - k_{12}'^{\mathrm{i}}\int_{-h}^{h}\theta_{,2}' dx_1', \\ &\int_{-h}^{h} h_2' dx_1' = -k_{12}'^{\mathrm{i}}\left[\theta(h) - \theta(-h)\right] - k_{22}'^{\mathrm{i}}\int_{-h}^{h}\theta_{,2}' dx_1', \\ &\int_{-h}^{h} \tilde{\sigma}_{i1}' dx_1' = Q_{ik}'^{\mathrm{i}}\left[\tilde{u}_k'(h) - \tilde{u}_k'(-h)\right] + R_{ik}'^{\mathrm{i}}\int_{-h}^{h}\tilde{u}_{k,2}' dx_1' - \tilde{\beta}_{i1}'^{\mathrm{i}}\int_{-h}^{h}\theta dx_1', \\ &\int_{-h}^{h} \tilde{\sigma}_{i2}' dx_1' = R_{ki}'^{\mathrm{i}}\left[\tilde{u}_k'(h) - \tilde{u}_k'(-h)\right] + T_{ik}'^{\mathrm{i}}\int_{-h}^{h}\tilde{u}_{k,2}' dx_1' - \tilde{\beta}_{i2}'^{\mathrm{i}}\int_{-h}^{h}\theta dx_1'. \end{aligned} \tag{73}$$

With the account of the balance equations (1) and contact conditions $h_n^{\pm} = -h_n^{\mathrm{i}\pm}$, $\tilde{t}_i^{\pm} = -\tilde{t}_i^{\mathrm{i}\pm}$ using the coupling principle for continua of different dimension the following relations should hold

$$\begin{aligned} &\int_{-h}^{h} h_2' dx_1' = H(\mathbf{y}), \quad H(\mathbf{y}) = -H^0 + \int_{\mathbf{y}_0}^{\mathbf{y}} \Sigma h_n(s)\, ds; \\ &\int_{-h}^{h} \tilde{\sigma}_{i2}' dx_1' = \tilde{P}_i'(\mathbf{y}) = \Omega_{ij}(\mathbf{y})\tilde{P}_j(\mathbf{y}), \quad \tilde{P}_j(\mathbf{y}) = -\tilde{P}_j^0 + \int_{\mathbf{y}_0}^{\mathbf{y}} \Sigma\tilde{t}_j(s)\, ds, \end{aligned} \tag{74}$$

where s is an arc coordinate of the mathematical cut Γ_C; $\tilde{P}_j^0$ are the force and electric charge at the left end of the inclusion, which position vector is defined by a point $\mathbf{y}_0$; H^0 is a heat flux at the left end of the inclusion. According to the mean value theorem,

$$\begin{aligned} &\int_{-h}^{h} h_1' dx_1' = 2h\cdot h_1'^{\mathrm{avr}} \approx h(\mathbf{y})\left[h_n^{\mathrm{i}}(h) - h_n^{\mathrm{i}}(-h)\right] = h(\mathbf{y})\Delta h_n(\mathbf{y}), \\ &\int_{-h}^{h} \theta_{,2}' dx_1' = 2h\cdot\theta_{,2}'^{\mathrm{avr}} \approx h(\mathbf{y})\left[\theta_{,2}'(h) + \theta_{,2}'(-h)\right] = h(\mathbf{y})\Sigma\theta_{,2}'(\mathbf{y}), \\ &\int_{-h}^{h} \theta dx_1' = 2h\cdot\theta^{\mathrm{avr}} \approx h(\mathbf{y})\left[\theta(h) + \theta(-h)\right] = h(\mathbf{y})\Sigma\theta(\mathbf{y}); \\ &\int_{-h}^{h} \tilde{\sigma}_{i1}' dx_1' = 2h\tilde{\sigma}_{i1}'^{\mathrm{avr}} \approx h(\mathbf{y})\left[\tilde{t}_i'^{\mathrm{i}}(h) - \tilde{t}_i'^{\mathrm{i}}(-h)\right] = h(\mathbf{y})\Delta\tilde{t}_i'(\mathbf{y}), \\ &\int_{-h}^{h} \tilde{u}_{k,2}' dx_1' = 2h\tilde{u}_{k,2}'^{\mathrm{avr}} \approx h(\mathbf{y})\left[\tilde{u}_{k,2}'(h) + \tilde{u}_{k,2}'(-h)\right] = h(\mathbf{y})\Sigma\tilde{u}_{k,2}'(\mathbf{y}). \end{aligned} \tag{75}$$

Similar to [15], for simplification of the model one can withdraw the interaction of thermo-electro-mechanical fields in the directions normal and tangential to the

inclusion's median line (as in the model of Winkler elastic foundation) by assuming that $k_{12}^{\prime i}=0$ and $R_{ik}^{\prime i}=0$. Then, according to Eqs. (73)–(75), one can obtain

$$\Delta h_n(\mathbf{y})=\frac{k_{11}^{\prime i}(\mathbf{y})}{h(\mathbf{y})}\left[\Delta\theta(\mathbf{y})+\Delta\theta^*(\mathbf{y})\right],\quad \Sigma\theta'_{,2}(\mathbf{y})=-\frac{H(\mathbf{y})-H^*(\mathbf{y})}{h(\mathbf{y})k_{22}^{\prime i}(\mathbf{y})};$$

$$\Delta\tilde{t}_i'(\mathbf{y})=-\frac{Q_{ik}^{\prime i}(\mathbf{y})}{h(\mathbf{y})}\left[\Delta\tilde{u}_k'(\mathbf{y})+\Delta\tilde{u}_k'^*(\mathbf{y})\right]-\tilde{\beta}_{i1}^{\prime i}\Sigma\theta(\mathbf{y}),\qquad (76)$$

$$T_{ik}^{\prime i}(\mathbf{y})\Sigma\tilde{u}'_{k,2}(\mathbf{y})=\frac{1}{h(\mathbf{y})}\left[\tilde{P}_i'(\mathbf{y})+\tilde{P}_i'^*(\mathbf{y})\right]+\tilde{\beta}_{i2}^{\prime i}\Sigma\theta(\mathbf{y}).$$

Similar to Ref. [15], a system of correcting functions $\Delta\theta^*$, H^*, $\Delta\tilde{u}_i'^*$, $\tilde{P}_i'^*$ is introduced into Eq. (76). According to Refs. [15, 24, 25], the correcting functions for very thin inclusions can be assumed zero ones.

Denoting $\mathbf{N}^1=\left(\mathbf{T}'^i\right)^{-1}$ and $\tilde{\alpha}_{i2}'^i=N_{ij}^1\tilde{\beta}_{j2}'^i$ with the account that $\Sigma\theta'_{,2}=\partial\Sigma\theta/\partial s$, $\Sigma\tilde{u}'_{k,2}=\partial\Sigma\tilde{u}_k'/\partial s$ one can obtain the following relations between discontinuity functions at the thin inclusion

$$\Delta h_n(\mathbf{y})=\frac{k_{11}^{\prime i}(\mathbf{y})}{h(\mathbf{y})}\left[\Delta\theta(\mathbf{y})+\Delta\theta^*(\mathbf{y})\right],\quad \frac{\partial\Sigma\theta(\mathbf{y})}{\partial s}=-\frac{H(\mathbf{y})-H^*(\mathbf{y})}{h(\mathbf{y})k_{22}^{\prime i}(\mathbf{y})};$$

$$\Delta\tilde{t}_i'(\mathbf{y})=-\frac{Q_{ik}^{\prime i}(\mathbf{y})}{h(\mathbf{y})}\left[\Delta\tilde{u}_k'(\mathbf{y})+\Delta\tilde{u}_k'^*(\mathbf{y})\right]-\tilde{\beta}_{i1}^{\prime i}\Sigma\theta(\mathbf{y}),\qquad (77)$$

$$\frac{\partial\Sigma\tilde{u}_i'(\mathbf{y})}{\partial s}=\frac{N_{ij}^1}{h(\mathbf{y})}\left[\tilde{P}_j'(\mathbf{y})+\tilde{P}_j'^*(\mathbf{y})\right]+\tilde{\alpha}_{i2}^{\prime i}\Sigma\theta(\mathbf{y}).$$

Transforming (77) to global coordinates and integrating $\partial\Sigma\theta/\partial s$ and $\partial\Sigma\tilde{u}_k/\partial s$ along the discontinuity line Γ_C from the left end $\mathbf{y}_0$ to the collocation point $\mathbf{y}$ the following model of the thin thermoelectroelastic inclusion is obtained

$$\Delta h_n(\mathbf{y})=\frac{k_{11}^{\prime i}(\mathbf{y})}{h(\mathbf{y})}\left[\Delta\theta(\mathbf{y})+\Delta\theta^*(\mathbf{y})\right],\quad \Sigma\theta(\mathbf{y})=2\theta^0-\int_{\mathbf{y}_0}^{\mathbf{y}}\frac{H(s)-H^*(s)}{h(s)k_{22}^{\prime i}(s)}ds;$$

$$\Delta\tilde{\mathbf{t}}(\mathbf{y})=-\frac{\mathbf{V}(\mathbf{y})\left[\Delta\tilde{\mathbf{u}}(\mathbf{y})+\Delta\tilde{\mathbf{u}}^*(\mathbf{y})\right]}{h(\mathbf{y})}-\mathbf{v}(\mathbf{y})\Sigma\theta(\mathbf{y}),\qquad (78)$$

$$\Sigma\tilde{\mathbf{u}}(\mathbf{y})=2\tilde{\mathbf{u}}^0+\int_{\mathbf{y}_0}^{\mathbf{y}}\frac{\mathbf{W}(s)\left[\tilde{\mathbf{P}}(s)+\tilde{\mathbf{P}}^*(s)\right]}{h(s)}ds+\int_{\mathbf{y}_0}^{\mathbf{y}}\mathbf{w}(s)\Sigma\theta(s)ds.$$

Here $\mathbf{V}=\mathbf{\Omega}^{\mathrm{T}}\mathbf{Q}'^i\mathbf{\Omega}$, $\mathbf{W}=\mathbf{\Omega}^{\mathrm{T}}\mathbf{N}^1\mathbf{\Omega}$, $\mathbf{v}=\mathbf{\Omega}^{\mathrm{T}}\tilde{\boldsymbol{\beta}}_1'^i$, and $\mathbf{w}=\mathbf{\Omega}^{\mathrm{T}}\tilde{\boldsymbol{\alpha}}_2'^i$; θ^0 is an average temperature change at the left end of the inclusion; $\tilde{\mathbf{u}}^0$ are the mean displacements and electric potential at the left end of the inclusion. Model (78) for an isothermal case ($\theta\equiv 0$) is equivalent to the piezoelectric inclusion model developed in Ref. [15].

Average values of temperature, displacements and electric potential at the left end of the thin inclusion can be determined, when the integral equations (68)–(71) and equations (78) of the pyroelectric inclusion model are supplied with the equilibrium and heat balance equations for a thin inhomogeneity,

$$\tilde{P}_j^n+\tilde{P}_j^0-\int_{\Gamma_C^+}\Sigma\tilde{t}_j(\mathbf{x})d\Gamma(\mathbf{x})=0,\quad H^0+H^n-\int_{\Gamma_C^+}\Sigma h_n(\mathbf{x})d\Gamma(\mathbf{x})=0,\qquad (79)$$

where $\tilde{P}_j^n$ are forces and surface electric charges applied at the right end of the inclusion; H^n is a heat at the right end of the inhomogeneity.

To study thin curved and crooked inclusions or solids with thin inhomogeneities under a non-uniform load, one should extend the model (78) with the account of bending effect using Eq. (A.5) of Ref. [15] or Eq. (19) of Ref. [25].

If one assumes elastic moduli of an inclusion to be close to zero, and its permittivity in the direction perpendicular to the median line to be very high, the model (78) allows modeling permeable cracks [15]. Meanwhile, the variation of the heat conduction coefficients in the model (78) allows studying insulated or thermo-conductive cracks and cracks with an imperfect thermal contact of their faces. If one assumes the permittivity in Eq. (78) close to zero, a model of an impermeable crack (or inclusion) can be established [15]. If inclusion's permittivity κ_{ij}^i is very high comparing to the corresponding of a medium, based on the inclusion model (78) one can obtain that when $\kappa^i \to \infty$ the electric potential discontinuity $\Delta\phi$ at the inclusion tends to zero, i.e. faces of the inclusion have a constant electric potential. Physically these conditions correspond to an electricity-conductive inclusion in a dielectric solid [15].

Therefore, the model (78) of a thin inclusion allows modeling impermeable and permeable cracks, and rigid conductive line inclusions, if one assumes its elastic moduli and permittivity to be close to zero or tend to infinity. It is clear, that for the case of intermediate values of elastic and dielectric constants the model (78) describes semi-permeable cracks and thin pyroelectric inclusions.

Boundary integral equations (68)–(71) along with the model of a thin inclusion (78), (79) can be introduced into the computational algorithm [15] of the boundary element method. According to Refs. [15, 24], it is necessary to consider the square root singularity of heat flux, stress and electric displacement at the tips of a thin inclusion. This singularity can be accounted for by utilizing special shape functions [15] for modeling of temperature, heat flux, electric potential, displacement, stress and electric displacement discontinuities at the ends of the discontinuity line Γ_C, which replaces the inhomogeneity. The account of a thermal expansion and a pyroeffect in Eqs. (68)–(71), (78) does not influence the solution structure, and hence, the singularity of stress and electric displacement fields. Therefore, according to [15], the strength of the fields' singularity at tips of a thin inhomogeneity is described by generalized stress and electric displacement intensity factors (SEDIF), which are determined through the discontinuity functions in the local rectangular coordinate system with the origin at the tip of an inhomogeneity by the following formulae

$$\tilde{\mathbf{k}}^{(1)} = \lim_{s\to 0}\sqrt{\frac{\pi}{8s}}\mathbf{L}\cdot\Delta\tilde{\mathbf{u}}(s), \quad \tilde{\mathbf{k}}^{(2)} = -\lim_{s\to 0}\sqrt{\frac{\pi s}{2}}\Sigma\tilde{\mathbf{t}}(s), \tag{80}$$

where $\tilde{\mathbf{k}}^{(1)} = \left[K_{21}, K_{11}, K_{31}, K_{41}\right]^{\mathrm{T}}$, $\tilde{\mathbf{k}}^{(2)} = \left[K_{12}^{(2)}, K_{22}^{(2)}, K_{32}, K_{42}\right]^{\mathrm{T}}$; K_{ij} are the generalised SEDIF. For a crack $K_{11} = K_{\mathrm{I}}$, $K_{21} = K_{\mathrm{II}}$, $K_{31} = K_{\mathrm{III}}$, $K_{41} = K_{\mathrm{IV}} \equiv K_D$, and $\tilde{\mathbf{k}}^{(2)} = \mathbf{0}$, where K_{I}, K_{II}, K_{III}, $K_{\mathrm{IV}} \equiv K_D$ are classical SEDIF of the cracks theory [4, 11]; $\mathbf{L} = -2\sqrt{-1}\mathbf{B}\mathbf{B}^{\mathrm{T}}$ is a real Barnett–Lothe tensor [11].

Two first components $K_{12}^{(2)}$ and $K_{22}^{(2)}$ of the generalized SEDIF vector $\tilde{\mathbf{k}}^{(2)}$ are denoted with a superscript to distinguish them from the generalized stress intensity factors K_{12} and K_{22} of thin elastic inclusions introduced by Sulym [24], which are defined as

$$K_{11}+K_{12}=\lim_{r\to 0}\sqrt{2\pi r}\,\sigma_{22}(r,\theta)\big|_{\theta=0},\quad K_{21}+K_{22}=\lim_{r\to 0}\sqrt{2\pi r}\,\sigma_{12}(r,\theta)\big|_{\theta=0}, \tag{81}$$

where the factors K_{11} and K_{21} are introduced by Eq. (80). To determine the factors K_{12} and K_{22}, according to Ref. [15], one should use the following equation

$$k_i^{(2)}=S_{ji}\tilde{k}_j^{(2)}\quad (i=1,2;\ j=1,..,4). \tag{82}$$

Here $\mathbf{k}^{(2)}=[K_{22},K_{12}]^{\mathrm{T}}$ is a vector of generalized stress intensity factors; $\mathbf{S}=\sqrt{-1}\left(2\mathbf{A}\mathbf{B}^{\mathrm{T}}-\mathbf{I}\right)$ is the second real Barnett–Lothe tensor [11].

Extended stress function and displacement vector in the local coordinate system with the origin at the inclusion tip and Ox_1 axis directed along a median line are related to the generalized SEDIF by the following asymptotic formulae [15]

$$\tilde{\boldsymbol{\varphi}}=\sqrt{\frac{2}{\pi}}\,\mathrm{Im}\left\{\mathbf{B}\left\langle\sqrt{z_*}\right\rangle\left(\sqrt{-1}\mathbf{B}^{-1}\tilde{\mathbf{k}}^{(1)}-2\mathbf{A}^{\mathrm{T}}\tilde{\mathbf{k}}^{(2)}\right)\right\}+O\left(z^{3/2}\right), \tag{83}$$

$$\tilde{\mathbf{u}}=\sqrt{\frac{2}{\pi}}\,\mathrm{Im}\left\{\mathbf{A}\left\langle\sqrt{z_*}\right\rangle\left(\sqrt{-1}\mathbf{B}^{-1}\tilde{\mathbf{k}}^{(1)}-2\mathbf{A}^{\mathrm{T}}\tilde{\mathbf{k}}^{(2)}\right)\right\}+O\left(z^{3/2}\right). \tag{84}$$

1.5. Numerical examples

1.5.1. Electric displacement in a homogeneous square pyroelectric solid under a uniform heat flux

Consider a plane strain state of a square thermoelectroelastic solid, whose height and width equal $2a$, occupying a domain $\{x_1,x_2\,|-a\le x_1\le a,-a\le x_2\le a\}$. The solid is made of $BaTiO_3$ ceramics. According to [26], this material is transversely isotropic and when it is polarized along the Ox_2 it has the following properties: $c_{11}=150$ GPa, $c_{12}=66$ GPa, $c_{13}=66$ GPa, $c_{44}=44$ GPa; $\alpha_{11}=8.53\cdot 10^{-6}$ K^{-1}, $\alpha_{22}=1.99\cdot 10^{-6}$ K^{-1}; $\lambda_2=13.3\cdot 10^{-6}$ GV/(m·K); $e_{21}=-4.35$ C/m^2, $e_{22}=17.5$ C/m^2, $e_{16}=11.4$ C/m^2; $\kappa_{11}=1115\varepsilon_0$, $\kappa_{22}=1260\varepsilon_0$; $k_{11}=k_{22}=2.5$ W/(m·K). Here $\varepsilon_0=8.85\cdot 10^{-3}$ nF/m is the electric constant. The boundary of the solid is free of surface tractions and electric charges.

When a steady-state heat flows uniformly along the polarization direction Ox_2 the system of linear algebraic equations (62) is consistent, and stress and electric displacement are zero in the entire solid, which is also proved by the boundary element analysis of this problem. However, if the heat h_0 flows steady along Ox_1 axis, which is normal to the polarization direction, Eqs. (62) are inconsistent. Thus, the stress and electric displacement are not zero inside the solid, and the tertiary pyroelectric effect is observed. Due to the same structure of matrices of elastic and piezoelectric constants, this behavior is possessed by other transversely isotropic ferroelectrics, such as Cadmium Selenide and PZT-4.

Fig. 2 depicts the contour plots of the components of electric displacement vector obtained by the developed boundary element method. The contour step equals $0.1D_0$. The normalization factor equals $D_0 = h_0 a \chi_2 / k_{11}$. The boundary element mesh consists of $20 \times 4 = 80$ discontinuous quadratic boundary elements distributed uniformly at the sides of the square. Here and further the number of boundary elements is selected under the condition, that its increase does not influence the obtained numerical results.

One can see in Fig. 2 that electric displacement in the solid is not constant and has essentially nonlinear distribution. Electric displacement D_i is proportional to the linear dimension a. Thus, when $a \to \infty$ $\sup D_i \to \infty$, and hence, for the infinite medium stress and electric displacement boundedness condition (63) does not hold. Therefore, thermoelectroelastic problems for the infinite medium under the uniform steady-state heat flux are well-posed only if Eqs. (62) are consistent.

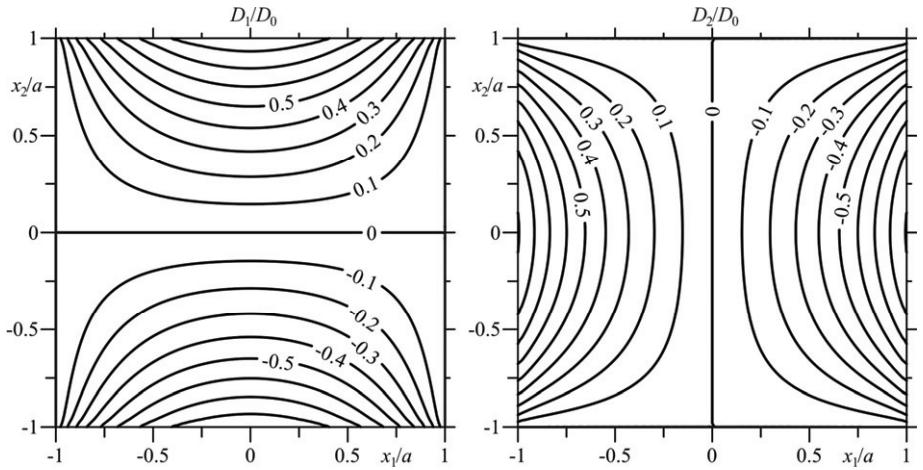

Fig. 2. Components of the electric displacement vector in a square solid under a uniform heat flux

The authors verified the numerical results obtained by the developed BEM using the combined method of power series and least squares, which is proposed in Refs. [6, 7]. Stroh complex functions were expanded into power series with unknown complex factors. The latter were determined through minimization of the squared deviation of stress and electric displacement at the boundary from that prescribed by the boundary conditions. The collocation points were distributed uniformly at the boundary. When 10 terms of power series for Stroh complex functions are considered, the difference between the obtained results and the BEM data does not exceed 0.5 %.

1.5.2. Thermally insulated impermeable crack in a square pyroelectric domain

Consider a square solid with sides of a length $2W$ containing a central impermeable thermally insulated crack of a length $2a$ (Fig. 3). The solid is made of a $BaTiO_3$ ceramics. Two sides of the square are parallel to the polarization axis Ox_2, and the crack is perpendicular to it, i.e. the crack lays on the Ox_1 axis. The sides of the square are free of surface tractions and electric displacement. At the sides, parallel to Ox_1 axis, the uniform heat flux h_2 is set, and at the sides, parallel to Ox_2 axis, the uniform heat h_1 is given. Table 1 contains the nonzero values of the normalized stress and electric displacement intensity factors at the right tip of the crack for different ratios a/W of a crack length and a side of the square. The normalization factors are equal to $K_\sigma^0 = h_0\beta_{11}a\sqrt{\pi a}/k_{11}$, $K_D^0 = h_0\chi_2 a\sqrt{\pi a}/k_{11}$. The boundary element mesh consists of 80 elements at the sides of the square and 20 elements distributed uniformly along the crack surface.

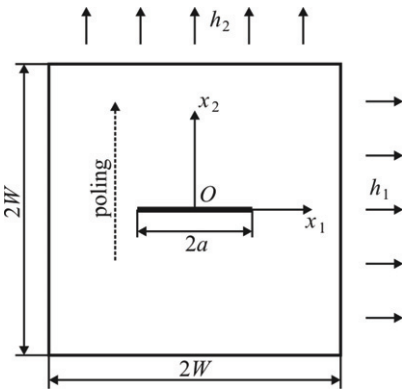

Fig. 3. Square pyroelectric solid with a central crack

Table 1. SEDIF of the impermeable thermally insulated crack in a square domain

a/W	0.1	0.2	0.3	0.4	0.5	0.6	0.7	0.8	0.9
$h_1 = 0,\ h_2 = h_0$									
$-K_{II}/K_\sigma^0$	0.1792	0.1798	0.1816	0.1860	0.1947	0.2108	0.2396	0.2942	0.4264
$h_1 = h_0,\ h_2 = 0$									
$-K_D/K_D^0$	0.3256	0.3288	0.3343	0.3424	0.3535	0.3684	0.3888	0.4195	0.4815
$10^3\, K_I/K_\sigma^0$	0.158	0.153	0.145	0.134	0.120	0.102	0.083	0.065	0.053

When the heat flux h_0 flows along the polarization axis Ox_2 ($h_1 = 0,\ h_2 = h_0$) the system of equations (62) is consistent, and stress and electric displacement vanish in the unnotched solid. As well as for the infinite orthotropic thermoelastic medium

[16], for a finite pyroelectric solid with a central crack the only nonzero SIF is K_{II}. When the crack is small comparing with the side of the square ($a/W = 0.1$), SIF K_{II} differs only by 0.24 % from the analytical solution for a thermally insulated impermeable crack in the infinite medium, which can be easily obtained from the thermoelastic solution [16]:

$$\tilde{\mathbf{k}}^{(1)} = \frac{\sqrt{\pi} h_0}{2k_t} a^{3/2} \operatorname{Re}\left\{\tilde{\boldsymbol{\gamma}}_2^*\right\}, \quad \tilde{\boldsymbol{\gamma}}_2^* = \left(\mathbf{S}^{\mathrm{T}} - i\mathbf{I}\right)\mathbf{d} - \mathbf{L}\mathbf{c}\,. \tag{85}$$

As well as for a finite thermoelastic solid [27], the SIF K_{II} given in Table 1 for a crack in a pyroelectric square domain increases with a growth of the crack length.

When the heat flows along the crack faces ($h_1 = h_0$, $h_2 = 0$), temperature field is the same as in the uncracked square domain. However, in this case the heat flows perpendicularly to the polarization direction, which produces non-uniform distribution of electric displacement inside the solid due to the tertiary pyroelectric effect. Consequently, the electric displacement field is perturbed by the presence of the impermeable crack. This causes the essentially nonzero values of EDIF K_D. In turn, the piezoelectric effect causes perturbation of the stress field, and hence, the nonzero SIF K_I (SIF K_I is equal to zero, when the electroelastic coupling is neglected, i.e. the piezoelectric constants e_{ijk} are assumed zero). Thus, unlike the anisotropic thermoelasticity, for which the steady uniform heat flowing along the crack does not produce thermal stress [16], for thermoelectroelasticity this effect is not observed.

When the crack is permeable and the heat flows along it, the pyroelectric effect causes the perturbation of the stress field, and consequently the nonzero SIF K_I, which is close to that presented in Table 1. However, the EDIF K_D is a thousand times smaller than that of the impermeable crack. This is due to the fact that the permeable crack does not perturb the electric displacement field. Nevertheless, small but nonzero values of the EDIF K_D are caused by the piezoelectric effect. It is obvious, that for a semi-permeable crack the EDIF K_D acquires some intermediate value between those of permeable and impermeable cracks.

1.5.3. Thin electricity and heat conductive inclusion in a pyroelectric medium

Consider an infinite pyroelectric $BaTiO_3$ medium that contains thin isotropic electricity-conductive inclusion with high heat conductivity. One can obtain these properties of the thin inhomogeneity, when it is assumed that in the model (78) $k^{\mathrm{i}} \to \infty$ and $\kappa^{\mathrm{i}} \to \infty$ (for the numerical computations it is assumed that $k^{\mathrm{i}} = 10^{10} k$ and $\kappa^{\mathrm{i}} = 10^{10} \varepsilon_0$). The inclusion of a length $2a$ and a thickness $2h$ ($h = 0.01a$) is placed at the Ox_1 axis, and the medium is polarized along the Ox_2 direction. A relative rigidity of the inclusion is equal to $\mu = G^{\mathrm{i}}/c_{44}$, where G^{i} is a shear modulus of inclusion's material. The Poisson ratio of the inclusion equals 0.3. At the infinity the heat h_0 flows steady and uniformly in the positive of Ox_2 axis. Therefore, equations (62) are

consistent, and stress and electric displacement vanish at the infinity. Under the considered thermal load the temperature of the medium is zero along the Ox_1 axis, therefore the thermal expansion of the inclusion does not influence the solution. The sketch of the problem and the plot of normalized SEDIF at the right tip of the inclusion versus its relative rigidity μ are depicted in Fig. 4. The normalization factors are the same as in the previous example. The boundary element mesh consists of only 20 elements distributed uniformly along the inclusion's median line.

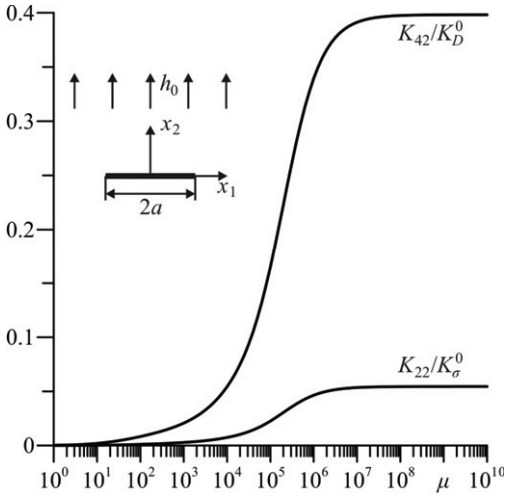

Fig. 4. Generalized SEDIF of a thin electricity and heat conductive elastic inclusion

One can see in Fig. 4 that the increase of inclusion's relative rigidity μ causes a growth of the generalized SEDIF K_{22} and K_{42}. The rest of SEDIF are zero. According to Eq. (81), the nonzero value of the generalized SIF K_{22} produces essential shear stress near inclusion's tips. This can cause delamination of inclusion's tips or a shear crack initiation. In addition, it is necessary to consider the EDIF K_{42}, which significantly influences the energy density at the inclusion tip, and hence, fracture initiation.

1.5.4. Thin dielectric thermally insulated inclusion

Consider an infinite pyroelectric $BaTiO_3$ medium containing a thin isotropic inclusion of a length $2a$ and a thickness $2h$ ($h = 0.01a$), which is made of a material that does not polarize ($\kappa^i = \varepsilon_0$) and does not conduct heat ($k^i \to 0$). The inclusion is collinear with the Ox_1 axis. At the infinity the heat h_0 flows steady and uniformly along the positive Ox_2 direction. The medium is polarized along the Ox_2 axis. Under the considered thermal load the temperature of inclusion faces is anti-symmetric with respect to the Ox_1 axis, thus, according to Eq. (78) the thermal expansion of the

inclusion does not influence the solution, since Eq. (78) considers only average temperatures of inclusion's cross-sections. The plots of the generalized SIF at the right tip of the inclusion versus its relative rigidity μ are depicted in Fig. 5. The boundary element mesh consists of 20 elements.

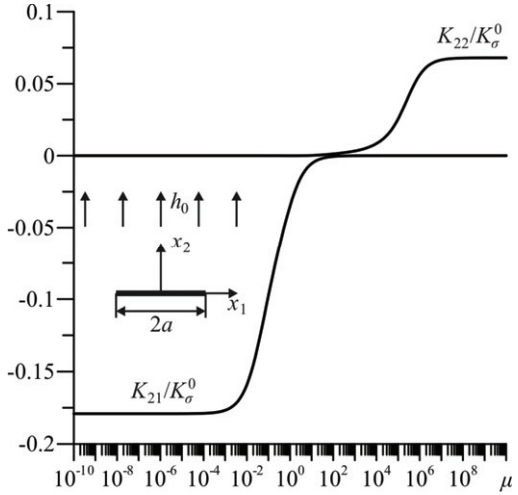

Fig. 5. Generalized SIF of a thin dielectric thermally insulated elastic inclusion

Fig. 5 shows that for very soft inclusions ($\mu = 10^{-10}$) the SIF $K_{21} = K_{\text{II}}$ differs only by 0.2 % from K_{II} of an impermeable crack in the infinite pyroelectric medium defined by Eq. (85). With the increase of the relative rigidity, the SIF K_{21} tends to zero. The generalized SIF K_{22} increases, when the relative rigidity of inclusion $\mu > 10$. For very rigid inclusions, the generalized SIF K_{22} is approximately 25 % greater than that of an electricity and heat conductive rigid line inclusion. The EDIF K_{42} is much smaller than that of the electricity-conductive inclusion; therefore, in the general scale of the plot it cannot be distinguished from zero. Thus, the main influence on energy density at inclusion's tips is caused by the generalized stress intensity factors K_{21} and K_{22}.

1.5.5. Cracked pyroelectric solid with mixed thermal boundary conditions

Consider a square solid with sides of a length $2W$ containing a central inclined impermeable crack of a length $2a$ (Fig. 6). The solid is made of a $BaTiO_3$ ceramics. Boundaries of the solid and the crack are free of tractions and surface charges. However, the mixed thermal boundary conditions are given. Two sides $|x_1| \le W$, $x_2 = \pm W$ are thermally insulated, and other sides $|x_2| \le W$, $x_1 = \pm W$ are maintained at a constant temperature θ_0. The crack is maintained at the reference temperature

$(\theta(x_1,0)=0\ \forall x_1\in(-a,a))$. Thus, there is no temperature discontinuity, and the boundary element method developed in Refs. [11, 12] is unsuitable for the solution of this problem. However, the proposed approach can be used here, since it considers both temperature and heat flux discontinuities. Table 2 presents the results of the numerical analysis of the problem by means of the proposed boundary element approach. The boundary element mesh consists of 80 elements at the sides of the square and 20 elements distributed uniformly along the crack surface.

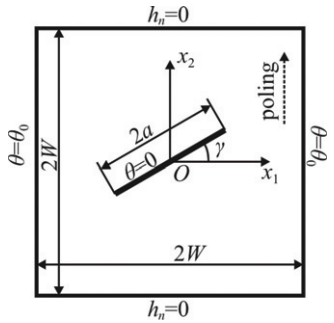

Fig. 6. Cracked square solid with mixed thermal boundary conditions

Table 2 contains SEDIF at the right tip of the crack for different values of the ratio a/W and the crack inclination angle γ. The normalization factors are equal to $K_\sigma^1=\theta_0\beta_{11}\sqrt{\pi a}$, $K_D^1=\theta_0\chi_2\sqrt{\pi a}$. As well as for an isotropic solid [27], the applied thermal load causes only mode I SIF for symmetric cases of $\gamma=0$ and $\gamma=90^\circ$. However, in the case of thermoelectroelastic solid for $\gamma=0$ the electric displacement intensity factor K_D is also nonzero, mainly due to the tertiary pyroelectric effect. Table 2 shows that normalized SIF $K_{\mathrm{I}}/K_\sigma^1$ decreases with the increase of the crack's length. In contrast, the normalized EDIF K_D/K_D^1 increases with the increase of the ratio a/W. For $\gamma=30^\circ$ the normalized SIF $K_{\mathrm{II}}/K_\sigma^1$ increases with the increase of a/W, and for $\gamma=60^\circ$ this behavior is not monotonous.

Conclusions

Both reciprocity approach and the complex variable approach allow development of the Somigliana type boundary integral equations of thermoelectroelasticity, which do not contain domain integral terms in the absence of body forces and distributed heat. The Stroh formalism combined with the complex variable approach gives strict mathematical proof of the correctness of the obtained integral equations and their kernels.

Consequently, obtained truly boundary integral equations allow development of the efficient boundary element method for the analysis of pyroelectric solids with cracks and thin inclusions.

To model permeable, impermeable and semi-permeable cracks and other types of thin inhomogeneities one can use the developed linear model of a thin inclusion, which allows varying its heat conductivity, electric permittivity and rigidity in the entire spectrum of these values.

Unlike the anisotropic thermoelasticity, the uniform steady-state heat flux can cause the nonzero stress and electric displacement in the unnotched pyroelectric medium due to the tertiary pyroelectric effect. In the case of a transversely isotropic pyroelectric solid the stress and electric displacement vanish, if the heat flows along the polarization direction.

The heat, which flows perpendicularly to the polarization direction, causes essential field intensity at the tips of impermeable cracks, even when it flows along their faces.

Electric permittivity and heat conductivity of a thin inclusion or a crack medium essentially influences the field intensity at the tips of thin inhomogeneities. Therefore, these properties should be accounted for in calculation of the pyroelectric materials with cracks and thin inclusions.

Table 2. SEDIF of and inclined crack, whose faces are maintained at a constant temperature

a/W	$K_{\mathrm{I}}/K_{\sigma}^{1}$	$K_{\mathrm{II}}/K_{\sigma}^{1}$	K_{D}/K_{D}^{1}	$K_{\mathrm{I}}/K_{\sigma}^{1}$	$K_{\mathrm{II}}/K_{\sigma}^{1}$	K_{D}/K_{D}^{1}
	$\gamma=0$			$\gamma=30^{\circ}$		
0.1	0.1799	0.0000	-0.0613	0.1865	-0.0180	-0.0604
0.2	0.1646	0.0000	-0.0122	0.1666	-0.0121	-0.0212
0.3	0.1550	0.0000	0.0306	0.1530	-0.0071	0.0120
0.4	0.1475	0.0000	0.0688	0.1423	-0.0024	0.0415
0.5	0.1397	0.0000	0.1006	0.1332	0.0021	0.0675
0.6	0.1295	0.0000	0.1232	0.1246	0.0064	0.0897
0.7	0.1149	0.0000	0.1334	0.1157	0.0101	0.1073
0.8	0.0942	0.0000	0.1271	0.1054	0.0128	0.1186
	$\gamma=60^{\circ}$			$\gamma=90^{\circ}$		
0.1	0.2014	-0.0191	-0.0436	0.2096	0.0000	0.0000
0.2	0.1759	-0.0156	-0.0253	0.1831	0.0000	0.0000
0.3	0.1596	-0.0144	-0.0118	0.1683	0.0000	0.0000
0.4	0.1484	-0.0149	-0.0021	0.1602	0.0000	0.0000
0.5	0.1405	-0.0166	0.0045	0.1558	0.0000	0.0000
0.6	0.1349	-0.0192	0.0081	0.1525	0.0000	0.0000
0.7	0.1308	-0.0224	0.0094	0.1476	0.0000	0.0000
0.8	0.1273	-0.0255	0.0089	0.1377	0.0000	0.0000

Appendix 1.A. Green's function for a point heat source

Consider an infinite thermoelectroelastic medium, in which all fields are assumed to depend on in-plane coordinates x_1 and x_2 only. According to [11], for an infinite space subjected to a line heat source h^* located at the point $\mathbf{x}^*$, the function $g'(z_t)$ (see Eq. (4)) is equal to

$$g'(z_t) = -\frac{h^*}{4\pi k_t}\ln\left(z_t - Z_t(\mathbf{x}^*)\right). \tag{A.1}$$

The function $g(z_t)$ is obtained by integrating Eq. (A.1), which yields

$$g(z_t) = -\frac{h^*}{4\pi k_t} f^*\left(z_t - Z_t(\mathbf{x}^*)\right), \tag{A.2}$$

where $f^*(z) = z(\ln z - 1)$.

Stroh complex functions $\mathbf{f}(z_*)$ are assumed to have the same structure as (A.2):

$$\mathbf{f}(z_*) = \left\langle f^*\left(z_* - Z_*(\mathbf{x}^*)\right)\right\rangle \mathbf{q}, \tag{A.3}$$

where $\mathbf{q}$ is a complex vector to be determined; $\langle F(z_*)\rangle = \mathrm{diag}\left[F_1(z_1),...,F_4(z_4)\right]$; $Z_\alpha(\mathbf{x}) = x_1 + p_\alpha x_2$ ($\alpha = 1,..,4$).

According to Eqs. (4), (A.2) and (A.3), extended displacement and stress function at the arbitrary point $\boldsymbol{\xi}$ (or alternatively, $z = \xi_1 + i\xi_2$) of the medium equal

$$\begin{aligned}
\tilde{\mathbf{u}}^*(\boldsymbol{\xi},\mathbf{x}^*) &= \tilde{\mathbf{u}}^*(z,\mathbf{x}^*) = 2\,\mathrm{Re}\left\{\mathbf{A}\mathbf{f}(z_*) + \mathbf{c}g(z_t)\right\} = 2\,\mathrm{Re}\left\{\mathbf{A}\left\langle f^*\left(Z_*(\boldsymbol{\xi}-\mathbf{x}^*)\right)\right\rangle \mathbf{q} + \mathbf{c}g\left(Z_t(\boldsymbol{\xi})\right)\right\},\\
\tilde{\boldsymbol{\varphi}}^*(\boldsymbol{\xi},\mathbf{x}^*) &= \tilde{\boldsymbol{\varphi}}^*(z,\mathbf{x}^*) = 2\,\mathrm{Re}\left\{\mathbf{B}\mathbf{f}(z_*) + \mathbf{d}g(z_t)\right\} = 2\,\mathrm{Re}\left\{\mathbf{B}\left\langle f^*\left(Z_*(\boldsymbol{\xi}-\mathbf{x}^*)\right)\right\rangle \mathbf{q} + \mathbf{d}g\left(Z_t(\boldsymbol{\xi})\right)\right\}.
\end{aligned} \tag{A.4}$$

Due to the physical considerations extended displacement and stress function are to be continuous in the entire medium, therefore,

$$\tilde{\mathbf{u}}^*\left(z\,\mathrm{e}^{2\pi i},\mathbf{x}^*\right) - \tilde{\mathbf{u}}^*(z,\mathbf{x}^*) = 0, \quad \tilde{\boldsymbol{\varphi}}^*\left(z\,\mathrm{e}^{2\pi i},\mathbf{x}^*\right) - \tilde{\boldsymbol{\varphi}}^*(z,\mathbf{x}^*) = 0. \tag{A.5}$$

Satisfying conditions (A.5) one can obtain that the vector $\mathbf{q}$ in Eq. (A.4) should be equal to

$$\mathbf{q} = \frac{ih^*}{2\pi k_t}\left(\mathbf{B}^{\mathrm{T}}\,\mathrm{Im}[\mathbf{c}] + \mathbf{A}^{\mathrm{T}}\,\mathrm{Im}[\mathbf{d}]\right). \tag{A.6}$$

Therefore, Green's function for an infinite medium subjected to a line heat source h^* equals to

$$\begin{aligned}
\tilde{\mathbf{u}}^*(\boldsymbol{\xi},\mathbf{x}^*) &= 2\,\mathrm{Re}\left\{\mathbf{A}\left\langle f^*\left(Z_*(\boldsymbol{\xi}-\mathbf{x}^*)\right)\right\rangle \mathbf{q} + \mathbf{c}g\left(Z_t(\boldsymbol{\xi})\right)\right\}\\
&= -\frac{h^*}{\pi k_t}\,\mathrm{Im}\left\{\mathbf{A}\left\langle f^*\left(Z_*(\boldsymbol{\xi}-\mathbf{x}^*)\right)\right\rangle\left(\mathbf{A}^{\mathrm{T}}\,\mathrm{Im}[\mathbf{d}] + \mathbf{B}^{\mathrm{T}}\,\mathrm{Im}[\mathbf{c}]\right)\right\}\\
&\quad -\frac{h^*}{2\pi k_t}\,\mathrm{Re}\left\{\mathbf{c}f^*\left(Z_t(\boldsymbol{\xi}-\mathbf{x}^*)\right)\right\}.
\end{aligned} \tag{A.7}$$

Based on the identity (9) one can prove that

$$\tilde{\mathbf{u}}^*(\boldsymbol{\xi},\mathbf{x}^*) = -\tilde{\mathbf{u}}^*(\mathbf{x}^*,\boldsymbol{\xi}). \tag{A.8}$$

Therefore,

$$V_i(\mathbf{x},\boldsymbol{\xi}) = -\frac{1}{h^*}\tilde{u}_i^*(\boldsymbol{\xi},\mathbf{x}) = \frac{1}{h^*}u_i^*(\mathbf{x},\boldsymbol{\xi}). \tag{A.9}$$

Appendix 1.B. Proof of Eq. (27) for $V_i(\mathbf{x},\boldsymbol{\xi})$ given by Eq. (35)

Differentiation of Eq. (35) yields

$$\begin{aligned} k_{pq}\frac{\partial^2 V_i(\mathbf{x},\boldsymbol{\xi})}{\partial x_p \partial x_q} = &-\frac{1}{\pi k_t}\operatorname{Im}\left[A_{i\alpha}\frac{\left(k_{22}p_\alpha^2 + 2k_{12}p_\alpha + k_{11}\right)}{Z_\alpha(\mathbf{x}-\boldsymbol{\xi})}\left(A_{j\alpha}\operatorname{Im}\{d_j\} + B_{j\alpha}\operatorname{Im}\{c_j\}\right)\right] - \\ &-\frac{1}{2\pi k_t}\operatorname{Re}\left[c_i\left(k_{22}p_t^2 + 2k_{12}p_t + k_{11}\right)\Big/ Z_t(\mathbf{x}-\boldsymbol{\xi})\right]. \end{aligned} \tag{B.1}$$

According Eq. (5), the last term in the right hand side of Eq. (B.1) vanishes. Applying to Eq. (B.1) the identity (9) and noting that $k_{22}p_t + 2k_{12} = -k_{12} + ik_t + 2k_{12} = k_{12} + ik_t$ one obtains

$$\begin{aligned} k_{pq}\frac{\partial^2 V_i(\mathbf{x},\boldsymbol{\xi})}{\partial x_p \partial x_q} &= -\frac{1}{\pi k_t}\operatorname{Im}\left[A_{i\alpha}\frac{\left(k_{22}p_\alpha^2 + 2k_{12}p_\alpha + k_{11}\right)}{Z_\alpha(\mathbf{x}-\boldsymbol{\xi})}\left(A_{j\alpha}\operatorname{Im}\{d_j\} + B_{j\alpha}\operatorname{Im}\{c_j\}\right)\right] \\ &= -\frac{1}{\pi k_t}\operatorname{Im}\left[\frac{A_{i\alpha}p_\alpha}{Z_\alpha(\mathbf{x}-\boldsymbol{\xi})}\left(A_{j\alpha}\operatorname{Im}\{(k_{12}+ik_t)d_j\} + B_{j\alpha}\operatorname{Im}\{(k_{12}+ik_t)c_j\}\right)\right] \\ &\quad -\frac{k_{11}}{\pi k_t}\operatorname{Im}\left[\frac{A_{i\alpha}}{Z_\alpha(\mathbf{x}-\boldsymbol{\xi})}\left(A_{j\alpha}\operatorname{Im}\{d_j\} + B_{j\alpha}\operatorname{Im}\{c_j\}\right)\right] \\ &= -\frac{1}{\pi}\operatorname{Im}\left[\frac{A_{i\alpha}p_\alpha}{Z_\alpha(\mathbf{x}-\boldsymbol{\xi})}\left(A_{j\alpha}\operatorname{Re}\{d_j\} + B_{j\alpha}\operatorname{Re}\{c_j\}\right)\right] \\ &\quad -\frac{1}{\pi k_t}\operatorname{Im}\left[\frac{A_{i\alpha}}{Z_\alpha(\mathbf{x}-\boldsymbol{\xi})}\left(A_{j\alpha}\operatorname{Im}\{(k_{11}+p_tk_{12})d_j\} + B_{j\alpha}\operatorname{Im}\{(k_{11}+p_tk_{12})c_j\}\right)\right]. \end{aligned} \tag{B.2}$$

Since based on Eq. (5) $k_{12}p_t + k_{11} = -ik_tp_t$, Eq. (B.2) can be rewritten as

$$\begin{aligned} k_{pq}\frac{\partial^2 V_i(\mathbf{x},\boldsymbol{\xi})}{\partial x_p \partial x_q} = &-\frac{1}{\pi}\operatorname{Im}\left[\frac{A_{i\alpha}p_\alpha}{Z_\alpha(\mathbf{x}-\boldsymbol{\xi})}\left(A_{j\alpha}\operatorname{Re}\{d_j\} + B_{j\alpha}\operatorname{Re}\{c_j\}\right)\right] \\ &+\frac{1}{\pi}\operatorname{Im}\left[\frac{A_{i\alpha}}{Z_\alpha(\mathbf{x}-\boldsymbol{\xi})}\left(A_{j\alpha}\operatorname{Re}\{p_td_j\} + B_{j\alpha}\operatorname{Re}\{p_tc_j\}\right)\right]. \end{aligned} \tag{B.3}$$

According to Eqs. (6)–(8), one can obtain that

$$\mathbf{P}\mathbf{B}^{\mathrm{T}}\operatorname{Re}\{\mathbf{c}\} + \mathbf{P}\mathbf{A}^{\mathrm{T}}\operatorname{Re}\{\mathbf{d}\} = \mathbf{B}^{\mathrm{T}}\operatorname{Re}\{p_t\mathbf{c}\} + \mathbf{A}^{\mathrm{T}}\operatorname{Re}\{p_t\mathbf{d}\} - \left(\mathbf{A}^{\mathrm{T}}\boldsymbol{\beta}_1 + \mathbf{A}^{\mathrm{T}}\mathbf{N}_1^{\mathrm{T}}\boldsymbol{\beta}_2 + \mathbf{B}^{\mathrm{T}}\mathbf{N}_2\boldsymbol{\beta}_2\right). \tag{B.4}$$

Since [11]

$$\mathbf{B}^{\mathrm{T}} = \mathbf{A}^{\mathrm{T}}\mathbf{R} + \mathbf{P}\mathbf{A}^{\mathrm{T}}\mathbf{T}, \quad \mathbf{N}_2 = \mathbf{T}^{-1}, \quad \mathbf{N}_1^{\mathrm{T}} = -\mathbf{R}\mathbf{T}^{-1}, \tag{B.5}$$

thus,

$$\mathbf{A}^{\mathrm{T}}\boldsymbol{\beta}_1 + \mathbf{A}^{\mathrm{T}}\mathbf{N}_1^{\mathrm{T}}\boldsymbol{\beta}_2 + \mathbf{B}^{\mathrm{T}}\mathbf{N}_2\boldsymbol{\beta}_2 = \mathbf{A}^{\mathrm{T}}\boldsymbol{\beta}_1 - \mathbf{A}^{\mathrm{T}}\mathbf{R}\mathbf{T}^{-1}\boldsymbol{\beta}_2 + \mathbf{A}^{\mathrm{T}}\mathbf{R}\mathbf{T}^{-1}\boldsymbol{\beta}_2 + \mathbf{P}\mathbf{A}^{\mathrm{T}}\boldsymbol{\beta}_2 = \mathbf{A}^{\mathrm{T}}\boldsymbol{\beta}_1 + \mathbf{P}\mathbf{A}^{\mathrm{T}}\boldsymbol{\beta}_2, \tag{B.6}$$

and Eq. (B.4) can be rewritten as

$$\mathbf{B}^{\mathrm{T}}\operatorname{Re}\{p_t\mathbf{c}\} + \mathbf{A}^{\mathrm{T}}\operatorname{Re}\{p_t\mathbf{d}\} - \mathbf{P}\left(\mathbf{B}^{\mathrm{T}}\operatorname{Re}\{\mathbf{c}\} + \mathbf{A}^{\mathrm{T}}\operatorname{Re}\{\mathbf{d}\}\right) = \mathbf{A}^{\mathrm{T}}\boldsymbol{\beta}_1 + \mathbf{P}\mathbf{A}^{\mathrm{T}}\boldsymbol{\beta}_2, \tag{B.7}$$

or in the index notations

$$A_{j\alpha}\,\mathrm{Re}\{p_i d_j\}+B_{j\alpha}\,\mathrm{Re}\{p_i c_j\}-p_\alpha\left(A_{j\alpha}\,\mathrm{Re}\{d_j\}+B_{j\alpha}\,\mathrm{Re}\{c_j\}\right)=A_{j\alpha}\tilde{\beta}_{j1}+p_\alpha A_{j\alpha}\tilde{\beta}_{j2}. \quad \text{(B.8)}$$

Based on Eq. (B.8), Eq. (B.3) writes as

$$k_{pq}\frac{\partial^2 V_i(\mathbf{x},\boldsymbol{\xi})}{\partial x_p \partial x_q}=\frac{1}{\pi}\mathrm{Im}\left[\frac{A_{i\alpha}A_{j\alpha}\left(\tilde{\beta}_{j1}+p_\alpha\tilde{\beta}_{j2}\right)}{Z_\alpha(\mathbf{x}-\boldsymbol{\xi})}\right]. \quad \text{(B.9)}$$

According to Eq. (19),

$$\tilde{\beta}_{jk}\frac{\partial}{\partial x_k}U_{ij}(\mathbf{x},\boldsymbol{\xi})=\frac{\tilde{\beta}_{jk}}{\pi}\mathrm{Im}\left[A_{i\alpha}A_{j\alpha}\frac{\partial}{\partial x_k}\ln Z_\alpha(\mathbf{x}-\boldsymbol{\xi})\right]=\frac{1}{\pi}\mathrm{Im}\left[\frac{A_{i\alpha}A_{j\alpha}\left(\tilde{\beta}_{j1}+p_\alpha\tilde{\beta}_{j2}\right)}{Z_\alpha(\mathbf{x}-\boldsymbol{\xi})}\right]. \quad \text{(B.10)}$$

Hence, right hand sides of Eqs. (B.9) and (B.10) are identical, and this proves that the kernel $V_i(\mathbf{x},\boldsymbol{\xi})$ given by Eq. (35) satisfies Eq. (27).

Appendix 1.C. Derivation of the integral identities using the complex variable approach

According to Eq. (50), Stroh complex functions in the domain S are related to the extended displacement and stress function at the boundary ∂S through the following equation

$$\begin{aligned}\mathbf{f}\left(Z_*(\boldsymbol{\xi})\right)=&\frac{1}{2\pi i}\int_{\partial S}\left\langle\frac{dZ_*(\mathbf{x})}{Z_*(\mathbf{x}-\boldsymbol{\xi})}\right\rangle\left(\mathbf{A}^{\mathrm{T}}\tilde{\boldsymbol{\varphi}}(\mathbf{x})+\mathbf{B}^{\mathrm{T}}\tilde{\mathbf{u}}(\mathbf{x})\right)\\&-\frac{1}{2\pi i}\int_{\partial S}\left\langle\frac{dZ_*(\mathbf{x})}{Z_*(\mathbf{x}-\boldsymbol{\xi})}\right\rangle\left(\mathbf{A}^{\mathrm{T}}\tilde{\boldsymbol{\varphi}}^t(\mathbf{x})+\mathbf{B}^{\mathrm{T}}\tilde{\mathbf{u}}^t(\mathbf{x})\right).\end{aligned} \quad \text{(C.1)}$$

To transform Eq. (C.1), first note that according to Eq. (4),

$$\frac{\partial\tilde{\boldsymbol{\varphi}}}{\partial s}=\frac{\partial\tilde{\boldsymbol{\varphi}}}{\partial x_1}\frac{\partial x_1}{\partial s}+\frac{\partial\tilde{\boldsymbol{\varphi}}}{\partial x_2}\frac{\partial x_2}{\partial s}=-\tilde{\boldsymbol{\sigma}}_2 n_2-\tilde{\boldsymbol{\sigma}}_1 n_1=-\tilde{\boldsymbol{\sigma}}_j n_j=-\tilde{\mathbf{t}}, \quad \text{(C.2)}$$

therefore,

$$\begin{aligned}\int_{\partial S}\left\langle\frac{dZ_*(\mathbf{x})}{Z_*(\mathbf{x}-\boldsymbol{\xi})}\right\rangle\mathbf{A}^{\mathrm{T}}\tilde{\boldsymbol{\varphi}}(\mathbf{x})=&\left\langle\ln Z_*(\mathbf{x}-\boldsymbol{\xi})\right\rangle\tilde{\boldsymbol{\varphi}}(\mathbf{x})\Big|_a^b+\int_{\partial S}\left\langle\ln Z_*(\mathbf{x}-\boldsymbol{\xi})\right\rangle\mathbf{A}^{\mathrm{T}}\tilde{\mathbf{t}}(\mathbf{x})d\Gamma(\mathbf{x})\\=&\int_{\partial S}\left\langle\ln Z_*(\mathbf{x}-\boldsymbol{\xi})\right\rangle\mathbf{A}^{\mathrm{T}}\tilde{\mathbf{t}}(\mathbf{x})d\Gamma(\mathbf{x}),\end{aligned} \quad \text{(C.3)}$$

since due to the stress continuity condition and balance equation (1) $\tilde{\boldsymbol{\varphi}}(a)=\tilde{\boldsymbol{\varphi}}(b)=0$, where a and b are the starting and end points of the integration path ∂S.

According to Eq. (49),

$$\frac{\partial\tilde{\boldsymbol{\varphi}}^t}{\partial s}=-2\,\mathrm{Re}\left\{\mathbf{d}\left(n_2-n_1 p_t\right)g'(z_t)\right\},\quad \frac{\partial\tilde{\mathbf{u}}^t}{\partial s}=-2\,\mathrm{Re}\left\{\mathbf{c}\left(n_2-n_1 p_t\right)g'(z_t)\right\}, \quad \text{(C.4)}$$

therefore,

$$
\begin{aligned}
&\int_{\partial S}\left\langle\frac{dZ_*(\mathbf{x})}{Z_*(\mathbf{x}-\boldsymbol{\xi})}\right\rangle\left(\mathbf{A}^{\mathrm{T}}\tilde{\boldsymbol{\varphi}}^t(\mathbf{x})+\mathbf{B}^{\mathrm{T}}\tilde{\mathbf{u}}^t(\mathbf{x})\right)=\left\langle\ln Z_*(\mathbf{x}-\boldsymbol{\xi})\right\rangle\left(\mathbf{A}^{\mathrm{T}}\tilde{\boldsymbol{\varphi}}^t(\mathbf{x})+\mathbf{B}^{\mathrm{T}}\tilde{\mathbf{u}}^t(\mathbf{x})\right)\Big|_a^b\\
&\quad-\int_{\partial S}\left\langle\ln Z_*(\mathbf{x}-\boldsymbol{\xi})\right\rangle\left(\mathbf{A}^{\mathrm{T}}\frac{\partial\tilde{\boldsymbol{\varphi}}^t(\mathbf{x})}{\partial s}+\mathbf{B}^{\mathrm{T}}\frac{\partial\tilde{\mathbf{u}}^t(\mathbf{x})}{\partial s}\right)d\Gamma(\mathbf{x})\\
&\quad=-\int_{\partial S}\left\langle\ln Z_*(\mathbf{x}-\boldsymbol{\xi})\right\rangle\left(\mathbf{A}^{\mathrm{T}}\frac{\partial\tilde{\boldsymbol{\varphi}}^t(\mathbf{x})}{\partial s}+\mathbf{B}^{\mathrm{T}}\frac{\partial\tilde{\mathbf{u}}^t(\mathbf{x})}{\partial s}\right)d\Gamma(\mathbf{x})\\
&\quad=2\int_{\partial S}\left\langle\ln Z_*(\mathbf{x}-\boldsymbol{\xi})\right\rangle\left(\mathbf{A}^{\mathrm{T}}\operatorname{Re}\left\{\mathbf{d}(n_2-p_tn_1)g'(Z_t(\mathbf{x}))\right\}\right)d\Gamma(\mathbf{x})\\
&\quad+2\int_{\partial S}\left\langle\ln Z_*(\mathbf{x}-\boldsymbol{\xi})\right\rangle\left(\mathbf{B}^{\mathrm{T}}\operatorname{Re}\left\{\mathbf{c}(n_2-p_tn_1)g'(Z_t(\mathbf{x}))\right\}\right)d\Gamma(\mathbf{x}).
\end{aligned}
\tag{C.5}
$$

Eq. (C.5) accounts for the stress and displacement continuity conditions $\tilde{\boldsymbol{\varphi}}^t(a)=\tilde{\boldsymbol{\varphi}}^t(b)=0$, $\tilde{\mathbf{u}}^t(a)=\tilde{\mathbf{u}}(b)$ and singlevaluedness of Stroh complex functions.

Substitution of Eq. (40) into Eq. (C.5) yields

$$
\begin{aligned}
&\int_{\partial S}\left\langle\frac{dZ_*(\mathbf{x})}{Z_*(\mathbf{x}-\boldsymbol{\xi})}\right\rangle\left(\mathbf{A}^{\mathrm{T}}\tilde{\boldsymbol{\varphi}}^t(\mathbf{x})+\mathbf{B}^{\mathrm{T}}\tilde{\mathbf{u}}^t(\mathbf{x})\right)\\
&\quad=\int_{\partial S}\left\langle\ln Z_*(\mathbf{x}-\boldsymbol{\xi})\right\rangle\left(\mathbf{A}^{\mathrm{T}}\operatorname{Re}\left\{\mathbf{d}(n_2-p_tn_1)\left(\theta(\mathbf{x})+i\frac{\vartheta(\mathbf{x})}{k_t}\right)\right\}\right)d\Gamma(\mathbf{x})\\
&\quad+\int_{\partial S}\left\langle\ln Z_*(\mathbf{x}-\boldsymbol{\xi})\right\rangle\left(\mathbf{B}^{\mathrm{T}}\operatorname{Re}\left\{\mathbf{c}(n_2-p_tn_1)\left(\theta(\mathbf{x})+i\frac{\vartheta(\mathbf{x})}{k_t}\right)\right\}\right)d\Gamma(\mathbf{x})\\
&\quad=\int_{\partial S}\left\langle\ln Z_*(\mathbf{x}-\boldsymbol{\xi})\right\rangle\left(\mathbf{A}^{\mathrm{T}}\operatorname{Re}\left\{\mathbf{d}(n_2-n_1p_t)\right\}+\mathbf{B}^{\mathrm{T}}\operatorname{Re}\left\{\mathbf{c}(n_2-n_1p_t)\right\}\right)\theta(\mathbf{x})\,d\Gamma(\mathbf{x})\\
&\quad-\frac{1}{k_t}\int_{\partial S}\left\langle\ln Z_*(\mathbf{x}-\boldsymbol{\xi})\right\rangle\left(\mathbf{A}^{\mathrm{T}}\operatorname{Im}\left\{\mathbf{d}(n_2-n_1p_t)\right\}+\mathbf{B}^{\mathrm{T}}\operatorname{Im}\left\{\mathbf{c}(n_2-n_1p_t)\right\}\right)\vartheta(\mathbf{x})\,d\Gamma(\mathbf{x}).
\end{aligned}
\tag{C.6}
$$

Using the identity (9) the last term in Eq. (C.6) can be rewritten as

$$
\begin{aligned}
&-\frac{1}{k_t}\int_{\partial S}\left\langle\ln Z_*(\mathbf{x}-\boldsymbol{\xi})\right\rangle\left(\mathbf{A}^{\mathrm{T}}\operatorname{Im}\left\{\mathbf{d}(n_2-n_1p_t)\right\}+\mathbf{B}^{\mathrm{T}}\operatorname{Im}\left\{\mathbf{c}(n_2-n_1p_t)\right\}\right)\vartheta(\mathbf{x})\,d\Gamma(\mathbf{x})\\
&\quad=-\frac{1}{k_t}\int_{\partial S}\left\langle\ln Z_*(\mathbf{x}-\boldsymbol{\xi})\right\rangle\left(\mathbf{A}^{\mathrm{T}}\operatorname{Im}\{\mathbf{d}\}+\mathbf{B}^{\mathrm{T}}\operatorname{Im}\{\mathbf{c}\}\right)\vartheta(\mathbf{x})\,n_2\,d\Gamma(\mathbf{x})\\
&\quad+\frac{1}{k_t}\int_{\partial S}\left\langle\ln Z_*(\mathbf{x}-\boldsymbol{\xi})\right\rangle\left(\mathbf{A}^{\mathrm{T}}\operatorname{Im}\{p_t\mathbf{d}\}+\mathbf{B}^{\mathrm{T}}\operatorname{Im}\{p_t\mathbf{c}\}\right)\vartheta(\mathbf{x})\,n_1\,d\Gamma(\mathbf{x})\\
&\quad=-\frac{1}{k_t}\int_{\partial S}\left\langle\ln Z_*(\mathbf{x}-\boldsymbol{\xi})\right\rangle\left(\mathbf{A}^{\mathrm{T}}\operatorname{Im}\{\mathbf{d}\}+\mathbf{B}^{\mathrm{T}}\operatorname{Im}\{\mathbf{c}\}\right)\vartheta(\mathbf{x})\,n_2\,d\Gamma(\mathbf{x})\\
&\quad+\frac{1}{k_t}\int_{\partial S}\left\langle\ln Z_*(\mathbf{x}-\boldsymbol{\xi})\right\rangle\mathbf{P}\left(\mathbf{A}^{\mathrm{T}}\operatorname{Im}\{\mathbf{d}\}+\mathbf{B}^{\mathrm{T}}\operatorname{Im}\{\mathbf{c}\}\right)\vartheta(\mathbf{x})\,n_1\,d\Gamma(\mathbf{x})\\
&\quad=-\frac{1}{k_t}\int_{\partial S}\left\langle\ln Z_*(\mathbf{x}-\boldsymbol{\xi})\,dZ_*(\mathbf{x})\right\rangle\left(\mathbf{A}^{\mathrm{T}}\operatorname{Im}\{\mathbf{d}\}+\mathbf{B}^{\mathrm{T}}\operatorname{Im}\{\mathbf{c}\}\right)\vartheta(\mathbf{x}).
\end{aligned}
\tag{C.7}
$$

Integrating Eq. (C.7) by parts one obtains

$$
\begin{aligned}
&-\frac{1}{k_t}\int_{\partial S}\left\langle \ln Z_*\left(\mathbf{x}-\boldsymbol{\xi}\right)d Z_*\left(\mathbf{x}\right)\right\rangle\left(\mathbf{A}^{\mathrm{T}}\,\mathrm{Im}\{\mathbf{d}\}+\mathbf{B}^{\mathrm{T}}\,\mathrm{Im}\{\mathbf{c}\}\right)\vartheta\left(\mathbf{x}\right)\\
&\quad=-\left\langle f^*\left(Z_*\left(\mathbf{x}-\boldsymbol{\xi}\right)\right)\right\rangle\left(\mathbf{A}^{\mathrm{T}}\,\mathrm{Im}\{\mathbf{d}\}+\mathbf{B}^{\mathrm{T}}\,\mathrm{Im}\{\mathbf{c}\}\right)\frac{\vartheta\left(\mathbf{x}\right)}{k_t}\Bigg|_a^b\\
&\quad-\frac{1}{k_t}\int_{\partial S}\left\langle f^*\left(Z_*\left(\mathbf{x}-\boldsymbol{\xi}\right)\right)\right\rangle\left(\mathbf{A}^{\mathrm{T}}\,\mathrm{Im}\{\mathbf{d}\}+\mathbf{B}^{\mathrm{T}}\,\mathrm{Im}\{\mathbf{c}\}\right)h_n\left(\mathbf{x}\right)d\Gamma\left(\mathbf{x}\right)\\
&\quad=-\frac{1}{k_t}\int_{\partial S}\left\langle f^*\left(Z_*\left(\mathbf{x}-\boldsymbol{\xi}\right)\right)\right\rangle\left(\mathbf{A}^{\mathrm{T}}\,\mathrm{Im}\{\mathbf{d}\}+\mathbf{B}^{\mathrm{T}}\,\mathrm{Im}\{\mathbf{c}\}\right)h_n\left(\mathbf{x}\right)d\Gamma\left(\mathbf{x}\right).
\end{aligned}
\tag{C.8}
$$

Substituting Eqs. (C.3), (C.6)–(C.8) into Eq. (C.1) the following integral formula relating Stroh complex functions with the boundary values of temperature, heat flux, extended displacements and tractions can be obtained

$$
\begin{aligned}
\mathbf{f}\left(Z_*\left(\boldsymbol{\xi}\right)\right)&=\frac{1}{2\pi i}\int_{\partial S}\left\langle \ln Z_*\left(\mathbf{x}-\boldsymbol{\xi}\right)\right\rangle\mathbf{A}^{\mathrm{T}}\tilde{\mathbf{t}}\left(\mathbf{x}\right)d\Gamma\left(\mathbf{x}\right)\\
&-\frac{1}{2\pi i}\int_{\partial S}\left\langle\frac{n_2-n_1p_*}{Z_*\left(\mathbf{x}-\boldsymbol{\xi}\right)}\right\rangle\mathbf{B}^{\mathrm{T}}\tilde{\mathbf{u}}\left(\mathbf{x}\right)d\Gamma\left(\mathbf{x}\right)\\
&-\frac{1}{2\pi i}\int_{\partial S}\left\langle \ln Z_*\left(\mathbf{x}-\boldsymbol{\xi}\right)\right\rangle\left(\mathbf{A}^{\mathrm{T}}\,\mathrm{Re}\left\{\mathbf{d}\left(n_2-n_1p_t\right)\right\}+\mathbf{B}^{\mathrm{T}}\,\mathrm{Re}\left\{\mathbf{c}\left(n_2-n_1p_t\right)\right\}\right)\theta\left(\mathbf{x}\right)d\Gamma\left(\mathbf{x}\right)\\
&-\frac{1}{2\pi ik_t}\int_{\partial S}\left\langle f^*\left(Z_*\left(\mathbf{x}-\boldsymbol{\xi}\right)\right)\right\rangle\left(\mathbf{A}^{\mathrm{T}}\,\mathrm{Im}\{\mathbf{d}\}+\mathbf{B}^{\mathrm{T}}\,\mathrm{Im}\{\mathbf{c}\}\right)h_n\left(\mathbf{x}\right)d\Gamma\left(\mathbf{x}\right).
\end{aligned}
\tag{C.9}
$$

References

[1] S.B. Lang, Pyroelectricity: from ancient curiosity to modern imaging tools, Physics Today (August 2005) 31–36.

[2] P. Lu, M.J. Tan, K.M. Liew, Piezothermoelastic analysis of a piezoelectric material with an elliptic cavity under uniform heat flow, Archive of Applied Mechanics 68 (1998) 719–733.

[3] Liu Jinxi, Zhang Xiaosong, Liu Xianglin, Zheng Jian, Anisotropic thermopiezoelectric solids with an elliptic inclusion or a hole under uniform heat flow,/ Acta Mechanica Sinica 16, No. 2 (2000) 148–163.

[4] C.-F. Gao, M.-Z. Wang, Collinear permeable cracks in thermopiezoelectric materials, Mechanics of Materials 33 (2001) 1–9.

[5] C.-F. Gao, H. Kessler, H. Balke, Fracture analysis of electromagnetic thermoelastic solids, European Journal of Mechanics A/Solids 22 (2003) 433–442.

[6] S.A. Kaloerov, K.G. Khoroshev, Thermoelectroelastic state of a multiply connected anisotropic plate, International Applied Mechanics 41, No. 11 (2005) 1306–1315.

[7] S.A. Kaloerov, K.G. Khoroshev, Thermoelectroelastic state of an anisotropic plate with holes and cracks, Theoretical and applied mechanics 41 (2005) 124–133. (in Russian)

[8] Q.H. Qin, Green's function for thermopiezoelectric plates with holes of various shapes, Archive of Applied Mechanics 69 (1999) 406–418.

[9] Q.H. Qin, 2D Green's functions of defective magnetoelectroelastic solids under thermal loading, Eng. Anal. Bound. Elem. 29, No. 6 (2005) 577–585.

[10] P.F. Hou, 2D fundamental solution for orthotropic pyroelectric media, Acta Mech. 206 (2009) 225–235.

[11] Q.H. Qin, Green's function and boundary elements of multifield materials, Elsevier, Oxford, 2007.

[12] Q.H. Qin, Fracture analysis of cracked thermopiezoelectric materials by BEM, Electronic Journal of Boundary Elements 1, No. 2 (2003) 283–301.

[13] Q.H. Qin, M. Lu, BEM for crack-inclusion problems of plane thermopiezoelectric solids, Int. J. Numer. Meth. Eng. 48 (2000) 1071–1088.

[14] Q.H. Qin, Y.W. Mai, BEM for crack-hole problems in thermopiezoelectric materials, Engineering Fracture Mechanics 69, No. 5 (2002) 577–588.

[15] Ia. Pasternak, Coupled 2D electric and mechanical fields in piezoelectric solids containing cracks and thin inhomogeneities, Engng. Anal. Bound. Elem. 35, No. 4 (2011) 678–690.

[16] C. Hwu, Anisotropic elastic plates, Springer, London, 2010.

[17] T.C.T. Ting, Anisotropic elasticity: theory and applications, Oxford University Press, New York, 1996.

[18] Ia. Pasternak, Boundary integral equations and the boundary element method for fracture mechanics analysis in 2D anisotropic thermoelasticity, Engng. Anal. Bound. Elem. 36, No. 12 (2012) 1931–1941.

[19] Y.C. Shiah, C.L. Tan, Exact boundary integral transformation of the thermoelastic domain integral in BEM for general 2D anisotropic elasticity, Computational Mechanics 23 (1999) 87–96.

[20] N.I. Muskhelishvili, Singular integral equations, Dover publications, New York, 2008.

[21] A.M. Lin'kov, Boundary integral equations in elasticity theory, Kluwer academic publishers, Dordrecht, 2002.

[22] C.C. Lin, C. Hwu, Uniform heat flow disturbed by an elliptical rigid inclusion embedded in an anisotropic elastic matrix, J. Thermal Stress 16 (1993) 119–133.

[23] J.T. Chen, H.K. Hong, Review of dual boundary element methods with emphasis on hypersingular integrals and divergent series, Appl. Mech. Rev. 52, No. 1 (1999) 17–33.

[24] H.T. Sulym, Bases of mathematical theory of thermo-elastic equilibrium of solids containing thin inclusions, Research and Publishing center of NTSh, Lviv, 2007. (in Ukrainian)

[25] Ia. Pasternak, H. Sulym, Stress state of solids containing thin elastic crooked inclusions, J. Eng. Math. Doi: 10.1007/s10665-011-9486-0.

[26] M.L. Dunn, Micromechanics of coupled electroelastic composites: effective thermal expansion and pyroelectric coefficients, J. Appl. Phys. 73 (1993) 5131–5140.

[27] Y. Murakami (ed.), Stress intensity factor handbook, Pergamon Press, New York, 1987.

CHAPTER 2. Boundary element analysis of 2D defective thermomagnetoelectroelastic bimaterials

2.1. Introduction

Ferroelectric materials are widely used in modern technologies, especially precise devices, due to the highest values of electro-mechanical coupling among other piezoelectric materials. In turn, all ferroelectric materials are pyroelectric ones [1], thus, polarize when heated or cooled. This behavior should be definitely accounted for in the design of smart devices containing ferroelectric parts, which are not maintained at a constant temperature. The presence of different defects (e.g. cracks or inclusions) can additionally cause high stress and electric displacement intensity under the applied thermal load, especially, when the pyroelectric material is not homogeneous, or consists of homogeneous parts bonded together.

The study of anisotropic and piezoelectric bimaterial solids is widely covered in the scientific literature. Pan and Amadei [2] developed a single domain boundary element approach for fracture analysis of anisotropic bimaterials. Yang et al. [3] and Tian and Gabbert [4] studied cracks near the interface of piezoelectric and magnetoelectroelastic bimaterials. Pan and Yuan [5] developed a 3D Green's function in piezoelectric bimaterial. Ou and Chen [6] studied near-tip stress fields near interfacial cracks.

However, the problems for thermoelectroelastic bimaterials are more challenging, since thermal expansion and pyroelectric phenomenon should be additionally accounted for. There are fewer publications concerning these problems. Hwu [7] obtained the solution for an interfacial crack in an anisotropic thermoelastic bimaterial. Wang and Pan [8] derived the 2D Green's function for a thermoelastic anisotropic bimaterial with imperfect interface. Qin [9, 10], Qin and Mai [11, 12] derived 2D Green's functions and developed a boundary element technique for defective thermomagnetoelectroelastic solids. However, Pasternak et al. [13] has shown that thermoelectroelastic Green's function for a line heat derived by Qin [9, 10] for an infinite medium lacks terms, which should account for stress and displacement continuity conditions. As it is shown below, the same concerns the Green's functions [9, 10] for a thermoelectroelastic bimaterial, which are also incomplete.

Therefore, this chapter utilizes authors' novel complex variable approach [13–16] for obtaining of the Somigliana type boundary integral equations and fundamental solutions for an anisotropic thermoelectroelastic bimaterial in a strict and straightforward manner.

2.2. Governing equations of thermoelectroelasticity. Extended Stroh formalism

In a fixed rectangular system of coordinates $Ox_1x_2x_3$ under the assumption that all fields depend only on in-plane coordinates x_1 and x_2 the balance equations for

stress, electric displacement and heat flux, and constitutive laws can be written in the following compact form [10, 17–19]:

$$\tilde{\sigma}_{ij,j} + \tilde{f}_i = 0\,, \quad h_{i,i} - f_h = 0 \quad (i = 1,..,4;\, j = 1,2)\,; \tag{1}$$

$$\tilde{\sigma}_{ij} = \tilde{C}_{ijkm}\tilde{u}_{k,m} - \tilde{\beta}_{ij}\theta\,, \quad h_i = -k_{ij}\theta_{,j} \quad (i,k = 1,..,4;\, j,m = 1,2) \tag{2}$$

with

$$\begin{aligned} &\tilde{u}_i = u_i,\ \tilde{u}_4 = \phi;\ \tilde{f}_i = f_i,\ \tilde{f}_4 = -q;\ \tilde{\sigma}_{ij} = \sigma_{ij},\ \tilde{\sigma}_{4j} = D_j;\ \tilde{\beta}_{ij} = \beta_{ij},\ \tilde{\beta}_{4j} = -\chi_j;\\ &\tilde{C}_{ijkm} = C_{ijkm},\ \tilde{C}_{ij4m} = e_{mij},\ \tilde{C}_{4jkm} = e_{jkm},\ \tilde{C}_{4j4m} = -\kappa_{jm} \quad (i,k = 1,2,3;\, j,m = 1,2), \end{aligned} \tag{3}$$

where σ_{ij} is a stress tensor; h_i is a heat flux; D_i is an electric displacement; f_i is a body force vector; q is a free charge volume density; f_h is a distributed heat source density; u_i is a displacement; ϕ is an electric potential; θ is a temperature change with respect to the reference temperature; C_{ijkm} are elastic moduli; k_{ij} are heat conduction coefficients; $\beta_{ij} = C_{ijkm}\alpha_{km} + e_{mij}\lambda_m\ (i,j,k,m = 1,..,3)$ are thermal moduli (thermal stress coefficients); α_{ij} are thermal expansion coefficients; e_{ijk} are piezoelectric constants; κ_{ij} are dielectric constants; $\chi_i = -e_{ikm}\alpha_{km} + \kappa_{ij}\lambda_j$ are pyroelectric coefficients; and λ_i are pyroelectric constants. Tensors C_{ijkm}, k_{ij}, κ_{ij} and β_{ij} are assumed to be symmetric. Here and further, the Einstein summation convention is used. A comma at subscript denotes differentiation with respect to a coordinate indexed after the comma, i.e. $u_{i,j} = \partial u_i / \partial x_j$.

If the temperature, electric potential and displacement depend only on in-plane coordinates x_1 and x_2, according to the extended Stroh formalism [10], the general homogeneous (i.e. for $\tilde{f}_i \equiv 0$ and $f_h \equiv 0$) solution of Eqs. (1), (2) can be expressed in terms of complex analytic functions as follows

$$\begin{aligned} &\theta = 2\,\mathrm{Re}\{g'(z_t)\}\,, \quad \vartheta = 2k_t\,\mathrm{Im}\{g'(z_t)\}\,, \quad h_1 = -\vartheta_{,2}\,, \quad h_2 = \vartheta_{,1}\,, \quad k_t = \sqrt{k_{11}k_{22} - k_{12}^{\ 2}}\,;\\ &\tilde{\mathbf{u}} = 2\,\mathrm{Re}\{\mathbf{A}\mathbf{f}(z_*) + \mathbf{c}g(z_t)\}\,, \quad \tilde{\boldsymbol{\varphi}} = 2\,\mathrm{Re}\{\mathbf{B}\mathbf{f}(z_*) + \mathbf{d}g(z_t)\}\,; \quad \tilde{\sigma}_{i1} = -\tilde{\varphi}_{i,2}\,, \quad \tilde{\sigma}_{i2} = \tilde{\varphi}_{i,1}\,;\\ &z_t = x_1 + p_t x_2\,; \quad z_\alpha = x_1 + p_\alpha x_2\,; \quad \mathbf{f}(z_*) = \left[F_1(z_1), F_2(z_2), F_3(z_3), F_4(z_4)\right]^{\mathrm{T}}, \end{aligned} \tag{4}$$

where ϑ is a heat flux function; $g(z_t)$ and $F_\alpha(z_\alpha)$ are complex analytic functions with respect to their arguments; the complex constant p_t is a root (with a positive imaginary part) of the characteristic equation for heat conduction

$$k_{22}p_t^2 + 2k_{12}p_t + k_{11} = 0\,; \tag{5}$$

4x4 complex matrices $\mathbf{A} \equiv [A_{i\alpha}] = [\mathbf{a}_\alpha]$, $\mathbf{B} \equiv [B_{i\alpha}] = [\mathbf{b}_\alpha]$ and constants $p_\alpha\ (\alpha = 1,..,4)$ are determined from the 8x8 Stroh eigenvalue problem [10, 17, 19]:

$$\mathbf{N} = \begin{bmatrix} \mathbf{N}_1 & \mathbf{N}_2 \\ \mathbf{N}_3 & \mathbf{N}_1^{\mathrm{T}} \end{bmatrix}, \quad \begin{aligned} &\mathbf{N}\boldsymbol{\xi} = p\boldsymbol{\xi},\\ &\mathbf{N}^{\mathrm{T}}\boldsymbol{\eta} = p\boldsymbol{\eta}, \end{aligned} \tag{6}$$

and vectors $\mathbf{c}$ and $\mathbf{d}$ satisfy the following matrix equation [17, 19]:

$$\mathbf{N}\boldsymbol{\zeta} = p_t\boldsymbol{\zeta} + \boldsymbol{\gamma}\,, \quad \boldsymbol{\zeta} = \begin{bmatrix} \mathbf{c} \\ \mathbf{d} \end{bmatrix}, \quad \boldsymbol{\gamma} = -\begin{bmatrix} \mathbf{0} & \mathbf{N}_2 \\ \mathbf{I} & \mathbf{N}_1^{\mathrm{T}} \end{bmatrix}\begin{bmatrix} \boldsymbol{\beta}_1 \\ \boldsymbol{\beta}_2 \end{bmatrix}, \tag{7}$$

where $\mathbf{N}_1 = -\mathbf{T}^{-1}\mathbf{R}^{\mathrm{T}}$, $\mathbf{N}_2 = \mathbf{T}^{-1}$, $\mathbf{N}_3 = \mathbf{R}\mathbf{T}^{-1}\mathbf{R}^{\mathrm{T}} - \mathbf{Q}$; $\boldsymbol{\beta}_1 = \left[\tilde{\beta}_{i1}\right]$, $\boldsymbol{\beta}_2 = \left[\tilde{\beta}_{i2}\right]$; $\boldsymbol{\xi} = [\mathbf{a}, \mathbf{b}]^{\mathrm{T}}$ is a right eigenvector and $\boldsymbol{\eta} = [\mathbf{b}, \mathbf{a}]^{\mathrm{T}}$ is a left eigenvector of the fundamental electro-elasticity matrix $\mathbf{N}$; superscript "T" denotes matrix transpose. The components of 4x4 matrices $\mathbf{Q}$, $\mathbf{R}$ and $\mathbf{T}$ are defined as $Q_{ik} = \tilde{C}_{i1k1}$, $T_{ik} = \tilde{C}_{i2k2}$, $R_{ik} = \tilde{C}_{i1k2} = \tilde{C}_{k2i1}$. Matrices $\mathbf{Q}$ and $\mathbf{T}$ are symmetric due to the symmetry of the tensor $\tilde{C}_{ijkm}$ [18]: $\tilde{C}_{ijkm} = \tilde{C}_{kmij}$.

Since eigenvectors of the matrix $\mathbf{N}$ are unique up to an arbitrary multiplier, matrices $\mathbf{A}$ and $\mathbf{B}$ are normalized such that [10, 17, 19]:

$$\begin{bmatrix} \mathbf{B}^{\mathrm{T}} & \mathbf{A}^{\mathrm{T}} \\ \overline{\mathbf{B}}^{\mathrm{T}} & \overline{\mathbf{A}}^{\mathrm{T}} \end{bmatrix} \begin{bmatrix} \mathbf{A} & \overline{\mathbf{A}} \\ \mathbf{B} & \overline{\mathbf{B}} \end{bmatrix} = \begin{bmatrix} \mathbf{I} & \mathbf{0} \\ \mathbf{0} & \mathbf{I} \end{bmatrix}. \tag{8}$$

According to [15], based on Eqs. (6)–(8) one can obtain the following identity

$$\mathbf{P}\mathbf{B}^{\mathrm{T}}\,\mathrm{Im}\{\mathbf{c}\} + \mathbf{P}\mathbf{A}^{\mathrm{T}}\,\mathrm{Im}\{\mathbf{d}\} = \mathbf{B}^{\mathrm{T}}\,\mathrm{Im}\{p_t\mathbf{c}\} + \mathbf{A}^{\mathrm{T}}\,\mathrm{Im}\{p_t\mathbf{d}\}, \quad \mathbf{P} = \mathrm{diag}[p_1, p_2, p_3, p_4]. \tag{9}$$

Stroh orthogonality conditions (8) allow obtaining the following relations between the Stroh complex functions and vectors of extended displacement and stress function [15]:

$$\mathbf{f}(z_*) = \mathbf{B}^{\mathrm{T}}\tilde{\mathbf{u}} + \mathbf{A}^{\mathrm{T}}\tilde{\boldsymbol{\varphi}} - \mathbf{B}^{\mathrm{T}}\tilde{\mathbf{u}}^t - \mathbf{A}^{\mathrm{T}}\tilde{\boldsymbol{\varphi}}^t, \quad \tilde{\mathbf{u}}^t = 2\,\mathrm{Re}\{\mathbf{c}g(z_t)\}, \quad \tilde{\boldsymbol{\varphi}}^t = 2\,\mathrm{Re}\{\mathbf{d}g(z_t)\}. \tag{10}$$

Based on Eq. (4) one can derive the following relation between the function $g'(z_t)$ and temperature and heat flux function:

$$g'(z_t) = \frac{1}{2}\left(\theta + i\frac{\vartheta}{k_t}\right). \tag{11}$$

2.3. Derivation of the integral formulae for the Stroh complex functions for a bimaterial

Consider a plane problem of thermoelectroelasticity for two half-spaces $x_2 > 0$ and $x_2 < 0$ (actually only the cross-sections (half-planes) S_1 as S_2 normal to the axis x_3 are studied as depicted in Fig. 1), which are bonded along the plane $x_2 = 0$ such that the following conditions of a perfect contact are satisfied for thermal fields

$$\theta^{(1)}(x_1, x_2)\big|_{x_2=0} = \theta^{(2)}(x_1, x_2)\big|_{x_2=0}, \quad \vartheta^{(1)}(x_1, x_2)\big|_{x_2=0} = \vartheta^{(2)}(x_1, x_2)\big|_{x_2=0} \quad \forall x_1 \in (-\infty; \infty) \tag{12}$$

and electric and mechanical fields

$$\tilde{\mathbf{u}}^{(1)}(x_1, x_2)\big|_{x_2=0} = \tilde{\mathbf{u}}^{(2)}(x_1, x_2)\big|_{x_2=0}, \quad \tilde{\boldsymbol{\varphi}}^{(1)}(x_1, x_2)\big|_{x_2=0} = \tilde{\boldsymbol{\varphi}}^{(2)}(x_1, x_2)\big|_{x_2=0} \quad \forall x_1 \in (-\infty; \infty). \tag{13}$$

Each of the half-spaces contains a system of cylindrical voids, which are referred as corresponding holes in the 2D half-planes S_1 and S_2 that are bounded by plane contours $\Gamma_1 = \cup_j \Gamma_j^{(1)}$ and $\Gamma_2 = \cup_j \Gamma_j^{(2)}$ respectively (fig. 1).

For derivation of the integral formulae for the Stroh complex functions for bonded half-spaces one can use the Cauchy integral formula [20], which relates values of an arbitrary analytic function $\phi(\tau)$ at the boundary ∂S of the domain S with its value $\phi(z)$ inside this domain:

$$\frac{1}{2\pi i}\int_{\partial S}\frac{\phi(\tau)d\tau}{\tau-z}=\begin{cases}\phi(z) & \forall z\in S,\\ 0 & \forall z\notin S,\end{cases} \tag{14}$$

where $\tau, z\in\mathbb{C}$ are complex variables, which define the position of the source and field points, respectively. Herewith, if the domain S is infinite it is assumed that the function $\phi(z)$ vanishes at $z\to\infty$.

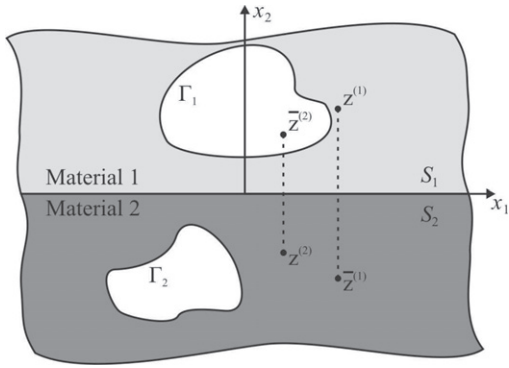

Fig. 1. The sketch of the problem

2.3.1. Derivation of the integral formulae for heat conduction in a bimaterial

Due to the linearity of the problem of heat conduction one can present its solution as a superposition of the homogeneous solution given by the functions $g_{1\infty}\left(z_t^{(1)}\right)$ and $g_{2\infty}\left(z_t^{(2)}\right)$ (which should definitely satisfy the boundary conditions (12)) and the perturbed solution caused by the presence of the contours Γ_1 and Γ_2, and certain boundary conditions set on them. Denoting the Cauchy integrals of the complex temperature functions $g_i'\left(z_t^{(i)}\right)$ as

$$q_t^{(i)}\left(z_t^{(j)}\right)=\int_{\Gamma_i}\frac{g_i'\left(\tau_t^{(i)}\right)d\tau_t^{(i)}}{\tau_t^{(i)}-z_t^{(j)}},\quad \overline{q}_t^{(i)}\left(z_t^{(j)}\right)=\int_{\Gamma_i}\frac{\overline{g_i'\left(\tau_t^{(i)}\right)}d\overline{\tau}_t^{(i)}}{\overline{\tau}_t^{(i)}-z_t^{(j)}}, \tag{15}$$

and the improper integrals over the infinite path $-\infty<x_1<\infty$ as

$$m_t\left(z_t^{(j)}\right)=\int_{-\infty}^{\infty}\frac{\vartheta(x_1)dx_1}{x_1-z_t^{(j)}},\quad p_t\left(z_t^{(j)}\right)=\int_{-\infty}^{\infty}\frac{\theta(x_1)dx_1}{x_1-z_t^{(j)}}, \tag{16}$$

based on Eqs. (11) and (14), satisfying the contact conditions (12) one obtains the following integral formulae for the functions $g_i'\left(z_t^{(i)}\right)$:

$$g_1'\left(z_t^{(1)}\right)=g_{1\infty}'\left(z_t^{(1)}\right)+\frac{1}{2\pi i}q_t^{(1)}\left(z_t^{(1)}\right)+\frac{1}{4\pi i}p_t\left(z_t^{(1)}\right)+\frac{1}{4\pi k_t^{(1)}}m_t\left(z_t^{(1)}\right)\quad\forall\,\mathrm{Im}\left(z_t^{(1)}\right)>0; \tag{17}$$

$$g_2'\left(z_t^{(2)}\right)=g_{2\infty}'\left(z_t^{(2)}\right)+\frac{1}{2\pi i}q_t^{(2)}\left(z_t^{(2)}\right)-\frac{1}{4\pi i}p_t\left(z_t^{(2)}\right)-\frac{1}{4\pi k_t^{(2)}}m_t\left(z_t^{(2)}\right)\quad\forall\,\mathrm{Im}\left(z_t^{(2)}\right)>0 \tag{18}$$

and a system of equations for determination of the improper integrals (16) through the Cauchy integrals (15):

$$\begin{aligned} \operatorname{Im}\left(z_t^{(1)}\right)>0: \quad & \overline{q}_t^{(1)}\left(z_t^{(1)}\right)+\frac{1}{2}p_t\left(z_t^{(1)}\right)-\frac{i}{2k_t^{(1)}}m_t\left(z_t^{(1)}\right)=0, \\ & q_t^{(2)}\left(z_t^{(1)}\right)-\frac{1}{2}p_t\left(z_t^{(1)}\right)-\frac{i}{2k_t^{(2)}}m_t\left(z_t^{(1)}\right)=0; \end{aligned} \tag{19}$$

$$\begin{aligned} \operatorname{Im}\left(z_t^{(2)}\right)<0: \quad & \overline{q}_t^{(2)}\left(z_t^{(2)}\right)-\frac{1}{2}p_t\left(z_t^{(2)}\right)+\frac{i}{2k_t^{(2)}}m_t\left(z_t^{(2)}\right)=0, \\ & q_t^{(1)}\left(z_t^{(2)}\right)+\frac{1}{2}p_t\left(z_t^{(2)}\right)+\frac{i}{2k_t^{(1)}}m_t\left(z_t^{(2)}\right)=0. \end{aligned} \tag{20}$$

The superscripts 1 or 2 denote corresponding half-space, which the temperature complex function belongs to. A positive orientation of a contour is selected under the condition that as we traverse the path following the positive orientation the domain occupied by the solid must always be on the left.

Solving Eqs. (19) and (20) for the unknowns (16) one can obtain that

$$\begin{aligned} p_t\left(z_t^{(1)}\right)&=(1-K)q_t^{(2)}\left(z_t^{(1)}\right)-(1+K)\overline{q}_t^{(1)}\left(z_t^{(1)}\right), \\ m_t\left(z_t^{(1)}\right)&=-ik_t^{(1)}(1-K)\left[\overline{q}_t^{(1)}\left(z_t^{(1)}\right)+q_t^{(2)}\left(z_t^{(1)}\right)\right]; \end{aligned} \tag{21}$$

$$\begin{aligned} p_t\left(z_t^{(2)}\right)&=(1-K)\overline{q}_t^{(2)}\left(z_t^{(2)}\right)-(1+K)q_t^{(1)}\left(z_t^{(2)}\right), \\ m_t\left(z_t^{(2)}\right)&=ik_t^{(2)}(1+K)\left[\overline{q}_t^{(2)}\left(z_t^{(2)}\right)+q_t^{(1)}\left(z_t^{(2)}\right)\right], \end{aligned} \tag{22}$$

where $K=\left(k_t^{(1)}-k_t^{(2)}\right)\Big/\left(k_t^{(1)}+k_t^{(2)}\right)$.

Substituting Eq. (21) into Eq. (17), and Eq. (22) into Eq. (18) one obtains the following integral formulae for the temperature functions $g_i'\left(z_t^{(i)}\right)$, which do not contain improper integrals along the infinite bimaterial interface:

$$g_1'\left(z_t^{(1)}\right)=g_{1\infty}'\left(z_t^{(1)}\right)+\frac{1}{2\pi i}\left[q_t^{(1)}\left(z_t^{(1)}\right)-K\overline{q}_t^{(1)}\left(z_t^{(1)}\right)+(1-K)q_t^{(2)}\left(z_t^{(1)}\right)\right] \quad \forall \operatorname{Im}\left(z_t^{(1)}\right)>0; \tag{23}$$

$$g_2'\left(z_t^{(2)}\right)=g_{2\infty}'\left(z_t^{(2)}\right)+\frac{1}{2\pi i}\left[q_t^{(2)}\left(z_t^{(2)}\right)+K\overline{q}_t^{(2)}\left(z_t^{(2)}\right)+(1+K)q_t^{(1)}\left(z_t^{(2)}\right)\right] \quad \forall \operatorname{Im}\left(z_t^{(2)}\right)<0. \tag{24}$$

Based on Eq. (11) the Cauchy integral formulae (15) can be easily rewritten through the boundary values of physical functions of the temperature θ and the heat flux function ϑ:

$$\begin{aligned} q_t^{(i)}\left(z_t^{(j)}\right)&=\int_{\Gamma_i}\frac{g_i'\left(\tau_t^{(i)}\right)d\tau_t^{(i)}}{\tau_t^{(i)}-z_t^{(j)}}=\frac{1}{2}\int_{\Gamma_i}\frac{\theta\left(\tau_t^{(i)}\right)d\tau_t^{(i)}}{\tau_t^{(i)}-z_t^{(j)}}+\frac{i}{2k_t^{(i)}}\int_{\Gamma_i}\frac{\vartheta\left(\tau_t^{(i)}\right)d\tau_t^{(i)}}{\tau_t^{(i)}-z_t^{(j)}}, \\ \overline{q}_t^{(i)}\left(z_t^{(j)}\right)&=\overline{\int_{\Gamma_i}\frac{g_i'\left(\tau_t^{(i)}\right)d\tau_t^{(i)}}{\overline{\tau}_t^{(i)}-z_t^{(j)}}}=\frac{1}{2}\int_{\Gamma_i}\frac{\theta\left(\overline{\tau}_t^{(i)}\right)d\overline{\tau}_t^{(i)}}{\overline{\tau}_t^{(i)}-z_t^{(j)}}-\frac{i}{2k_t^{(i)}}\int_{\Gamma_i}\frac{\vartheta\left(\overline{\tau}_t^{(i)}\right)d\overline{\tau}_t^{(i)}}{\overline{\tau}_t^{(i)}-z_t^{(j)}}. \end{aligned} \tag{25}$$

Now one can account for the relation

$$d\tau_*=dx_1+p_*dx_2=-\left(n_2(s)-p_*n_1(s)\right)ds, \tag{26}$$

where $ds = \sqrt{dx_1^2 + dx_2^2}$ is a real differential of arcs Γ_1 or Γ_2; n_j are the components of a unit outwards normal vector $\mathbf{n}$; and convert (25) to line integrals of the first kind. According to Eq. (4),

$$\frac{\partial \vartheta}{\partial s} = \frac{\partial \vartheta}{\partial x_1}\frac{\partial x_1}{\partial s} + \frac{\partial \vartheta}{\partial x_2}\frac{\partial x_2}{\partial s} = h_2\left(-n_2\right) - h_1 n_1 = -h_n, \tag{27}$$

thus, integral formulae (25) can be reduced to the following line integrals of the first kind

$$\begin{aligned} q_t^{(i)}\left(z_t^{(j)}\right) &= -\frac{1}{2}\int_{\Gamma_i}\frac{n_2(s) - p_t^{(i)} n_1(s)}{\tau_t^{(i)}(s) - z_t^{(j)}}\theta(s)\,ds + \frac{i}{2k_t^{(i)}}\int_{\Gamma_i}\ln\left(\tau_t^{(i)}(s) - z_t^{(j)}\right)h_n(s)\,ds, \\ \overline{q}_t^{(i)}\left(z_t^{(j)}\right) &= -\frac{1}{2}\int_{\Gamma_i}\frac{n_2(s) - \overline{p}_t^{(i)} n_1(s)}{\overline{\tau}_t^{(i)}(s) - z_t^{(j)}}\theta(s)\,ds - \frac{i}{2k_t^{(i)}}\int_{\Gamma_i}\ln\left(\overline{\tau}_t^{(i)}(s) - z_t^{(j)}\right)h_n(s)\,ds. \end{aligned} \tag{28}$$

Based on Eq. (28) one can write explicit expressions for integral formulae (23) and (24) through the boundary values of the temperature θ and the normal component h_n of a heat flux vector:

$$\begin{aligned} g_1'\left(z_t^{(1)}\right) &= g_{1\infty}'\left(z_t^{(1)}\right) + \frac{1}{4\pi k_t^{(1)}}\int_{\Gamma_1}\left[\ln\left(\tau_t^{(1)}(s) - z_t^{(1)}\right) + K\ln\left(\overline{\tau}_t^{(1)}(s) - z_t^{(1)}\right)\right]h_n(s)\,ds - \\ &- \frac{1}{4\pi i}\int_{\Gamma_1}\left[\frac{n_2(s) - p_t^{(1)} n_1(s)}{\tau_t^{(1)}(s) - z_t^{(1)}} - K\frac{n_2(s) - \overline{p}_t^{(1)} n_1(s)}{\overline{\tau}_t^{(1)}(s) - z_t^{(1)}}\right]\theta(s)\,ds + \\ &+ \frac{1-K}{4\pi k_t^{(2)}}\int_{\Gamma_2}\ln\left(\tau_t^{(2)}(s) - z_t^{(1)}\right)h_n(s)\,ds - \frac{1-K}{4\pi i}\int_{\Gamma_2}\frac{n_2(s) - p_t^{(2)} n_1(s)}{\tau_t^{(2)}(s) - z_t^{(1)}}\theta(s)\,ds; \end{aligned} \tag{29}$$

$$\begin{aligned} g_2'\left(z_t^{(2)}\right) &= g_{2\infty}'\left(z_t^{(2)}\right) + \frac{1}{4\pi k_t^{(2)}}\int_{\Gamma_2}\left[\ln\left(\tau_t^{(2)}(s) - z_t^{(2)}\right) - K\ln\left(\overline{\tau}_t^{(2)}(s) - z_t^{(2)}\right)\right]h_n(s)\,ds - \\ &- \frac{1}{4\pi i}\int_{\Gamma_2}\left[\frac{n_2(s) - p_t^{(2)} n_1(s)}{\tau_t^{(2)}(s) - z_t^{(2)}} + K\frac{n_2(s) - \overline{p}_t^{(2)} n_1(s)}{\overline{\tau}_t^{(2)}(s) - z_t^{(2)}}\right]\theta(s)\,ds + \\ &+ \frac{1+K}{4\pi k_t^{(1)}}\int_{\Gamma_1}\ln\left(\tau_t^{(1)}(s) - z_t^{(2)}\right)h_n(s)\,ds - \frac{1+K}{4\pi i}\int_{\Gamma_1}\frac{n_2(s) - p_t^{(1)} n_1(s)}{\tau_t^{(1)}(s) - z_t^{(2)}}\theta(s)\,ds. \end{aligned} \tag{30}$$

In turn, application of the Stroh formalism relations (4) to Eqs. (29) and (30) allows obtaining the Somigliana type integral formulae for temperature and heat flux in a bimaterial:

$$\begin{aligned} \theta(\boldsymbol{\xi}) &= \begin{cases} 2\,\mathrm{Re}\left[g_1'\left(Z_t^{(1)}(\boldsymbol{\xi})\right)\right] & (\forall \boldsymbol{\xi} \in S_1), \\ 2\,\mathrm{Re}\left[g_2'\left(Z_t^{(2)}(\boldsymbol{\xi})\right)\right] & (\forall \boldsymbol{\xi} \in S_2) \end{cases} = \\ &= \int_{\Gamma}\left[\Theta^{\mathrm{bm}*}(\mathbf{x},\boldsymbol{\xi})\,h_n(\mathbf{x}) - H^{\mathrm{bm}*}(\mathbf{x},\boldsymbol{\xi})\,\theta(\mathbf{x})\right]ds(\mathbf{x}) + \theta^{\infty}(\boldsymbol{\xi}); \end{aligned} \tag{31}$$

$$\begin{aligned} h_i(\boldsymbol{\xi}) &= \begin{cases} 2k_t^{(1)}\,\mathrm{Im}\left[\left(\delta_{2i} - \delta_{1i} p_t^{(1)}\right)g_1''\left(Z_t^{(1)}(\boldsymbol{\xi})\right)\right] & (\forall \boldsymbol{\xi} \in S_1), \\ 2k_t^{(2)}\,\mathrm{Im}\left[\left(\delta_{2i} - \delta_{1i} p_t^{(2)}\right)g_2''\left(Z_t^{(2)}(\boldsymbol{\xi})\right)\right] & (\forall \boldsymbol{\xi} \in S_2) \end{cases} = \\ &= \int_{\Gamma}\left[\Theta_i^{\mathrm{bm}**}(\mathbf{x},\boldsymbol{\xi})\,h_n(\mathbf{x}) - H_i^{\mathrm{bm}**}(\mathbf{x},\boldsymbol{\xi})\,\theta(\mathbf{x})\right]ds(\mathbf{x}) + h_i^{\infty}(\boldsymbol{\xi}), \end{aligned} \tag{32}$$

where δ_{ij} is a Kronecker delta; $Z_t^{(i)}(\xi)=\xi_1+p_t^{(i)}\xi_2$; $\Gamma=\Gamma_1\cup\Gamma_2$ is a set of all internal contours in a bimaterial. The functions $\theta^{\infty}(\xi)$ and $h_i^{\infty}(\xi)$ define the particular homogeneous solution for an unnotched bimaterial as

$$\theta^{\infty}(\xi)=\begin{cases}2\,\mathrm{Re}\left[g_{1\infty}'\left(Z_t^{(1)}(\xi)\right)\right] & (\forall\xi\in S_1),\\ 2\,\mathrm{Re}\left[g_{2\infty}'\left(Z_t^{(2)}(\xi)\right)\right] & (\forall\xi\in S_2);\end{cases}$$

$$h_i(\xi)=\begin{cases}2k_t^{(1)}\,\mathrm{Im}\left[\left(\delta_{2i}-\delta_{1i}p_t^{(1)}\right)g_{1\infty}''\left(Z_t^{(1)}(\xi)\right)\right] & (\forall\xi\in S_1),\\ 2k_t^{(2)}\,\mathrm{Im}\left[\left(\delta_{2i}-\delta_{1i}p_t^{(2)}\right)g_{2\infty}''\left(Z_t^{(2)}(\xi)\right)\right] & (\forall\xi\in S_2).\end{cases}$$

According to Eqs. (4), (29), and (30), the explicit expression for the kernels of the integral formulae (31) and (32) are as follows

$\mathbf{x}\in S_1\wedge\xi\in S_1$:

$$\Theta^{\mathrm{bm}*}(\mathbf{x},\xi)=\frac{1}{2\pi k_t^{(1)}}\left[\ln\left|Z_t^{(1)}(\mathbf{x}-\xi)\right|+K\ln\left|\overline{Z}_t^{(1)}(\mathbf{x})-Z_t^{(1)}(\xi)\right|\right];$$

$$H^{\mathrm{bm}*}(\mathbf{x},\xi)=\frac{1}{2\pi}\,\mathrm{Im}\left[\frac{n_2(\mathbf{x})-p_t^{(1)}n_1(\mathbf{x})}{Z_t^{(1)}(\mathbf{x}-\xi)}-K\frac{n_2(\mathbf{x})-\overline{p}_t^{(1)}n_1(\mathbf{x})}{\overline{Z}_t^{(1)}(\mathbf{x})-Z_t^{(1)}(\xi)}\right];$$

$$\Theta_i^{\mathrm{bm}**}(\mathbf{x},\xi)=-\frac{1}{2\pi}\,\mathrm{Im}\left[\frac{\delta_{i2}-p_t^{(1)}\delta_{i1}}{Z_t^{(1)}(\mathbf{x}-\xi)}+\frac{K\left(\delta_{i2}-p_t^{(1)}\delta_{i1}\right)}{\overline{Z}_t^{(1)}(\mathbf{x})-Z_t^{(1)}(\xi)}\right];$$

$$H_i^{\mathrm{bm}**}(\mathbf{x},\xi)=-\frac{k_t^{(1)}}{2\pi}\,\mathrm{Re}\left[\left(\delta_{i2}-p_t^{(1)}\delta_{i1}\right)\left[\frac{n_2(\mathbf{x})-p_t^{(1)}n_1(\mathbf{x})}{\left[Z_t^{(1)}(\mathbf{x}-\xi)\right]^2}-K\frac{n_2(s)-\overline{p}_t^{(1)}n_1(\mathbf{x})}{\left[\overline{Z}_t^{(1)}(\mathbf{x})-Z_t^{(1)}(\xi)\right]^2}\right]\right];$$

$\mathbf{x}\in S_2\wedge\xi\in S_1$:

$$\Theta^{\mathrm{bm}*}(\mathbf{x},\xi)=\frac{1-K}{2\pi k_t^{(2)}}\ln\left|Z_t^{(2)}(\mathbf{x})-Z_t^{(1)}(\xi)\right|;\quad H^{\mathrm{bm}*}(\mathbf{x},\xi)=\frac{1-K}{2\pi}\,\mathrm{Im}\left[\frac{n_2(\mathbf{x})-p_t^{(2)}n_1(\mathbf{x})}{Z_t^{(2)}(\mathbf{x})-Z_t^{(1)}(\xi)}\right];$$

$$\Theta_i^{\mathrm{bm}**}(\mathbf{x},\xi)=-\frac{(1-K)k_t^{(1)}}{2\pi k_t^{(2)}}\,\mathrm{Im}\left[\frac{\delta_{i2}-p_t^{(1)}\delta_{i1}}{Z_t^{(2)}(\mathbf{x})-Z_t^{(1)}(\xi)}\right];$$

$$H_i^{\mathrm{bm}**}(\mathbf{x},\xi)=-\frac{(1-K)k_t^{(1)}}{2\pi}\,\mathrm{Re}\left[\left(\delta_{i2}-p_t^{(1)}\delta_{i1}\right)\frac{n_2(\mathbf{x})-p_t^{(2)}n_1(\mathbf{x})}{\left[Z_t^{(2)}(\mathbf{x})-Z_t^{(1)}(\xi)\right]^2}\right];$$

$\mathbf{x}\in S_1 \wedge \boldsymbol{\xi}\in S_2$:

$$\Theta^{\mathrm{bm}^*}(\mathbf{x},\boldsymbol{\xi})=\frac{1+K}{2\pi k_t^{(1)}}\ln\left|Z_t^{(1)}(\mathbf{x})-Z_t^{(2)}(\boldsymbol{\xi})\right|;\quad H^{\mathrm{bm}^*}(\mathbf{x},\boldsymbol{\xi})=\frac{1+K}{2\pi}\operatorname{Im}\left[\frac{n_2(\mathbf{s})-p_t^{(1)}n_1(\mathbf{x})}{Z_t^{(1)}(\mathbf{x})-Z_t^{(2)}(\boldsymbol{\xi})}\right];$$

$$\Theta_i^{\mathbf{bm}^{**}}(\mathbf{x},\boldsymbol{\xi})=-\frac{(1+K)k_t^{(2)}}{2\pi k_t^{(1)}}\operatorname{Im}\left[\frac{\delta_{i2}-p_t^{(2)}\delta_{i1}}{Z_t^{(1)}(\mathbf{x})-Z_t^{(2)}(\boldsymbol{\xi})}\right];$$

$$H_i^{\mathbf{bm}^{**}}(\mathbf{x},\boldsymbol{\xi})=-\frac{(1+K)k_t^{(2)}}{2\pi}\operatorname{Re}\left[\left(\delta_{i2}-p_t^{(2)}\delta_{i1}\right)\frac{n_2(\mathbf{x})-p_t^{(1)}n_1(\mathbf{x})}{\left[Z_t^{(1)}(\mathbf{x})-Z_t^{(2)}(\boldsymbol{\xi})\right]^2}\right];$$

$\mathbf{x}\in S_2 \wedge \boldsymbol{\xi}\in S_2$:

$$\Theta^{\mathrm{bm}^*}(\mathbf{x},\boldsymbol{\xi})=\frac{1}{2\pi k_t^{(2)}}\left[\ln\left|Z_t^{(2)}(\mathbf{x}-\boldsymbol{\xi})\right|-K\ln\left|\overline{Z}_t^{(2)}(\mathbf{x})-Z_t^{(2)}(\boldsymbol{\xi})\right|\right];$$

$$H^{\mathrm{bm}^*}(\mathbf{x},\boldsymbol{\xi})=\frac{1}{2\pi}\operatorname{Im}\left[\frac{n_2(\mathbf{x})-p_t^{(2)}n_1(\mathbf{x})}{Z_t^{(2)}(\mathbf{x}-\boldsymbol{\xi})}+K\frac{n_2(\mathbf{x})-\overline{p}_t^{(2)}n_1(\mathbf{x})}{\overline{Z}_t^{(2)}(\mathbf{x})-Z_t^{(2)}(\boldsymbol{\xi})}\right];$$

$$\Theta_i^{\mathbf{bm}^{**}}(\mathbf{x},\boldsymbol{\xi})=-\frac{1}{2\pi}\operatorname{Im}\left[\frac{\delta_{i2}-p_t^{(2)}\delta_{i1}}{Z_t^{(2)}(\mathbf{x}-\boldsymbol{\xi})}-\frac{K\left(\delta_{i2}-p_t^{(2)}\delta_{i1}\right)}{\overline{Z}_t^{(2)}(\mathbf{x})-Z_t^{(2)}(\boldsymbol{\xi})}\right];$$

$$H_i^{\mathbf{bm}^{**}}(\mathbf{x},\boldsymbol{\xi})=-\frac{k_t^{(2)}}{2\pi}\operatorname{Re}\left[\left(\delta_{i2}-p_t^{(2)}\delta_{i1}\right)\left[\frac{n_2(\mathbf{x})-p_t^{(2)}n_1(\mathbf{x})}{\left[Z_t^{(2)}(\mathbf{x}-\boldsymbol{\xi})\right]^2}+K\frac{n_2(\mathbf{x})-\overline{p}_t^{(2)}n_1(\mathbf{x})}{\left[\overline{Z}_t^{(2)}(\mathbf{x})-Z_t^{(2)}(\boldsymbol{\xi})\right]^2}\right]\right]. \tag{33}$$

According to Eqs. (4) and (6), for derivation of the integral formulae for extended displacement and stress it is necessary to calculate the anti-derivatives (integrals) of the functions $g_i'\left(z_t^{(i)}\right)$, $m_t(z)$, and $p_t(z)$:

$$g_i\left(z_t^{(i)}\right)=\int g_i'\left(z_t^{(i)}\right)dz_t^{(i)}; \tag{34}$$

$$M_t(z)=\int m_t(z)\,dz=-\int_{-\infty}^{\infty}\ln(x_1-z)\,\vartheta(x_1)\,dx_1; \tag{35}$$

$$P_t(z)=\int p_t(z)\,dz=-\int_{-\infty}^{\infty}\ln(x_1-z)\,\theta(x_1)\,dx_1. \tag{36}$$

According to Eqs. (21)–(24), one obtains

$$\begin{aligned}
&P_t\left(z_t^{(1)}\right)=(1-K)Q_t^{(2)}\left(z_t^{(1)}\right)-(1+K)\overline{Q}_t^{(1)}\left(z_t^{(1)}\right),\\
&M_t\left(z_t^{(1)}\right)=-ik_t^{(1)}(1-K)\left[\overline{Q}_t^{(1)}\left(z_t^{(1)}\right)+Q_t^{(2)}\left(z_t^{(1)}\right)\right],\\
&g_1\left(z_t^{(1)}\right)=g_{1\infty}\left(z_t^{(1)}\right)+\frac{1}{2\pi i}\left[Q_t^{(1)}\left(z_t^{(1)}\right)-K\overline{Q}_t^{(1)}\left(z_t^{(1)}\right)+(1-K)Q_t^{(2)}\left(z_t^{(1)}\right)\right]\quad\left(\forall\operatorname{Im}\left(z_t^{(1)}\right)>0\right);
\end{aligned} \tag{37}$$

$$P_t\left(z_t^{(2)}\right)=(1-K)\bar{Q}_t^{(2)}\left(z_t^{(2)}\right)-(1+K)Q_t^{(1)}\left(z_t^{(2)}\right),$$
$$M_t\left(z_t^{(2)}\right)=ik_t^{(2)}(1+K)\left[\bar{Q}_t^{(2)}\left(z_t^{(2)}\right)+Q_t^{(1)}\left(z_t^{(2)}\right)\right], \tag{38}$$
$$g_2\left(z_t^{(2)}\right)=g_{2\infty}\left(z_t^{(2)}\right)+\frac{1}{2\pi i}\left[Q_t^{(2)}\left(z_t^{(2)}\right)+K\bar{Q}_t^{(2)}\left(z_t^{(2)}\right)+(1+K)Q_t^{(1)}\left(z_t^{(2)}\right)\right]\ \left(\forall \operatorname{Im}\left(z_t^{(2)}\right)<0\right),$$

where according to Eqs. (28) and (34)–(35),

$$\begin{aligned}
Q_t^{(i)}(z)&=\int q_t^{(i)}(z)\,dz=\\
&=\frac{1}{2}\int_{\Gamma_i}\left(n_2(s)-p_t^{(i)}n_1(s)\right)\ln\left(\tau_t^{(i)}(s)-z\right)\theta(s)\,ds-\frac{i}{2k_t^{(i)}}\int_{\Gamma_i}f^*\left(\tau_t^{(i)}(s)-z\right)h_n(s)\,ds,\\
\bar{Q}_t^{(i)}(z)&=\int \bar{q}_t^{(i)}(z)\,dz=\\
&=\frac{1}{2}\int_{\Gamma_i}\left(n_2(s)-\bar{p}_t^{(i)}n_1(s)\right)\ln\left(\bar{\tau}_t^{(i)}(s)-z\right)\theta(s)\,ds+\frac{i}{2k_t^{(i)}}\int_{\Gamma_i}f^*\left(\bar{\tau}_t^{(i)}(s)-z\right)h_n(s)\,ds,
\end{aligned} \tag{39}$$

and $f^*(z)=z(\ln z-1)$ is an anti-derivative (integral) of a logarithmic function.

2.3.2. Integral formulae for thermoelectroelasticity of a bimaterial

For obtaining the integral formulae of thermoelectroelasticity one should write the Cauchy integral formula (14) for the Stroh complex vector functions $\mathbf{f}^{(1)}\left(z_*^{(1)}\right)$ and $\mathbf{f}^{(2)}\left(z_*^{(2)}\right)$, which are analytic in the domains S_1 and S_2, respectively. Since the Cauchy integral formula define the analytic function that vanishes at the infinity, the complete solution of the problem can be presented as a sum of the perturbed solution defined by the Cauchy formula and a homogeneous solution given by the functions $\mathbf{f}_\infty^{(1)}\left(z_*^{(1)}\right)$ and $\mathbf{f}_\infty^{(2)}\left(z_*^{(2)}\right)$, which satisfy interface boundary conditions (13). Consequently, one obtains

$$\mathbf{f}^{(1)}\left(z_*^{(1)}\right)=\mathbf{f}_\infty^{(1)}\left(z_*^{(1)}\right)+\frac{1}{2\pi i}\left[\int_{\Gamma_1}\left\langle\frac{d\tau_*^{(1)}}{\tau_*^{(1)}-z_*^{(1)}}\right\rangle\mathbf{f}^{(1)}\left(\tau_*^{(1)}\right)+\int_{-\infty}^{\infty}\left\langle\frac{dx_1}{x_1-z_*^{(1)}}\right\rangle\mathbf{f}^{(1)}(x_1)\right]\ \left(\operatorname{Im}z_*^{(1)}>0\right); \tag{40}$$

$$\int_{\Gamma_1}\left\langle\frac{d\tau_*^{(1)}}{\tau_*^{(1)}-\bar{z}_\beta^{(1)}}\right\rangle\mathbf{f}^{(1)}\left(\tau_*^{(1)}\right)+\int_{-\infty}^{\infty}\frac{dx_1}{x_1-\bar{z}_\beta^{(1)}}\mathbf{f}^{(1)}(x_1)=\mathbf{0}\ \left(\operatorname{Im}z_\beta^{(1)}>0\right); \tag{41}$$

$$\int_{\Gamma_2}\left\langle\frac{d\tau_*^{(2)}}{\tau_*^{(2)}-z_\beta^{(1)}}\right\rangle\mathbf{f}^{(2)}\left(\tau_*^{(2)}\right)-\int_{-\infty}^{\infty}\frac{dx_1}{x_1-z_\beta^{(1)}}\mathbf{f}^{(2)}(x_1)=\mathbf{0}\ \left(\operatorname{Im}z_\beta^{(1)}>0\right); \tag{42}$$

$$\mathbf{f}^{(2)}\left(z_*^{(2)}\right)=\mathbf{f}_\infty^{(2)}\left(z_*^{(2)}\right)+\frac{1}{2\pi i}\left[\int_{\Gamma_2}\left\langle\frac{d\tau_*^{(2)}}{\tau_*^{(2)}-z_*^{(2)}}\right\rangle\mathbf{f}^{(2)}\left(\tau_*^{(2)}\right)-\int_{-\infty}^{\infty}\left\langle\frac{dx_1}{x_1-z_*^{(2)}}\right\rangle\mathbf{f}^{(2)}(x_1)\right]\ \left(\operatorname{Im}z_*^{(2)}<0\right); \tag{43}$$

$$\int_{\Gamma_1}\left\langle\frac{d\tau_*^{(1)}}{\tau_*^{(1)}-z_\beta^{(2)}}\right\rangle\mathbf{f}^{(1)}\left(\tau_*^{(1)}\right)+\int_{-\infty}^{\infty}\frac{dx_1}{x_1-z_\beta^{(2)}}\mathbf{f}^{(1)}(x_1)=\mathbf{0}\ \left(\operatorname{Im}z_\beta^{(2)}<0\right); \tag{44}$$

$$\int_{\Gamma_2}\left\langle\frac{d\tau_*^{(2)}}{\tau_*^{(2)}-\bar{z}_\beta^{(2)}}\right\rangle\mathbf{f}^{(2)}\left(\tau_*^{(2)}\right)-\int_{-\infty}^{\infty}\frac{dx_1}{x_1-\bar{z}_\beta^{(2)}}\mathbf{f}^{(2)}(x_1)=\mathbf{0}\ \left(\operatorname{Im}z_\beta^{(2)}<0\right), \tag{45}$$

where $\left\langle F\left(z_*\right)\right\rangle = \operatorname{diag}\left[F_1\left(z_1\right), F_2\left(z_2\right), F_3\left(z_3\right), F_4\left(z_4\right)\right]$; and $z_\alpha^{(j)} = x_1 + p_\alpha^{(j)} x_2$ $(\alpha = 1,...,4)$.

Accounting for Eqs. (10) and (13), the integrals over the infinite bimaterial interface included in Eqs. (40)–(45) can be rewritten as,

$$\int\limits_{-\infty}^{\infty} \frac{\mathbf{f}^{(j)}\left(x_1\right) dx_1}{x_1 - z_\beta^{(i)}} = \mathbf{A}_j^{\mathrm{T}} \mathbf{m}\left(z_\beta^{(i)}\right) + \mathbf{B}_j^{\mathrm{T}} \mathbf{p}\left(z_\beta^{(i)}\right) - 2\int\limits_{-\infty}^{\infty} \frac{\left(\mathbf{A}_j^{\mathrm{T}} \operatorname{Re}\left[\mathbf{d}_j g_j\left(x_1\right)\right] + \mathbf{B}_j^{\mathrm{T}} \operatorname{Re}\left[\mathbf{c}_j g_j\left(x_1\right)\right]\right) dx_1}{x_1 - z_\beta^{(i)}}, \quad (46)$$

where the following notations are used

$$\mathbf{m}\left(z_\beta^{(j)}\right) = \int\limits_{-\infty}^{\infty} \frac{\tilde{\boldsymbol{\varphi}}\left(x_1\right) dx_1}{x_1 - z_\beta^{(j)}}, \quad \mathbf{p}\left(z_\beta^{(j)}\right) = \int\limits_{-\infty}^{\infty} \frac{\tilde{\mathbf{u}}\left(x_1\right) dx_1}{x_1 - z_\beta^{(j)}}. \quad (47)$$

After integration of the last term in the right-hand side of Eq. (46) and accounting for Eqs. (11), (35), and (36), Eq. (46) rewrites as,

$$\begin{aligned} \int\limits_{-\infty}^{\infty} \frac{\mathbf{f}^{(j)}\left(x_1\right) dx_1}{x_1 - z_\beta^{(i)}} &= \mathbf{A}_j^{\mathrm{T}} \mathbf{m}\left(z_\beta^{(i)}\right) + \mathbf{B}_j^{\mathrm{T}} \mathbf{p}\left(z_\beta^{(i)}\right) + \\ &+ 2\int\limits_{-\infty}^{\infty} \left(\mathbf{A}_j^{\mathrm{T}} \operatorname{Re}\left[\mathbf{d}_j g_j'\left(x_1\right)\right] + \mathbf{B}_j^{\mathrm{T}} \operatorname{Re}\left[\mathbf{c}_j g_j'\left(x_1\right)\right]\right) \ln\left(x_1 - z_\beta^{(i)}\right) dx_1 = , \quad (48) \\ &= \mathbf{A}_j^{\mathrm{T}} \mathbf{m}\left(z_\beta^{(i)}\right) + \mathbf{B}_j^{\mathrm{T}} \mathbf{p}\left(z_\beta^{(i)}\right) + \boldsymbol{\mu}_j M_t\left(z_\beta^{(i)}\right) - \boldsymbol{\lambda}_j P_t\left(z_\beta^{(i)}\right), \end{aligned}$$

where the complex vector constants $\boldsymbol{\mu}_j$ and $\boldsymbol{\lambda}_j$ are defined by the following equations

$$\boldsymbol{\mu}_j = \frac{1}{k_t^{(j)}}\left(\mathbf{A}_j^{\mathrm{T}} \operatorname{Im}\left[\mathbf{d}_j\right] + \mathbf{B}_j^{\mathrm{T}} \operatorname{Im}\left[\mathbf{c}_j\right]\right), \quad \boldsymbol{\lambda}_j = \mathbf{A}_j^{\mathrm{T}} \operatorname{Re}\left[\mathbf{d}_j\right] + \mathbf{B}_j^{\mathrm{T}} \operatorname{Re}\left[\mathbf{c}_j\right]. \quad (49)$$

Denoting the Cauchy integrals of the Stroh complex functions as

$$\mathbf{q}_j\left(z_\beta^{(i)}\right) = \int\limits_{\Gamma_j} \left\langle \frac{d\tau_*^{(j)}}{\tau_*^{(j)} - z_\beta^{(i)}} \right\rangle \mathbf{f}^{(j)}\left(\tau_*^{(j)}\right), \quad \overline{\mathbf{q}}_j\left(z_\beta^{(i)}\right) = \int\limits_{\Gamma_j} \left\langle \frac{d\overline{\tau}_*^{(j)}}{\overline{\tau}_*^{(j)} - z_\beta^{(i)}} \right\rangle \overline{\mathbf{f}^{(j)}\left(\tau_*^{(j)}\right)}, \quad (50)$$

based on Eqs. (40)–(45), (47), and (48) one can obtain that

$$\begin{aligned} &\mathbf{f}^{(1)}\left(z_*^{(1)}\right) = \mathbf{f}_\infty^{(1)}\left(z_*^{(1)}\right) + \\ &+ \frac{1}{2\pi i}\left[\mathbf{q}_1\left(z_*^{(1)}\right) + \sum_{\beta=1}^{4} \mathbf{I}_\beta \left(\mathbf{A}_1^{\mathrm{T}} \mathbf{m}\left(z_\beta^{(1)}\right) + \mathbf{B}_1^{\mathrm{T}} \mathbf{p}\left(z_\beta^{(1)}\right)\right) + \left\langle M_t\left(z_*^{(1)}\right)\right\rangle \boldsymbol{\mu}_1 - \left\langle P_t\left(z_*^{(1)}\right)\right\rangle \boldsymbol{\lambda}_1\right]; \quad (51) \\ &\overline{\mathbf{A}}_1^{\mathrm{T}} \mathbf{m}\left(z_\beta^{(1)}\right) + \overline{\mathbf{B}}_1^{\mathrm{T}} \mathbf{p}\left(z_\beta^{(1)}\right) = -\overline{\mathbf{q}}_1\left(z_\beta^{(1)}\right) + \overline{\boldsymbol{\lambda}}_1 P_t\left(z_\beta^{(1)}\right) - \overline{\boldsymbol{\mu}}_1 M_t\left(z_\beta^{(1)}\right); \quad (52) \\ &\mathbf{A}_2^{\mathrm{T}} \mathbf{m}\left(z_\beta^{(1)}\right) + \mathbf{B}_2^{\mathrm{T}} \mathbf{p}\left(z_\beta^{(1)}\right) = \mathbf{q}_2\left(z_\beta^{(1)}\right) + \boldsymbol{\lambda}_2 P_t\left(z_\beta^{(1)}\right) - \boldsymbol{\mu}_2 M_t\left(z_\beta^{(1)}\right); \quad (53) \\ &\mathbf{f}^{(2)}\left(z_*^{(2)}\right) = \mathbf{f}_\infty^{(2)}\left(z_*^{(2)}\right) + \\ &+ \frac{1}{2\pi i}\left[\mathbf{q}_2\left(z_*^{(2)}\right) - \sum_{\beta=1}^{4} \mathbf{I}_\beta \left(\mathbf{A}_2^{\mathrm{T}} \mathbf{m}\left(z_\beta^{(2)}\right) + \mathbf{B}_2^{\mathrm{T}} \mathbf{p}\left(z_\beta^{(2)}\right)\right) - \left\langle M_t\left(z_*^{(2)}\right)\right\rangle \boldsymbol{\mu}_2 + \left\langle P_t\left(z_*^{(2)}\right)\right\rangle \boldsymbol{\lambda}_2\right]; \quad (54) \\ &\mathbf{A}_1^{\mathrm{T}} \mathbf{m}\left(z_\beta^{(2)}\right) + \mathbf{B}_1^{\mathrm{T}} \mathbf{p}\left(z_\beta^{(2)}\right) = -\mathbf{q}_1\left(z_\beta^{(2)}\right) + \boldsymbol{\lambda}_1 P_t\left(z_\beta^{(2)}\right) - \boldsymbol{\mu}_1 M_t\left(z_\beta^{(2)}\right); \quad (55) \\ &\overline{\mathbf{A}}_2^{\mathrm{T}} \mathbf{m}\left(z_\beta^{(2)}\right) + \overline{\mathbf{B}}_2^{\mathrm{T}} \mathbf{p}\left(z_\beta^{(2)}\right) = \overline{\mathbf{q}}_2\left(z_\beta^{(2)}\right) + \overline{\boldsymbol{\lambda}}_2 P_t\left(z_\beta^{(2)}\right) - \overline{\boldsymbol{\mu}}_2 M_t\left(z_\beta^{(2)}\right), \quad (56) \end{aligned}$$

where $\mathbf{I}_1 = \operatorname{diag}[1,0,0,0]$, $\mathbf{I}_2 = \operatorname{diag}[0,1,0,0]$, $\mathbf{I}_3 = \operatorname{diag}[0,0,1,0]$, and $\mathbf{I}_4 = \operatorname{diag}[0,0,0,1]$.

Eqs. (52), (53), (55), and (56) allow to express the improper integrals (47) over the infinite bimaterial interface through the integrals over the finite contours Γ_j:

$$\begin{aligned}
&\mathbf{m}\left(z_\beta^{(1)}\right)=\left(\overline{\mathbf{A}}_1\overline{\mathbf{B}}_1^{-1}-\mathbf{A}_2\mathbf{B}_2^{-1}\right)^{-\mathrm{T}}\left(\overline{\mathbf{B}}_1^{-\mathrm{T}}\mathbf{y}_1\left(z_\beta^{(1)}\right)-\mathbf{B}_2^{-\mathrm{T}}\mathbf{y}_2\left(z_\beta^{(1)}\right)\right);\\
&\mathbf{p}\left(z_\beta^{(1)}\right)=\left(\overline{\mathbf{B}}_1\overline{\mathbf{A}}_1^{-1}-\mathbf{B}_2\mathbf{A}_2^{-1}\right)^{-\mathrm{T}}\left(\overline{\mathbf{A}}_1^{-\mathrm{T}}\mathbf{y}_1\left(z_\beta^{(1)}\right)-\mathbf{A}_2^{-\mathrm{T}}\mathbf{y}_2\left(z_\beta^{(1)}\right)\right);\\
&\mathbf{y}_1\left(z_\beta^{(1)}\right)=-\overline{\mathbf{q}}_1\left(z_\beta^{(1)}\right)+\overline{\boldsymbol{\lambda}}_1P_t\left(z_\beta^{(1)}\right)-\overline{\boldsymbol{\mu}}_1M_t\left(z_\beta^{(1)}\right);\\
&\mathbf{y}_2\left(z_\beta^{(1)}\right)=\mathbf{q}_2\left(z_\beta^{(1)}\right)+\boldsymbol{\lambda}_2P_t\left(z_\beta^{(1)}\right)-\boldsymbol{\mu}_2M_t\left(z_\beta^{(1)}\right);
\end{aligned}\tag{57}$$

$$\begin{aligned}
&\mathbf{m}\left(z_\beta^{(2)}\right)=\left(\overline{\mathbf{A}}_2\overline{\mathbf{B}}_2^{-1}-\mathbf{A}_1\mathbf{B}_1^{-1}\right)^{-\mathrm{T}}\left(\overline{\mathbf{B}}_2^{-\mathrm{T}}\mathbf{y}_3\left(z_\beta^{(2)}\right)-\mathbf{B}_1^{-\mathrm{T}}\mathbf{y}_4\left(z_\beta^{(2)}\right)\right);\\
&\mathbf{p}\left(z_\beta^{(2)}\right)=\left(\overline{\mathbf{B}}_2\overline{\mathbf{A}}_2^{-1}-\mathbf{B}_1\mathbf{A}_1^{-1}\right)^{-\mathrm{T}}\left(\overline{\mathbf{A}}_2^{-\mathrm{T}}\mathbf{y}_3\left(z_\beta^{(2)}\right)-\mathbf{A}_1^{-\mathrm{T}}\mathbf{y}_4\left(z_\beta^{(2)}\right)\right);\\
&\mathbf{y}_3\left(z_\beta^{(2)}\right)=\overline{\mathbf{q}}_2\left(z_\beta^{(2)}\right)+\overline{\boldsymbol{\lambda}}_2P_t\left(z_\beta^{(2)}\right)-\overline{\boldsymbol{\mu}}_2M_t\left(z_\beta^{(2)}\right);\\
&\mathbf{y}_4\left(z_\beta^{(2)}\right)=-\mathbf{q}_1\left(z_\beta^{(2)}\right)+\boldsymbol{\lambda}_1P_t\left(z_\beta^{(2)}\right)-\boldsymbol{\mu}_1M_t\left(z_\beta^{(2)}\right).
\end{aligned}\tag{58}$$

Substituting Eqs. (57), (58) into Eqs. (51) and (54) one can obtain the integral formulae for the Stroh complex functions for a bimaterial, which do not contain improper integrals over the infinite path (bimaterial interface):

$$\begin{aligned}
\mathbf{f}^{(1)}\left(z_*^{(1)}\right)=\mathbf{f}_\infty^{(1)}\left(z_*^{(1)}\right)+\frac{1}{2\pi i}\Bigg[&\mathbf{q}_1\left(z_*^{(1)}\right)+\sum_{\beta=1}^{4}\mathbf{I}_\beta\left(\mathbf{G}_1^{(1)}\overline{\mathbf{q}}_1\left(z_\beta^{(1)}\right)+\mathbf{G}_2^{(1)}\mathbf{q}_2\left(z_\beta^{(1)}\right)\right)+\\
&+\left\langle M_t\left(z_*^{(1)}\right)\right\rangle\left(\mathbf{G}_1^{(1)}\overline{\boldsymbol{\mu}}_1-\mathbf{G}_2^{(1)}\boldsymbol{\mu}_2+\boldsymbol{\mu}_1\right)+\left\langle P_t\left(z_*^{(1)}\right)\right\rangle\left(\mathbf{G}_2^{(1)}\boldsymbol{\lambda}_2-\mathbf{G}_1^{(1)}\overline{\boldsymbol{\lambda}}_1-\boldsymbol{\lambda}_1\right)\Bigg]\quad\forall\,\mathrm{Im}\,z_*^{(1)}>0;
\end{aligned}\tag{59}$$

$$\begin{aligned}
\mathbf{f}^{(2)}\left(z_*^{(2)}\right)=\mathbf{f}_\infty^{(2)}\left(z_*^{(2)}\right)+\frac{1}{2\pi i}\Bigg[&\mathbf{q}_2\left(z_*^{(2)}\right)-\sum_{\beta=1}^{4}\mathbf{I}_\beta\left(\mathbf{G}_1^{(2)}\mathbf{q}_1\left(z_\beta^{(2)}\right)+\mathbf{G}_2^{(2)}\overline{\mathbf{q}}_2\left(z_\beta^{(2)}\right)\right)+\\
&+\left\langle M_t\left(z_*^{(2)}\right)\right\rangle\left(\mathbf{G}_2^{(2)}\overline{\boldsymbol{\mu}}_2-\mathbf{G}_1^{(2)}\boldsymbol{\mu}_1-\boldsymbol{\mu}_2\right)+\left\langle P_t\left(z_*^{(2)}\right)\right\rangle\left(\mathbf{G}_1^{(2)}\boldsymbol{\lambda}_1-\mathbf{G}_2^{(2)}\overline{\boldsymbol{\lambda}}_2+\boldsymbol{\lambda}_1\right)\Bigg]\quad\forall\,\mathrm{Im}\,z_*^{(2)}>0,
\end{aligned}\tag{60}$$

where

$$\begin{aligned}
&\mathbf{G}_1^{(1)}=-\left[\mathbf{A}_1^{\mathrm{T}}\left(\overline{\mathbf{A}}_1\overline{\mathbf{B}}_1^{-1}-\mathbf{A}_2\mathbf{B}_2^{-1}\right)^{-\mathrm{T}}\overline{\mathbf{B}}_1^{-\mathrm{T}}+\mathbf{B}_1^{\mathrm{T}}\left(\overline{\mathbf{B}}_1\overline{\mathbf{A}}_1^{-1}-\mathbf{B}_2\mathbf{A}_2^{-1}\right)^{-\mathrm{T}}\overline{\mathbf{A}}_1^{-\mathrm{T}}\right];\\
&\mathbf{G}_2^{(1)}=-\left[\mathbf{A}_1^{\mathrm{T}}\left(\overline{\mathbf{A}}_1\overline{\mathbf{B}}_1^{-1}-\mathbf{A}_2\mathbf{B}_2^{-1}\right)^{-\mathrm{T}}\mathbf{B}_2^{-\mathrm{T}}+\mathbf{B}_1^{\mathrm{T}}\left(\overline{\mathbf{B}}_1\overline{\mathbf{A}}_1^{-1}-\mathbf{B}_2\mathbf{A}_2^{-1}\right)^{-\mathrm{T}}\mathbf{A}_2^{-\mathrm{T}}\right];\\
&\mathbf{G}_1^{(2)}=-\left[\mathbf{A}_2^{\mathrm{T}}\left(\mathbf{A}_1\mathbf{B}_1^{-1}-\overline{\mathbf{A}}_2\overline{\mathbf{B}}_2^{-1}\right)^{-\mathrm{T}}\mathbf{B}_1^{-\mathrm{T}}+\mathbf{B}_2^{\mathrm{T}}\left(\mathbf{B}_1\mathbf{A}_1^{-1}-\overline{\mathbf{B}}_2\overline{\mathbf{A}}_2^{-1}\right)^{-\mathrm{T}}\mathbf{A}_1^{-\mathrm{T}}\right];\\
&\mathbf{G}_2^{(2)}=-\left[\mathbf{A}_2^{\mathrm{T}}\left(\mathbf{A}_1\mathbf{B}_1^{-1}-\overline{\mathbf{A}}_2\overline{\mathbf{B}}_2^{-1}\right)^{-\mathrm{T}}\overline{\mathbf{B}}_2^{-\mathrm{T}}+\mathbf{B}_2^{\mathrm{T}}\left(\mathbf{B}_1\mathbf{A}_1^{-1}-\overline{\mathbf{B}}_2\overline{\mathbf{A}}_2^{-1}\right)^{-\mathrm{T}}\overline{\mathbf{A}}_2^{-\mathrm{T}}\right].
\end{aligned}\tag{61}$$

By means of the impedance tensor [17, 19]

$$\mathbf{M}=-i\mathbf{B}\mathbf{A}^{-1},\quad\mathbf{M}^{-1}=i\mathbf{A}\mathbf{B}^{-1},\tag{62}$$

which has the following useful property [17, 19]

$$\mathbf{M}+\overline{\mathbf{M}}=-i\mathbf{A}^{-\mathrm{T}}\mathbf{A}^{-1},\tag{63}$$

Eq. (61) can be reduced to a simpler form

$$\begin{aligned}
&\mathbf{G}_1^{(1)}=\left[\overline{\mathbf{A}}_1^{-1}\left(\overline{\mathbf{M}}_1+\mathbf{M}_2\right)^{-1}\left(\mathbf{M}_1-\mathbf{M}_2\right)\mathbf{A}_1\right]^{\mathrm{T}};\quad\mathbf{G}_2^{(1)}=-i\left[\mathbf{A}_2^{-1}\left(\overline{\mathbf{M}}_1+\mathbf{M}_2\right)^{-1}\mathbf{A}_1^{-\mathrm{T}}\right]^{\mathrm{T}};\\
&\mathbf{G}_1^{(2)}=i\left[\mathbf{A}_1^{-1}\left(\mathbf{M}_1+\overline{\mathbf{M}}_2\right)^{-1}\mathbf{A}_2^{-\mathrm{T}}\right]^{\mathrm{T}};\quad\mathbf{G}_2^{(2)}=\left[\overline{\mathbf{A}}_2^{-1}\left(\mathbf{M}_1+\overline{\mathbf{M}}_2\right)^{-1}\left(\mathbf{M}_1-\mathbf{M}_2\right)\mathbf{A}_2\right]^{\mathrm{T}}.
\end{aligned}\tag{64}$$

Substituting Eqs. (37) and (38) into Eqs. (59) and (60) one can obtain that

$$\mathbf{f}^{(1)}\left(z_*^{(1)}\right)=\mathbf{f}_\infty^{(1)}\left(z_*^{(1)}\right)+\frac{1}{2\pi i}\Bigg[\mathbf{q}_1\left(z_*^{(1)}\right)+\sum_{\beta=1}^{4}\mathbf{I}_\beta\left(\mathbf{G}_1^{(1)}\overline{\mathbf{q}}_1\left(z_\beta^{(1)}\right)+\mathbf{G}_2^{(1)}\mathbf{q}_2\left(z_\beta^{(1)}\right)\right)+$$
$$+\left\langle\overline{Q}_t^{(1)}\left(z_*^{(1)}\right)\right\rangle\boldsymbol{\delta}_1^{(1)}+\left\langle Q_t^{(2)}\left(z_*^{(1)}\right)\right\rangle\boldsymbol{\delta}_2^{(1)}\Bigg]\quad\forall\,\mathrm{Im}\,z_*^{(1)}>0; \tag{65}$$

$$\mathbf{f}^{(2)}\left(z_*^{(2)}\right)=\mathbf{f}_\infty^{(2)}\left(z_*^{(2)}\right)+\frac{1}{2\pi i}\Bigg[\mathbf{q}_2\left(z_*^{(2)}\right)-\sum_{\beta=1}^{4}\mathbf{I}_\beta\left(\mathbf{G}_1^{(2)}\mathbf{q}_1\left(z_\beta^{(2)}\right)+\mathbf{G}_2^{(2)}\overline{\mathbf{q}}_2\left(z_\beta^{(2)}\right)\right)+$$
$$+\left\langle Q_t^{(1)}\left(z_*^{(2)}\right)\right\rangle\boldsymbol{\delta}_1^{(2)}+\left\langle\overline{Q}_t^{(2)}\left(z_*^{(2)}\right)\right\rangle\boldsymbol{\delta}_2^{(2)}\Bigg]\quad\forall\,\mathrm{Im}\,z_*^{(2)}>0, \tag{66}$$

where

$$\begin{aligned}
\boldsymbol{\delta}_1^{(1)}&=-ik_t^{(1)}\left(1-K\right)\left(\mathbf{G}_1^{(1)}\overline{\boldsymbol{\mu}}_1-\mathbf{G}_2^{(1)}\boldsymbol{\mu}_2+\boldsymbol{\mu}_1\right)-\left(1+K\right)\left(\mathbf{G}_2^{(1)}\boldsymbol{\lambda}_2-\mathbf{G}_1^{(1)}\overline{\boldsymbol{\lambda}}_1-\boldsymbol{\lambda}_1\right);\\
\boldsymbol{\delta}_2^{(1)}&=-ik_t^{(1)}\left(1-K\right)\left(\mathbf{G}_1^{(1)}\overline{\boldsymbol{\mu}}_1-\mathbf{G}_2^{(1)}\boldsymbol{\mu}_2+\boldsymbol{\mu}_1\right)+\left(1-K\right)\left(\mathbf{G}_2^{(1)}\boldsymbol{\lambda}_2-\mathbf{G}_1^{(1)}\overline{\boldsymbol{\lambda}}_1-\boldsymbol{\lambda}_1\right);\\
\boldsymbol{\delta}_1^{(2)}&=ik_t^{(2)}\left(1+K\right)\left(\mathbf{G}_2^{(2)}\overline{\boldsymbol{\mu}}_2-\mathbf{G}_1^{(2)}\boldsymbol{\mu}_1-\boldsymbol{\mu}_2\right)-\left(1+K\right)\left(\mathbf{G}_1^{(2)}\boldsymbol{\lambda}_1-\mathbf{G}_2^{(2)}\overline{\boldsymbol{\lambda}}_2+\boldsymbol{\lambda}_2\right);\\
\boldsymbol{\delta}_2^{(2)}&=ik_t^{(2)}\left(1+K\right)\left(\mathbf{G}_2^{(2)}\overline{\boldsymbol{\mu}}_2-\mathbf{G}_1^{(2)}\boldsymbol{\mu}_1-\boldsymbol{\mu}_2\right)+\left(1-K\right)\left(\mathbf{G}_1^{(2)}\boldsymbol{\lambda}_1-\mathbf{G}_2^{(2)}\overline{\boldsymbol{\lambda}}_2+\boldsymbol{\lambda}_2\right).
\end{aligned} \tag{67}$$

According to [13, 15], based on Eqs. (4), (9)–(11) the Cauchy integrals (50) can be expressed through the physical boundary functions as

$$\begin{aligned}
\mathbf{q}_j\left(z_\beta^{(i)}\right)&=\int_{\Gamma_j}\left\langle\ln\left(\tau_*^{(j)}(s)-z_\beta^{(i)}\right)\right\rangle\mathbf{A}_j^{\mathrm{T}}\tilde{\mathbf{t}}(s)\,ds-\int_{\Gamma_j}\left\langle\frac{n_2(s)-p_*^{(j)}n_1(s)}{\tau_*^{(j)}(s)-z_\beta^{(i)}}\right\rangle\mathbf{B}_j^{\mathrm{T}}\tilde{\mathbf{u}}(s)\,ds-\\
&-\int_{\Gamma_j}\left\langle\ln\left(\tau_*^{(j)}(s)-z_\beta^{(i)}\right)\right\rangle\left(\boldsymbol{\lambda}_j n_2(s)-\boldsymbol{\rho}_j n_1(s)\right)\theta(s)\,ds-\int_{\Gamma_j}\left\langle f^*\left(\tau_*^{(j)}(s)-z_\beta^{(i)}\right)\right\rangle\boldsymbol{\mu}_j h_n(s)\,ds;\\
\overline{\mathbf{q}}_j\left(z_\beta^{(i)}\right)&=\int_{\Gamma_j}\left\langle\ln\left(\overline{\tau}_*^{(j)}(s)-z_\beta^{(i)}\right)\right\rangle\overline{\mathbf{A}}_j^{\mathrm{T}}\tilde{\mathbf{t}}(s)\,ds-\int_{\Gamma_j}\left\langle\frac{n_2(s)-\overline{p}_*^{(j)}n_1(s)}{\overline{\tau}_*^{(j)}(s)-z_\beta^{(i)}}\right\rangle\overline{\mathbf{B}}_j^{\mathrm{T}}\tilde{\mathbf{u}}(s)\,ds-\\
&-\int_{\Gamma_j}\left\langle\ln\left(\overline{\tau}_*^{(j)}(s)-z_\beta^{(i)}\right)\right\rangle\left(\overline{\boldsymbol{\lambda}}_j n_2(s)-\overline{\boldsymbol{\rho}}_j n_1(s)\right)\theta(s)\,ds-\int_{\Gamma_j}\left\langle f^*\left(\overline{\tau}_*^{(j)}(s)-z_\beta^{(i)}\right)\right\rangle\overline{\boldsymbol{\mu}}_j h_n(s)\,ds,
\end{aligned} \tag{68}$$

where $\tilde{t}_i=\tilde{\sigma}_{ij}n_j$ is an extended traction vector, and

$$\boldsymbol{\rho}_j=\mathbf{A}_j^{\mathrm{T}}\,\mathrm{Re}\left[p_t^{(j)}\mathbf{d}_j\right]+\mathbf{B}_j^{\mathrm{T}}\,\mathrm{Re}\left[p_t^{(j)}\mathbf{c}_j\right]. \tag{69}$$

According to Eqs. (39) and (68), expressions (65) and (66) for the Stroh complex functions are the integral formulae relating the latter at the internal points of the thermoelectroelastic bimaterial with the boundary values of the temperature θ, the heat flux h_n, the extended displacement vector $\tilde{\mathbf{u}}$ and the traction vector $\tilde{\mathbf{t}}$ at the contours Γ_j. Consequently, Eqs. (4), (65), (66), and (68) allow to derive the Somigliana type integral formula for a thermoelectroelastic bimaterial

$$\begin{aligned}
\tilde{\mathbf{u}}(\boldsymbol{\xi})&=\begin{cases}2\,\mathrm{Re}\left[\mathbf{A}_1\mathbf{f}^{(1)}\left(Z_*^{(1)}(\boldsymbol{\xi})\right)+\mathbf{c}_1 g_1\left(Z_t^{(1)}(\boldsymbol{\xi})\right)\right] & (\forall\boldsymbol{\xi}\in S_1),\\ 2\,\mathrm{Re}\left[\mathbf{A}_2\mathbf{f}^{(2)}\left(Z_*^{(2)}(\boldsymbol{\xi})\right)+\mathbf{c}_2 g_2\left(Z_t^{(2)}(\boldsymbol{\xi})\right)\right] & (\forall\boldsymbol{\xi}\in S_2)\end{cases}=\\
&=\tilde{\mathbf{u}}^{\infty}(\boldsymbol{\xi})+\int_{\Gamma}\left[\mathbf{U}^{\mathrm{bm}}(\mathbf{x},\boldsymbol{\xi})\tilde{\mathbf{t}}(\mathbf{x})-\mathbf{T}^{\mathrm{bm}}(\mathbf{x},\boldsymbol{\xi})\tilde{\mathbf{u}}(\mathbf{x})+\mathbf{r}^{\mathrm{bm}}(\mathbf{x},\boldsymbol{\xi})\theta(\mathbf{x})+\mathbf{v}^{\mathrm{bm}}(\mathbf{x},\boldsymbol{\xi})h_n(\mathbf{x})\right]ds(\mathbf{x}),
\end{aligned} \tag{70}$$

where the kernels are defined as,

$\mathbf{x}\in S_1 \wedge \boldsymbol{\xi}\in S_1$:

$$\mathbf{U}^{\text{bm}}(\mathbf{x},\boldsymbol{\xi}) = \frac{1}{\pi}\operatorname{Im}\left\{\mathbf{A}_1\left[\left\langle \ln\left(Z_*^{(1)}(\mathbf{x}-\boldsymbol{\xi})\right)\right\rangle \mathbf{A}_1^{\mathrm{T}} + \sum_{\beta=1}^{4}\left\langle \ln\left(\overline{Z}_\beta^{(1)}(\mathbf{x}) - Z_*^{(1)}(\boldsymbol{\xi})\right)\right\rangle \mathbf{G}_1^{(1)}\mathbf{I}_\beta\overline{\mathbf{A}}_1^{\mathrm{T}}\right]\right\};$$

$$\mathbf{T}^{\text{bm}}(\mathbf{x},\boldsymbol{\xi}) = \frac{1}{\pi}\operatorname{Im}\left\{\mathbf{A}_1\left[\left\langle \frac{n_2(\mathbf{x}) - p_*^{(1)}n_1(\mathbf{x})}{Z_*^{(1)}(\mathbf{x}-\boldsymbol{\xi})}\right\rangle \mathbf{B}_1^{\mathrm{T}} + \sum_{\beta=1}^{4}\left\langle \frac{n_2(\mathbf{x}) - \overline{p}_\beta^{(1)}n_1(\mathbf{x})}{\overline{Z}_\beta^{(1)}(\mathbf{x}) - Z_*^{(1)}(\boldsymbol{\xi})}\right\rangle \mathbf{G}_1^{(1)}\mathbf{I}_\beta\overline{\mathbf{B}}_1^{\mathrm{T}}\right]\right\};$$

$$\begin{aligned}\mathbf{r}^{\text{bm}}(\mathbf{x},\boldsymbol{\xi}) = \frac{1}{\pi}\operatorname{Im}\Bigg\{\mathbf{A}_1\Bigg[&-\left\langle \ln\left(Z_*^{(1)}(\mathbf{x}-\boldsymbol{\xi})\right)\right\rangle\left(\boldsymbol{\lambda}_1 n_2(\mathbf{x}) - \boldsymbol{\rho}_1 n_1(\mathbf{x})\right) - \\ &- \sum_{\beta=1}^{4}\left\langle \ln\left(\overline{Z}_\beta^{(1)}(\mathbf{x}) - Z_*^{(1)}(\boldsymbol{\xi})\right)\right\rangle \mathbf{G}_1^{(1)}\mathbf{I}_\beta\left(\overline{\boldsymbol{\lambda}}_1 n_2(\mathbf{x}) - \overline{\boldsymbol{\rho}}_1 n_1(\mathbf{x})\right) + \\ &+ \frac{1}{2}\left(n_2(\mathbf{x}) - \overline{p}_t^{(1)}n_1(\mathbf{x})\right)\left\langle \ln\left(\overline{Z}_t^{(1)}(\mathbf{x}) - Z_*^{(1)}(\boldsymbol{\xi})\right)\right\rangle \boldsymbol{\delta}_1^{(1)}\Bigg] + \\ &+ \frac{\mathbf{c}_1}{2}\left(n_2(\mathbf{x}) - p_t^{(1)}n_1(\mathbf{x})\right)\ln\left(Z_t^{(1)}(\mathbf{x}-\boldsymbol{\xi})\right) - \\ &- \frac{\mathbf{c}_1}{2}K\left(n_2(\mathbf{x}) - \overline{p}_t^{(1)}n_1(\mathbf{x})\right)\ln\left(\overline{Z}_t^{(1)}(\mathbf{x}) - Z_t^{(1)}(\boldsymbol{\xi})\right)\Bigg\};\end{aligned}$$

$$\begin{aligned}\mathbf{v}^{\text{bm}}(\mathbf{x},\boldsymbol{\xi}) = \frac{1}{\pi}\operatorname{Im}\Bigg\{\mathbf{A}_1\Bigg[&-\left\langle f^*\left(Z_*^{(1)}(\mathbf{x}-\boldsymbol{\xi})\right)\right\rangle \boldsymbol{\mu}_1 - \\ &- \sum_{\beta=1}^{4}\left\langle f^*\left(\overline{Z}_\beta^{(1)}(\mathbf{x}) - Z_*^{(1)}(\boldsymbol{\xi})\right)\right\rangle \mathbf{G}_1^{(1)}\mathbf{I}_\beta\overline{\boldsymbol{\mu}}_1 + \frac{i}{2k_t^{(1)}}\left\langle f^*\left(\overline{Z}_t^{(1)}(\mathbf{x}) - Z_*^{(1)}(\boldsymbol{\xi})\right)\right\rangle \boldsymbol{\delta}_1^{(1)}\Bigg] - \\ &- \frac{i\mathbf{c}_1}{2k_t^{(1)}}\left[f^*\left(Z_t^{(1)}(\mathbf{x}-\boldsymbol{\xi})\right) + Kf^*\left(\overline{Z}_t^{(1)}(\mathbf{x}) - Z_t^{(1)}(\boldsymbol{\xi})\right)\right]\Bigg\};\end{aligned}$$

$\mathbf{x}\in S_2 \wedge \boldsymbol{\xi}\in S_1$:

$$\mathbf{U}^{\text{bm}}(\mathbf{x},\boldsymbol{\xi}) = \frac{1}{\pi}\operatorname{Im}\left\{\mathbf{A}_1\sum_{\beta=1}^{4}\left[\left\langle \ln\left(Z_\beta^{(2)}(\mathbf{x}) - Z_*^{(1)}(\boldsymbol{\xi})\right)\right\rangle \mathbf{G}_2^{(1)}\mathbf{I}_\beta\right]\mathbf{A}_2^{\mathrm{T}}\right\};$$

$$\mathbf{T}^{\text{bm}}(\mathbf{x},\boldsymbol{\xi}) = \frac{1}{\pi}\operatorname{Im}\left\{\mathbf{A}_1\sum_{\beta=1}^{4}\left[\left\langle \frac{n_2(\mathbf{x}) - p_\beta^{(2)}n_1(\mathbf{x})}{Z_\beta^{(2)}(\mathbf{x}) - Z_*^{(1)}(\boldsymbol{\xi})}\right\rangle \mathbf{G}_2^{(1)}\mathbf{I}_\beta\right]\mathbf{B}_2^{\mathrm{T}}\right\};$$

$$\begin{aligned}\mathbf{r}^{\text{bm}}(\mathbf{x},\boldsymbol{\xi}) = \frac{1}{\pi}\operatorname{Im}\Bigg\{\mathbf{A}_1\Bigg[&-\sum_{\beta=1}^{4}\left\langle \ln\left(Z_\beta^{(2)}(\mathbf{x}) - Z_*^{(1)}(\boldsymbol{\xi})\right)\right\rangle \mathbf{G}_2^{(1)}\mathbf{I}_\beta\left(\boldsymbol{\lambda}_2 n_2(\mathbf{x}) - \boldsymbol{\rho}_2 n_1(\mathbf{x})\right) + \\ &+ \frac{1}{2}\left(n_2(\mathbf{x}) - p_t^{(2)}n_1(\mathbf{x})\right)\left\langle \ln\left(Z_t^{(2)}(\mathbf{x}) - Z_*^{(1)}(\boldsymbol{\xi})\right)\right\rangle \boldsymbol{\delta}_2^{(1)}\Bigg] + \\ &+ \frac{\mathbf{c}_1}{2}(1-K)\left(n_2(\mathbf{x}) - p_t^{(2)}n_1(\mathbf{x})\right)\ln\left(Z_t^{(2)}(\mathbf{x}) - Z_t^{(1)}(\boldsymbol{\xi})\right)\Bigg\};\end{aligned}$$

$$\begin{aligned}\mathbf{v}^{\text{bm}}(\mathbf{x},\boldsymbol{\xi}) = \frac{1}{\pi}\operatorname{Im}\Bigg\{\mathbf{A}_1\Bigg[&-\sum_{\beta=1}^{4}\left\langle f^*\left(Z_\beta^{(2)}(\mathbf{x}) - Z_*^{(1)}(\boldsymbol{\xi})\right)\right\rangle \mathbf{G}_2^{(1)}\mathbf{I}_\beta\boldsymbol{\mu}_2 - \\ &- \frac{i}{2k_t^{(2)}}\left\langle f^*\left(Z_t^{(2)}(\mathbf{x}) - Z_*^{(1)}(\boldsymbol{\xi})\right)\right\rangle \boldsymbol{\delta}_2^{(1)}\Bigg] - \frac{i\mathbf{c}_1}{2k_t^{(2)}}(1-K)f^*\left(Z_t^{(2)}(\mathbf{x}) - Z_t^{(1)}(\boldsymbol{\xi})\right)\Bigg\};\end{aligned}$$

$\mathbf{x}\in S_1\wedge\boldsymbol{\xi}\in S_2$:

$$\mathbf{U}^{\text{bm}}(\mathbf{x},\boldsymbol{\xi})=-\frac{1}{\pi}\operatorname{Im}\left\{\mathbf{A}_2\sum_{\beta=1}^{4}\left[\left\langle\ln\left(Z_\beta^{(1)}(\mathbf{x})-Z_*^{(2)}(\boldsymbol{\xi})\right)\right\rangle\mathbf{G}_1^{(2)}\mathbf{I}_\beta\right]\mathbf{A}_1^{\mathrm{T}}\right\};$$

$$\mathbf{T}^{\text{bm}}(\mathbf{x},\boldsymbol{\xi})=-\frac{1}{\pi}\operatorname{Im}\left\{\mathbf{A}_2\sum_{\beta=1}^{4}\left[\left\langle\frac{n_2(\mathbf{x})-p_\beta^{(1)}n_1(\mathbf{x})}{Z_\beta^{(1)}(\mathbf{x})-Z_*^{(2)}(\boldsymbol{\xi})}\right\rangle\mathbf{G}_1^{(2)}\mathbf{I}_\beta\right]\mathbf{B}_1^{\mathrm{T}}\right\};$$

$$\begin{aligned}\mathbf{r}^{\text{bm}}(\mathbf{x},\boldsymbol{\xi})=\frac{1}{\pi}\operatorname{Im}\Bigg\{\mathbf{A}_2\Bigg[&\sum_{\beta=1}^{4}\left\langle\ln\left(Z_\beta^{(1)}(\mathbf{x})-Z_*^{(2)}(\boldsymbol{\xi})\right)\right\rangle\mathbf{G}_1^{(2)}\mathbf{I}_\beta\left(\boldsymbol{\lambda}_1n_2(\mathbf{x})-\boldsymbol{\rho}_1n_1(\mathbf{x})\right)+\\&+\frac{1}{2}\left(n_2(\mathbf{x})-p_t^{(1)}n_1(\mathbf{x})\right)\left\langle\ln\left(Z_t^{(1)}(\mathbf{x})-Z_*^{(2)}(\boldsymbol{\xi})\right)\right\rangle\boldsymbol{\delta}_1^{(2)}\Bigg]+\\&+\frac{\mathbf{c}_2}{2}(1+K)\left(n_2(\mathbf{x})-p_t^{(1)}n_1(\mathbf{x})\right)\ln\left(Z_t^{(1)}(\mathbf{x})-Z_t^{(2)}(\boldsymbol{\xi})\right)\Bigg\};\end{aligned}$$

$$\begin{aligned}\mathbf{v}^{\text{bm}}(\mathbf{x},\boldsymbol{\xi})=\frac{1}{\pi}\operatorname{Im}\Bigg\{\mathbf{A}_2\Bigg[&\sum_{\beta=1}^{4}\left\langle f^*\left(Z_\beta^{(1)}(\mathbf{x})-Z_*^{(2)}(\boldsymbol{\xi})\right)\right\rangle\mathbf{G}_1^{(2)}\mathbf{I}_\beta\boldsymbol{\mu}_1-\\&-\frac{i}{2k_t^{(1)}}\left\langle f^*\left(Z_t^{(1)}(\mathbf{x})-Z_*^{(2)}(\boldsymbol{\xi})\right)\right\rangle\boldsymbol{\delta}_1^{(2)}\Bigg]-\frac{i\mathbf{c}_2}{2k_t^{(1)}}(1+K)f^*\left(Z_t^{(1)}(\mathbf{x})-Z_t^{(2)}(\boldsymbol{\xi})\right)\Bigg\};\end{aligned}$$

$\mathbf{x}\in S_2\wedge\boldsymbol{\xi}\in S_2$:

$$\mathbf{U}^{\text{bm}}(\mathbf{x},\boldsymbol{\xi})=\frac{1}{\pi}\operatorname{Im}\left\{\mathbf{A}_2\left[\left\langle\ln\left(Z_*^{(2)}(\mathbf{x}-\boldsymbol{\xi})\right)\right\rangle\mathbf{A}_2^{\mathrm{T}}-\sum_{\beta=1}^{4}\left\langle\ln\left(\overline{Z}_\beta^{(2)}(\mathbf{x})-Z_*^{(2)}(\boldsymbol{\xi})\right)\right\rangle\mathbf{G}_2^{(2)}\mathbf{I}_\beta\overline{\mathbf{A}}_2^{\mathrm{T}}\right]\right\};$$

$$\mathbf{T}^{\text{bm}}(\mathbf{x},\boldsymbol{\xi})=\frac{1}{\pi}\operatorname{Im}\left\{\mathbf{A}_2\left[\left\langle\frac{n_2(\mathbf{x})-p_*^{(2)}n_1(\mathbf{x})}{Z_*^{(2)}(\mathbf{x}-\boldsymbol{\xi})}\right\rangle\mathbf{B}_2^{\mathrm{T}}-\sum_{\beta=1}^{4}\left\langle\frac{n_2(\mathbf{x})-\overline{p}_\beta^{(2)}n_1(\mathbf{x})}{\overline{Z}_\beta^{(2)}(\mathbf{x})-Z_*^{(2)}(\boldsymbol{\xi})}\right\rangle\mathbf{G}_2^{(2)}\mathbf{I}_\beta\overline{\mathbf{B}}_2^{\mathrm{T}}\right]\right\}.$$

$$\begin{aligned}\mathbf{r}^{\text{bm}}(\mathbf{x},\boldsymbol{\xi})=\frac{1}{\pi}\operatorname{Im}\Bigg\{\mathbf{A}_2\Bigg[&-\left\langle\ln\left(Z_*^{(2)}(\mathbf{x}-\boldsymbol{\xi})\right)\right\rangle\left(\boldsymbol{\lambda}_2n_2(\mathbf{x})-\boldsymbol{\rho}_2n_1(\mathbf{x})\right)+\\&+\sum_{\beta=1}^{4}\left\langle\ln\left(\overline{Z}_\beta^{(2)}(\mathbf{x})-Z_*^{(2)}(\boldsymbol{\xi})\right)\right\rangle\mathbf{G}_2^{(2)}\mathbf{I}_\beta\left(\overline{\boldsymbol{\lambda}}_2n_2(\mathbf{x})-\overline{\boldsymbol{\rho}}_2n_1(\mathbf{x})\right)+\\&+\frac{1}{2}\left(n_2(\mathbf{x})-\overline{p}_t^{(2)}n_1(\mathbf{x})\right)\left\langle\ln\left(\overline{Z}_t^{(2)}(\mathbf{x})-Z_*^{(2)}(\boldsymbol{\xi})\right)\right\rangle\boldsymbol{\delta}_2^{(2)}\Bigg]+\\&+\frac{\mathbf{c}_2}{2}\left(n_2(\mathbf{x})-p_t^{(2)}n_1(\mathbf{x})\right)\ln\left(Z_t^{(2)}(\mathbf{x}-\boldsymbol{\xi})\right)+\\&+\frac{\mathbf{c}_2}{2}K\left(n_2(\mathbf{x})-\overline{p}_t^{(2)}n_1(\mathbf{x})\right)\ln\left(\overline{Z}_t^{(2)}(\mathbf{x})-Z_t^{(2)}(\boldsymbol{\xi})\right)\Bigg\};\end{aligned}$$

$$\mathbf{v}^{\mathrm{bm}}(\mathbf{x},\boldsymbol{\xi})=\frac{1}{\pi}\operatorname{Im}\Big\{\mathbf{A}_2\Big[-\Big\langle f^*\left(Z_*^{(2)}(\mathbf{x}-\boldsymbol{\xi})\right)\Big\rangle\boldsymbol{\mu}_2+$$

$$+\sum_{\beta=1}^{4}\Big\langle f^*\left(\overline{Z}_\beta^{(2)}(\mathbf{x})-Z_*^{(2)}(\boldsymbol{\xi})\right)\Big\rangle\mathbf{G}_2^{(2)}\mathbf{I}_\beta\overline{\boldsymbol{\mu}}_2+\frac{i}{2k_t^{(2)}}\Big\langle f^*\left(\overline{Z}_t^{(2)}(\mathbf{x})-Z_*^{(2)}(\boldsymbol{\xi})\right)\Big\rangle\boldsymbol{\delta}_2^{(2)}\Big]-$$

$$-\frac{i\mathbf{c}_2}{2k_t^{(2)}}\Big[f^*\left(Z_t^{(2)}(\mathbf{x}-\boldsymbol{\xi})\right)-Kf^*\left(\overline{Z}_t^{(2)}(\mathbf{x})-Z_t^{(2)}(\boldsymbol{\xi})\right)\Big]\Big\}. \tag{71}$$

And the following notation is used in Eq. (71): $Z_*^{(i)}(\mathbf{x})=x_1+p_*^{(i)}x_2$.

Based on Eqs. (4), (29), (30), (65), (66), and (68) one can also derive the integral formula for the extended stress tensor at the arbitrary internal point of a thermoelectroelastic bimaterial:

$$\tilde{\boldsymbol{\sigma}}_j(\boldsymbol{\xi})=\begin{cases}2\operatorname{Re}\Big[\mathbf{B}_1\left\langle\delta_{2j}-\delta_{1j}p_*^{(1)}\right\rangle\mathbf{f}'\left(Z_*^{(1)}(\boldsymbol{\xi})\right)+\mathbf{d}_1\left(\delta_{2j}-\delta_{1j}p_t^{(1)}\right)g_1'\left(Z_t^{(1)}(\boldsymbol{\xi})\right)\Big] & (\boldsymbol{\xi}\in S_1),\\ 2\operatorname{Re}\Big[\mathbf{B}_2\left\langle\delta_{2j}-\delta_{1j}p_*^{(2)}\right\rangle\mathbf{f}'\left(Z_*^{(2)}(\boldsymbol{\xi})\right)+\mathbf{d}_2\left(\delta_{2j}-\delta_{1j}p_t^{(2)}\right)g_2'\left(Z_t^{(2)}(\boldsymbol{\xi})\right)\Big] & (\boldsymbol{\xi}\in S_2)\end{cases}= \tag{72}$$

$$=\tilde{\boldsymbol{\sigma}}_j^{\infty}(\boldsymbol{\xi})+\int_\Gamma\Big[\mathbf{D}_j^{\mathrm{bm}}(\mathbf{x},\boldsymbol{\xi})\tilde{\mathbf{t}}(\mathbf{x})-\mathbf{S}_j^{\mathrm{bm}}(\mathbf{x},\boldsymbol{\xi})\tilde{\mathbf{u}}(\mathbf{x})+\mathbf{q}_j^{\mathrm{bm}}(\mathbf{x},\boldsymbol{\xi})\theta(\mathbf{x})+\mathbf{w}_j^{\mathrm{bm}}(\mathbf{x},\boldsymbol{\xi})h_n(\mathbf{x})\Big]d\Gamma(\mathbf{x}).$$

The kernels in Eq. (72) are defined as,

$\mathbf{x}\in S_1\wedge\boldsymbol{\xi}\in S_1$:

$$\mathbf{D}_j^{\mathrm{bm}}(\mathbf{x},\boldsymbol{\xi})=-\frac{1}{\pi}\operatorname{Im}\left\{\mathbf{B}_1\left[\left\langle\frac{\delta_{2j}-\delta_{1j}p_*^{(1)}}{Z_*^{(1)}(\mathbf{x}-\boldsymbol{\xi})}\right\rangle\mathbf{A}_1^{\mathrm{T}}+\sum_{\beta=1}^{5}\left\langle\frac{\delta_{2j}-\delta_{1j}p_*^{(1)}}{\overline{Z}_\beta^{(1)}(\mathbf{x})-Z_*^{(1)}(\boldsymbol{\xi})}\right\rangle\mathbf{G}_1^{(1)}\mathbf{I}_\beta\overline{\mathbf{A}}_1^{\mathrm{T}}\right]\right\};$$

$$\mathbf{S}_j^{\mathrm{bm}}(\mathbf{x},\boldsymbol{\xi})=\frac{1}{\pi}\operatorname{Im}\left\{\mathbf{B}_1\left\langle\delta_{2j}-\delta_{1j}p_*^{(1)}\right\rangle\left[\left\langle\frac{n_2(\mathbf{x})-p_*^{(1)}n_1(\mathbf{x})}{\left[Z_*^{(1)}(\mathbf{x}-\boldsymbol{\xi})\right]^2}\right\rangle\mathbf{B}_1^{\mathrm{T}}+\right.\right.$$

$$\left.\left.+\sum_{\beta=1}^{5}\left\langle\frac{n_2(\mathbf{x})-\overline{p}_\beta^{(1)}n_1(\mathbf{x})}{\left[\overline{Z}_\beta^{(1)}(\mathbf{x})-Z_*^{(1)}(\boldsymbol{\xi})\right]^2}\right\rangle\mathbf{G}_1^{(1)}\mathbf{I}_\beta\overline{\mathbf{B}}_1^{\mathrm{T}}\right]\right\};$$

$$\mathbf{q}_j^{\mathrm{bm}}(\mathbf{x},\boldsymbol{\xi})=\frac{1}{\pi}\operatorname{Im}\left\{\mathbf{B}_1\left[\left\langle\frac{\delta_{2j}-\delta_{1j}p_*^{(1)}}{Z_*^{(1)}(\mathbf{x}-\boldsymbol{\xi})}\right\rangle\left(\boldsymbol{\lambda}_1n_2(\mathbf{x})-\boldsymbol{\rho}_1n_1(\mathbf{x})\right)+\right.\right.$$

$$+\sum_{\beta=1}^{4}\left\langle\frac{\delta_{2j}-\delta_{1j}p_*^{(1)}}{\overline{Z}_\beta^{(1)}(\mathbf{x})-Z_*^{(1)}(\boldsymbol{\xi})}\right\rangle\mathbf{G}_1^{(1)}\mathbf{I}_\beta\left(\overline{\boldsymbol{\lambda}}_1n_2(\mathbf{x})-\overline{\boldsymbol{\rho}}_1n_1(\mathbf{x})\right)-$$

$$-\frac{1}{2}\left(n_2(\mathbf{x})-\overline{p}_t^{(1)}n_1(\mathbf{x})\right)\left\langle\frac{\delta_{2j}-\delta_{1j}p_*^{(1)}}{\overline{Z}_t^{(1)}(\mathbf{x})-Z_*^{(1)}(\boldsymbol{\xi})}\right\rangle\boldsymbol{\delta}_1^{(1)}\Big]+$$

$$\left.-\frac{\mathbf{d}_1}{2}\left(\delta_{2j}-\delta_{1j}p_t^{(1)}\right)\left[\frac{n_2(\mathbf{x})-p_t^{(1)}n_1(\mathbf{x})}{Z_t^{(1)}(\mathbf{x}-\boldsymbol{\xi})}-K\frac{n_2(\mathbf{x})-\overline{p}_t^{(1)}n_1(\mathbf{x})}{\overline{Z}_t^{(1)}(\mathbf{x})-Z_t^{(1)}(\boldsymbol{\xi})}\right]\right\};$$

$$\mathbf{w}_j^{\text{bm}}(\mathbf{x},\boldsymbol{\xi})=\frac{1}{\pi}\operatorname{Im}\Big\{\mathbf{B}_1\left\langle\delta_{2j}-\delta_{1j}p_*^{(1)}\right\rangle\Big[\left\langle\ln\left(Z_*^{(1)}(\mathbf{x}-\boldsymbol{\xi})\right)\right\rangle\boldsymbol{\mu}_1+$$

$$+\sum_{\beta=1}^{4}\left\langle\ln\left(\overline{Z}_\beta^{(1)}(\mathbf{x})-Z_*^{(1)}(\boldsymbol{\xi})\right)\right\rangle\mathbf{G}_1^{(1)}\mathbf{I}_\beta\overline{\boldsymbol{\mu}}_1-\frac{i}{2k_t^{(1)}}\left\langle\ln\left(\overline{Z}_t^{(1)}(\mathbf{x})-Z_*^{(1)}(\boldsymbol{\xi})\right)\right\rangle\boldsymbol{\delta}_1^{(1)}\Big]+$$

$$+\frac{i\mathbf{d}_1}{2k_t^{(1)}}\left(\delta_{2j}-\delta_{1j}p_t^{(1)}\right)\Big[\ln\left(Z_t^{(1)}(\mathbf{x}-\boldsymbol{\xi})\right)+K\ln\left(\overline{Z}_t^{(1)}(\mathbf{x})-Z_t^{(1)}(\boldsymbol{\xi})\right)\Big]\Big\};$$

$\mathbf{x}\in S_2\wedge\boldsymbol{\xi}\in S_1$:

$$\mathbf{D}_j^{\text{bm}}(\mathbf{x},\boldsymbol{\xi})=-\frac{1}{\pi}\operatorname{Im}\left\{\mathbf{B}_1\sum_{\beta=1}^{5}\left[\left\langle\frac{\delta_{2j}-\delta_{1j}p_*^{(1)}}{Z_\beta^{(2)}(\mathbf{x})-Z_*^{(1)}(\boldsymbol{\xi})}\right\rangle\mathbf{G}_2^{(1)}\mathbf{I}_\beta\right]\mathbf{A}_2^{\text{T}}\right\};$$

$$\mathbf{S}_j^{\text{bm}}(\mathbf{x},\boldsymbol{\xi})=\frac{1}{\pi}\operatorname{Im}\left\{\mathbf{B}_1\left\langle\delta_{2j}-\delta_{1j}p_*^{(1)}\right\rangle\sum_{\beta=1}^{5}\left[\left\langle\frac{n_2(\mathbf{x})-p_\beta^{(2)}n_1(\mathbf{x})}{\left[Z_\beta^{(2)}(\mathbf{x})-Z_*^{(1)}(\boldsymbol{\xi})\right]^2}\right\rangle\mathbf{G}_2^{(1)}\mathbf{I}_\beta\right]\mathbf{B}_2^{\text{T}}\right\};$$

$$\mathbf{q}_j^{\text{bm}}(\mathbf{x},\boldsymbol{\xi})=\frac{1}{\pi}\operatorname{Im}\left\{\mathbf{B}_1\left[\sum_{\beta=1}^{4}\left\langle\frac{\delta_{2j}-\delta_{1j}p_*^{(1)}}{Z_\beta^{(2)}(\mathbf{x})-Z_*^{(1)}(\boldsymbol{\xi})}\right\rangle\mathbf{G}_2^{(1)}\mathbf{I}_\beta\left(\boldsymbol{\lambda}_2n_2(\mathbf{x})-\boldsymbol{\rho}_2n_1(\mathbf{x})\right)-\right.\right.$$

$$-\frac{1}{2}\left(n_2(\mathbf{x})-p_t^{(2)}n_1(\mathbf{x})\right)\left\langle\frac{\delta_{2j}-\delta_{1j}p_*^{(1)}}{Z_t^{(2)}(\mathbf{x})-Z_*^{(1)}(\boldsymbol{\xi})}\right\rangle\boldsymbol{\delta}_2^{(1)}\Big]-$$

$$\left.\left.-\frac{\mathbf{d}_1}{2}(1-K)\left(\delta_{2j}-\delta_{1j}p_t^{(1)}\right)\frac{n_2(\mathbf{x})-p_t^{(2)}n_1(\mathbf{x})}{Z_t^{(2)}(\mathbf{x})-Z_t^{(1)}(\boldsymbol{\xi})}\right\};$$

$$\mathbf{w}_j^{\text{bm}}(\mathbf{x},\boldsymbol{\xi})=\frac{1}{\pi}\operatorname{Im}\left\{\mathbf{B}_1\left\langle\delta_{2j}-\delta_{1j}p_*^{(1)}\right\rangle\left[\sum_{\beta=1}^{4}\left\langle\ln\left(Z_\beta^{(2)}(\mathbf{x})-Z_*^{(1)}(\boldsymbol{\xi})\right)\right\rangle\mathbf{G}_2^{(1)}\mathbf{I}_\beta\boldsymbol{\mu}_2+\right.\right.$$

$$+\frac{i}{2k_t^{(2)}}\left\langle\ln\left(Z_t^{(2)}(\mathbf{x})-Z_*^{(1)}(\boldsymbol{\xi})\right)\right\rangle\boldsymbol{\delta}_2^{(1)}\Big]+$$

$$\left.+\frac{i\mathbf{d}_1}{2k_t^{(2)}}(1-K)\left(\delta_{2j}-\delta_{1j}p_t^{(1)}\right)\ln\left(Z_t^{(2)}(\mathbf{x})-Z_t^{(1)}(\boldsymbol{\xi})\right)\right\};$$

$\mathbf{x}\in S_1\wedge\boldsymbol{\xi}\in S_2$:

$$\mathbf{D}_j^{\text{bm}}(\mathbf{x},\boldsymbol{\xi})=\frac{1}{\pi}\operatorname{Im}\left\{\mathbf{B}_2\sum_{\beta=1}^{5}\left[\left\langle\frac{\delta_{2j}-\delta_{1j}p_*^{(2)}}{Z_\beta^{(1)}(\mathbf{x})-Z_*^{(2)}(\boldsymbol{\xi})}\right\rangle\mathbf{G}_1^{(2)}\mathbf{I}_\beta\right]\mathbf{A}_1^{\text{T}}\right\};$$

$$\mathbf{S}_j^{\text{bm}}(\mathbf{x},\boldsymbol{\xi})=-\frac{1}{\pi}\operatorname{Im}\left\{\mathbf{B}_2\left\langle\delta_{2j}-\delta_{1j}p_*^{(2)}\right\rangle\sum_{\beta=1}^{5}\left[\left\langle\frac{n_2(\mathbf{x})-p_\beta^{(1)}n_1(\mathbf{x})}{\left[Z_\beta^{(1)}(\mathbf{x})-Z_*^{(2)}(\boldsymbol{\xi})\right]^2}\right\rangle\mathbf{G}_1^{(2)}\mathbf{I}_\beta\right]\mathbf{B}_1^{\text{T}}\right\};$$

$$\mathbf{q}_j^{\mathrm{bm}}(\mathbf{x},\boldsymbol{\xi})=\frac{1}{\pi}\operatorname{Im}\left\{\mathbf{B}_2\left[-\sum_{\beta=1}^{4}\left\langle\frac{\delta_{2j}-\delta_{1j}p_*^{(2)}}{Z_\beta^{(1)}(\mathbf{x})-Z_*^{(2)}(\boldsymbol{\xi})}\right\rangle\mathbf{G}_1^{(2)}\mathbf{I}_\beta\left(\boldsymbol{\lambda}_1 n_2(\mathbf{x})-\boldsymbol{\rho}_1 n_1(\mathbf{x})\right)-\right.\right.$$

$$-\frac{1}{2}\left(n_2(\mathbf{x})-p_t^{(1)}n_1(\mathbf{x})\right)\left\langle\frac{\delta_{2j}-\delta_{1j}p_*^{(2)}}{Z_t^{(1)}(\mathbf{x})-Z_*^{(2)}(\boldsymbol{\xi})}\right\rangle\boldsymbol{\delta}_1^{(2)}\Bigg]-$$

$$\left.-\frac{\mathbf{d}_2}{2}(1+K)\left(\delta_{2j}-\delta_{1j}p_t^{(2)}\right)\frac{n_2(\mathbf{x})-p_t^{(1)}n_1(\mathbf{x})}{Z_t^{(1)}(\mathbf{x})-Z_t^{(2)}(\boldsymbol{\xi})}\right\};$$

$$\mathbf{w}_j^{\mathrm{bm}}(\mathbf{x},\boldsymbol{\xi})=\frac{1}{\pi}\operatorname{Im}\left\{\mathbf{B}_2\left\langle\delta_{2j}-\delta_{1j}p_*^{(2)}\right\rangle\left[-\sum_{\beta=1}^{4}\left\langle\ln\left(Z_\beta^{(1)}(\mathbf{x})-Z_*^{(2)}(\boldsymbol{\xi})\right)\right\rangle\mathbf{G}_1^{(2)}\mathbf{I}_\beta\boldsymbol{\mu}_1+\right.\right.$$

$$+\frac{i}{2k_t^{(1)}}\left\langle\ln\left(Z_t^{(1)}(\mathbf{x})-Z_*^{(2)}(\boldsymbol{\xi})\right)\right\rangle\boldsymbol{\delta}_1^{(2)}\Bigg]+$$

$$\left.+\frac{i\mathbf{d}_2}{2k_t^{(1)}}(1+K)\left(\delta_{2j}-\delta_{1j}p_t^{(2)}\right)\ln\left(Z_t^{(1)}(\mathbf{x})-Z_t^{(2)}(\boldsymbol{\xi})\right)\right\};$$

$\mathbf{x}\in S_2\wedge\boldsymbol{\xi}\in S_2$:

$$\mathbf{D}_j^{\mathrm{bm}}(\mathbf{x},\boldsymbol{\xi})=-\frac{1}{\pi}\operatorname{Im}\left\{\mathbf{B}_2\left[\left\langle\frac{\delta_{2j}-\delta_{1j}p_*^{(2)}}{Z_*^{(2)}(\mathbf{x}-\boldsymbol{\xi})}\right\rangle\mathbf{A}_2^{\mathrm{T}}-\sum_{\beta=1}^{5}\left\langle\frac{\delta_{2j}-\delta_{1j}p_*^{(2)}}{\overline{Z}_\beta^{(2)}(\mathbf{x})-Z_*^{(2)}(\boldsymbol{\xi})}\right\rangle\mathbf{G}_2^{(2)}\mathbf{I}_\beta\overline{\mathbf{A}}_2^{\mathrm{T}}\right]\right\};$$

$$\mathbf{S}_j^{\mathrm{bm}}(\mathbf{x},\boldsymbol{\xi})=\frac{1}{\pi}\operatorname{Im}\left\{\mathbf{B}_2\left\langle\delta_{2j}-\delta_{1j}p_*^{(2)}\right\rangle\left[\left\langle\frac{n_2(\mathbf{x})-p_*^{(2)}n_1(\mathbf{x})}{Z_*^{(2)}(\mathbf{x}-\boldsymbol{\xi})}\right\rangle\mathbf{B}_2^{\mathrm{T}}-\right.\right.$$

$$\left.\left.-\sum_{\beta=1}^{5}\left\langle\frac{n_2(\mathbf{x})-\overline{p}_\beta^{(2)}n_1(\mathbf{x})}{\overline{Z}_\beta^{(2)}(\mathbf{x})-Z_*^{(2)}(\boldsymbol{\xi})}\right\rangle\mathbf{G}_2^{(2)}\mathbf{I}_\beta\overline{\mathbf{B}}_2^{\mathrm{T}}\right]\right\}.$$

$$\mathbf{q}_j^{\mathrm{bm}}(\mathbf{x},\boldsymbol{\xi})=\frac{1}{\pi}\operatorname{Im}\left\{\mathbf{B}_2\left[\left\langle\frac{\delta_{2j}-\delta_{1j}p_*^{(2)}}{Z_*^{(2)}(\mathbf{x}-\boldsymbol{\xi})}\right\rangle\left(\boldsymbol{\lambda}_2 n_2(\mathbf{x})-\boldsymbol{\rho}_2 n_1(\mathbf{x})\right)-\right.\right.$$

$$-\sum_{\beta=1}^{4}\left\langle\frac{\delta_{2j}-\delta_{1j}p_*^{(2)}}{\overline{Z}_\beta^{(2)}(\mathbf{x})-Z_*^{(2)}(\boldsymbol{\xi})}\right\rangle\mathbf{G}_2^{(2)}\mathbf{I}_\beta\left(\overline{\boldsymbol{\lambda}}_2 n_2(\mathbf{x})-\overline{\boldsymbol{\rho}}_2 n_1(\mathbf{x})\right)-$$

$$-\frac{1}{2}\left(n_2(\mathbf{x})-\overline{p}_t^{(2)}n_1(\mathbf{x})\right)\left\langle\frac{\delta_{2j}-\delta_{1j}p_*^{(2)}}{\overline{Z}_t^{(2)}(\mathbf{x})-Z_*^{(2)}(\boldsymbol{\xi})}\right\rangle\boldsymbol{\delta}_2^{(2)}\Bigg]-$$

$$\left.-\frac{\mathbf{d}_2}{2}\left(\delta_{2j}-\delta_{1j}p_t^{(2)}\right)\left[\frac{n_2(\mathbf{x})-p_t^{(2)}n_1(\mathbf{x})}{Z_t^{(2)}(\mathbf{x}-\boldsymbol{\xi})}+K\frac{n_2(\mathbf{x})-\overline{p}_t^{(2)}n_1(\mathbf{x})}{\overline{Z}_t^{(2)}(\mathbf{x})-Z_t^{(2)}(\boldsymbol{\xi})}\right]\right\};$$

$$\mathbf{w}_j^{\mathrm{bm}}(\mathbf{x},\boldsymbol{\xi}) = \frac{1}{\pi}\operatorname{Im}\Big\{\mathbf{B}_2\Big\langle\delta_{2j} - \delta_{1j}p_*^{(2)}\Big\rangle\Big[\Big\langle\ln\big(Z_*^{(2)}(\mathbf{x}-\boldsymbol{\xi})\big)\Big\rangle\boldsymbol{\mu}_2 -$$

$$-\sum_{\beta=1}^{4}\Big\langle\ln\big(\overline{Z}_\beta^{(2)}(\mathbf{x}) - Z_*^{(2)}(\boldsymbol{\xi})\big)\Big\rangle\mathbf{G}_2^{(2)}\mathbf{I}_\beta\overline{\boldsymbol{\mu}}_2 - \frac{i}{2k_t^{(2)}}\Big\langle\ln\big(\overline{Z}_t^{(2)}(\mathbf{x}) - Z_*^{(2)}(\boldsymbol{\xi})\big)\Big\rangle\boldsymbol{\delta}_2^{(2)}\Big] +$$

$$+\frac{i\mathbf{d}_2}{2k_t^{(2)}}\big(\delta_{2j} - \delta_{1j}p_t^{(2)}\big)\Big[\ln\big(Z_t^{(2)}(\mathbf{x}-\boldsymbol{\xi})\big) - K\ln\big(\overline{Z}_t^{(2)}(\mathbf{x}) - Z_t^{(2)}(\boldsymbol{\xi})\big)\Big]\Big\}. \tag{73}$$

The functions $\tilde{\mathbf{u}}^{\infty}(\boldsymbol{\xi})$ and $\tilde{\boldsymbol{\sigma}}_j^{\infty}(\boldsymbol{\xi})$ define the influence of the remote load and are related to the homogeneous parts of the Stroh complex functions through the following expressions:

$$\tilde{\mathbf{u}}_{\infty}(\boldsymbol{\xi}) = \begin{cases} 2\operatorname{Re}\Big[\mathbf{A}_1\mathbf{f}_{\infty}^{(1)}\big(Z_*^{(1)}(\boldsymbol{\xi})\big) + \mathbf{c}_1 g_{1\infty}\big(Z_t^{(1)}(\boldsymbol{\xi})\big)\Big] & (\forall\boldsymbol{\xi}\in S_1), \\ 2\operatorname{Re}\Big[\mathbf{A}_2\mathbf{f}_{\infty}^{(2)}\big(Z_*^{(2)}(\boldsymbol{\xi})\big) + \mathbf{c}_2 g_{2\infty}\big(Z_t^{(2)}(\boldsymbol{\xi})\big)\Big] & (\forall\boldsymbol{\xi}\in S_2); \end{cases}$$

$$\tilde{\boldsymbol{\sigma}}_j(\boldsymbol{\xi}) = \begin{cases} 2\operatorname{Re}\Big[\mathbf{B}_1\Big\langle\delta_{2j} - \delta_{1j}p_*^{(1)}\Big\rangle\mathbf{f}_{\infty}'\big(Z_*^{(1)}(\boldsymbol{\xi})\big) + \mathbf{d}_1\big(\delta_{2j} - \delta_{1j}p_t^{(1)}\big)g_{1\infty}'\big(Z_t^{(1)}(\boldsymbol{\xi})\big)\Big] & (\boldsymbol{\xi}\in S_1), \\ 2\operatorname{Re}\Big[\mathbf{B}_2\Big\langle\delta_{2j} - \delta_{1j}p_*^{(2)}\Big\rangle\mathbf{f}_{\infty}'\big(Z_*^{(2)}(\boldsymbol{\xi})\big) + \mathbf{d}_2\big(\delta_{2j} - \delta_{1j}p_t^{(2)}\big)g_{2\infty}'\big(Z_t^{(2)}(\boldsymbol{\xi})\big)\Big] & (\boldsymbol{\xi}\in S_2). \end{cases}$$

The kernels $\mathbf{U}^{\mathrm{bm}}(\mathbf{x},\boldsymbol{\xi})$ and $\mathbf{T}^{\mathrm{bm}}(\mathbf{x},\boldsymbol{\xi})$ given by Eq. (71) coincide with the corresponding fundamental solutions obtained for an anisotropic electroelastic bimaterial in Refs. [17, 19]. Other kernels for the thermoelectroelastic bimaterial defined by Eqs. (71) and (73) are obtained for the first time.

2.4. Relations between the kernels and fundamental solutions of thermoelectroelasticity

It is easy to verify that the kernels (33) of heat conduction integral formulae correspond to Green's functions for steady-state heat conduction in a bimaterial composite solid [21]. This fact verifies these equations. The same verification can be provided for thermoelectroelastic integral formulae.

Pasternak et al. [13] using the reciprocity approach derived extended Somigliana identity for plane thermoelectroelasticity, and proved that the matrix transpose of the kernel $\mathbf{U}(\mathbf{x},\boldsymbol{\xi})$ corresponds to the extended displacement field caused by the action of the extended concentrated force applied at the point $\mathbf{x}$; and the kernel $\mathbf{v}(\mathbf{x},\boldsymbol{\xi})$ defines the extended displacement at the point $\boldsymbol{\xi}$ induced by a unit line heat drain applied at the point $\mathbf{x}$. Regarding the generality of the given proof [13], the same should concern a bimaterial thermoelectroelastic solid. Thus, the proof of the corresponding relations for a thermoelectroelastic bimaterial can serve as an additional verification of the obtained integral formulae.

Direct comparison of the kernel $\mathbf{U}^{\mathrm{bm}}(\mathbf{x},\boldsymbol{\xi})$ with a corresponding fundamental solution for an electroelastic bimaterial given in Refs. [17, 19] proves that this kernel is identical to the Green's function for an infinite bimaterial. Unfortunately, in

derivation of the fundamental solutions of thermoelectroelasticity for the action of a unit line heat source (which corresponds to the kernel $\mathbf{v}^{\mathrm{bm}}(\mathbf{x},\boldsymbol{\xi})$) Qin [10] does not account for the stress and displacement continuity conditions for arbitrary closed curve enclosing the heat source [13], therefore, the fundamental solution of Ref. [10] is incomplete. Thus, it is necessary to prove, that the function $\mathbf{v}^{\mathrm{bm}}(\mathbf{x},\boldsymbol{\xi})$ given by Eq. (71) is the Green's function for a thermoelectroelastic bimaterial.

To proceed with this, first consider that a line heat drain is located in the domain S_1, i.e. $\mathbf{x}\in S_1$. Thus, according to Eqs. (4), (33) and (71), consider the following Stroh complex functions

$$\begin{aligned}
\mathbf{f}_{11}\left(z_*^{(1)}\right) &= \frac{1}{2\pi i}\left[-\left\langle f^*\left(\tau_*^{(1)}-z_*^{(1)}\right)\right\rangle\boldsymbol{\mu}_1-\sum_{\beta}\left\langle f^*\left(\overline{\tau}_*^{(1)}-z_*^{(1)}\right)\right\rangle\mathbf{G}_1^{(1)}\mathbf{I}_\beta\overline{\boldsymbol{\mu}}_1+\right.\\
&\qquad\left.+\frac{i}{2k_t^{(1)}}\left\langle f^*\left(\overline{\tau}_t^{(1)}-z_*^{(1)}\right)\right\rangle\boldsymbol{\delta}_1^{(1)}\right];\\
g_{11}\left(z_t^{(1)}\right) &= \frac{1}{2\pi i}\left[-\frac{i}{2k_t^{(1)}}\left(f^*\left(\tau_t^{(1)}-z_t^{(1)}\right)+Kf^*\left(\overline{\tau}_t^{(1)}-z_t^{(1)}\right)\right)\right];\\
\mathbf{f}_{12}\left(z_*^{(2)}\right) &= \frac{1}{2\pi i}\left[\sum_{\beta}\left\langle f^*\left(\tau_\beta^{(1)}-z_*^{(2)}\right)\right\rangle\mathbf{G}_1^{(2)}\mathbf{I}_\beta\boldsymbol{\mu}_1-\frac{i}{2k_t^{(1)}}\left\langle f^*\left(\tau_t^{(1)}-z_*^{(2)}\right)\right\rangle\boldsymbol{\delta}_1^{(2)}\right];\\
g_{12}\left(z_t^{(2)}\right) &= \frac{1}{2\pi i}\left[-\frac{i(1+K)}{2k_t^{(1)}}f^*\left(\tau_t^{(1)}-z_t^{(2)}\right)\right].
\end{aligned}\tag{74}$$

Assuming that $z_*^{(j)}=Z_*^{(j)}(\boldsymbol{\xi})$, $\tau_*^{(j)}=Z_*^{(j)}(\mathbf{x})$, and substituting Eq. (74) into Eq. (4) one obtains the extended displacement field similar to that given for the case $\mathbf{x}\in S_1$ by the kernel $\mathbf{v}(\mathbf{x},\boldsymbol{\xi})$ from Eq. (71). Thus, according to [13], the Stroh complex functions (74), as well as the kernel $\mathbf{v}(\mathbf{x},\boldsymbol{\xi})$, should correspond to the fundamental solution for a unit line heat drain located inside the domain $\mathbf{v}(\mathbf{x},\boldsymbol{\xi})$. The proof of this statement is presented below.

One can see from Eq. (74) that the Stroh complex functions $\mathbf{f}_{12}\left(z_*^{(2)}\right)$ and $g_{12}\left(z_t^{(2)}\right)$ are continuous in the entire domain S_2. As we traverse an arbitrary closed path enclosing the point $\tau_t^{(1)}\sim\mathbf{x}$ the function $g_{11}'\left(z_t^{(1)}\right)$ obtains the following increment:

$$g_{11}'\left(z_t^{(1)}\mathrm{e}^{2\pi i}\right)-g_{11}'\left(z_t^{(1)}\right)=\frac{i}{2k_t^{(1)}}.\tag{75}$$

Thus, according to Eqs. (4) and (75), the temperature θ is continuous along the arbitrary closed contour enclosing the point $\mathbf{x}$, and the heat flux function ϑ increase at

$$\vartheta\left(z^{(1)}\mathrm{e}^{2\pi i}\right)-\vartheta\left(z^{(1)}\right)=2k_t^{(1)}\,\mathrm{Im}\left[g_{11}'\left(z_t^{(1)}\mathrm{e}^{2\pi i}\right)-g_{11}'\left(z_t^{(1)}\right)\right]=1,\tag{76}$$

therefore, according to Eq. (4), this testifies the presence of a unit heat drain at the point $\mathbf{x}$.

Besides, accounting for the identity $k_t^{(2)}(1+K)=k_t^{(1)}(1-K)$, the temperature and heat flux function defined by the complex functions g_{11} and g_{12} in accordance with Eq. (4) are continuous at transition through the bimaterial interface. Therefore, the functions g_{11} and g_{12} define the fundamental solution of heat conductivity for a bimaterial. According to Eq. (4), one can also verify that these functions also define the kernels (33) of heat conductivity.

Due to the physical considerations the extended displacement and stress fields caused by a unit heat drain should be continuous both at the bimaterial interface and at the arbitrary closed contour enclosing the line heat drain (or source). Therefore, one should prove that the field defined by the complex functions (74) satisfies these conditions.

The function $f^*\left(Z_*(\mathbf{x})-Z_*(\boldsymbol{\xi})\right)$ gains an increment of $-2\pi ir$ as one traverse a closed contour enclosing the heat drain at the point $\mathbf{x}$. Therefore, according to Eqs. (4), (8), (49) and (74), one obtains

$$\begin{aligned}
&\tilde{\mathbf{u}}\left(z^{(1)}\mathrm{e}^{2\pi i}\right)-\tilde{\mathbf{u}}\left(z^{(1)}\right)=2r\,\mathrm{Re}\left[\mathbf{A}_1\boldsymbol{\mu}_1+\frac{i\mathbf{c}_1}{2k_t^{(1)}}\right]=0,\\
&\tilde{\boldsymbol{\varphi}}\left(z^{(1)}\mathrm{e}^{2\pi i}\right)-\tilde{\boldsymbol{\varphi}}\left(z^{(1)}\right)=2r\,\mathrm{Re}\left[\mathbf{B}_1\boldsymbol{\mu}_1+\frac{i\mathbf{d}_1}{2k_t^{(1)}}\right]=0.
\end{aligned} \tag{77}$$

According to Eqs. (8), (49), (64) and (67), the following relations can be obtained for the complex constants included in Eq. (74):

$$\begin{aligned}
&\bar{\mathbf{A}}_1\bar{\mathbf{G}}_1^{(1)}-\mathbf{A}_2\mathbf{G}_1^{(2)}-\mathbf{A}_1=0,\quad \bar{\mathbf{A}}_1\bar{\boldsymbol{\delta}}_1^{(1)}+\mathbf{A}_2\boldsymbol{\delta}_1^{(2)}-\mathbf{c}_1-K\overline{\mathbf{c}}_1+\mathbf{c}_2(1+K)=0,\\
&\bar{\mathbf{A}}_2\bar{\mathbf{G}}_2^{(2)}-\mathbf{A}_1\mathbf{G}_2^{(1)}+\mathbf{A}_2=0,\quad \bar{\mathbf{A}}_2\bar{\boldsymbol{\delta}}_2^{(2)}+\mathbf{A}_1\boldsymbol{\delta}_2^{(1)}-\mathbf{c}_2+K\overline{\mathbf{c}}_1+\mathbf{c}_1(1-K)=0,\\
&\bar{\mathbf{B}}_1\bar{\mathbf{G}}_1^{(1)}-\mathbf{B}_2\mathbf{G}_1^{(2)}-\mathbf{B}_1=0,\quad \bar{\mathbf{B}}_1\bar{\boldsymbol{\delta}}_1^{(1)}+\mathbf{B}_2\boldsymbol{\delta}_1^{(2)}-\mathbf{d}_1-K\overline{\mathbf{d}}_1+\mathbf{d}_2(1+K)=0,\\
&\bar{\mathbf{B}}_2\bar{\mathbf{G}}_2^{(2)}-\mathbf{B}_1\mathbf{G}_2^{(1)}+\mathbf{B}_2=0,\quad \bar{\mathbf{B}}_2\bar{\boldsymbol{\delta}}_2^{(2)}+\mathbf{B}_1\boldsymbol{\delta}_2^{(1)}-\mathbf{d}_2+K\overline{\mathbf{d}}_1+\mathbf{d}_1(1-K)=0.
\end{aligned} \tag{78}$$

Thus, based on Eqs. (4), (74) and (78), for $\xi_2=0$ one obtains

$$\begin{aligned}
&\tilde{\mathbf{u}}^{(1)}(\xi_1)-\tilde{\mathbf{u}}^{(2)}(\xi_1)=2\,\mathrm{Re}\left[\mathbf{A}_1\mathbf{f}_{11}(\xi_1)-\mathbf{A}_2\mathbf{f}_{12}(\xi_1)+\mathbf{c}_1g_{11}(\xi_1)-\mathbf{c}_2g_{12}(\xi_1)\right]=\\
&\quad=\frac{1}{\pi}\mathrm{Im}\left[\left(\bar{\mathbf{A}}_1\bar{\mathbf{G}}_1^{(1)}-\mathbf{A}_2\mathbf{G}_1^{(2)}-\mathbf{A}_1\right)\left\langle f^*\left(\tau_*^{(1)}-\xi_1\right)\right\rangle\boldsymbol{\mu}_1\right]+\\
&\quad+\frac{1}{2\pi k_t^{(1)}}\mathrm{Re}\left[\left(\bar{\mathbf{A}}_1\bar{\boldsymbol{\delta}}_1^{(1)}+\mathbf{A}_2\boldsymbol{\delta}_1^{(2)}-\mathbf{c}_1-K\overline{\mathbf{c}}_1+\mathbf{c}_2(1+K)\right)f^*\left(\tau_t^{(1)}-\xi_1\right)\right]=\mathbf{0},\\
&\tilde{\boldsymbol{\varphi}}^{(1)}(\xi_1)-\tilde{\boldsymbol{\varphi}}^{(2)}(\xi_1)=2\,\mathrm{Re}\left[\mathbf{B}_1\mathbf{f}_{11}(\xi_1)-\mathbf{B}_2\mathbf{f}_{12}(\xi_1)+\mathbf{d}_1g_{11}(\xi_1)-\mathbf{d}_2g_{12}(\xi_1)\right]=\\
&\quad=\frac{1}{\pi}\mathrm{Im}\left[\left(\bar{\mathbf{B}}_1\bar{\mathbf{G}}_1^{(1)}-\mathbf{B}_2\mathbf{G}_1^{(2)}-\mathbf{B}_1\right)\left\langle f^*\left(\tau_*^{(1)}-\xi_1\right)\right\rangle\boldsymbol{\mu}_1\right]+\\
&\quad+\frac{1}{2\pi k_t^{(1)}}\mathrm{Re}\left[\left(\bar{\mathbf{B}}_1\bar{\boldsymbol{\delta}}_1^{(1)}+\mathbf{B}_2\boldsymbol{\delta}_1^{(2)}-\mathbf{d}_1-K\overline{\mathbf{d}}_1+\mathbf{d}_2(1+K)\right)f^*\left(\tau_t^{(1)}-\xi_1\right)\right]=\mathbf{0}.
\end{aligned} \tag{79}$$

Eqs. (76), (77) and (79) prove that the Stroh complex functions (74), as well as the kernel $\mathbf{v}(\mathbf{x},\boldsymbol{\xi})$ given by Eq. (71), define the fundamental solution for a thermoelectroelastic bimaterial containing a unit line heat drain at the point $\mathbf{x}\in S_2$. Besides, it is easy to verify that the fundamental solution given by Eqs. (3.45)–(3.48)

of Ref. [10] does not satisfy continuity conditions (77), therefore, the latter is incomplete.

According to Eq. (79) thermoelectroelastic Green's functions are continuous at transition through the bimaterial interface, therefore, the special case that a source point and a field point are both located at the interface can be treated without any restrictions.

2.5. Action of internal body forces, electric charges and distributed heat

Assume that concentrated forces $\mathbf{F}^k$ and free electric charges q^k are applied at the points $\mathbf{x}^{k*}$ of a thermoelectroelastic medium. According to notations used in Eq. (3), these internal factors can be described by the following extended vector: $\tilde{\mathbf{F}}^k = \left[\mathbf{F}^k, -q^k\right]^{\mathrm{T}}$. The action of these factors can be accounted for in Eqs. (70) and (72) by introduction of the additional opened contour Γ_F that passes through the points $\mathbf{x}^{k*}$ and does not cross the curves Γ. Since the action of concentrated forces and free electric charges does not cause the discontinuities of displacement, electric potential, temperature and heat flux, therefore, $\Delta\tilde{\mathbf{u}}(\mathbf{x}) = 0$, $\Delta\theta(\mathbf{x}) = 0$, $\Sigma h_n(\mathbf{x}) = 0 \quad \forall \mathbf{x} \in \Gamma_F$, where $\Sigma(\bullet) = (\bullet)^+ + (\bullet)^-$, $\Delta(\bullet) = (\bullet)^+ - (\bullet)^-$, and signs "+" and "–" denote functions concerned with faces Γ_F^+ and Γ_F^- of the mathematical cut Γ_F.

Thus, the discontinuities of stress and electric displacement $\Sigma\tilde{\mathbf{t}}$ at Γ_F are zero except the points $\mathbf{x}^{k*}$ of the curve Γ_F, where the extended stress function gains the increment of $\tilde{\mathbf{F}}^k$. Therefore,

$$\Sigma\tilde{\mathbf{t}}(\mathbf{x}) = \sum_k \tilde{\mathbf{F}}^k \delta\left(\mathbf{x} - \mathbf{x}^{k*}\right) \quad \forall \mathbf{x} \in \Gamma_F, \tag{80}$$

where $\delta\left(\mathbf{x} - \mathbf{x}^{k*}\right)$ is the Dirac delta-function. Accounting for the rules of integration of generalized functions, based on Eqs. (70), (72) and (80) one can obtain the terms, which should be added to the right-hand sides of Eqs. (70), (72) in a case of action of concentrated forces and free electric charges

$$\tilde{\mathbf{u}}^F(\boldsymbol{\xi}) = \sum_k \mathbf{U}^{\mathrm{bm}}\left(\mathbf{x}^{k*}, \boldsymbol{\xi}\right)\tilde{\mathbf{F}}^k, \quad \tilde{\boldsymbol{\sigma}}_j^F(\boldsymbol{\xi}) = \sum_k \mathbf{D}_j^{\mathrm{bm}}\left(\mathbf{x}^{k*}, \boldsymbol{\xi}\right)\tilde{\mathbf{F}}^k. \tag{81}$$

Assume that besides electric and mechanical load, the line heat sources h^{*k} are applied at the points $\mathbf{x}^{k*}$ of a thermoelectroelastic bimaterial. As well as in the case of action of the concentrated forces, one can consider an additional contour Γ_h, which passes through the points $\mathbf{x}^{k*}$ and does not cross the curves Γ. Since the action of the concentrated heat sources does not induce any discontinuities of displacements, electric potential, stress, electric displacement and temperature in a continuous solid, therefore, $\Delta\tilde{\mathbf{u}}(\mathbf{x}) = 0$, $\Sigma\tilde{\mathbf{t}}(\mathbf{x}) = 0$, $\Delta\theta(\mathbf{x}) = 0 \quad \forall \mathbf{x} \in \Gamma_h$. Nevertheless, the heat flux function gains an increment of h^{*k} at the points $\mathbf{x}^{k*}$. Therefore, the heat flux discontinuity function at the curve Γ_h is equal to $\Sigma h_n = -\sum_k h^{*k}\delta\left(\mathbf{x} - \mathbf{x}^{k*}\right) \quad \forall \mathbf{x} \in \Gamma_h$. A minus sign in the right hand side of the last equation is caused by the selected direction of a normal $\mathbf{n} = \mathbf{n}^+$ to a contour Γ_h. Accounting for the rules of integration of the generalized

functions, one can obtain the following terms, which in the case of action of line heat sources are to be added to Eqs. (31), (32) of heat conductivity:

$$\theta^h(\xi) = -\sum_k h^{*k}\Theta^{\mathrm{bm}*}\left(\mathbf{x}^{k*},\xi\right), \quad h_j^h(\xi) = -\sum_k h^{*k}\Theta_j^{\mathrm{bm}**}\left(\mathbf{x}^{k*},\xi\right), \tag{82}$$

and to Eqs. (70), (72) of thermoelectroelasticity:

$$\tilde{\mathbf{u}}^h(\xi) = -\sum_k h^{*k}\mathbf{v}^{\mathrm{bm}}\left(\mathbf{x}^{k*},\xi\right), \quad \tilde{\boldsymbol{\sigma}}_j^h(\xi) = -\sum_k h^{*k}\mathbf{w}_j^{\mathrm{bm}}\left(\mathbf{x}^{k*},\xi\right). \tag{83}$$

If the distributed volume forces, electric charges or heat sources are present, their influence can be accounted for, when one rewrites Eqs. (81)–(83) in the following way

$$\begin{aligned}
&\theta^{\mathrm{in.l.}}(\xi) = -\iint_{S_0}\Theta^{\mathrm{bm}*}(\mathbf{x},\xi)f_h(\mathbf{x})dS_0(\mathbf{x}), \quad h_j^{\mathrm{in.l.}}(\xi) = -\iint_{S_0}\Theta_j^{\mathrm{bm}**}(\mathbf{x},\xi)f_h(\mathbf{x})dS_0(\mathbf{x}),\\
&\tilde{\mathbf{u}}^{\mathrm{in.l.}}(\xi) = \iint_{S_0}\left(\mathbf{U}^{\mathrm{bm}}(\mathbf{x},\xi)\tilde{\mathbf{f}}(\mathbf{x}) - \mathbf{v}^{\mathrm{bm}}(\mathbf{x},\xi)f_h(\mathbf{x})\right)dS_0(\mathbf{x}),\\
&\tilde{\boldsymbol{\sigma}}_j^{\mathrm{in.l.}}(\xi) = \iint_{S_0}\left(\mathbf{D}_j^{\mathrm{bm}}(\mathbf{x},\xi)\tilde{\mathbf{f}}(\mathbf{x}) - \mathbf{w}_j^{\mathrm{bm}}(\mathbf{x},\xi)f_h(\mathbf{x})\right)dS_0(\mathbf{x}).
\end{aligned} \tag{84}$$

Thus, the integral identities (31), (32), (70) and (72) are generalized to account for the internal load:

$$\theta(\xi) = \theta^{\infty}(\xi) + \theta^{\mathrm{in.l.}}(\xi) + \int_\Gamma\left[\Theta^{\mathrm{bm}*}(\mathbf{x},\xi)h_n(\mathbf{x}) - H^{\mathrm{bm}*}(\mathbf{x},\xi)\theta(\mathbf{x})\right]ds(\mathbf{x}), \tag{85}$$

$$h_i(\xi) = h_i^{\infty}(\xi) + h_i^{\mathrm{in.l.}}(\xi) + \int_\Gamma\left[\Theta_i^{\mathrm{bm}**}(\mathbf{x},\xi)h_n(\mathbf{x}) - H_i^{\mathrm{bm}**}(\mathbf{x},\xi)\theta(\mathbf{x})\right]ds(\mathbf{x}), \tag{86}$$

$$\begin{aligned}
\tilde{\mathbf{u}}(\xi) &= \tilde{\mathbf{u}}^{\infty}(\xi) + \tilde{\mathbf{u}}^{\mathrm{in.l.}}(\xi) +\\
&+ \int_\Gamma\left[\mathbf{U}^{\mathrm{bm}}(\mathbf{x},\xi)\tilde{\mathbf{t}}(\mathbf{x}) - \mathbf{T}^{\mathrm{bm}}(\mathbf{x},\xi)\tilde{\mathbf{u}}(\mathbf{x}) + \mathbf{r}^{\mathrm{bm}}(\mathbf{x},\xi)\theta(\mathbf{x}) + \mathbf{v}^{\mathrm{bm}}(\mathbf{x},\xi)h_n(\mathbf{x})\right]ds(\mathbf{x}),
\end{aligned} \tag{87}$$

$$\begin{aligned}
\tilde{\boldsymbol{\sigma}}_j(\xi) &= \tilde{\boldsymbol{\sigma}}_j^{\infty}(\xi) + \tilde{\boldsymbol{\sigma}}_j^{\mathrm{in.l.}}(\xi) +\\
&+ \int_\Gamma\left[\mathbf{D}_j^{\mathrm{bm}}(\mathbf{x},\xi)\tilde{\mathbf{t}}(\mathbf{x}) - \mathbf{S}_j^{\mathrm{bm}}(\mathbf{x},\xi)\tilde{\mathbf{u}}(\mathbf{x}) + \mathbf{q}_j^{\mathrm{bm}}(\mathbf{x},\xi)\theta(\mathbf{x}) + \mathbf{w}_j^{\mathrm{bm}}(\mathbf{x},\xi)h_n(\mathbf{x})\right]ds(\mathbf{x}).
\end{aligned} \tag{88}$$

The functions $\tilde{\mathbf{f}}(\mathbf{x})$ and $f_h(\mathbf{x})$ describe extended body force vector and internal heat volume density distributed in the local domain S_0 of a thermoelectroelastic bimaterial solid.

2.6. Derivation of the Stroh complex functions that define the homogeneous solution

Assume that a thermoelectroelastic bimaterial is heated (or cooled) by a certain temperature θ_0 with respect to the reference temperature. According to [13, 15], in this case the complex functions of heat conduction are as follows

$$g_{1\infty}\left(z_t^{(1)}\right) = \frac{1}{2}\theta_0 z_t^{(1)}, \quad g_{2\infty}\left(z_t^{(2)}\right) = \frac{1}{2}\theta_0 z_t^{(2)}. \tag{89}$$

According to Eq. (4), the complex functions (89) satisfy boundary conditions (12) at the bimaterial interface. To satisfy the boundary conditions (13) the Stroh complex functions can be written as,

$$\mathbf{f}_{\infty}^{(1)}\left(z_*^{(1)}\right) = \left\langle z_*^{(1)}\right\rangle\left(\mathbf{A}_1^{\mathrm{T}}\mathbf{s}_a^{(1)} + \mathbf{B}_1^{\mathrm{T}}\mathbf{s}_b^{(1)}\right), \quad \mathbf{f}_{\infty}^{(2)}\left(z_*^{(2)}\right) = \left\langle z_*^{(2)}\right\rangle\left(\mathbf{A}_2^{\mathrm{T}}\mathbf{s}_a^{(2)} + \mathbf{B}_2^{\mathrm{T}}\mathbf{s}_b^{(2)}\right), \tag{90}$$

where the constant real vectors $\mathbf{s}_a^{(1)}$, $\mathbf{s}_b^{(1)}$, $\mathbf{s}_a^{(2)}$, and $\mathbf{s}_b^{(2)}$ are to be determined.

According to Eqs. (4), (89) and (90), boundary conditions (13) produce the following system of linear algebraic equations

$$\begin{aligned} &2\,\mathrm{Re}\left[\mathbf{A}_1\left(\mathbf{A}_1^{\mathrm{T}}\mathbf{s}_a^{(1)}+\mathbf{B}_1^{\mathrm{T}}\mathbf{s}_b^{(1)}\right)+\frac{1}{2}\mathbf{c}_1\theta_0\right]=2\,\mathrm{Re}\left[\mathbf{A}_2\left(\mathbf{A}_2^{\mathrm{T}}\mathbf{s}_a^{(2)}+\mathbf{B}_2^{\mathrm{T}}\mathbf{s}_b^{(2)}\right)+\frac{1}{2}\mathbf{c}_2\theta_0\right],\\ &2\,\mathrm{Re}\left[\mathbf{B}_1\left(\mathbf{A}_1^{\mathrm{T}}\mathbf{s}_a^{(1)}+\mathbf{B}_1^{\mathrm{T}}\mathbf{s}_b^{(1)}\right)+\frac{1}{2}\mathbf{d}_1\theta_0\right]=2\,\mathrm{Re}\left[\mathbf{B}_2\left(\mathbf{A}_2^{\mathrm{T}}\mathbf{s}_a^{(2)}+\mathbf{B}_2^{\mathrm{T}}\mathbf{s}_b^{(2)}\right)+\frac{1}{2}\mathbf{d}_2\theta_0\right]. \end{aligned} \tag{91}$$

Using the orthogonality relations (8), the system of equations (91) can be reduced to

$$\mathbf{s}_b^{(1)}+\mathrm{Re}\left[\mathbf{c}_1\right]\theta_0=\mathbf{s}_b^{(2)}+\mathrm{Re}\left[\mathbf{c}_2\right]\theta_0,\quad \mathbf{s}_a^{(1)}+\mathrm{Re}\left[\mathbf{d}_1\right]\theta_0=\mathbf{s}_a^{(2)}+\mathrm{Re}\left[\mathbf{d}_2\right]\theta_0. \tag{92}$$

According to Eqs. (4), (89), (90) and (92), at the remote points of the domains S_1 and S_2:

$$\begin{aligned} \tilde{\boldsymbol{\sigma}}_1^{(j)\infty}&=-2\,\mathrm{Re}\left[\mathbf{B}_j\mathbf{P}_j\left(\mathbf{A}_j^{\mathrm{T}}\mathbf{s}_a^{(j)}+\mathbf{B}_j^{\mathrm{T}}\mathbf{s}_b^{(j)}\right)+\frac{1}{2}\mathbf{d}_j p_t^{(j)}\theta_0\right]=\\ &=-2\,\mathrm{Re}\left[\mathbf{B}_j\mathbf{P}_j\mathbf{A}_j^{\mathrm{T}}\right]\mathbf{s}_a^{(j)}-2\,\mathrm{Re}\left[\mathbf{B}_j\mathbf{P}_j\mathbf{B}_j^{\mathrm{T}}\right]\mathbf{s}_b^{(j)}-\mathrm{Re}\left[\mathbf{d}_j p_t^{(j)}\right]\theta_0,\\ \tilde{\boldsymbol{\sigma}}_2^{(j)\infty}&=2\,\mathrm{Re}\left[\mathbf{B}_j\left(\mathbf{A}_j^{\mathrm{T}}\mathbf{s}_a^{(j)}+\mathbf{B}_j^{\mathrm{T}}\mathbf{s}_b^{(j)}\right)+\frac{1}{2}\mathbf{d}_j\theta_0\right]=\\ &=2\,\mathrm{Re}\left[\mathbf{B}_j\mathbf{A}_j^{\mathrm{T}}\right]\mathbf{s}_a^{(j)}+2\,\mathrm{Re}\left[\mathbf{B}_j\mathbf{B}_j^{\mathrm{T}}\right]\mathbf{s}_b^{(j)}+\mathrm{Re}\left[\mathbf{d}_j\right]\theta_0\quad\left(\measuredangle_j\right). \end{aligned} \tag{93}$$

According to Ref. [19],

$$2\,\mathrm{Re}\left[\mathbf{B}_j\mathbf{P}_j\mathbf{A}_j^{\mathrm{T}}\right]=\left[\mathbf{N}_1^{(j)}\right]^{\mathrm{T}},\quad 2\,\mathrm{Re}\left[\mathbf{B}_j\mathbf{P}_j\mathbf{B}_j^{\mathrm{T}}\right]=\mathbf{N}_3^{(j)},\quad 2\,\mathrm{Re}\left[\mathbf{B}_j\mathbf{A}_j^{\mathrm{T}}\right]=\mathbf{I},\quad \mathrm{Re}\left[\mathbf{B}_j\mathbf{B}_j^{\mathrm{T}}\right]=\mathbf{0},$$

therefore, Eq. (93) writes as,

$$\mathbf{s}_a^{(j)}=\tilde{\boldsymbol{\sigma}}_2^{(j)\infty}-\mathrm{Re}\left[\mathbf{d}_j\right]\theta_0,\quad \mathbf{N}_3^{(j)}\mathbf{s}_b^{(j)}=-\tilde{\boldsymbol{\sigma}}_1^{(j)\infty}-\left[\mathbf{N}_1^{(j)}\right]^{\mathrm{T}}\mathbf{s}_a^{(j)}-\mathrm{Re}\left[\mathbf{d}_j p_t^{(j)}\right]\theta_0\quad\left(\measuredangle_j\right). \tag{94}$$

Thus, for a uniformly heated (or cooled) bimaterial the mechanical and electric load $\tilde{\boldsymbol{\sigma}}_1^{\infty}$ and $\tilde{\boldsymbol{\sigma}}_2^{\infty}$ at the infinity should satisfy the conditions (92) and (94). In particular, accounting for the second equation in (92) and the first one in (94), the following equality should hold: $\tilde{\boldsymbol{\sigma}}_2^{1\infty}=\tilde{\boldsymbol{\sigma}}_2^{2\infty}$.

According to Ref. [19], the matrix $\mathbf{N}_3$ is a singular one (the second row is zero-vector), therefore, for determination of the vectors $\mathbf{s}_b^{(j)}$ except Eq. (94) one should use some additional conditions, in particular, one can assume that the rigid rotation of one of the domains S_1 or S_2 is equal to zero.

2.7. Derivation of the boundary integral equations for a thermoelectroelastic bimaterial

It is obvious that boundary conditions at the contours Γ define only a half of functions $\theta(\mathbf{x})$, $h_n(\mathbf{x})$, $\tilde{\mathbf{u}}(\mathbf{x})$ and $\tilde{\mathbf{t}}(\mathbf{x})$ $(\forall\mathbf{x}\in\Gamma)$. However, according to Eqs. (85)–(88), it is necessary to know all of these functions to calculate the temperature, heat flux, extended displacement and stress at an arbitrary point of a bimaterial. To determine unknown boundary functions one should approach the interior point to the boundary one at the contours Γ to obtain boundary integral equations of the problem. The complex variable analysis used in this chapter allows direct obtaining of these

boundary integral equations by means of the Sokhotskii-Plemelj formula. The latter relates the limit value of the Cauchy integral with its principal value. In instance, for a smooth closed curve Γ the Sokhotskii-Plemelj formula writes as [20]

$$\lim_{z\to\tau_0}\frac{1}{2\pi i}\int_\Gamma\frac{\phi(\tau)\,d\tau}{\tau-z}=\frac{1}{2}\phi(\tau_0)+\frac{1}{2\pi i}\mathrm{CPV}\int_\Gamma\frac{\phi(\tau)\,d\tau}{\tau-\tau_0}, \tag{95}$$

where it is assumed that the point z approaches to the boundary point τ_0 placed at Γ from inside the domain; CPV stands for the Cauchy Principal Value of an integral.

Thus, according to Eqs. (85)–(88) and (95), for smooth closed contours Γ inside the thermoelectroelastic bimaterial one can obtain the following boundary integral equations to determine unknown boundary functions:

$$\begin{aligned}
&\frac{1}{2}\theta(\mathbf{y})=\theta^{\infty}(\xi)+\theta^{\mathrm{in.l.}}(\xi)+\mathrm{RPV}\int_\Gamma\Theta^{\mathrm{hs}*}(\mathbf{x},\mathbf{y})h_n(\mathbf{x})\,ds(\mathbf{x})-\mathrm{CPV}\int_\Gamma H^{\mathrm{hs}*}(\mathbf{x},\mathbf{y})\theta(\mathbf{x})\,ds(\mathbf{x}),\\
&\frac{1}{2}\tilde{\mathbf{u}}(\mathbf{y})=\tilde{\mathbf{u}}^{\infty}(\xi)+\tilde{\mathbf{u}}^{\mathrm{in.l.}}(\xi)+\mathrm{RPV}\int_\Gamma\mathbf{U}^{\mathrm{hs}}(\mathbf{x},\mathbf{y})\tilde{\mathbf{t}}(\mathbf{x})\,ds(\mathbf{x})-\mathrm{CPV}\int_\Gamma\mathbf{T}^{\mathrm{hs}}(\mathbf{x},\mathbf{y})\tilde{\mathbf{u}}(\mathbf{x})\,ds(\mathbf{x})+\\
&\quad+\mathrm{RPV}\int_\Gamma\mathbf{r}^{\mathrm{hs}}(\mathbf{x},\mathbf{y})\theta(\mathbf{x})\,ds(\mathbf{x})+\int_\Gamma\mathbf{v}^{\mathrm{hs}}(\mathbf{x},\mathbf{y})h_n(\mathbf{x})\,ds(\mathbf{x}),
\end{aligned} \tag{96}$$

where RPV stands for a Riemann improper integral (Riemann Principal Value).

Nevertheless, boundary integral equations (96) degenerate, when some of closed contours Γ_j of a line Γ transform into the faces of the mathematical cuts Γ_{Cj} (simple opened arcs). Therefore, for this case it is necessary to develop a system of dual boundary integral equations. The latter can be derived within the framework of the complex variable analysis based on the following holomorphy theorem for piecewise-analytic functions [20]:

$$\frac{1}{2}\Sigma\phi(\tau_0)=\frac{1}{2\pi i}\left[\mathrm{CPV}\int_{\Gamma_C}\frac{\Delta\phi(\tau)}{\tau-\tau_0}d\tau+\int_\Gamma\frac{\phi(\tau)}{\tau-\tau_0}d\tau\right]\quad\forall\,\tau_0\in\Gamma_C, \tag{97}$$

where $\Sigma(\bullet)=(\bullet)^+ +(\bullet)^-$, $\Delta(\bullet)=(\bullet)^+ -(\bullet)^-$; $\Gamma_C=\bigcup_j\Gamma_{Cj}$ is a set of opened contours in a complex plane; signs "+" and "–" denote functions concerned with faces Γ_C^+ and Γ_C^- of the mathematical cuts Γ_C.

Based on Eqs. (85)–(88) and (97) one can obtain the following system of dual boundary integral equations for a thermoelectroelastic bimaterial:

- collocation point $\mathbf{y}$ is placed at the smooth segment of the closed contour Γ:

$$\begin{aligned}
&\frac{1}{2}\theta(\mathbf{y})=\theta^{\infty}(\xi)+\theta^{\mathrm{in.l.}}(\xi)+\mathrm{RPV}\int_\Gamma\Theta^{\mathrm{hs}*}(\mathbf{x},\mathbf{y})h_n(\mathbf{x})\,ds(\mathbf{x})-\\
&\quad-\mathrm{CPV}\int_\Gamma H^{\mathrm{hs}*}(\mathbf{x},\mathbf{y})\theta(\mathbf{x})\,ds(\mathbf{x})+\int_{\Gamma_C}\left[\Theta^{\mathrm{hs}*}(\mathbf{x},\mathbf{y})\Sigma h_n(\mathbf{x})-H^{\mathrm{hs}*}(\mathbf{x},\mathbf{y})\Delta\theta(\mathbf{x})\right]ds(\mathbf{x}),\\
&\frac{1}{2}\tilde{\mathbf{u}}(\mathbf{y})=\tilde{\mathbf{u}}^{\infty}(\xi)+\tilde{\mathbf{u}}^{\mathrm{in.l.}}(\xi)+\mathrm{RPV}\int_\Gamma\mathbf{U}^{\mathrm{hs}}(\mathbf{x},\mathbf{y})\tilde{\mathbf{t}}(\mathbf{x})\,ds(\mathbf{x})-\mathrm{CPV}\int_\Gamma\mathbf{T}^{\mathrm{hs}}(\mathbf{x},\mathbf{y})\tilde{\mathbf{u}}(\mathbf{x})\,ds(\mathbf{x})+\\
&\quad+\mathrm{RPV}\int_\Gamma\mathbf{r}^{\mathrm{hs}}(\mathbf{x},\mathbf{y})\theta(\mathbf{x})\,ds(\mathbf{x})+\int_\Gamma\mathbf{v}^{\mathrm{hs}}(\mathbf{x},\mathbf{y})h_n(\mathbf{x})\,ds(\mathbf{x})+\\
&\quad+\int_{\Gamma_C}\left[\mathbf{U}^{\mathrm{hs}}(\mathbf{x},\mathbf{y})\Sigma\tilde{\mathbf{t}}(\mathbf{x})-\mathbf{T}^{\mathrm{hs}}(\mathbf{x},\mathbf{y})\Delta\tilde{\mathbf{u}}(\mathbf{x})+\mathbf{r}^{\mathrm{hs}}(\mathbf{x},\mathbf{y})\Delta\theta(\mathbf{x})+\mathbf{v}^{\mathrm{hs}}(\mathbf{x},\mathbf{y})\Sigma h_n(\mathbf{x})\right]ds(\mathbf{x});
\end{aligned} \tag{98}$$

- collocation point $\mathbf{y}$ is placed at the smooth segment of the opened line Γ_C:

$$\frac{1}{2}\Sigma\theta(\mathbf{y}) = \theta^{\infty}(\boldsymbol{\xi}) + \theta^{\text{in.l.}}(\boldsymbol{\xi}) + \text{RPV}\int_{\Gamma_C}\Theta^{\text{hs*}}(\mathbf{x},\mathbf{y})\Sigma h_n(\mathbf{x})\,ds(\mathbf{x}) -$$
$$-\text{CPV}\int_{\Gamma_C}H^{\text{hs*}}(\mathbf{x},\mathbf{y})\Delta\theta(\mathbf{x})\,ds(\mathbf{x}) + \int_{\Gamma}\left[\Theta^{\text{hs*}}(\mathbf{x},\mathbf{y})h_n(\mathbf{x}) - H^{\text{hs*}}(\mathbf{x},\mathbf{y})\theta(\mathbf{x})\right]ds(\mathbf{x}),$$

$$\frac{1}{2}\Delta h_n(\mathbf{y}) = n_i(\mathbf{y})\left[h_i^{\infty}(\boldsymbol{\xi}) + h_i^{\text{in.l.}}(\boldsymbol{\xi}) + \text{CPV}\int_{\Gamma_C}\Theta_i^{\text{hs**}}(\mathbf{x},\mathbf{y})\Sigma h_n(\mathbf{x})\,d\Gamma(\mathbf{x}) -\right.$$
$$\left.-\text{HPV}\int_{\Gamma_C}H_i^{\text{hs**}}(\mathbf{x},\mathbf{y})\Delta\theta(\mathbf{x})\,ds(\mathbf{x}) + \int_{\Gamma}\left[\Theta_i^{\text{hs**}}(\mathbf{x},\mathbf{y})h_n(\mathbf{x}) - H_i^{\text{hs**}}(\mathbf{x},\mathbf{y})\theta(\mathbf{x})\right]d\Gamma(\mathbf{x})\right],$$

$$\frac{1}{2}\Sigma\tilde{\mathbf{u}}(\mathbf{y}) = \tilde{\mathbf{u}}^{\infty}(\boldsymbol{\xi}) + \tilde{\mathbf{u}}^{\text{in.l.}}(\boldsymbol{\xi}) + \text{RPV}\int_{\Gamma_C}\mathbf{U}^{\text{hs}}(\mathbf{x},\mathbf{y})\Sigma\tilde{\mathbf{t}}(\mathbf{x})\,ds(\mathbf{x}) - \text{CPV}\int_{\Gamma_C}\mathbf{T}^{\text{hs}}(\mathbf{x},\mathbf{y})\Delta\tilde{\mathbf{u}}(\mathbf{x})\,ds(\mathbf{x}) +$$
$$+\text{RPV}\int_{\Gamma_C}\mathbf{r}^{\text{hs}}(\mathbf{x},\mathbf{y})\Delta\theta(\mathbf{x})\,ds(\mathbf{x}) + \int_{\Gamma_C}\mathbf{v}^{\text{hs}}(\mathbf{x},\mathbf{y})\Sigma h_n(\mathbf{x})\,ds(\mathbf{x}) +$$
$$+\int_{\Gamma}\left[\mathbf{U}^{\text{hs}}(\mathbf{x},\mathbf{y})\tilde{\mathbf{t}}(\mathbf{x}) - \mathbf{T}^{\text{hs}}(\mathbf{x},\mathbf{y})\tilde{\mathbf{u}}(\mathbf{x}) + \mathbf{r}^{\text{hs}}(\mathbf{x},\mathbf{y})\theta(\mathbf{x}) + \mathbf{v}^{\text{hs}}(\mathbf{x},\mathbf{y})h_n(\mathbf{x})\right]ds(\mathbf{x}),$$

$$\frac{1}{2}\Delta\tilde{\mathbf{t}}(\mathbf{y}) = n_j^{+}(\mathbf{y})\left[\tilde{\boldsymbol{\sigma}}_j^{\infty}(\boldsymbol{\xi}) + \tilde{\boldsymbol{\sigma}}_j^{\text{in.l.}}(\boldsymbol{\xi}) + \text{CPV}\int_{\Gamma_C}\mathbf{D}_j^{\text{hs}}(\mathbf{x},\mathbf{y})\Sigma\tilde{\mathbf{t}}(\mathbf{x})\,ds(\mathbf{x}) -\right.$$
$$-\text{HPV}\int_{\Gamma_C}\mathbf{S}_j^{\text{hs}}(\mathbf{x},\mathbf{y})\Delta\tilde{\mathbf{u}}(\mathbf{x})\,ds(\mathbf{x}) +$$
$$+\text{CPV}\int_{\Gamma_C}\mathbf{q}_j^{\text{hs}}(\mathbf{x},\mathbf{y})\Delta\theta(\mathbf{x})\,ds(\mathbf{x}) + \text{RPV}\int_{\Gamma_C}\mathbf{w}_j^{\text{hs}}(\mathbf{x},\mathbf{y})\Sigma h_n(\mathbf{x})\,ds(\mathbf{x}) +$$
$$\left.+\int_{\Gamma}\left[\mathbf{D}_j^{\text{hs}}(\mathbf{x},\mathbf{y})\tilde{\mathbf{t}}(\mathbf{x}) - \mathbf{S}_j^{\text{hs}}(\mathbf{x},\mathbf{y})\tilde{\mathbf{u}}(\mathbf{x}) + \mathbf{q}_j^{\text{hs}}(\mathbf{x},\mathbf{y})\theta(\mathbf{x}) + \mathbf{w}_j^{\text{hs}}(\mathbf{x},\mathbf{y})h_n(\mathbf{x})\right]ds(\mathbf{x})\right], \tag{99}$$

where HPV stands for the Hadamard Principal Value (finite part) of an integral.

The system of dual boundary integral equations (98), (99) accompanied with the models of thin thermoelectroelastic inclusions [13], which can be presented within the following functional dependences

$$\begin{aligned}&\Sigma\theta(\mathbf{y}) = F^{\theta}\left(\mathbf{y},\Sigma h_n,\Delta\theta\right), \quad \Delta h_n(\mathbf{y}) = F^{h}\left(\mathbf{y},\Sigma h_n,\Delta\theta\right),\\ &\Sigma\tilde{\mathbf{u}}(\mathbf{y}) = \mathbf{F}^{u}\left(\mathbf{y},\Sigma\tilde{\mathbf{t}},\Delta\tilde{\mathbf{u}},\Sigma\theta,\Delta\theta\right), \quad \Delta\tilde{\mathbf{t}}(\mathbf{y}) = \mathbf{F}^{t}\left(\mathbf{y},\Sigma\tilde{\mathbf{t}},\Delta\tilde{\mathbf{u}},\Sigma\theta,\Delta\theta\right)\end{aligned} \tag{100}$$

allow to consider 2D problems for a thermoelectroelastic half-space containing holes, cracks and thin inclusions. The boundary element approach developed in Ref. [18] can be easily adopted for the numerical solution of these problems.

According to [13, 18], the strength of the fields' singularity at tips of a thin inhomogeneity is described by generalized stress and electric displacement intensity factors (SEDIF), which are determined through the discontinuity functions in the local rectangular coordinate system with the origin at the tip of an inhomogeneity by the following formulae

$$\tilde{\mathbf{k}}^{(1)} = \lim_{s\to 0}\sqrt{\frac{\pi}{8s}}\mathbf{L}\cdot\Delta\tilde{\mathbf{u}}(s), \quad \tilde{\mathbf{k}}^{(2)} = -\lim_{s\to 0}\sqrt{\frac{\pi s}{2}}\Sigma\tilde{\mathbf{t}}(s), \tag{101}$$

where $\tilde{\mathbf{k}}^{(1)} = \left[K_{21}, K_{11}, K_{31}, K_{41}\right]^{\mathrm{T}}$, $\tilde{\mathbf{k}}^{(2)} = \left[K_{12}^{(2)}, K_{22}^{(2)}, K_{32}, K_{42}\right]^{\mathrm{T}}$; K_{ij} are the generalized SEDIF. For a crack $K_{11} = K_{\mathrm{I}}$, $K_{21} = K_{\mathrm{II}}$, $K_{31} = K_{\mathrm{III}}$, $K_{41} = K_{\mathrm{IV}} \equiv K_D$, and $\tilde{\mathbf{k}}^{(2)} = \mathbf{0}$, where K_{I}, K_{II}, K_{III}, $K_{\mathrm{IV}} \equiv K_D$ are classical SEDIF of the cracks theory [10]; $\mathbf{L} = -2\sqrt{-1}\mathbf{B}\mathbf{B}^{\mathrm{T}}$ is a real Barnett–Lothe tensor [10].

Two first components $K_{12}^{(2)}$ and $K_{22}^{(2)}$ of the generalized SEDIF vector $\tilde{\mathbf{k}}^{(2)}$ are denoted with a superscript to distinguish them from the generalized stress intensity factors K_{12} and K_{22} of thin elastic inclusions introduced by Sulym [22] for elastic problems. The factors K_{12} and K_{22} are determined based on the components of the vector $\tilde{\mathbf{k}}^{(2)}$ through the following formula [18]

$$k_i^{(2)} = S_{ji}\tilde{k}_j^{(2)} \quad (i = 1,2;\ j = 1,..,4), \tag{102}$$

where $\mathbf{k}^{(2)} = \left[K_{22}, K_{12}\right]^{\mathrm{T}}$ is a vector of generalized stress intensity factors; $\mathbf{S} = \sqrt{-1}\left(2\mathbf{A}\mathbf{B}^{\mathrm{T}} - \mathbf{I}\right)$ is the second real Barnett–Lothe tensor [10].

Extended stress function and displacement vector in the local coordinate system with the origin at the inclusion tip and Ox_1 axis directed along a median line are related to the generalized SEDIF by the following asymptotic formulae [13, 18]:

$$\tilde{\boldsymbol{\varphi}} = \sqrt{\frac{2}{\pi}}\,\mathrm{Im}\left\{\mathbf{B}\left\langle\sqrt{Z_*}\right\rangle\left(\sqrt{-1}\mathbf{B}^{-1}\tilde{\mathbf{k}}^{(1)} - 2\mathbf{A}^{\mathrm{T}}\tilde{\mathbf{k}}^{(2)}\right)\right\}; \tag{103}$$

$$\tilde{\mathbf{u}} = \sqrt{\frac{2}{\pi}}\,\mathrm{Im}\left\{\mathbf{A}\left\langle\sqrt{Z_*}\right\rangle\left(\sqrt{-1}\mathbf{B}^{-1}\tilde{\mathbf{k}}^{(1)} - 2\mathbf{A}^{\mathrm{T}}\tilde{\mathbf{k}}^{(2)}\right)\right\}. \tag{104}$$

Thus, the generalized SEDIF completely characterize the asymptotic field of stress and electric displacement near the tips of cracks and thin inclusions.

Introducing the generalized heat flux intensity factors with the formulae

$$K_{h1} = -\lim_{s\to 0}\sqrt{\frac{\pi}{8s}}k_t\Delta\theta(s), \quad K_{h2} = -\lim_{s\to 0}\sqrt{\frac{\pi s}{2}}\Sigma h_n(s), \tag{105}$$

similarly to the abovementioned one can obtain the following one-term asymptotic relations for the temperature change and heat flux function at the vicinity of the tip of a thin inhomogeneity:

$$\vartheta = \sqrt{\frac{2}{\pi}}\,\mathrm{Im}\left\{\left(\sqrt{-1}K_{h1} - K_{h2}\right)\sqrt{Z_t}\right\}; \quad \theta = \frac{1}{k_t}\sqrt{\frac{2}{\pi}}\,\mathrm{Im}\left\{\left(K_{h1} + \sqrt{-1}K_{h2}\right)\sqrt{Z_t}\right\}. \tag{106}$$

2.8. Numerical examples

2.8.1. Verification of the obtained equations

To verify the developed approach, consider an infinite medium made of two isotropic half-spaces with the shear moduli G_1 and G_2, and Poisson ratios ν_1 and ν_2, respectively. Without loss in generality, in numerical calculations it was assumed that $\nu_1 = \nu_2 = 0{,}3$. The elastic moduli C_{ijkm} of each half-space are calculated based on the values of G and ν under the assumption of plane stress [17, 19]. At the infinity of the upper half-space the uniform stress $\sigma_{11}^{(1)\infty} = \sigma^{(1)}$ acts, and the stress

$\sigma_{11}^{(2)\infty} \equiv \sigma^{(2)} = G_2 / G_1 \sigma^{(1)}$ is applied to the lower one. The medium contains a crack of length $2a$, which is perpendicular to the bimaterial interface (**Fig. 2**). This defect is modeled by a thin inclusion of very small rigidity ($G^{\mathrm{i}} = 10^{-10} G_1$).

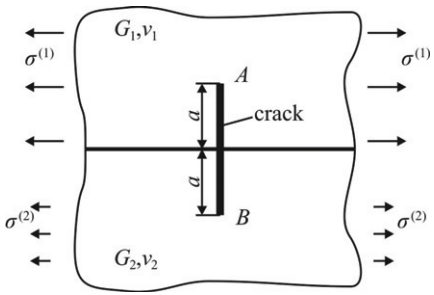

Fig. 2. A crack perpendicular to the bimaterial interface

Table 1 compares SIFs obtained based on the volume force approach [23], single domain boundary element method [2] and the present boundary element approach. One can observe good agreement of data obtained with these approaches that proves the reliability and also the efficiency of the proposed boundary element method, since only 20 three-node boundary elements, including two special that model a square-root singularity at the crack tips, are used to mesh the crack.

Since the authors did not find any numeric or analytic reliable results of the study of thin inclusions in thermoelectroelastic bimaterials, the developed approach was verified in this case based on the analysis of an infinite thermoelectroelastic space and a half-space containing thin inhomogeneities. The integral equations of these problems can be obtained from the derived one taking the limit values of thermo-electro-elastic constants of one of the materials, which compose a bimaterial solid. This analysis resulted in perfect agreement of the obtained data with the known solutions [13, 16] for an infinite space and a half-space with thin inclusions.

Table 1. SIFs of a crack perpendicular to the bimaterial interface

G_2 / G_1	Ref. [23]		Ref. [2]		Present approach	
	$\frac{K_{\mathrm{I}}^A}{\sigma^{(1)}\sqrt{\pi a}}$	$\frac{K_{\mathrm{I}}^B}{\sigma^{(2)}\sqrt{\pi a}}$	$\frac{K_{\mathrm{I}}^A}{\sigma^{(1)}\sqrt{\pi a}}$	$\frac{K_{\mathrm{I}}^B}{\sigma^{(2)}\sqrt{\pi a}}$	$\frac{K_{\mathrm{I}}^A}{\sigma^{(1)}\sqrt{\pi a}}$	$\frac{K_{\mathrm{I}}^B}{\sigma^{(2)}\sqrt{\pi a}}$
0.1	1.062	1.153	1.063	1.156	1.063	1.154
0.3	1.015	1.064	1.016	1.066	1.016	1.065
0.5	1.000	1.028	1.001	1.029	1.001	1.029
0.8	0.997	1.006	0.998	1.007	0.997	1.006

2.8.2. Uniform heat at the crack parallel to the bimaterial interface

Consider a thermoelectroelastic bimaterial consisting of two half-spaces made of barium titanate $BaTiO_3$ ($x_2 > 0$) and cadmium selenide CdSe ($x_2 < 0$), which are both

polarized along the Ox_2 axis. According to Refs. [24, 25], in this case the thermoelectroelastic properties of these materials are as follows:

$BaTiO_3$:

- elastic moduli (GPa): $C_{11} = C_{33} = 150$; $C_{22} = 146$; $C_{12} = C_{13} = C_{23} = 66$; $C_{44} = C_{66} = 44$; $C_{55} = 42$;
- piezoelectric constants (C/m^2): $e_{21} = e_{23} = -4.35$; $e_{22} = 17.5$; $e_{16} = e_{34} = 11.4$;
- dielectric constants (nF/m): $\kappa_{11} = 9.86775$; $\kappa_{22} = 11.151$;
- heat conduction coefficients (W/(m·K)): $k_{11} = k_{22} = 2.5$;
- thermal expansion coefficients (K^{-1}): $\alpha_{11} = 8.53 \cdot 10^{-6}$; $\alpha_{22} = 1.99 \cdot 10^{-6}$;
- pyroelectric constants (GV/(m·K)): $\lambda_2 = 13.3 \cdot 10^{-6}$;

CdSe:

- elastic moduli (GPa): $C_{11} = C_{33} = 74.1$; $C_{22} = 83.6$; $C_{12} = C_{23} = 39.3$; $C_{13} = 45.2$; $C_{44} = C_{66} = 13.17$; $C_{55} = 14.45$;
- piezoelectric constants (C/m^2): $e_{21} = e_{23} = -0.160$; $e_{22} = 0.347$; $e_{16} = e_{34} = -0.138$;
- dielectric constants (nF/m): $\kappa_{11} = 0.0826$; $\kappa_{22} = 0.0903$;
- heat conduction coefficients (W/(m·K)): $k_{11} = 1$; $k_{22} = 2.5$ (*since there is no available data in the literature, these coefficients are chosen such that they provide anisotropy of heat conduction in different directions and are of the same order of magnitude as the corresponding coefficients of barium titanate*);
- thermal moduli (MPa/K): $\beta_{11} = \beta_{33} = 0.621$; $\beta_{22} = 0.551$;
- pyroelectric coefficients ($C/(m^2 \cdot K)$): $\chi_2 = -2.94 \times 10^{-6}$.

A crack of length $2a$ is parallel to the bimaterial interface. The crack faces are loaded with a uniform heat flux h_0 such that $\Delta h_n = 2h_0$ and $\Sigma h_n = 0$ at the crack. **Figure 3** depicts the normalized SEDIF at the right crack tip versus the distance d between the crack and the bimaterial interface. Negative values of d correspond to the case of the crack lying at the bottom half-space. The normalization coefficients are determined based on the applied load, linear dimensions, thermal moduli and pyroelectric constants through the following dependences: $K_\sigma^0 = h_0 a \sqrt{\pi a} \beta_{11}^{(1)} / k_{11}^{(1)}$, $K_D^0 = h_0 a \sqrt{\pi a} \chi_2^{(1)} / k_{11}^{(1)}$.

The SEDIF of a crack placed far from the bimaterial interface are close to those obtained for a crack in the infinite homogeneous medium [13] and agree with the particular analytic solutions for a thermoelastic anisotropic medium [17]. This additionally verifies the validity of the derived boundary integral equations and the boundary element approach based on them.

As a crack approaches the bimaterial interface the SIF K_I increases in its magnitude. Moreover, as a crack is placed in the $BaTiO_3$ half-space the SIF K_I is positive at both tips, which testifies that the crack opens. Instead, when the crack is placed near the bimaterial interface in the cadmium selenide half-space, the SIF K_I is negative at both tips. This behavior testifies that this problem should be considered separately with the account of contact of crack faces.

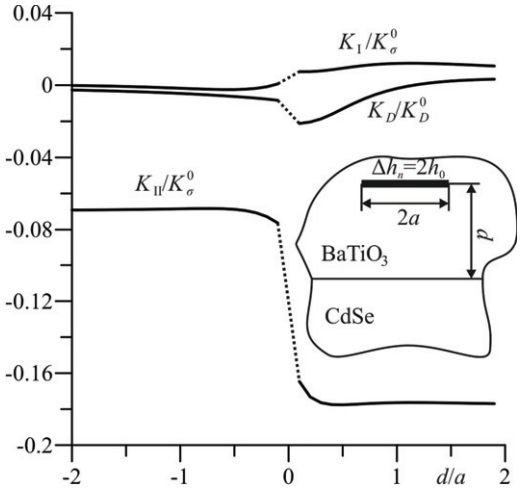

Fig. 3. SEDIF of a crack in the bimaterial under the action of a uniform heat distributed at its faces

However, the EDIF K_D gains the most intensive change with the approach to the bimaterial interface. It is natural, since the dielectric constants of top and bottom half-spaces differ by two orders of magnitude.

2.8.3. Elastic inclusion that crosses the bimaterial interface

Consider a $BaTiO_3$ – CdSe bimaterial containing a thin isotropic elastic inclusion of length $2a$ and thickness $2h$ ($h = 0.01a$), which perpendicularly crosses the bimaterial interface. The relative rigidity of the inclusion is defined by the equation $\mu = G^{\mathrm{i}} / C_{66}^{(1)}$, where G^{i} is a shear modulus of the inclusion's material. The inclusion is assumed not to expand due to the temperature change. Two opposite heat sources of a magnitude q are applied at the points $(0, 2a)$ and $(0, -2a)$. **Figure 4** depicts the generalized SEDIF at both tips of the inclusion in their dependence on the relative rigidity μ. Four types of inclusions are considered depending on their electric permeability and heat conduction. The normalization factors for the generalized SEDIF obtained for the action of concentrated heat are defined as $K_\sigma^1 = q\sqrt{\pi a}\,\beta_{11}^{(1)} / k_{11}^{(1)}$, $K_D^1 = q\sqrt{\pi a}\,\chi_2^{(1)} / k_{11}^{(1)}$.

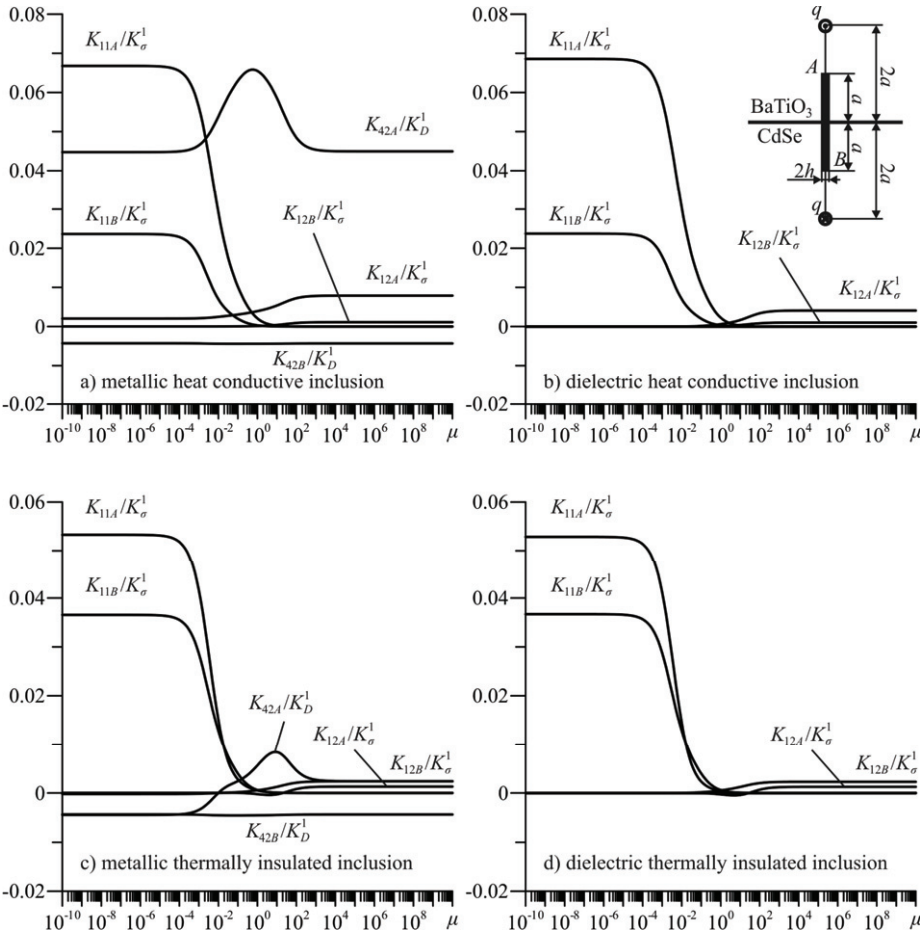

Fig. 4. Generalized SEDIF of a thin elastic inclusion, which perpendicularly crosses the bimaterial interface

One can see in Fig. 4 that the generalized SIF K_{11} at the tip A of soft inclusions ($\mu < 1$) is greater for heat conductive inclusions comparing to thermally insulated ones. In contrast, generalized SIF K_{11} at the tip B demonstrates an opposite behavior. Thus, the change in the heat conduction coefficients of the inclusion causes the redistribution of the normal stress intensity at both of its tips.

For an electricity-conductive (metallic) inclusion the generalized EDIF K_{42} possesses greatest values at the tip A. It is natural, since the tip A is placed at the barium titanate half-space, which dielectric coefficients are higher by two orders of magnitude comparing to cadmium selenide. Instead, for an inclusion made of a dielectric material that does not polarize the electric displacement intensity factors are close to zero.

Another case when a thin inclusion crosses the bimaterial interface at an angle of 45° is presented in **Fig. 5**. The SIF K_{11} of an inclined soft inclusion decreases approximately twice. Instead, the generalized SIF K_{12} of an inclined rigid inclusion is higher comparing to the inclusions, which are perpendicular to the bimaterial interface.

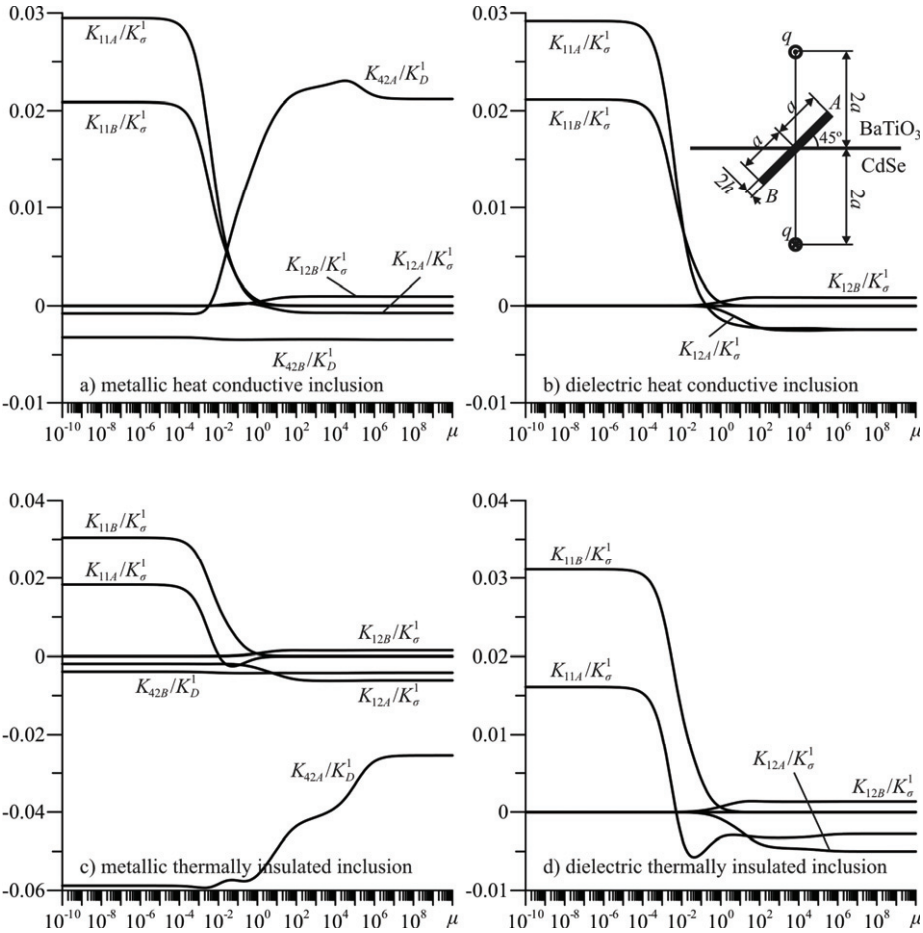

Fig. 5. Generalized SEDIF of a thin elastic inclusion crossing the bimaterial interface at an angle of 45°

The dependence of the generalized EDIF K_{42} on the relative rigidity of an inclined thin inclusion demonstrates monotonously increasing behavior. Again the nonzero values of the generalized EDIF K_{42} are observed only for metallic inclusions (or dielectric inclusions with considerable dielectric coefficients).

Conclusion

The chapter presents a strict and straightforward approach for obtaining the Somigliana type integral formulae and corresponding dual boundary integral equations for a thermoelectroelastic bimaterial. This approach is advantageous comparing to those previously used, since it does not depend on the a priori assumptions on the structure of the kernels of these integral identities. Moreover, the complex variable approach used has possible future applications in the derivation of boundary integral equations and fundamental solutions for a thermoelectroelastic strip or a medium containing holes or inclusions.

It is shown that the kernels of the obtained integral formulae correspond to the fundamental solutions of electroelasticity and thermoelectroelasticity. Thus, the complex variable approach developed also gives a straightforward technique for obtaining the 2D thermoelectroelastic Green's functions. The latter are shown to be physically correct, since they additionally satisfy extended displacement and stress continuity conditions, which yet have not been referenced for bimaterial solids. Instead, Green's functions previously obtained in literature leak those terms accounting for stress and displacement continuity due to the a priori assumptions on their structure.

Obtained boundary integral equations are introduced into the boundary element computational algorithm. The numerical analysis held proved their validity and high accuracy in calculation of the generalized stress and electric displacement intensity factors of cracks and thin inclusions. It is shown that thermo-electro-elastic properties of thin inclusions and the bimaterial sufficiently influence the intensity factors at their tips, therefore, sufficient analysis should be definitely held in the corresponding problems raised by the industrial applications.

References

[1] J.F. Nye, Physical properties of crystals: their representation by tensors and matrices, Oxford University Press, Toronto, 2006.

[2] E. Pan, B. Amadei, Boundary element analysis of fracture mechanics in anisotropic bimaterials, Eng. Anal. Bound. Elem. 23 (1999) 683–691.

[3] P.S. Yang, J.Y. Liou, J.C. Sung, Subinterface crack in an anisotropic piezoelectric bimaterial, Int. J. Sol. Struct. 45 (2008) 4990–5014.

[4] W. Tian, U. Gabbert, Parallel crack near the interface of magnetoelectroelastic bimaterials, Comp. Mat. Sci. 32 (2005) 562–567.

[5] E. Pan, F.G. Yuan, Three-dimensional Green's functions in anisotropic piezoelectric bimaterials, Int. J. Eng. Sci. 38 (2000) 1939–1960.

[6] Z.C. Ou, Y.H. Chen, Near-tip stress fields and intensity factors for an interface crack in metal/piezoelectric bimaterials, Int. J. Eng. Sci. 42 (2004) 1407–1438.

[7] C. Hwu, Thermoelastic interface crack problems in dissimilar anisotropic media, Int. J. Solids Struct. 18 (1992) 2077–2090.

[8] X. Wang, E. Pan, Thermal Green's functions in plane anisotropic bimaterials with spring-type and Kapitza-type imperfect interface, Acta Mech. 209 (2010) 115–128.

[9] Q.H. Qin, 2D Green's functions of defective magnetoelectroelastic solids under thermal loading, Eng. Anal. Bound. Elem. 29 (2005) 577–585.
[10] Q.H. Qin, Green's function and boundary elements of multifield materials, Elsevier, Oxford, 2007.
[11] Q.H. Qin, Y.W. Mai, Multiple cracks in thermoelectroelastic bimaterials, Theor. Appl. Fract. Mech. 29 (1998) 141–150.
[12] Q.H. Qin, Y.W. Mai, A closed crack tip model for interface cracks in thermopiezoelectric materials, Int. J. Sol. Struct. 36 (1999) 2463–2479.
[13] Ia. Pasternak, R. Pasternak, H. Sulym, A comprehensive study on the 2D boundary element method for anisotropic thermoelectroelastic solids with cracks and thin inhomogeneities, Eng. Anal. Bound. Elem. 37 (2013) 419–433.
[14] Ia. Pasternak, H. Sulym, Stroh formalism based boundary integral equations for 2D magnetoelectroelasticity, Eng. Anal. Bound. Elem. 37 (2013) 167–175.
[15] Ia. Pasternak, Boundary integral equations and the boundary element method for fracture mechanics analysis in 2D anisotropic thermoelasticity, Eng. Anal. Bound. Elem. 36 (2012) 1931–1941.
[16] Ia. Pasternak, R. Pasternak, H. Sulym, Boundary integral equations for 2D thermoelectroelasticity of a half-space with cracks and thin inclusions, Eng. Anal. Bound. Elem. 37 (2013) 1514–1523.
[17] C. Hwu, Anisotropic elastic plates, Springer, London, 2010.
[18] Ia. Pasternak, Coupled 2D electric and mechanical fields in piezoelectric solids containing cracks and thin inhomogeneities, Eng. Anal. Bound. Elem. 35 (2011) 678–690.
[19] T.C.T. Ting, Anisotropic elasticity: theory and applications, Oxford University Press, New York, 1996.
[20] N.I. Muskhelishvili, Singular integral equations, Dover publications, New York, 2008.
[21] J.R. Berger, J.L. Skilowitz, V.K. Tewary, Green's function for steady-state heat conduction in a bimaterial composite solid, Computational Mechanics 25 (2000) 627–634.
[22] H.T. Sulym, Bases of mathematical theory of thermo-elastic equilibrium of solids containing thin inclusions, Research and Publishing center of NTSh, Lviv, 2007. (in Ukrainian)
[23] M. Isida, H. Noguchi, Plane elastostatic problems of bonded dissimilar materials with an interface crack and arbitrarily located cracks, Trans. Jap. Soc. Mech. Engng. 49 (1983) 137–146 (in Japanese).
[24] D. Berlincourt, H. Jaffe, L.R. Shiozawa, Electroelastic properties of the sulfides, selenides, and tellurides of zinc and cadmium, Physical Review 129 (1963) 1009–1017.
[25] M.L. Dunn, Micromechanics of coupled electroelastic composites: effective thermal expansion and pyroelectric coefficients, J. Appl. Phys. 73 (1993) 5131–5140.

CHAPTER 3. Boundary element analysis of 3D thermomagnetoelectroelastic solids

3.1. Introduction

Nowadays anisotropic thermoelastic, thermoelectroelastic, and thermomagnetoelectroelastic materials are widely used in modern micro-electro-mechanical systems, smart structures and devices as sensors, actuators, positioning elements etc. This raises great scientific interest to the development of experimental [1] analytic [1, 2] and numerical techniques [2] for quantitative analysis of these materials.

Among the analytic and numerical approaches boundary integral techniques (in particular boundary element method) are prospective ones in the study of solids of complex shape, since they require only the boundary mesh [2]. Nevertheless, when the thermal effects are considered, the extra volume integral terms arise in the integral equations, which negate the advantages of the boundary element techniques. For the case of isotropic solids volume integrals can be transformed to the boundary ones. Gao [3], Prasad et al. [4], Mukherjee et al. [5], Koshelev and Ghassemi [6] utilized this transformation approach in the BEM for studying of cracked isotropic thermoelastic solids. However, in the case of anisotropic solids the transformation of the volume integral to the boundary one is a challenging and complicated problem.

In the case of 2D thermoelectroelasticity of anisotropic solids a general complex variable approach was developed based on the Stroh formalism, which results in truly boundary integral formulae and equations for inhomogeneous [7], half-space [8] and bimaterial [9, 10] solids. Also it was shown that the kernels of boundary integral equations are closely related to the Green's functions of thermoelectroelasticity [7]. It seems natural that these results should be extended to 3D problems.

For a 3D solid of an arbitrary shape, several methods have been used to evaluate the temperature volume integral term. Deb and Banerjee [11] and Deb et al. [12] developed the particular integral approach, which involves sub-dividing of the domain occupied by a solid and carrying out multiple regression analyses to approximate the temperature field in each of the sub-domains as simple polynomials. Recently, Shiah and Tan [13, 14, 15, 16] proposed the algorithm of exact volume-to-surface integral transformation both for 2D and 3D anisotropic thermoelasticity. However, the latter requires some of the boundary integrals to be evaluated in the mapped temperature domain, which complicates corresponding boundary element technique. Therefore, to this end there are no truly boundary integral equations of 3D anisotropic thermomagnetoelectroelasticity in the real domain.

The same concerns 3D anisotropic thermoelastic (thermomagnetoelectroelastic) Green's functions. There are a few publications concerning this topic. In particular, Hou et al. [17, 18] obtained 3D thermoelastic Green's function for transversely isotropic space, half-space and bimaterial using the Fabrikant's approach. However, it is more convenient for further applications to obtain these functions for general anisotropic thermoelasticity (thermomagnetoelectroelasticity) using the Radon

transform [19] or the Stroh formalism [20], which are successfully applied in the obtaining of 3D anisotropic fundamental solutions [21, 22, 23, 24, 25].

Therefore, this chapter utilizes the general concepts of field theory and the Radon transform to obtain truly boundary integral equations and Green's functions for 3D thermomagnetoelectroelasticity of generally anisotropic solids.

3.2. Governing equations of heat conduction and thermomagnetoelectroelasticity

According to [2, 7, 23, 25], in a fixed Cartesian coordinate system $Ox_1x_2x_3$ the equilibrium equations, the Maxwell equations (Gauss theorem for electric and magnetic fields), and the balance equations of heat conduction in the steady-state case take the form

$$\sigma_{ij,j} + f_i = 0, \quad D_{i,i} - q = 0, \quad B_{i,i} + b_m = 0, \quad h_{i,i} - f_h = 0 \quad (i, j = 1,2,3), \tag{1}$$

where σ_{ij} is a stress tensor; f_i is a body force vector; D_i is an electric displacement vector; q is a free charge volume density; B_i is a magnetic induction vector; b_m is a body current; h_i is a heat flux; f_h is a distributed heat source density. Here and further, the Einstein summation convention is used. A comma at subscript denotes differentiation with respect to a coordinate indexed after the comma, i.e. $u_{i,j} = \partial u_i / \partial x_j$.

In the assumption of small strains and fields' strengths the constitutive equations of linear thermomagnetoelectroelasticity are as follows [2]

$$\begin{aligned} \sigma_{ij} &= C_{ijkm}u_{k,m} - e_{pij}E_p - h_{pij}H_p - \beta_{ij}\theta, \\ D_i &= e_{ikm}u_{k,m} + \kappa_{ip}E_p + \gamma_{ip}H_p + \chi_i\theta, \\ B_i &= h_{ikm}u_{k,m} + \gamma_{ip}E_p + \mu_{ip}H_p - \nu_i\theta, \\ h_i &= -k_{ij}\theta_{,j}, \end{aligned} \tag{2}$$

where u_i is a displacement vector; $E_i = -\phi_{,i}$, $H_i = -\psi_{,i}$ are the electric and magnetic fields strengths, respectively; ϕ, ψ are the electric and magnetic potentials, respectively; θ is a temperature change with respect to the reference temperature; C_{ijkm} are the elastic stiffnesses (elastic moduli); k_{ij} are heat conduction coefficients; e_{ijk}, h_{ijk} are piezoelectric and piezomagnetic constants; κ_{ij}, μ_{ij}, γ_{ij} are dielectric permittivities, magnetic permeabilities and electromagnetic constants, respectively; β_{ij}, χ_i and ν_i are thermal moduli, pyroelectric coefficients and pyromagnetic coefficients, respectively.

With respect to the symmetry properties of thermal, elastic, electric, magnetic and electromagnetic tensors

$$C_{ijkm} = C_{jikm} = C_{kmji}, \quad e_{kij} = e_{kji}, \quad h_{kij} = h_{kji}, \quad \kappa_{ij} = \kappa_{ji}, \quad \mu_{ij} = \mu_{ji}, \quad \gamma_{ij} = \gamma_{ji}, \quad \beta_{ij} = \beta_{ji} \tag{3}$$

Eqs. (1) and (2) can be presented in the compact unified form as

$$\tilde{\sigma}_{Ij,j} + \tilde{f}_I = 0, \quad h_{i,i} - f_h = 0; \tag{4}$$

$$\tilde{\sigma}_{Ij} = \tilde{C}_{IjKm}\tilde{u}_{K,m} - \tilde{\beta}_{Ij}\theta, \quad h_i = -k_{ij}\theta_{,j}, \tag{5}$$

where

$$
\begin{aligned}
&\tilde{u}_i = u_i,\ \tilde{u}_4 = \phi,\ \tilde{u}_5 = \psi\ ;\ \tilde{f}_i = f_i,\ \tilde{f}_4 = -q,\ \tilde{f}_5 = b_m;\\
&\tilde{\sigma}_{ij} = \sigma_{ij},\ \tilde{\sigma}_{4j} = D_j,\ \tilde{\sigma}_{5j} = B_j;\\
&\tilde{C}_{ijkm} = C_{ijkm},\ \tilde{C}_{ij4m} = e_{mij},\ \tilde{C}_{4jkm} = e_{jkm},\ \tilde{C}_{4j4m} = -\kappa_{jm},\\
&\tilde{C}_{ij5m} = h_{mij},\ \tilde{C}_{5jkm} = h_{jkm},\ \tilde{C}_{5j5m} = -\mu_{jm},\\
&\tilde{C}_{4j5m} = -\gamma_{jm},\ \tilde{C}_{5j4m} = -\gamma_{jm};\\
&\tilde{\beta}_{ij} = \beta_{ij},\ \tilde{\beta}_{4j} = -\chi_j,\ \tilde{\beta}_{5j} = \nu_j\ \ (i,j,k,m = 1,2,3).
\end{aligned}
\tag{6}
$$

Here and further the capital index varies from 1 to 5, while the lower case index varies from 1 to 3, i.e. $I = 1,2,...,5$; $i = 1,2,3$.

According to (6) obtained extended magnetoelectroelastic tensor $\tilde{C}_{IjKm}$ has the following symmetry property

$$\tilde{C}_{IjKm} = \tilde{C}_{KmIj}. \tag{7}$$

3.3. Derivation of truly boundary integral equations for 3D anisotropic thermomagnetoelectroelasticity

It can be verified by the direct differentiation that for two arbitrary functions ϕ and ψ of spatial coordinates x_i and a constant tensor k_{pq} the following differential relation holds

$$\frac{\partial}{\partial x_p}\left(\phi k_{pq}\psi_{,q} - \psi k_{pq}\phi_{,q}\right) = \phi k_{pq}\psi_{,pq} - \psi k_{pq}\phi_{,pq} + k_{pq}\phi_{,p}\psi_{,q} - k_{pq}\psi_{,p}\phi_{,q}. \tag{8}$$

If the tensor k_{pq} is symmetric, i.e. $k_{pq} = k_{qp}$, then the last two terms in Eq. (8) vanish and it holds that

$$\frac{\partial}{\partial x_p}\left(\phi k_{pq}\psi_{,q} - \psi k_{pq}\phi_{,q}\right) = \phi k_{pq}\psi_{,pq} - \psi k_{pq}\phi_{,pq}. \tag{9}$$

Integrating (9) over the 3D domain $\mathfrak{B}$ and utilizing the divergence theorem one obtains

$$
\begin{aligned}
&\iiint_{\mathfrak{B}} \frac{\partial}{\partial x_p}\left(\phi k_{pq}\psi_{,q} - \psi k_{pq}\phi_{,q}\right) dV\\
&\quad = \iint_{\partial\mathfrak{B}} \left(\phi k_{pq}\psi_{,q} - \psi k_{pq}\phi_{,q}\right) n_p\, dS = \iiint_{\mathfrak{B}} \left(\phi k_{pq}\psi_{,pq} - \psi k_{pq}\phi_{,pq}\right) dV,
\end{aligned}
\tag{10}
$$

where $\partial\mathfrak{B}$ is a boundary of the domain $\mathfrak{B}$; n_p is a unit outwards normal vector to the surface $\partial\mathfrak{B}$. Assuming that the tensor k_{pq} is an identity tensor ($k_{pq} = \delta_{pq}$, where δ_{pq} is a Kronecker delta) Eq. (10) transforms into the Green's second integral identity

$$\iint_{\partial\mathfrak{B}} \left(\phi\psi_{,p} - \psi\phi_{,p}\right) n_p\, dS = \iiint_{\mathfrak{B}} \left(\phi\psi_{,pp} - \psi\phi_{,pp}\right) dV.$$

The same identity can be obtained for two arbitrary vector functions ϕ_I and ψ_I and symmetric extended tensor $\tilde{C}_{IjKm} = \tilde{C}_{KmIj}$

$$\iint_{\partial\mathfrak{B}} \left(\phi_I \tilde{C}_{IjKm}\psi_{K,m} - \psi_I \tilde{C}_{IjKm}\phi_{K,m}\right) n_j\, dS = \iiint_{\mathfrak{B}} \left(\phi_I \tilde{C}_{IjKm}\psi_{K,jm} - \psi_I \tilde{C}_{IjKm}\phi_{K,jm}\right) dV. \tag{11}$$

Eq. (10) is very useful in derivation of the boundary integral formulae for heat conduction. According to Eqs. (4) and (5), the temperature in the domain $\mathfrak{B}$ occupied be the solid should satisfy the following second-order partial differential equation

$$k_{ij}\theta_{,ij} = -f_h . \tag{12}$$

The fundamental solution $\Theta^*(\mathbf{x},\mathbf{x}_0)$ of Eq. (12) for a point unit heat drain $f_h = -\delta(\mathbf{x}-\mathbf{x}_0)$ at a point $\mathbf{x}_0$ satisfies the following equation

$$k_{ij}\Theta^*_{,ij}(\mathbf{x},\mathbf{x}_0) = \delta(\mathbf{x}-\mathbf{x}_0), \tag{13}$$

where $\delta(\mathbf{x})$ is the Dirac delta-function. Here and further the derivatives are evaluated for the variables x_i.

Denoting

$$H^*(\mathbf{x},\mathbf{x}_0) = -k_{ij}n_i(\mathbf{x})\Theta^*_{,j}(\mathbf{x},\mathbf{x}_0) \tag{14}$$

and assuming that $\phi = \theta$, $\psi = \Theta^*$ one obtains from Eq. (10) that

$$\begin{aligned}&\iint_{\partial\mathfrak{B}}\left(-\theta(\mathbf{x})H^*(\mathbf{x},\mathbf{x}_0)+\Theta^*(\mathbf{x},\mathbf{x}_0)h_n(\mathbf{x})\right)dS(\mathbf{x})\\ &\quad=\iiint_{\mathfrak{B}}\left[\theta(\mathbf{x})k_{pq}\Theta^*_{,pq}(\mathbf{x},\mathbf{x}_0)-\Theta^*(\mathbf{x},\mathbf{x}_0)k_{pq}\theta_{,pq}(\mathbf{x})\right]dV(\mathbf{x}),\end{aligned} \tag{15}$$

where $h_n = h_i n_i$.

Substituting (5) and (13) into (15) it's easy to obtain the integral formula for 3D steady-state heat conduction in an anisotropic solid

$$\theta(\mathbf{x}_0) = \iint_{\partial\mathfrak{B}}\left(\Theta^*(\mathbf{x},\mathbf{x}_0)h_n(\mathbf{x}) - \theta(\mathbf{x})H^*(\mathbf{x},\mathbf{x}_0)\right)dS(\mathbf{x}) - \iiint_{\mathfrak{B}}\Theta^*(\mathbf{x},\mathbf{x}_0)f_h(\mathbf{x})dV(\mathbf{x}). \tag{16}$$

The same way by means of Eq. (11) the extended Somigliana identity for anisotropic thermomagnetoelectroelasticity can be obtained. However, here the problem of extra temperature volume integral arises.

According to Eqs. (4) and (5), the fundamental solution $U_{LJ}(\mathbf{x},\mathbf{x}_0)$ of anisotropic magnetoelectroelasticity for the action of a concentrated unit extended forces $\tilde{f}_I^J = \delta_{LJ}\delta(\mathbf{x}-\mathbf{x}_0)$ at the point $\mathbf{x}_0$ satisfies the following equation

$$\tilde{C}_{IjKm}U_{QK,jm}(\mathbf{x},\mathbf{x}_0) = -\delta_{IQ}\delta(\mathbf{x}-\mathbf{x}_0). \tag{17}$$

Denoting

$$T_{QI}(\mathbf{x},\mathbf{x}_0) = \tilde{C}_{IjKm}n_j(\mathbf{x})U_{QK,m}(\mathbf{x},\mathbf{x}_0) \tag{18}$$

and assuming that in Eq. (11) $\phi_I = \tilde{u}_I$, $\psi_I = U_{QI}(\mathbf{x},\mathbf{x}_0)$ based on Eqs. (17) and (18) one obtains

$$\begin{aligned}\tilde{u}_Q(\mathbf{x}_0) = &\iint_{\partial\mathfrak{B}}\left(U_{QI}(\mathbf{x},\mathbf{x}_0)\tilde{C}_{IjKm}n_j(\mathbf{x})\tilde{u}_{K,m}(\mathbf{x}) - T_{QI}(\mathbf{x},\mathbf{x}_0)\tilde{u}_I(\mathbf{x})\right)dS(\mathbf{x})\\ &-\iiint_{\mathfrak{B}}U_{QI}(\mathbf{x},\mathbf{x}_0)\tilde{C}_{IjKm}\tilde{u}_{K,jm}(\mathbf{x})dV(\mathbf{x}).\end{aligned} \tag{19}$$

Since according to Eqs. (4) and (5)

$$\tilde{C}_{IjKm}\tilde{u}_{K,jm} = \tilde{\beta}_{Ij}\theta_{,j} - \tilde{f}_I, \quad \tilde{C}_{IjKm}\tilde{u}_{K,m} = \tilde{\sigma}_{Ij} + \tilde{\beta}_{Ij}\theta, \tag{20}$$

Eq. (19) can be rewritten as,

$$\tilde{u}_Q(\mathbf{x}_0) = \iint_{\partial\mathfrak{B}} \left(U_{QI}(\mathbf{x},\mathbf{x}_0)\tilde{t}_I(\mathbf{x}) - T_{QI}(\mathbf{x},\mathbf{x}_0)\tilde{u}_I(\mathbf{x}) \right) dS(\mathbf{x}) + \tilde{\beta}_{Ij} \iint_{\partial\mathfrak{B}} U_{QI}(\mathbf{x},\mathbf{x}_0) n_j(\mathbf{x}) \theta(\mathbf{x}) dS(\mathbf{x}) - \tilde{\beta}_{Ij} \iiint_{\mathfrak{B}} U_{QI}(\mathbf{x},\mathbf{x}_0) \theta_{,j}(\mathbf{x}) dV(\mathbf{x}) + \iiint_{\mathfrak{B}} U_{QI}(\mathbf{x},\mathbf{x}_0) \tilde{f}_I(\mathbf{x}) dV(\mathbf{x}), \tag{21}$$

where $\tilde{t}_I = \sigma_{Ij} n_j$ is an extended traction vector.

Integrating the last but one term in Eq. (21) by parts one obtains

$$\tilde{\beta}_{Ij} \iiint_{\mathfrak{B}} U_{QI}(\mathbf{x},\mathbf{x}_0) \theta_{,j}(\mathbf{x}) dV(\mathbf{x}) = \tilde{\beta}_{Ij} \iint_{\partial\mathfrak{B}} U_{QI}(\mathbf{x},\mathbf{x}_0) n_j(\mathbf{x}) \theta(\mathbf{x}) dS(\mathbf{x}) - \tilde{\beta}_{Ij} \iiint_{\mathfrak{B}} \theta(\mathbf{x}) U_{QI,j}(\mathbf{x},\mathbf{x}_0) dV(\mathbf{x}). \tag{22}$$

Accounting for Eq. (22), based on Eq. (21) one obtains

$$\tilde{u}_I(\mathbf{x}_0) = \iint_{\partial\mathfrak{B}} \left(U_{IJ}(\mathbf{x},\mathbf{x}_0)\tilde{t}_J(\mathbf{x}) - T_{IJ}(\mathbf{x},\mathbf{x}_0)\tilde{u}_J(\mathbf{x}) \right) dS(\mathbf{x}) + \iiint_{\mathfrak{B}} U_{IJ}(\mathbf{x},\mathbf{x}_0) \tilde{f}_J(\mathbf{x}) dV(\mathbf{x}) + \tilde{\beta}_{Jk} \iiint_{\mathfrak{B}} \theta(\mathbf{x}) U_{IJ,k}(\mathbf{x},\mathbf{x}_0) dV(\mathbf{x}). \tag{23}$$

Consider the last term in Eq. (23), which is a thermomagnetoelectroelastic domain integral. Denoting $\psi = V_I(\mathbf{x},\mathbf{x}_0)$, $\phi = \theta(\mathbf{x})$, and hence, according to Eq. (5), $k_{ij}\theta_{,j} = -h_i$, and using these notations in Eq. (10) yields

$$\iint_{\partial\mathfrak{B}} \left(\theta(\mathbf{x}) k_{mj} V_{I,j}(\mathbf{x},\mathbf{x}_0) n_m(\mathbf{x}) + V_I(\mathbf{x},\mathbf{x}_0) h_m(\mathbf{x}) n_m(\mathbf{x}) \right) dS(\mathbf{x}) = \iiint_{\mathfrak{B}} \left[\theta(\mathbf{x}) k_{mj} V_{I,mj}(\mathbf{x},\mathbf{x}_0) + V_I(\mathbf{x},\mathbf{x}_0) h_{m,m}(\mathbf{x}) \right] dV(\mathbf{x}). \tag{24}$$

As stated in Eq. (4), $h_{m,m} = f_h$, thus, rearranging terms in Eq. (24) one obtains

$$\iiint_{\mathfrak{B}} \theta(\mathbf{x}) k_{mj} V_{I,mj}(\mathbf{x},\mathbf{x}_0) dV(\mathbf{x}) = \iint_{\partial\mathfrak{B}} \left[R_I(\mathbf{x},\mathbf{x}_0)\theta(\mathbf{x}) + V_I(\mathbf{x},\mathbf{x}_0) h_n(\mathbf{x}) \right] dS(\mathbf{x}) - \iiint_{\mathfrak{B}} V_I(\mathbf{x},\mathbf{x}_0) f_h(\mathbf{x}) dV(\mathbf{x}). \tag{25}$$

Here

$$R_I(\mathbf{x},\mathbf{x}_0) = k_{mj} V_{I,j}(\mathbf{x},\mathbf{x}_0) n_m(\mathbf{x}). \tag{26}$$

Assuming that the function $V_I(\mathbf{x},\mathbf{x}_0)$ satisfies partial differential equation

$$k_{mj} V_{I,mj}(\mathbf{x},\mathbf{x}_0) = \tilde{\beta}_{Jk} U_{IJ,k}(\mathbf{x},\mathbf{x}_0), \tag{27}$$

the thermomagnetoelectroelastic domain integral in Eq. (23) can be transformed to a boundary one through Eq. (25) as

$$\tilde{\beta}_{Jk} \iiint_{\mathfrak{B}} \theta(\mathbf{x}) U_{IJ,k}(\mathbf{x},\mathbf{x}_0) dV(\mathbf{x}) = \iiint_{\mathfrak{B}} \theta(\mathbf{x}) k_{mj} V_{I,mj}(\mathbf{x},\mathbf{x}_0) dV(\mathbf{x}) = \iint_{\partial\mathfrak{B}} \left[R_I(\mathbf{x},\mathbf{x}_0)\theta(\mathbf{x}) + V_I(\mathbf{x},\mathbf{x}_0) h_n(\mathbf{x}) \right] dS(\mathbf{x}) - \iiint_{\mathfrak{B}} V_I(\mathbf{x},\mathbf{x}_0) f_h(\mathbf{x}) dV(\mathbf{x}). \tag{28}$$

Finally, substitution of Eq. (23) into Eq. (23) yields the extended Somigliana identity for 3D anisotropic thermomagnetoelectroelasticity

$$\tilde{u}_I(\mathbf{x}_0) = \iint_{\partial\mathfrak{B}} \left(U_{IJ}(\mathbf{x},\mathbf{x}_0)\tilde{t}_J(\mathbf{x}) - T_{IJ}(\mathbf{x},\mathbf{x}_0)\tilde{u}_J(\mathbf{x}) \right) dS(\mathbf{x}) + \iint_{\partial\mathfrak{B}} \left[R_I(\mathbf{x},\mathbf{x}_0)\theta(\mathbf{x}) + V_I(\mathbf{x},\mathbf{x}_0) h_n(\mathbf{x}) \right] dS(\mathbf{x}) + \iiint_{\mathfrak{B}} U_{IJ}(\mathbf{x},\mathbf{x}_0)\tilde{f}_J(\mathbf{x}) dV(\mathbf{x}) - \iiint_{\mathfrak{B}} V_I(\mathbf{x},\mathbf{x}_0) f_h(\mathbf{x}) dV(\mathbf{x}). \quad (29)$$

Eq. (29) contains volume integrals only if distributed heat $f_h(\mathbf{x})$ and extended body forces $\tilde{f}_I(\mathbf{x})$ are applied, which is advantageous comparing to existing equations. Besides, all integrals are to be evaluated in the real domains, but not mapped ones.

According to the approach used in Ref. [7] for 2D thermoelectroelasticity, another useful property of the kernel $V_I(\mathbf{x},\mathbf{x}_0)$ can be observed.

Consider an infinite thermoelectroelastic medium loaded by a unit heat source at the point $\mathbf{x}^*$. Since the infinite medium is considered, all path integrals in Eq. (29) and also domain integral containing extended body forces $\tilde{f}_I(\mathbf{x})$ should vanish. The only nonzero term remaining is

$$\tilde{u}_I^*(\mathbf{x}_0) = -\iiint_{\mathfrak{B}} V_I(\mathbf{x},\mathbf{x}_0)\delta(\mathbf{x}-\mathbf{x}^*) dV(\mathbf{x}) = -V_I(\mathbf{x}^*,\mathbf{x}_0). \quad (30)$$

Therefore, according to Eq. (30), the kernel $V_I(\mathbf{x},\mathbf{x}_0)$ corresponds to the extended displacements at the point $\mathbf{x}_0$ produced by a point heat drain of a unit magnitude applied at the point $\mathbf{x}$ of the infinite medium. Thus, $V_I(\mathbf{x},\mathbf{x}_0)$ is a fundamental solution of thermomagnetoelectroelasticity, which according to Eqs. (4), (5) and (13) satisfies the following partial differential equation

$$\tilde{C}_{IjKm} V_{K,jm}(\mathbf{x},\mathbf{x}_0) + \tilde{\beta}_{Ij}\Theta^*_{,j}(\mathbf{x},\mathbf{x}_0) = 0, \quad (31)$$

where the following property of the fundamental solution $V_I(\mathbf{x},\mathbf{x}_0)$ is utilized

$$V_I(\mathbf{x},\mathbf{x}_0) = -V_I(\mathbf{x}_0,\mathbf{x}). \quad (32)$$

Before application of the boundary integral formula (29), one should (a) obtain its kernels; and (b) strictly prove the equivalence of Eqs. (27) and (31). Till now these two problems were solved only for thermoelasticity of isotropic solids. The next section provides their solution for generally anisotropic thermomagnetoelectroelastic bodies.

3.4. Derivation of 3D fundamental solutions and kernels using the Radon transform

It is convenient to copy here the partial differential equations (13), (17), (26), (27), (31), which should be satisfied by the main kernels of heat conduction and thermomagnetoelectroelastic integral identities

$$k_{ij}\Theta^*_{,ij}(\mathbf{x},\mathbf{x}_0) = \delta(\mathbf{x}-\mathbf{x}_0), \quad (33)$$

$$\tilde{C}_{IjKm} U_{QK,jm}(\mathbf{x},\mathbf{x}_0) = -\delta_{IQ}\delta(\mathbf{x}-\mathbf{x}_0), \quad (34)$$

$$k_{mj} V_{I,mj}(\mathbf{x},\mathbf{x}_0) = \tilde{\beta}_{Jk} U_{IJ,k}(\mathbf{x},\mathbf{x}_0), \quad (35)$$

$$\tilde{C}_{IjKm} V_{K,jm}(\mathbf{x},\mathbf{x}_0) + \tilde{\beta}_{Ij}\Theta^*_{,j}(\mathbf{x},\mathbf{x}_0) = 0, \quad (36)$$

$$R_I(\mathbf{x},\mathbf{x}_0) = k_{mj} V_{I,j}(\mathbf{x},\mathbf{x}_0)\, n_m(\mathbf{x}). \tag{37}$$

As it was stated above, the problem is to find the unknown functions, and to prove the equivalence of Eqs. (35) and (36). Then other kernels can be obtained by differentiation of the sought functions through equations (14), (18).

Consider a Radon transform [19]

$$\breve{f}(p,\boldsymbol{\xi}) = \mathrm{R}\left(f(\mathbf{x})\right) = \iiint f(\mathbf{x})\,\delta(p-\boldsymbol{\xi}\cdot\mathbf{x})\,dx_1dx_2dx_3, \tag{38}$$

where $\boldsymbol{\xi}$ is a unit vector, normal to a plane $p-\boldsymbol{\xi}\cdot\mathbf{x}=0$. One of the useful properties of the Radon transform is that the transform of a derivative is equal to

$$\mathrm{R}\left(\frac{\partial f(\mathbf{x})}{\partial x_k}\right) = \xi_k \frac{\partial \breve{f}(p,\boldsymbol{\xi})}{\partial p}. \tag{39}$$

Since the Radon transform of Dirac delta-function equals

$$\mathrm{R}\left(\delta(\mathbf{x}-\mathbf{x}_0)\right) = \iiint \delta(\mathbf{x}-\mathbf{x}_0)\,\delta(p-\boldsymbol{\xi}\cdot\mathbf{x})\,dx_1dx_2dx_3 = \delta(p-\boldsymbol{\xi}\cdot\mathbf{x}_0), \tag{40}$$

the Radon transforms of Eqs. (33)–(37) yield

$$k_{ij}\xi_i\xi_j \frac{\partial^2}{\partial p^2}\breve{\Theta}^*(p,\boldsymbol{\xi}) = \delta(p-\boldsymbol{\xi}\cdot\mathbf{x}_0); \tag{41}$$

$$\tilde{C}_{IjKm}\xi_j\xi_m \frac{\partial^2}{\partial p^2}\breve{U}_{QK}(p,\boldsymbol{\xi}) = -\delta_{QI}\,\delta(p-\boldsymbol{\xi}\cdot\mathbf{x}_0); \tag{42}$$

$$\tilde{C}_{IjKm}\xi_j\xi_m \frac{\partial^2}{\partial p^2}\breve{V}_K(p,\boldsymbol{\xi}) = -\tilde{\beta}_{Ij}\xi_j \frac{\partial}{\partial p}\breve{\Theta}^*(p,\boldsymbol{\xi}), \tag{43}$$

$$k_{mn}\xi_m\xi_n \frac{\partial^2}{\partial p^2}\breve{V}_I(p,\boldsymbol{\xi}) = \frac{\partial}{\partial p}\breve{U}_{IJ}(p,\boldsymbol{\xi})\,\tilde{\beta}_{Jk}\xi_k, \tag{44}$$

$$\breve{R}_I(p,\boldsymbol{\xi}) = k_{mj}\xi_j n_m(\mathbf{x}) \frac{\partial}{\partial p}\breve{V}_I(p,\boldsymbol{\xi}). \tag{45}$$

Denoting $\Gamma_{IK}(\boldsymbol{\xi}) = \tilde{C}_{IjKm}\xi_j\xi_m$, due to the symmetry property (7) and the resulting symmetry $\Gamma_{IJ}(\boldsymbol{\xi}) = \Gamma_{JI}(\boldsymbol{\xi})$ based on Eqs. (41)–(45) one obtains

$$\frac{\partial^2}{\partial p^2}\breve{\Theta}^*(p,\boldsymbol{\xi}) = \frac{\delta(p-\boldsymbol{\xi}\cdot\mathbf{x}_0)}{k_{ij}\xi_i\xi_j}; \tag{46}$$

$$\frac{\partial^2}{\partial p^2}\breve{U}_{IJ}(p,\boldsymbol{\xi}) = -\Gamma^{-1}_{IJ}(\boldsymbol{\xi})\,\delta(p-\boldsymbol{\xi}\cdot\mathbf{x}_0); \tag{47}$$

$$\frac{\partial^2}{\partial p^2}\breve{V}_I(p,\boldsymbol{\xi}) = -\Gamma^{-1}_{IJ}(\boldsymbol{\xi})\,\tilde{\beta}_{Jk}\xi_k \frac{\partial}{\partial p}\breve{\Theta}^*(p,\boldsymbol{\xi}), \tag{48}$$

$$\frac{\partial^2}{\partial p^2}\breve{V}_I(p,\boldsymbol{\xi}) = \frac{\partial}{\partial p}\breve{U}_{IJ}(p,\boldsymbol{\xi})\frac{\tilde{\beta}_{Jk}\xi_k}{k_{mn}\xi_m\xi_n}, \tag{49}$$

$$\frac{\partial^2}{\partial p^2}\breve{R}_I(p,\boldsymbol{\xi}) = k_{mj}\xi_j n_m(\mathbf{x}) \frac{\partial^3}{\partial p^3}\breve{V}_I(p,\boldsymbol{\xi}). \tag{50}$$

where $\Gamma^{-1}_{IJ}(\boldsymbol{\xi})$ are the components of the matrix, which is inverse of the matrix $\Gamma_{IJ}(\boldsymbol{\xi})$, i.e. $\Gamma^{-1}_{IK}(\boldsymbol{\xi})\Gamma_{KJ}(\boldsymbol{\xi}) = \delta_{IJ}$.

Integrating Eqs. (46) and (47) over the variable p one obtains

$$\frac{\partial}{\partial p}\breve{\Theta}^*(p,\boldsymbol{\xi}) = \int_{-\infty}^{p} \frac{\partial^2}{\partial p^2}\breve{\Theta}^*(p,\boldsymbol{\xi})\,dp = \frac{H(p-\boldsymbol{\xi}\cdot\mathbf{x}_0)}{k_{ij}\xi_i\xi_j}; \tag{51}$$

$$\frac{\partial}{\partial p}\breve{U}_{IJ}(p,\boldsymbol{\xi})=\int_{-\infty}^{p}\frac{\partial^2}{\partial p^2}\breve{U}_{IJ}(p,\boldsymbol{\xi})\,dp=-\Gamma_{IJ}^{-1}(\boldsymbol{\xi})\,H(p-\boldsymbol{\xi}\cdot\mathbf{x}_0), \tag{52}$$

where $H(x)$ is a Heaviside step function.

Substitution of Eq. (51) into Eq. (48) yields

$$\frac{\partial^2}{\partial p^2}\breve{V}_I(p,\boldsymbol{\xi})=-\frac{\Gamma_{IJ}^{-1}(\boldsymbol{\xi})\tilde{\beta}_{Jk}\xi_k}{k_{qr}\xi_q\xi_r}H(p-\boldsymbol{\xi}\cdot\mathbf{x}_0). \tag{53}$$

It is easy to verify that the same result is obtained, when substituting Eq. (52) into Eq. (49). Since the Radon transform of a function of spatial variables is a unique function of transformed variables p, $\boldsymbol{\xi}$, this proves that equations (35) and (36) are equivalent, thus the physical assumption (30) is correct.

Substituting Eq. (53) into Eq. (50) one obtains

$$\frac{\partial^2}{\partial p^2}\breve{R}_I(p,\boldsymbol{\xi})=-\frac{\Gamma_{IJ}^{-1}(\boldsymbol{\xi})\tilde{\beta}_{Jk}\xi_k k_{ms}\xi_s}{k_{qr}\xi_q\xi_r}n_m(\mathbf{x})\,\delta(p-\boldsymbol{\xi}\cdot\mathbf{x}_0). \tag{54}$$

Application of the inverse Radon transform

$$f(\mathbf{x})=\mathrm{R}^{-1}\left(\breve{f}(p,\boldsymbol{\xi})\right)=-\frac{1}{8\pi^2}\iint_{|\boldsymbol{\xi}|=1}\frac{\partial^2}{\partial p^2}\breve{f}(p=\boldsymbol{\xi}\cdot\mathbf{x},\boldsymbol{\xi})\,dS(\boldsymbol{\xi}) \tag{55}$$

to Eqs. (46), (47), (53), (54) yields

$$\Theta^*(\mathbf{x},\mathbf{x}_0)=-\frac{1}{8\pi^2}\iint_{|\boldsymbol{\xi}|=1}\frac{\delta\left(\boldsymbol{\xi}\cdot(\mathbf{x}-\mathbf{x}_0)\right)}{k_{ij}\xi_i\xi_j}dS(\boldsymbol{\xi}); \tag{56}$$

$$U_{IJ}(\mathbf{x},\mathbf{x}_0)=\frac{1}{8\pi^2}\iint_{|\boldsymbol{\xi}|=1}\Gamma_{IJ}^{-1}(\boldsymbol{\xi})\,\delta\left(\boldsymbol{\xi}\cdot(\mathbf{x}-\mathbf{x}_0)\right)dS(\boldsymbol{\xi}); \tag{57}$$

$$V_I(\mathbf{x},\mathbf{x}_0)=\frac{1}{8\pi^2}\iint_{|\boldsymbol{\xi}|=1}\frac{\Gamma_{IJ}^{-1}(\boldsymbol{\xi})\tilde{\beta}_{Jk}\xi_k}{k_{qr}\xi_q\xi_r}H\left(\boldsymbol{\xi}\cdot(\mathbf{x}-\mathbf{x}_0)\right)dS(\boldsymbol{\xi}); \tag{58}$$

$$R_I(\mathbf{x},\mathbf{x}_0)=\frac{1}{8\pi^2}\iint_{|\boldsymbol{\xi}|=1}\frac{\Gamma_{IJ}^{-1}(\boldsymbol{\xi})\tilde{\beta}_{Jk}\xi_k k_{ms}\xi_s}{k_{qr}\xi_q\xi_r}n_m(\mathbf{x})\,\delta(p-\boldsymbol{\xi}\cdot\mathbf{x}_0)\,dS(\boldsymbol{\xi}), \tag{59}$$

where the integration is performed over a unit sphere $|\boldsymbol{\xi}|=1$.

Since

$$\delta\left(\boldsymbol{\xi}\cdot(\mathbf{x}-\mathbf{x}_0)\right)=\frac{\delta(\boldsymbol{\xi}\cdot\mathbf{t})}{|\mathbf{x}-\mathbf{x}_0|}, \tag{60}$$

Eqs. (56), (57), and (59) can be rewritten as contour integrals over a unit circle

$$\Theta^*(\mathbf{x},\mathbf{x}_0)=-\frac{1}{8\pi^2|\mathbf{x}-\mathbf{x}_0|}\oint_{|\boldsymbol{\lambda}|=1}\left(k_{ij}\lambda_i\lambda_j\right)^{-1}dl(\boldsymbol{\lambda}); \tag{61}$$

$$U_{IJ}(\mathbf{x},\mathbf{x}_0)=\frac{1}{8\pi^2|\mathbf{x}-\mathbf{x}_0|}\oint_{|\boldsymbol{\lambda}|=1}\Gamma_{IJ}^{-1}(\boldsymbol{\lambda})\,dl(\boldsymbol{\lambda}); \tag{62}$$

$$R_I(\mathbf{x},\mathbf{x}_0)=\frac{1}{8\pi^2|\mathbf{x}-\mathbf{x}_0|}\oint_{|\boldsymbol{\lambda}|=1}\frac{\Gamma_{IJ}^{-1}(\boldsymbol{\lambda})\tilde{\beta}_{Jk}\lambda_k k_{ms}\lambda_s}{k_{qr}\lambda_q\lambda_r}n_m(\mathbf{x})\,dl(\boldsymbol{\lambda}), \tag{63}$$

where $\mathbf{t}$ is a unit vector collinear with $\mathbf{x}-\mathbf{x}_0$; and $\boldsymbol{\lambda}$ is a unit vector normal to $\mathbf{x}-\mathbf{x}_0$ (see Fig. 1):

$$\mathbf{t} = \frac{\mathbf{x} - \mathbf{x}_0}{|\mathbf{x} - \mathbf{x}_0|}, \quad \boldsymbol{\lambda} \cdot \mathbf{t} = 0 . \tag{64}$$

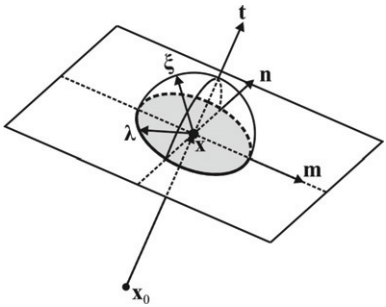

Fig. 1. Definition of the mutually orthogonal unit vectors $\mathbf{m}$, $\mathbf{n}$, $\mathbf{t}$

According to the definition of the Heaviside step function, Eq. (58) reduces to the regular surface integral over a half-sphere $\boldsymbol{\xi} \cdot \mathbf{t} > 0$

$$V_I(\mathbf{x}, \mathbf{x}_0) = \frac{1}{8\pi^2} \iint\limits_{\substack{|\boldsymbol{\xi}|=1, \\ \boldsymbol{\xi} \cdot \mathbf{t} > 0}} \frac{\Gamma_{IJ}^{-1}(\boldsymbol{\xi}) \tilde{\beta}_{Jk} \xi_k}{k_{qr} \xi_q \xi_r} dS(\boldsymbol{\xi}) . \tag{65}$$

Since $V_I(\mathbf{x}, \mathbf{x}_0) = -V_I(\mathbf{x}_0, \mathbf{x})$, Eq. (65) results in the following identity of anisotropic thermomagnetoelectroelasticity

$$\iint\limits_{|\boldsymbol{\xi}|=1} \frac{\Gamma_{IJ}^{-1}(\boldsymbol{\xi}) \tilde{\beta}_{Jk} \xi_k}{k_{qr} \xi_q \xi_r} dS(\boldsymbol{\xi}) = 0 , \tag{66}$$

which can be definitely used in further simplification of Eq. (65).

Eqs. (61) and (62) are well-known fundamental solutions of steady-state heat conduction and magnetoelectroelasticity [21, 23, 25]. The integrals present in these equations are all regular; therefore, they can be evaluated using the numerical quadratures or some other techniques (the Stroh formalism [25], the Cauchy residue theory [21], etc. [23]). The derivatives of these fundamental solutions are also known [23, 25]; therefore, the kernels (14), (18) can be easily calculated.

Eqs. (63), (65) for 3D anisotropic thermomagnetoelectroelastic kernels (fundamental solutions) are obtained for the first time. The line and surface integrals contained are regular; therefore, they can be also calculated with the numerical quadratures to a desired accuracy.

Using the obtained kernels, Eq. (29) can be readily introduced into the boundary element technique for calculation of 3D anisotropic thermomagnetoelectroelastic solids of a complex shape.

3.5. Verification of the obtained kernels and integral equations

3.5.1. Analytic verification

For verification of the obtained kernels consider a particular case of an isotropic thermoelastic material, which elastic, thermoelastic and heat conduction coefficients equal [20]

$$C_{ijkm}=\lambda\delta_{ij}\delta_{km}+\mu\left(\delta_{ik}\delta_{jm}+\delta_{im}\delta_{jk}\right),\quad \beta_{ij}=\alpha C_{ijkm}\delta_{km},\quad k_{ij}=k_t\delta_{ij}, \tag{67}$$

where $\lambda=\dfrac{2G\nu}{1-2\nu}$, $\mu=G$ are Lame constants; α is a thermal expansion coefficient; k_t is a heat conduction coefficient; G is a shear modulus; and ν is a Poisson ratio.

According to Eq. (67)

$$\Gamma_{ij}^{-1}\left(\boldsymbol{\xi}\right)=-\frac{1}{2G\left(1-\nu\right)}\xi_i\xi_j+\frac{\delta_{ij}}{G},\quad k_{ij}\xi_i\xi_j=k_t,\quad \beta_{ij}=\frac{2G\left(1+\nu\right)}{1-2\nu}\alpha\delta_{ij}, \tag{68}$$

therefore, for isotropic thermoelasticity Eqs. (61)–(63), (65) reduce to

$$\Theta^*\left(\mathbf{x},\mathbf{x}_0\right)=-\frac{1}{8\pi^2\left|\mathbf{x}-\mathbf{x}_0\right|k_t}\oint\limits_{|\boldsymbol{\lambda}|=1}dl\left(\boldsymbol{\lambda}\right); \tag{69}$$

$$U_{ij}\left(\mathbf{x},\mathbf{x}_0\right)=\frac{1}{8\pi^2\left|\mathbf{x}-\mathbf{x}_0\right|}\left[-\frac{1}{2G\left(1-\nu\right)}\oint\limits_{|\boldsymbol{\lambda}|=1}\lambda_i\lambda_j dl\left(\boldsymbol{\lambda}\right)+\frac{\delta_{ij}}{G}\oint\limits_{|\boldsymbol{\lambda}|=1}dl\left(\boldsymbol{\lambda}\right)\right]; \tag{70}$$

$$R_i\left(\mathbf{x},\mathbf{x}_0\right)=\frac{1}{8\pi^2\left|\mathbf{x}-\mathbf{x}_0\right|}\frac{1+\nu}{1-\nu}\alpha\oint\limits_{|\boldsymbol{\lambda}|=1}\lambda_i\lambda_j dl\left(\boldsymbol{\lambda}\right)n_j\left(\mathbf{x}\right), \tag{71}$$

$$V_i\left(\mathbf{x},\mathbf{x}_0\right)=\frac{1}{8\pi^2}\frac{\left(1+\nu\right)\alpha}{\left(1-\nu\right)k_t}\iint\limits_{\substack{|\boldsymbol{\xi}|=1,\\ \boldsymbol{\xi}\cdot\mathbf{t}>0}}\xi_i dS\left(\boldsymbol{\xi}\right). \tag{72}$$

Since

$$\oint\limits_{|\boldsymbol{\lambda}|=1}dl\left(\boldsymbol{\lambda}\right)=2\pi,\quad \oint\limits_{|\boldsymbol{\lambda}|=1}\lambda_i\lambda_j dl\left(\boldsymbol{\lambda}\right)=\pi\left(\delta_{ij}-t_it_j\right),\quad \iint\limits_{\substack{|\boldsymbol{\xi}|=1,\\ \boldsymbol{\xi}\cdot\mathbf{t}>0}}\xi_i dS\left(\boldsymbol{\xi}\right)=\pi t_i, \tag{73}$$

Eqs. (69)–(72) result in

$$\Theta^*\left(\mathbf{x},\mathbf{x}_0\right)=-\frac{1}{4\pi\left|\mathbf{x}-\mathbf{x}_0\right|k_t}; \tag{74}$$

$$U_{ij}\left(\mathbf{x},\mathbf{x}_0\right)=\frac{1}{16\pi G\left(1-\nu\right)\left|\mathbf{x}-\mathbf{x}_0\right|}\left[\left(3-4\nu\right)\delta_{ij}+t_it_j\right]; \tag{75}$$

$$R_i\left(\mathbf{x},\mathbf{x}_0\right)=\frac{1}{8\pi\left|\mathbf{x}-\mathbf{x}_0\right|}\frac{1+\nu}{1-\nu}\alpha\left(\delta_{ij}-t_it_j\right)n_j\left(\mathbf{x}\right), \tag{76}$$

$$V_i\left(\mathbf{x},\mathbf{x}_0\right)=\frac{1}{8\pi}\frac{\left(1+\nu\right)\alpha}{\left(1-\nu\right)k_t}t_i. \tag{77}$$

It is readily seen that the kernels (74)–(77) perfectly coincide with those obtained for the isotropic thermoelasticity in Refs. [4, 5, 20, 26], which additionally verifies the general solutions obtained in the present chapter for 3D anisotropic thermomagnetoelectroelasticity.

3.5.2. Convergence of numerical evaluation of thermomagnetoelectroelastic kernels

As it was stated above, Eqs. (61) and (62) are well-known fundamental solutions of steady-state heat conduction and magnetoelectroelasticity, which can be evaluated efficiently using different techniques [21, 23, 25]. The new kernels (63), (65) of anisotropic thermomagnetoelectroelasticity are reduced to the regular surface and line integrals; thus, it should be shown that numerical evaluation of these integrals converges fast. This provides the estimation of computations required for kernels evaluation, and therefore, shows the efficiency of the boundary element method implementation based on Eq. (29).

For numerical computations it is useful to rewrite the kernel (65) using the approach of Wang and Achenbach [27] as

$$V_I(\mathbf{x},\mathbf{x}_0)=\frac{1}{8\pi^2}\oint_{|\boldsymbol{\lambda}|=1}\int_0^1 \frac{\Gamma_{IJ}^{-1}\left(a(b)\boldsymbol{\lambda}+b\mathbf{t}\right)\tilde{\beta}_{Jk}\left(a(b)\lambda_k+bt_k\right)}{k_{qr}\left(a(b)\lambda_q+bt_q\right)\left(a(b)\lambda_r+bt_r\right)}dbdl(\boldsymbol{\lambda}), \tag{78}$$

where $a(b)=\sqrt{1-b^2}$. Eq. (78) is readily programmed for numerical evaluation using the Gaussian quadrature.

Since according to Eq. (37) the kernel R_I is a linear combination of the partial derivatives $V_{I,j}$ it is useful for numerical verification to evaluate these derivatives instead of R_I. According to Eqs. (63) and (65),

$$V_{I,s}(\mathbf{x},\mathbf{x}_0)=\frac{1}{8\pi^2|\mathbf{x}-\mathbf{x}_0|}\oint_{|\boldsymbol{\lambda}|=1}\frac{\Gamma_{IJ}^{-1}(\boldsymbol{\lambda})\tilde{\beta}_{Jk}\lambda_k\lambda_s}{k_{qr}\lambda_q\lambda_r}dl(\boldsymbol{\lambda}). \tag{79}$$

Table 1 compares values of V_I and $V_{I,j}$ obtained numerically by Eqs. (78), (79) using different number of Gaussian nodes with analytic solution. The computations are held for an isotropic material, which Poisson ratio is equal to 0.3. It is assumed that $\mathbf{x}-\mathbf{x}_0=[1,2,3]^{\mathrm{T}}a$, where $a=1$ m is the length normalization parameter. The normalization factors are equal to $V^*=\dfrac{\alpha}{k_t}$, $W^*=\dfrac{\alpha}{k_t a}$.

Good numerical convergence is observed from Table 1. One can see that for the isotropic material the kernel V_I and its derivatives can be evaluated up to 8 significant digits with only 10-point Gaussian quadrature.

Since the weak singularity in Eq. (79) is extracted from the integrand, the latter is a regular function, which does not depend on $|\mathbf{x}-\mathbf{x}_0|$. Therefore, the convergence of numerical evaluation of $V_{I,j}$ through Eq. (79) does not depend on $|\mathbf{x}-\mathbf{x}_0|$ too.

The same concerns anisotropic thermomagnetoelectroelastic materials. In instance, consider a transversely isotropic pyroelectric barium titanate ($BaTiO_3$), which has the following properties [28]:

- elastic moduli (GPa): $C_{11}=C_{22}=150$; $C_{33}=146$; $C_{12}=C_{13}=C_{23}=66$; $C_{44}=C_{55}=44$; $C_{66}=(C_{11}-C_{12})/2=42$;
- piezoelectric constants (C/m^2): $e_{31}=e_{32}=-4.35$; $e_{33}=17.5$; $e_{15}=e_{24}=11.4$;
- dielectric constants (nF/m): $\kappa_{11}=\kappa_{22}=9.86775$; $\kappa_{33}=11.151$;

- heat conduction coefficients (W/(m·K)): $k_{11} = k_{22} = k_{33} = 2.5$;
- thermal expansion coefficients (K^{-1}): $\alpha_{11} = \alpha_{22} = 8.53 \cdot 10^{-6}$; $\alpha_{33} = 1.99 \cdot 10^{-6}$;
- pyroelectric constants (GV/(m·K)): $\lambda_3 = 13.3 \cdot 10^{-6}$.

Table 1
Convergence of numerical evaluation of thermoelastic kernel and its derivatives for the isotropic material

	6-point quadrature	8-point quadrature	10-point quadrature	Analytic solution (77)
V_1/V^*	0.01974889961	0.01974883289	0.01974883288	0.01974883288
V_2/V^*	0.03949765242	0.03949766576	0.03949766577	0.03949766577
V_3/V^*	0.05924648530	0.05924649865	0.05924649865	0.05924649865
$V_{1,1}/W^*$	0.01831226653	0.01833813323	0.01833820190	0.01833820196
$V_{1,2}/W^*$	-0.002814870873	-0.002821244903	-0.002821261825	-0.002821261840
$V_{1,3}/W^*$	-0.00422750826	-0.004231881141	-0.004231892750	-0.004231892761
$V_{2,1}/W^*$	-0.002814870873	-0.002821244903	-0.002821261825	-0.002821261840
$V_{2,2}/W^*$	0.01412429309	0.01410635686	0.01410630925	0.01410630920
$V_{2,3}/W^*$	-0.008477905099	-0.008463822941	-0.008463785556	-0.008463785521
$V_{3,1}/W^*$	-0.00422750826	-0.004231881141	-0.004231892750	-0.004231892761
$V_{3,2}/W^*$	-0.008477905099	-0.008463822941	-0.008463785556	-0.008463785521
$V_{3,3}/W^*$	0.007061106153	0.007053175674	0.007053154621	0.007053154601

Table 2 contains the comparison of the values of V_I and $V_{I,j}$ obtained numerically for barium titanate material by Eqs. (78), (79) using different number of Gaussian nodes. The normalization factors are equal to $V^{**} = 10^{-6}$ m/W; $V^{***} = 10^3$ V/W; $W^{**} = 10^{-6}$ W^{-1}; $W^{***} = 10^3$ V/(m·W). The same as in the previous example, it is assumed that $\mathbf{x} - \mathbf{x}_0 = [1,2,3]^{\mathrm{T}} a$.

One can see that even 8-point Gaussian quadrature provides accurate evaluation of the thermoelectroelastic Green's function and its spatial derivatives. The 12-point quadrature evaluates these functions up to 4 significant digits. This proves that introduction of the obtained integral equations and kernels will not cause the enormous computational efforts. Moreover, the number of computations is reduced, since only the boundary mesh is required and no volume integration is needed.

Table 2

Convergence of numerical evaluation of thermoelectroelastic kernel and its derivative for $BaTiO_3$ medium

	8-point quadrature	10-point quadrature	12-point quadrature	14-point quadrature
V_1/V^{**}	0.05754299596	0.05758729346	0.05760621675	0.0576085965
V_2/V^{**}	0.115097828	0.1152203054	0.1152194639	0.115218077
V_3/V^{**}	0.05294005959	0.05287103244	0.05286700622	0.05286752099
V_4/V^{***}	0.3606560596	0.3605982597	0.3605940436	0.3605939944
$V_{1,1}/W^{**}$	0.05443631468	0.0543236663	0.05431774316	0.05431681205
$V_{1,2}/W^{**}$	-0.006521162818	-0.006578921208	-0.00658626293	-0.006584775656
$V_{1,3}/W^{**}$	-0.01379799635	-0.01372194129	-0.01371507243	-0.01371575358
$V_{2,1}/W^{**}$	-0.006521162818	-0.006578921208	-0.00658626293	-0.006584775656
$V_{2,2}/W^{**}$	0.04433456311	0.04443438953	0.04443992367	0.04444012877
$V_{2,3}/W^{**}$	-0.02738265447	-0.02742995262	-0.0274311948	-0.02743182729
$V_{3,1}/W^{**}$	-0.00106828011	-0.001013069298	-0.001016344202	-0.001017524135
$V_{3,2}/W^{**}$	-0.001985026647	-0.002034838318	-0.002034878194	-0.002035337878
$V_{3,3}/W^{**}$	0.001679444468	0.001694248645	0.001695366863	0.00169606663
$V_{4,1}/W^{***}$	-0.02500280544	-0.02498120387	-0.02498113211	-0.02498184126
$V_{4,2}/W^{***}$	-0.04994789938	-0.04996357202	-0.04996353366	-0.04996389935
$V_{r,3}/W^{***}$	0.04163286807	0.04163611597	0.04163606648	0.04163654666

3.5.3. Boundary element analysis based on the obtained integral equations

Consider a traction-free cube made of barium titanate, which edges and material axes are collinear to the reference ones. Edges of the cube are equal to a, and one of its vertices coincide with the origin O. The cube is uniformly heated by the temperature θ_0. Since barium titanate is a transversely isotropic material, it's easy to verify that the displacements and electric potential inside the cube are defined as

$$u_1 = \alpha_{11}\theta_0 x_1;\ \ u_2 = \alpha_{22}\theta_0 x_2;\ \ u_3 = \alpha_{33}\theta_0 x_3;\ \ \phi = \lambda_3\theta_0 x_3. \tag{80}$$

Here it is assumed that the origin is fixed and the cube does not perform rigid rotation; electric potential is assumed to be zero at the origin.

The same problem was solved with the boundary element approach, which utilizes derived boundary integral equations and kernels. Only 6 quadratic isoparametric rectangular boundary elements were used to mesh the boundary of the cube. No internal cells were introduced. 16-point Gaussian quadrature was used to evaluate kernels and to perform numerical integration over the boundary elements. Weakly-singular integrals were evaluated using the quadratures derived by Pina et al. [29]. Strongly singular integrals were evaluated using the rigid body motion technique [26].

Obtained internal displacements and electric potential are compared with the analytic solution (80). The relative error does not exceed 0.4 %, which proves the efficiency of the developed boundary element technique and derived boundary integral equations.

Conclusion

This chapter presents novel boundary integral equations for 3D thermomagnetoelectroelasticity of anisotropic solids. Their derivation is strict and transparent, and the kernels are given explicitly. The scientific community was very close to obtaining of these equations in the recent years. In particular, Shiah and Tan [15, 16] derived truly boundary integral equations of anisotropic thermoelasticity in the mapped temperature domain. It is easy to verify, that the identity (10) transforms into the well-known Green's second integral identity in this domain. The latter was utilized by Shiah and Tan to obtain their integral formulae in the mapped domain. However, the generalization (10) of this identity allows strict and direct obtaining of the boundary integral equations in the real domain occupied by the solid, as it is shown in this chapter.

Another interesting result of this chapter is that the kernels of the Somigliana type integral identity of anisotropic thermomagnetoelectroelasticity are closely related to the fundamental solutions of thermomagnetoelectroelasticity and magnetoelectroelasticity. Using the Radon transform, it is shown, that two equations (35) and (36), one of which is obtained as a result of volume-to-surface integral transform, and the other results from the solution for a point unit heat drain, are identical. This fact strictly proves the correctness of the volume-to-surface integral transform made, and provides equations for determination of the unknown kernels.

Using the Radon transform technique the 3D anisotropic thermomagnetoelectroelastic Green's functions and their derivatives are obtained explicitly. They are reduced to surface and line integrals, which are regular and can be calculated numerically to desired accuracy using the Gauss quadratures. Verification is provided for both isotropic thermoelastic and anisotropic thermoelectroelastic solids. Perfect agreement with the known solutions is observed.

These studies can be naturally continued with future publications, which will have contained the derivation of the dual boundary element method for the analysis of solids with degenerate boundary (cracks). Also the authors are engaged in further development of Green's functions for thermomagnetoelectroelastic solids, in particular using Eq. (66).

References

[1] Fang D, Liu J. Fracture mechanics of piezoelectric and ferroelectric solids. London: Springer; 2013.

[2] Qin QH. Green's function and boundary elements of multifield materials. Oxford: Elsevier; 2007.

[3] Gao XW. Boundary element analysis in thermoelasticity with and without internal cells. Int J Numer Meth Engng 2003; 57: 975–990.
[4] Prasad NNV, Aliabadi MH, Rooke DP. The dual boundary element method for thermoelastic crack problems. Int. J. Fract. 1994; 66: 255–272.
[5] Mukherjee YX, Shah K, Mukherjee S. Thermoelastic fracture mechanics with regularized hypersingular boundary integral equations. Eng Anal Bound Elem 1999; 23: 89–96.
[6] Koshelev V, Ghassemi A. Complex variable BEM for thermo- and poroelasticity. Eng Anal Bound Elem 2004; 28: 825–832.
[7] Pasternak I, Pasternak R, Sulym H. A comprehensive study on the 2D boundary element method for anisotropic thermoelectroelastic solids with cracks and thin inhomogeneities. Eng Anal Bound Elem 2013; 37: 419–433.
[8] Pasternak I, Pasternak R, Sulym H. Boundary integral equations for 2D thermoelectroelasticity of a half-space with cracks and thin inclusions. Eng Anal Bound Elem 2013; 37: 1514–1523.
[9] Pasternak I, Pasternak R, Sulym H. Boundary integral equations and Green's functions for 2D thermoelectroelastic bimaterial. Eng Anal Bound Elem 2014; 48: 87–101.
[10] Pasternak I, Pasternak R, Sulym H. 2D boundary element analysis of defective thermoelectroelastic bimaterial with thermally imperfect but mechanically and electrically perfect interface. Eng Anal Bound Elem 2015; 61: 194–206.
[11] Deb A, Banerjee PK. BEM for general anisotropic 2D elasticity using particular integrals. Commun Appl Num Meth 1990; 6: 111–119.
[12] Deb A, Henry Jr. DP, Wilson EB. Alternate BEM formulation for 2D and 3D anisotropic thermoelasticity. Int. J. Solids Struct. 1991; 27: 1721–1738.
[13] Shiah YC, Tan CL. Exact boundary integral transformation of the thermoelastic domain integral in BEM for general 2D anisotropic elasticity. Computational Mechanics 1999; 23: 87–96.
[14] Shiah YC, Tan CL. Fracture mechanics analysis in 2-D anisotropic thermoelasticity using BEM, CMES 1, No. 3 (2000) 91–99.
[15] Shiah YC, Tan CL. Boundary element method for thermoelastic analysis of three-dimensional transversely isotropic solids. Int J Sol Struct 2012; 49: 2924–2933.
[16] Shiah YC, Tan CL. The boundary integral equation for 3D general anisotropic thermoelasticity. CMES 2014; 102(No. 6): 425–447.
[17] Hou PF, Leung AYT, Chen CP. Fundamental solution for transversely isotropic thermoelastic materials. Int J Sol Struct 2008; 45: 392–408.
[18] Hou PF, Leung AYT, He YJ. Three-dimensional Green's functions for transversely isotropic thermoelastic bimaterials. Int J Sol Struct 2008; 45: 6100–6113.
[19] Deans SR. The Radon transform and some of its applications. New York: Wiley-Interscience Publication; 1983.
[20] Ting TCT. Anisotropic elasticity: theory and applications. New York: Oxford University Press; 1996.

[21] Buroni FC, Sáez A. Three-dimensional Green's function and its derivative for materials with general anisotropic magneto-electro-elastic coupling. Proc R Soc A 2010; 466: 515–537.
[22] Pan E, Yuan FG. Three-dimensional Green's functions in anisotropic bimaterials. Int J Sol Struct 2000; 37: 5329–5351.
[23] Pan E, Chen W. Static Green's functions in anisotropic media. New York: Cambridge University Press; 2015.
[24] Wu KC. Generalization of the Stroh formalism to 3-dimensional anisotropic elasticity. Journal of Elasticity 1998; 51: 213–225.
[25] Xie L, Zhang C, Hwu C, Sladek J, Sladek V. On two accurate methods for computing 3D Green's function and its first and second derivatives in piezoelectricity. Eng Anal Bound Elem 2015; 61: 183–193.
[26] Brebbia CA, Telles JCF, Wrobel LC. Boundary element techniques. Theory and applications in engineering. New York: Springer-Verlag; 1984.
[27] Wang CY, Achenbach JD. Three-dimensional time-harmonic elastodynamic Green's functions for anisotropic solids. Proc R Soc Lond 1995; A 449: 441–458.
[28] Dunn ML. Micromechanics of coupled electroelastic composites: effective thermal expansion and pyroelectric coefficients. J Appl Phys 1993; 73: 5131–5140.
[29] Pina HLG, Fernandes JLM, Brebbia CA. Some numerical integration formulae over triangles and squares with a 1/R singularity. Appl Math Modelling 1981; 5: 210–211.

CHAPTER 4. Boundary element modeling of 3D cracked thermomagnetoelectroelastic solids

4.1. Introduction

Thermomagnetoelectroelastic (TMEE) materials are used in the wide range of modern precise devices. Those are smart structures (pyroelectrics, pyromagnetics and composite materials containing both phases), which can convert different fields, and serve as sensors, actuators or even complex micro-electro-mechanical systems. The rapid development of modern multi-field materials and micro-electro-mechanical technologies raises increasing attention to their modeling and simulation. Particular interest is focused on the issues of fracture mechanics of TMEE materials [1]. Since TMEE materials are anisotropic by nature, their analysis is more complicated than those of isotropic materials.

The boundary element method (BEM) is widely applied in the linear fracture mechanics [2, 3, 4], since it allows accurate evaluation of field intensity factors at the crack front and requires only boundary mesh. Various boundary element techniques were proposed for 3D fracture mechanics analysis. Mi and Aliabadi [3] derived a 3D dual BEM for analysis of 3D cracks in isotropic linear elastic solids. Saez et al. [5] presented a boundary element formulation for crack analysis in transversely isotropic solids. Pan and Yuan [6] developed a single-domain BEM for 3D fracture mechanics analysis in generally anisotropic solids. Rungamornrat and Mear [7] derived a symmetric Galerkin BEM for analysis of cracks in 3D anisotropic media. These approaches are closely related to the techniques of anisotropic Green's functions evaluation [8, 9, 10], since the latter significantly influence efficiency and accuracy of the BEM.

Nevertheless, coupling of different fields in the solid's material significantly complicates boundary element formulations. Many researches address the issues of thermal expansion influence on fracture parameters. In instance, Dell'erba et al. [11] developed a dual BEM for 3D thermoelastic crack problems. Mukherjee et al. [12] derived regularized hypersingular boundary integral equations for isotropic thermoelastic fracture mechanics.

A number of works address piezoelectric, piezomagnetic and magnetoelectroelastic coupling. Rungamornrat and Mear [13] and Rungamornrat et al. [14] derived a symmetric Galerkin BEM for 3D fracture mechanics analysis of piezoelectric solids. Zhao et al. [15] presented the extended discontinuity boundary integral equation method for vertical cracks in magnetoelectroelastic medium. Muñoz-Reja et al. [16] presented the 3D BEM for fracture mechanics analysis of anisotropic magnetoelectroelastic materials.

However, to this end there is no general 3D BEM for analysis of 3D cracks in anisotropic medium, which couples both thermal and magneto-electro-mechanical fields. Several papers [17, 18, 19] address only the particular problems for a penny-shaped crack or two parallel concentric circular cracks in a thermopiezoelectric

medium. No works addressing TMEE medium containing 3D cracks of arbitrary shape were found in scientific literature.

Besides, there is no single and efficient approach for evaluation of anisotropic kernel functions, since the latter can be presented through the contour integrals or the particular eigenvalue problems. Different approaches [20, 21] are used; however, computational costs are high, which is essential in the derivation of fast BEM code.

Therefore, this chapter utilizes previously developed novel boundary integral equations [22] for obtaining the dual BEM for TMEE solids containing 3D cracks. All kernels are obtained explicitly. The issues on the efficient numerical evaluation of kernel functions, integration of singular and hypersingular integrals and accurate determination of field intensity factors are discussed in details.

4.2. Governing equations of heat conduction and thermomagnetoelectroelasticity

According to [22], in a fixed Cartesian coordinate system $Ox_1x_2x_3$ the equilibrium equations, the Maxwell equations (Gauss theorem for electric and magnetic fields), and the balance equations of heat conduction in the steady-state case can be presented in the following compact form

$$\tilde{\sigma}_{Ij,j} + \tilde{f}_I = 0, \quad h_{i,i} - f_h = 0, \tag{1}$$

where the capital index varies from 1 to 5, while the lower case index varies from 1 to 3, i.e. $I = 1,2,...,5$. $i = 1,2,3$. Here and further the Einstein summation convention is used. A comma at subscript denotes differentiation with respect to a coordinate indexed after the comma, i.e. $u_{i,j} = \partial u_i / \partial x_j$.

In the assumption of small strains and fields' strengths the constitutive equations of linear thermomagnetoelectroelasticity in the compact notations are as follows [22]

$$\tilde{\sigma}_{Ij} = \tilde{C}_{IjKm}\tilde{u}_{K,m} - \tilde{\beta}_{Ij}\theta, \quad h_i = -k_{ij}\theta_{,j}, \tag{2}$$

where

$$\begin{aligned}
&\tilde{u}_i = u_i,\ \tilde{u}_4 = \phi,\ \tilde{u}_5 = \psi\ ;\ \tilde{f}_i = f_i,\ \tilde{f}_4 = -q,\ \tilde{f}_5 = b_m;\\
&\tilde{\sigma}_{ij} = \sigma_{ij},\ \tilde{\sigma}_{4j} = D_j,\ \tilde{\sigma}_{5j} = B_j;\\
&\tilde{C}_{ijkm} = C_{ijkm},\ \tilde{C}_{ij4m} = e_{mij},\ \tilde{C}_{4jkm} = e_{jkm},\ \tilde{C}_{4j4m} = -\kappa_{jm},\\
&\tilde{C}_{ij5m} = h_{mij},\ \tilde{C}_{5jkm} = h_{jkm},\ \tilde{C}_{5j5m} = -\mu_{jm},\\
&\tilde{C}_{4j5m} = -\gamma_{jm},\ \tilde{C}_{5j4m} = -\gamma_{jm};\\
&\tilde{\beta}_{ij} = \beta_{ij},\ \tilde{\beta}_{4j} = -\chi_j,\ \tilde{\beta}_{5j} = \nu_j \quad (i,j,k,m = 1,2,3);
\end{aligned} \tag{3}$$

σ_{ij} is a stress tensor; f_i is a body force vector; D_i is an electric displacement vector; q is a free charge volume density; B_i is a magnetic induction vector; b_m is a body current; h_i is a heat flux; f_h is a distributed heat source density; u_i is a displacement vector; ϕ, ψ are the electric and magnetic potentials, respectively; θ is a temperature change with respect to the reference temperature; C_{ijkm} are the elastic stiffnesses (elastic moduli); k_{ij} are heat conduction coefficients; e_{ijk}, h_{ijk} are piezoelectric and piezomagnetic constants; κ_{ij}, μ_{ij}, γ_{ij} are dielectric permittivities, magnetic

permeabilities and electromagnetic constants, respectively; β_{ij}, χ_i and ν_i are thermal moduli, pyroelectric coefficients and pyromagnetic coefficients, respectively.

According to [22], the extended magnetoelectroelastic tensor $\tilde{C}_{IjKm}$ has the following useful symmetry property

$$\tilde{C}_{IjKm} = \tilde{C}_{KmIj}. \tag{4}$$

Thus, the problem of linear thermomagnetoelectroelasticity is to solve partial differential equations (1) and (2) under the given boundary conditions and volume loading. Since magneto-electro-mechanical fields do not influence temperature field in the considered problem (uncoupled thermomagnetoelectroelasticity) the first step is to solve the heat conduction equation and the second one is to determine mechanical, electric and magnetic fields acting in the solid.

4.3. Hypersingular boundary integral equations for 3D thermomagnetoelectroelasticity

Recently, novel truly boundary integral formulae were obtained for 3D anisotropic heat conduction and thermomagnetoelectroelasticity [22]

$$\theta(\mathbf{y}) = \iint_{\partial\mathfrak{B}} \left(\Theta^*(\mathbf{x},\mathbf{y}) h_n(\mathbf{x}) - H^*(\mathbf{x},\mathbf{y})\theta(\mathbf{x})\right) dS(\mathbf{x}) - \iiint_{\mathfrak{B}} \Theta^*(\mathbf{x},\mathbf{y}) f_h(\mathbf{x}) dV(\mathbf{x}), \tag{5}$$

$$\begin{aligned} \tilde{u}_I(\mathbf{y}) = & \iint_{\partial\mathfrak{B}} \left(U_{IJ}(\mathbf{x},\mathbf{y})\tilde{t}_J(\mathbf{x}) - T_{IJ}(\mathbf{x},\mathbf{y})\tilde{u}_J(\mathbf{x})\right) dS(\mathbf{x}) \\ & + \iint_{\partial\mathfrak{B}} \left[R_I(\mathbf{x},\mathbf{y})\theta(\mathbf{x}) + V_I(\mathbf{x},\mathbf{y}) h_n(\mathbf{x})\right] dS(\mathbf{x}) \\ & + \iiint_{\mathfrak{B}} U_{IJ}(\mathbf{x},\mathbf{y}) \tilde{f}_J(\mathbf{x}) dV(\mathbf{x}) - \iiint_{\mathfrak{B}} V_I(\mathbf{x},\mathbf{y}) f_h(\mathbf{x}) dV(\mathbf{x}), \end{aligned} \tag{6}$$

$$\Theta^*(\mathbf{x},\mathbf{y}) = -\frac{1}{8\pi^2 |\mathbf{x}-\mathbf{y}|} \oint_{|\boldsymbol{\lambda}|=1} \left(k_{ij}\lambda_i\lambda_j\right)^{-1} dl(\boldsymbol{\lambda}), \quad H^*(\mathbf{x},\mathbf{y}) = -k_{ij} n_i(\mathbf{x}) \Theta^*_{,j}(\mathbf{x},\mathbf{y}); \tag{7}$$

$$U_{IJ}(\mathbf{x},\mathbf{y}) = \frac{1}{8\pi^2 |\mathbf{x}-\mathbf{y}|} \oint_{|\boldsymbol{\lambda}|=1} \Gamma^{-1}_{IJ}(\boldsymbol{\lambda}) dl(\boldsymbol{\lambda}), \quad T_{QI}(\mathbf{x},\mathbf{y}) = \tilde{C}_{IjKm} n_j(\mathbf{x}) U_{QK,m}(\mathbf{x},\mathbf{y}); \tag{8}$$

$$V_I(\mathbf{x},\mathbf{y}) = \frac{1}{8\pi^2} \iint_{\substack{|\boldsymbol{\xi}|=1,\\ \boldsymbol{\xi}\cdot\mathbf{t}>0}} \frac{\Gamma^{-1}_{IJ}(\boldsymbol{\xi}) \tilde{\beta}_{Jk} \xi_k}{k_{qr}\xi_q\xi_r} dS(\boldsymbol{\xi}), \quad R_I(\mathbf{x},\mathbf{y}) = k_{mj} V_{I,j}(\mathbf{x},\mathbf{y}) n_m(\mathbf{x}), \tag{9}$$

where $\partial\mathfrak{B}$ is a boundary of the domain $\mathfrak{B}$ occupied by the solid; n_p is a unit outwards normal vector to the surface $\partial\mathfrak{B}$; $\tilde{t}_I = \tilde{\sigma}_{ij} n_j$ is an extended traction vector; $h_n = h_i n_i$; $\mathbf{t}$ is a unit vector collinear with $\mathbf{x}-\mathbf{y}$; and $\boldsymbol{\lambda}$ is a unit vector normal to $\mathbf{x}-\mathbf{y}$; $\mathbf{y}$ is an internal point in the domain $\mathfrak{B}$; $\Gamma^{-1}_{IJ}(\boldsymbol{\xi})$ are the components of the matrix, which is inverse of the matrix $\Gamma_{IK}(\boldsymbol{\xi}) = \tilde{C}_{IjKm}\xi_j\xi_m$, i.e. $\Gamma^{-1}_{IK}(\boldsymbol{\xi})\Gamma_{KJ}(\boldsymbol{\xi}) = \delta_{IJ}$. Here and further the derivatives are evaluated for the variables x_i.

Integral formulae are the basis for derivation of the boundary integral equations, which replaces the boundary value problem for partial differential equations (1), (2). Taking the limit when internal point $\mathbf{y}$ approaches the boundary point $\mathbf{x}_0 \in \partial\mathfrak{B}$ in the assumption that the boundary $\partial\mathfrak{B}$ is smooth at $\mathbf{x}_0$ one obtains

$$\frac{1}{2}\theta(\mathbf{x}_0) = \iint_{\partial\mathfrak{B}} \Theta^*(\mathbf{x},\mathbf{x}_0) h_n(\mathbf{x}) dS(\mathbf{x}) - \mathrm{CPV} \iint_{\partial\mathfrak{B}} H^*(\mathbf{x},\mathbf{x}_0)\theta(\mathbf{x}) dS(\mathbf{x}) - \iiint_{\mathfrak{B}} \Theta^*(\mathbf{x},\mathbf{x}_0) f_h(\mathbf{x}) dV(\mathbf{x}), \tag{10}$$

$$\frac{1}{2}\tilde{u}_I(\mathbf{x}_0) = \iint_{\partial\mathfrak{B}} U_{IJ}(\mathbf{x},\mathbf{x}_0)\tilde{t}_J(\mathbf{x}) dS(\mathbf{x}) - \mathrm{CPV} \iint_{\partial\mathfrak{B}} T_{IJ}(\mathbf{x},\mathbf{x}_0)\tilde{u}_J(\mathbf{x}) dS(\mathbf{x}) + \iint_{\partial\mathfrak{B}} \left[R_I(\mathbf{x},\mathbf{x}_0)\theta(\mathbf{x}) + V_I(\mathbf{x},\mathbf{x}_0) h_n(\mathbf{x}) \right] dS(\mathbf{x}) + \iiint_{\mathfrak{B}} U_{IJ}(\mathbf{x},\mathbf{x}_0)\tilde{f}_J(\mathbf{x}) dV(\mathbf{x}) - \iiint_{\mathfrak{B}} V_I(\mathbf{x},\mathbf{x}_0) f_h(\mathbf{x}) dV(\mathbf{x}), \tag{11}$$

where CPV stands for the Cauchy Principal Value of the integral. These equations allow obtaining the unknown boundary functions, which are not set by the boundary conditions. Thereafter, when all boundary functions are known Eqs (5), (6) allow determining thermal, magnetic, electric and mechanical fields at an arbitrary internal point of the solid.

Nevertheless, integral equations (10), (11) degenerate, when the boundary $\partial\mathfrak{B}$ or its part has the shape of a mathematical cut [23]. In this case both displacement and traction boundary integral equations should be used. Therefore, one should utilize Eqs (2), (5) and (6) to derive heat flux and extended stress integral formulae and then apply limiting procedure to obtain heat flux and extended traction integral equations.

Substituting Eqs (5), (6) into the constitutive relations (2) one obtains

$$h_i(\mathbf{y}) = \iint_{\partial\mathfrak{B}} \left(\Theta_i^{**}(\mathbf{x},\mathbf{y}) h_n(\mathbf{x}) - H_i^{**}(\mathbf{x},\mathbf{y})\theta(\mathbf{x}) \right) dS(\mathbf{x}) - \iiint_{\mathfrak{B}} \Theta_i^{**}(\mathbf{x},\mathbf{y}) f_h(\mathbf{x}) dV(\mathbf{x}), \tag{12}$$

$$\tilde{\sigma}_{Ij}(\mathbf{y}) = \iint_{\partial\mathfrak{B}} \left(D_{IjK}(\mathbf{x},\mathbf{y})\tilde{t}_K(\mathbf{x}) - S_{IjK}(\mathbf{x},\mathbf{y})\tilde{u}_K(\mathbf{x}) \right) dS(\mathbf{x}) + \iint_{\partial\mathfrak{B}} \left[Q_{Ij}(\mathbf{x},\mathbf{y})\theta(\mathbf{x}) + W_{Ij}(\mathbf{x},\mathbf{y}) h_n(\mathbf{x}) \right] dS(\mathbf{x}) + \iiint_{\mathfrak{B}} D_{IjK}(\mathbf{x},\mathbf{y})\tilde{f}_K(\mathbf{x}) dV(\mathbf{x}) - \iiint_{\mathfrak{B}} W_{Ij}(\mathbf{x},\mathbf{y}) f_h(\mathbf{x}) dV(\mathbf{x}), \tag{13}$$

where the kernels are equal to

$$\Theta_i^{**} = k_{ij}\Theta^*_{,j}, \quad H_i^{**} = -k_{ij}k_{mp}n_m\Theta^*_{,pj}; \tag{14}$$

$$D_{IjK} = -\tilde{C}_{IjMp}U_{MK,p}, \quad S_{IjK} = -\tilde{C}_{IjMp}\tilde{C}_{KqRs}n_q U_{MR,ps}, \tag{15}$$

$$W_{Ij} = -\left[\tilde{C}_{IjMp}V_{M,p} + \tilde{\beta}_{Ij}\Theta^* \right], \quad Q_{Ij} = -\left[\tilde{C}_{IjMp}V_{M,sp} + \tilde{\beta}_{Ij}\Theta^*_{,s} \right] k_{qs}n_q. \tag{16}$$

Here it is accounted for Eqs (7)–(9) and the identity $\frac{\partial}{\partial y} f(x-y) = -\frac{\partial}{\partial x} f(x-y)$.

However, prior to the limiting procedure the strength of singularity of the kernels should be studied. To obtain explicit expressions for kernels (14)–(16), one should write formulae for the derivatives of kernel functions Θ^*, U_{IJ} and V_I. This task can be performed with the approach presented by Buroni and Sáez [24]. The kernels' derivatives are rewritten as integrals over the unit sphere, and then their representation in the form given by Wang and Achenbach [25] is used to proceed with integration by parts. (The representation of kernels as integrals over a unit sphere is naturally obtained in their derivation procedure, which utilizes direct and

inverse Radon transforms [22].) Application of this approach to the kernel functions (7), (8), (9) leads to

$$\Theta^*_{,i}(\mathbf{x},\mathbf{y}) = -\frac{1}{8\pi^2}\oint\limits_{|\boldsymbol{\lambda}|=1}\int\limits_{-1}^{1}\frac{\xi_i\delta'(br)}{k_{qs}\xi_q\xi_s}dbdl(\boldsymbol{\lambda}),$$
$$\Theta^*_{,ij}(\mathbf{x},\mathbf{y}) = -\frac{1}{8\pi^2}\oint\limits_{|\boldsymbol{\lambda}|=1}\int\limits_{-1}^{1}\frac{\xi_i\xi_j\delta''(br)}{k_{qs}\xi_q\xi_s}dbdl(\boldsymbol{\lambda}); \tag{17}$$

$$U_{IJ,k}(\mathbf{x},\mathbf{y}) = \frac{1}{8\pi^2}\oint\limits_{|\boldsymbol{\lambda}|=1}\int\limits_{-1}^{1}\Gamma^{-1}_{IJ}(\boldsymbol{\xi})\xi_k\delta'(br)dbdl(\boldsymbol{\lambda}),$$
$$U_{IJ,km}(\mathbf{x},\mathbf{y}) = \frac{1}{8\pi^2}\oint\limits_{|\boldsymbol{\lambda}|=1}\int\limits_{-1}^{1}\Gamma^{-1}_{IJ}(\boldsymbol{\xi})\xi_k\xi_m\delta''(br)dbdl(\boldsymbol{\lambda}); \tag{18}$$

$$V_{I,p}(\mathbf{x},\mathbf{y}) = \frac{1}{8\pi^2}\oint\limits_{|\boldsymbol{\lambda}|=1}\int\limits_{-1}^{1}\frac{\Gamma^{-1}_{IJ}(\boldsymbol{\xi})\tilde{\beta}_{Jk}\xi_k\xi_p}{k_{qr}\xi_q\xi_r}\delta(br)dbdl(\boldsymbol{\lambda}),$$
$$V_{I,ps}(\mathbf{x},\mathbf{y}) = \frac{1}{8\pi^2}\oint\limits_{|\boldsymbol{\lambda}|=1}\int\limits_{-1}^{1}\frac{\Gamma^{-1}_{IJ}(\boldsymbol{\xi})\tilde{\beta}_{Jk}\xi_k\xi_p\xi_s}{k_{qr}\xi_q\xi_r}\delta'(br)dbdl(\boldsymbol{\lambda}), \tag{19}$$

where $\delta'(x)$ and $\delta''(x)$ are the first and the second derivatives of the Dirac delta-function $\delta(x)$; $\boldsymbol{\xi} = a\boldsymbol{\lambda} + b\mathbf{t}$; $a = \sqrt{1-b^2}$; $r = |\mathbf{x}-\mathbf{y}|$; $\mathbf{t} = (\mathbf{x}-\mathbf{y})/r$; $\boldsymbol{\lambda}\cdot\mathbf{t} = 0$; $\boldsymbol{\xi}\cdot(\mathbf{x}-\mathbf{y}) = br$.

Consider the inner integrals in the abovementioned equations. Accounting for the properties of generalized functions (distributions)

$$\int\limits_{-1}^{1}f(b)\delta(rb)db = \frac{1}{r}f(0),\quad \int\limits_{-1}^{1}f(b)\delta'(rb)db = -\frac{1}{r^2}f'(0),\quad \int\limits_{-1}^{1}f(b)\delta''(rb)db = \frac{1}{r^3}f''(0), \tag{20}$$

therefore, Eqs (17)–(19) can be reduced to

$$\Theta^*_{,i}(\mathbf{x},\mathbf{y}) = \frac{1}{8\pi^2 r^2}\oint\limits_{|\boldsymbol{\lambda}|=1}\left[t_i\gamma^{-1} - \lambda_i\gamma^{-2}k_{mn}(\lambda_m t_n + \lambda_n t_m)\right]dl(\boldsymbol{\lambda}),$$
$$\Theta^*_{,ij}(\mathbf{x},\mathbf{y}) = -\frac{1}{4\pi^2 r^3}\oint\limits_{|\boldsymbol{\lambda}|=1}\gamma^{-1}\left[t_i t_j + \omega(t_i\lambda_j + \lambda_i t_j) + \lambda_i\lambda_j\left[\omega^2 - \gamma^{-1}k_{mp}t_m t_p\right]\right]dl(\boldsymbol{\lambda}); \tag{21}$$

$$U_{IJ,k}(\mathbf{x},\mathbf{y}) = -\frac{1}{8\pi^2 r^2}\oint\limits_{|\boldsymbol{\lambda}|=1}\left[t_k\Gamma^{-1}_{IJ}(\boldsymbol{\lambda}) + \lambda_k F_{IJ}\right]dl(\boldsymbol{\lambda}),$$
$$\begin{aligned}U_{IJ,km}(\mathbf{x},\mathbf{y}) = \frac{1}{8\pi^2 r^3}\oint\limits_{|\boldsymbol{\lambda}|=1}\Big[&2\Gamma^{-1}_{IJ}(\boldsymbol{\lambda})t_k t_m + 2F_{IJ}(t_k\lambda_m + t_m\lambda_k)\\ &-\lambda_k\lambda_m\left[2\Gamma^{-1}_{IP}(\boldsymbol{\lambda})\tilde{C}_{PlQs}t_l t_s\Gamma^{-1}_{QJ}(\boldsymbol{\lambda})\right.\\ &\left.+\left(F_{IP}\Gamma^{-1}_{QJ}(\boldsymbol{\lambda}) + \Gamma^{-1}_{IP}(\boldsymbol{\lambda})F_{QJ}\right)\tilde{C}_{PlQs}(t_l\lambda_s + t_s\lambda_l)\right]\Big]dl(\boldsymbol{\lambda});\end{aligned} \tag{22}$$

$$V_{I,p}(\mathbf{x},\mathbf{y}) = \frac{1}{8\pi^2 r}\oint\limits_{|\boldsymbol{\lambda}|=1}\gamma^{-1}\Gamma^{-1}_{IJ}(\boldsymbol{\lambda})\tilde{\beta}_{Jk}\lambda_k\lambda_p dl(\boldsymbol{\lambda}),$$
$$V_{I,pq}(\mathbf{x},\mathbf{y}) = -\frac{1}{8\pi^2 r^2}\oint\limits_{|\boldsymbol{\lambda}|=1}\gamma^{-1}\tilde{\beta}_{Jk}\left[\left(F_{IJ} + \Gamma^{-1}_{IJ}(\boldsymbol{\lambda})\omega\right)\lambda_k\lambda_p\lambda_q + \Gamma^{-1}_{IJ}(\boldsymbol{\lambda})\mu_{kpq}\right]dl(\boldsymbol{\lambda}), \tag{23}$$

where $\gamma = k_{ij}\lambda_i\lambda_j$, $\omega = -\gamma^{-1}k_{mn}\left(t_m\lambda_n + t_n\lambda_m\right)$;

$F_{LJ} = \left.\dfrac{d\Gamma_{LJ}^{-1}(\boldsymbol{\xi})}{db}\right|_{b=0} = -\Gamma_{IK}^{-1}(\boldsymbol{\lambda})\tilde{C}_{KlMs}\Gamma_{MJ}^{-1}(\boldsymbol{\lambda})\left(t_l\lambda_s + t_s\lambda_l\right)$; $\mu_{kpq} = t_k\lambda_p\lambda_q + \lambda_k t_p\lambda_q + \lambda_k\lambda_p t_q$. In derivation of Eqs (21)–(23) the symmetry property (4) was utilized.

From Eqs (14)–(16) and (21)–(23) it is readily seen that kernels Θ_i^{**}, D_{ljK} and Q_{lj} are singular, kernels H_i^{**}, S_{ljK} are hypersingular, and W_{lj} is weakly singular. Therefore, for a smooth boundary surface at the point $\mathbf{x}_0 \in \partial\mathfrak{B}$ Eqs (12), (13) transform into the following boundary integral equations

$$\frac{1}{2}h_n(\mathbf{x}_0) = n_j(\mathbf{x}_0)\Bigg[\mathrm{CPV}\iint_{\partial\mathfrak{B}}\Theta_i^{**}(\mathbf{x},\mathbf{x}_0)h_n(\mathbf{x})\,dS(\mathbf{x}) - \mathrm{HFP}\iint_{\partial\mathfrak{B}}H_i^{**}(\mathbf{x},\mathbf{x}_0)\theta(\mathbf{x})\,dS(\mathbf{x}) - \iiint_{\mathfrak{B}}\Theta_i^{**}(\mathbf{x},\mathbf{x}_0)f_h(\mathbf{x})\,dV(\mathbf{x})\Bigg], \tag{24}$$

$$\begin{aligned}\frac{1}{2}\tilde{t}_I(\mathbf{x}_0) = n_j(\mathbf{x}_0)\Bigg[&\mathrm{CPV}\iint_{\partial\mathfrak{B}}D_{IjK}(\mathbf{x},\mathbf{x}_0)\tilde{t}_K(\mathbf{x})\,dS(\mathbf{x}) - \mathrm{HFP}\iint_{\partial\mathfrak{B}}S_{IjK}(\mathbf{x},\mathbf{x}_0)\tilde{u}_K(\mathbf{x})\,dS(\mathbf{x})\\ &+\mathrm{CPV}\iint_{\partial\mathfrak{B}}Q_{Ij}(\mathbf{x},\mathbf{x}_0)\theta(\mathbf{x})\,dS(\mathbf{x}) + \iint_{\partial\mathfrak{B}}W_{Ij}(\mathbf{x},\mathbf{x}_0)h_n(\mathbf{x})\,dS(\mathbf{x})\\ &+\iiint_{\mathfrak{B}}D_{IjK}(\mathbf{x},\mathbf{x}_0)\tilde{f}_K(\mathbf{x})\,dV(\mathbf{x}) - \iiint_{\mathfrak{B}}W_{Ij}(\mathbf{x},\mathbf{x}_0)f_h(\mathbf{x})\,dV(\mathbf{x})\Bigg],\end{aligned} \tag{25}$$

where HFP stands for the Hadamard Finite Part of the integral.

Consider a case when some part $C \in \partial\mathfrak{B}$ of the boundary $\partial\mathfrak{B}$ of the solid $\mathfrak{B}$ is a mathematical cut consisting of two faces C^+ and C^- (Fig. 1).

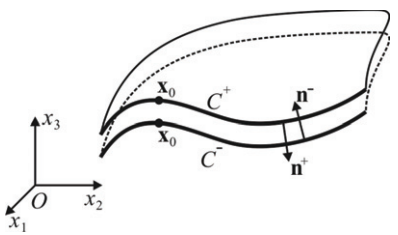

Fig. 1. Faces C^+ and C^- of the cut surface C

Since the boundary functions are discontinuous, at transition of the surface C they possess different values on its faces, which are denoted with corresponding superscripts "+" and "–". Kernel functions, which do not depend on the normal $\mathbf{n}$ to the surface, are the same on both faces C^+ and C^- of the cut C. Therefore,

$$\begin{aligned}&\iint_{C^+\cup C^-}\left(\Theta^*,\Theta_i^{**},U_{LJ},D_{IjK},V_I,W_{Ij}\right)^{\mathrm{T}}\left(h_n,h_n,\tilde{t}_I,\tilde{t}_K,h_n,h_n\right)dS =\\ &\iint_{C^+}\left(\Theta^*,\Theta_i^{**},U_{LJ},D_{IjK},V_I,W_{Ij}\right)^{\mathrm{T}}\left(\Sigma h_n,\Sigma h_n,\Sigma\tilde{t}_I,\Sigma\tilde{t}_K,\Sigma h_n,\Sigma h_n\right)dS,\end{aligned} \tag{26}$$

where $\Sigma f = f^+ + f^-$ and "T" stands for vector transpose. Since boundary functions h_n and $\tilde{t}_I$ depend on the normal vector and $\mathbf{n}^+(\mathbf{x}) = -\mathbf{n}^-(\mathbf{x})$ at the opposite faces of the cut

C, the function $\Sigma h_n = h_i^+ n_i^+ + h_i^- n_i^- = \left(h_i^+ - h_i^-\right) n_i^+$ is the heat flux discontinuity, and $\Sigma \tilde{t}_I = \left(\tilde{\sigma}_{Ij}^+ - \tilde{\sigma}_{Ij}^-\right) n_j^+$ is the extended stress discontinuity function.

Kernel functions, which depend on the normal $\mathbf{n}$, are opposite at the faces of the cut C, since $\mathbf{n}^+$ and $\mathbf{n}^-$ are opposite. Therefore

$$\iint\limits_{C^+ \cup C^-} \left(H^*, H_i^{**}, T_{IJ}, S_{IjK}, R_I, Q_{Ij}\right)^{\mathrm{T}} \left(\theta, \theta, \tilde{u}_I, \tilde{u}_K, \theta, \theta\right) dS = \iint\limits_{C^+} \left(H^*, H_i^{**}, T_{IJ}, S_{IjK}, R_I, Q_{Ij}\right)^{\mathrm{T}} \left(\Delta\theta, \Delta\theta, \Delta\tilde{u}_I, \Delta\tilde{u}_K, \Delta\theta, \Delta\theta\right) dS, \tag{27}$$

where $\Delta f = f^+ - f^-$, and thus $\Delta\theta$ is a temperature discontinuity at C and $\Delta\tilde{u}_I$ is an extended displacement discontinuity.

When $\mathbf{x}_0$ is collocated on C, the left hand sides of Eqs (10), (11), (24), (25) should be changed. It is obvious that both faces (C^+ and C^-) contribute the function at the left. When the surface C is smooth at $\mathbf{x}_0$ it is easy to verify that this contribution leads to the average value of the function at the left on C.

Therefore, when $\mathbf{x}_0 \in C$ the left hand side of Eq (10) looks as

$$\frac{1}{2}\left(\theta^+\left(\mathbf{x}_0\right) + \theta^-\left(\mathbf{x}_0\right)\right) = \frac{1}{2}\Sigma\theta\left(\mathbf{x}_0\right), \tag{28}$$

the left hand side of Eq (11) writes as

$$\frac{1}{2}\left(\tilde{u}_I^+\left(\mathbf{x}_0\right) + \tilde{u}_I^-\left(\mathbf{x}_0\right)\right) = \frac{1}{2}\Sigma\tilde{u}_I\left(x_0\right), \tag{29}$$

the left hand side of Eq (24) should be equal to

$$\frac{1}{2}\left(h_i^+\left(\mathbf{x}_0\right) + h_i^-\left(\mathbf{x}_0\right)\right) n_i^+\left(\mathbf{x}_0\right) = \frac{1}{2}\Delta h_n\left(\mathbf{x}_0\right), \tag{30}$$

and the left hand side of Eq (25) should be replaced with

$$\frac{1}{2}\left(\tilde{\sigma}_{Ij}^+\left(\mathbf{x}_0\right) + \tilde{\sigma}_{Ij}^-\left(\mathbf{x}_0\right)\right) n_j^+\left(\mathbf{x}_0\right) = \frac{1}{2}\Delta\tilde{t}_I\left(\mathbf{x}_0\right). \tag{31}$$

Thus, if one considers a solid containing a crack, Eqs (10), (11), (26), (27) are used when the collocation point $\mathbf{x}_0$ belongs to a smooth surface $\partial\mathfrak{B} \setminus C$ that bounds the solid, and a full system of equations (10), (11), (24), (25), (26), (27) is used (accounting for left hand sides given by Eqs (28)–(31)), when $\mathbf{x}_0$ belongs to a smooth crack surface C. This allows determining unknown components of the boundary functions θ, h_n, $\tilde{t}_I$ and $\tilde{u}_I$ at $\partial\mathfrak{B} \setminus C$ and all of the discontinuity functions $\Delta\theta$, Σh_n, $\Delta\tilde{u}_I$, $\Sigma\tilde{t}_I$ at C.

4.4. Boundary element solution of the obtained equations

4.4.1. Evaluation of kernels

When implemented in BEM analysis for 3D cases, the kernels given in integral form can require tremendous computational efforts, which perhaps can involve millions of computations for a simple 3D model. Therefore, it is essential to use special techniques for evaluation of kernels. In instance, for the magnetoelectroelastic

kernel (8) and its derivatives (22) (required for obtaining kernels (8), (15)) Xie et al. [20, 21] proposed three techniques, one of which is based on the direct numerical integration, and two others incorporate the residue theorem and reduce kernel evaluation to the Stroh eigenvalue problem.

The computational complexity of the direct numerical integration is $m \cdot O\left(n^3\right)$, where m is a number of quadrature nodes, and n is the dimension of the problem (5 for general thermomagnetoelectroelasticity, 4 for pyroelectric and 3 for thermoelastic materials), since matrix inversion is incorporated in kernels evaluation. The computational complexity of the Stroh eigenvalue problem is $\frac{2}{3}(2n)^3 + O\left(n^2\right) \approx 5.3n^3 + O\left(n^2\right)$ (if Householder transformations are used) or even higher. Therefore, computational costs of direct numerical integration are comparable to those of residue calculus, if the number of nodes is approximately about 10. However, special case of repeated eigenvalues should be considered separately in the residue calculus approach, which complicates corresponding computational algorithms. Thus, direct numerical integration approach is advantageous; however, one has to find the numerical quadrature, which provides the best accuracy at small number of nodes.

Since

$$\boldsymbol{\lambda} = \mathbf{n}\cos\phi + \mathbf{m}\sin\phi,$$

where $\mathbf{n}$ and $\mathbf{m}$ are two arbitrary orthogonal vectors in the oblique plane normal to $\mathbf{t}$, it is easy to show that the integrands in (7), (8), (17), (18), (19) are π-periodic functions in polar angle ϕ. Xie et al. [20, 21] used Gaussian quadrature for evaluation of these integrals. However, even at 25 Gaussian points the convergence of the results, especially for the second derivative, is not satisfactory.

Therefore, in this study it is proposed to use the trapezoid formula for numerical integration of the integrals involved in kernels. At first glance, it seems unreasonable, since it is known that Gaussian quadrature has the highest accuracy for polynomials. However, it was recently shown that trapezoid rule is exponentially convergent for integrals over a periodic interval [26, 27]. This useful feature is implemented in calculation of kernels (7), (8), (14)–(19). The only exception is the kernel (9), which is calculated the same as described in Ref. [22].

In the numerical examples section it is shown high convergence of the trapezoid rule applied to calculation of the kernels.

4.4.2. Boundary element mesh and special shape functions

At the first step (preprocessing) of the boundary element solution of derived boundary integral equations for a particular problem the surface $\partial\mathfrak{B}$ of the solid along with the crack surface C is meshed with quadrilateral quadratic discontinuous boundary elements. The local curvilinear coordinate system $O\xi\eta$ is associated with each boundary element, moreover, $-1 \le \xi \le 1$, $-1 \le \eta \le 1$. The collocation points are placed at nodes $\xi = (-2/3; 0; 2/3)$; $\eta = (-2/3; 0; 2/3)$. Therefore, there are 9 collocation points associated with each boundary element.

Boundary conditions along with unknown boundary and discontinuity functions are interpolated within the collocation points at each boundary element Γ_N as

$$\mathbf{b}_N(\xi,\eta)=\sum_{i=1}^{3}\sum_{j=1}^{3}\mathbf{b}_N^{i,j}\phi_i(\xi)\phi_j(\eta), \tag{32}$$

where $\mathbf{b}=\left(\theta,\Delta\theta,\Sigma\theta,h_n,\Sigma h_n,\Delta h_n,\tilde{u}_I,\Delta\tilde{u}_I,\Sigma\tilde{u}_I,\tilde{t}_I,\Sigma\tilde{t}_I,\Delta\tilde{t}_I\right)^{\mathrm{T}}$, and the discontinuous shape functions are given as [3]

$$\phi_1(\xi)=\xi\left(\frac{9}{8}\xi-\frac{3}{4}\right),\quad \phi_2(\xi)=\left(1-\frac{3}{2}\xi\right)\left(1+\frac{3}{2}\xi\right),\quad \phi_3(\xi)=\xi\left(\frac{9}{8}\xi+\frac{3}{4}\right). \tag{33}$$

If the side of the boundary element models the crack front, special shape functions are used for displacement and temperature discontinuity to capture the square root singularity [28, 29, 30] arising at crack front

$$\phi_i^{\Delta}(\xi)=\sqrt{1\pm\xi}\left(\Phi_{i1}^{\Delta}+\sum_{j=2}^{3}\Phi_{ij}^{\Delta}(1\pm\xi)^{j-1}\right). \tag{34}$$

Constants Φ_{ij}^{Δ} are determined from the system of equations $\phi_i(\xi_j)=\delta_{ij}$, where $\xi_j=(-2/3;0;2/3)$.

Special shape functions are also used for the heat flux discontinuity function Σh_n at the crack front boundary elements, when considering cracks with temperature boundary conditions given at their faces,

$$\phi_i^{\Sigma}(\xi)=\frac{1}{\sqrt{1\pm\xi}}\left(\Phi_{i1}^{\Sigma}+\sum_{j=2}^{3}\Phi_{ij}^{\Sigma}(1\pm\xi)^{j-1}\right). \tag{35}$$

Substituting (32) into the boundary integral equations (10), (11), (24), (25), (26), (27), one obtains the system of linear algebraic equations for unknown nodal values of the boundary and discontinuity functions.

4.4.3. Techniques for precise integration of regular, weakly, strongly and hyper-singular integrals

The coefficients of the obtained system of algebraic equations are the double integrals

$$I_{Nij}^{(1)}(\mathbf{x}_0)=\int_{-1}^{1}\int_{-1}^{1}\Theta^*\left(\mathbf{x}(\xi,\eta),\mathbf{x}_0\right)\phi_i(\xi)\phi_j(\eta)J_N(\xi,\eta)d\xi d\eta,$$

$$I_{Nij}^{(2)}(\mathbf{x}_0)=\int_{-1}^{1}\int_{-1}^{1}H^*\left(\mathbf{x}(\xi,\eta),\mathbf{x}_0\right)\phi_i(\xi)\phi_j(\eta)J_N(\xi,\eta)d\xi d\eta,$$

$$I_{Nijk}^{(3)}(\mathbf{x}_0)=\int_{-1}^{1}\int_{-1}^{1}\Theta_k^{**}\left(\mathbf{x}(\xi,\eta),\mathbf{x}_0\right)\phi_i(\xi)\phi_j(\eta)J_N(\xi,\eta)d\xi d\eta,$$

$$I_{Nijk}^{(4)}(\mathbf{x}_0)=\int_{-1}^{1}\int_{-1}^{1}H_k^{**}\left(\mathbf{x}(\xi,\eta),\mathbf{x}_0\right)\phi_i(\xi)\phi_j(\eta)J_N(\xi,\eta)d\xi d\eta,$$

$$I_{NijIJ}^{(5)}(\mathbf{x}_0)=\int_{-1}^{1}\int_{-1}^{1}U_{IJ}\left(\mathbf{x}(\xi,\eta),\mathbf{x}_0\right)\phi_i(\xi)\phi_j(\eta)J_N(\xi,\eta)d\xi d\eta,$$

$$I_{NijIJ}^{(6)}(\mathbf{x}_0)=\int_{-1}^{1}\int_{-1}^{1}T_{IJ}\left(\mathbf{x}(\xi,\eta),\mathbf{x}_0\right)\phi_i(\xi)\phi_j(\eta)J_N(\xi,\eta)d\xi d\eta,$$

$$I^{(7)}_{NijIkJ}(\mathbf{x}_0)=\int_{-1}^{1}\int_{-1}^{1} D_{IkJ}\left(\mathbf{x}(\xi,\eta),\mathbf{x}_0\right)\phi_i(\xi)\phi_j(\eta)J_N(\xi,\eta)d\xi d\eta,$$

$$I^{(8)}_{NijIkJ}(\mathbf{x}_0)=\int_{-1}^{1}\int_{-1}^{1} S_{IkJ}\left(\mathbf{x}(\xi,\eta),\mathbf{x}_0\right)\phi_i(\xi)\phi_j(\eta)J_N(\xi,\eta)d\xi d\eta,$$

$$I^{(9)}_{NijI}(\mathbf{x}_0)=\int_{-1}^{1}\int_{-1}^{1} V_I\left(\mathbf{x}(\xi,\eta),\mathbf{x}_0\right)\phi_i(\xi)\phi_j(\eta)J_N(\xi,\eta)d\xi d\eta,$$

$$I^{(10)}_{NijI}(\mathbf{x}_0)=\int_{-1}^{1}\int_{-1}^{1} R_I\left(\mathbf{x}(\xi,\eta),\mathbf{x}_0\right)\phi_i(\xi)\phi_j(\eta)J_N(\xi,\eta)d\xi d\eta,$$

$$I^{(11)}_{NijIk}(\mathbf{x}_0)=\int_{-1}^{1}\int_{-1}^{1} W_{Ik}\left(\mathbf{x}(\xi,\eta),\mathbf{x}_0\right)\phi_i(\xi)\phi_j(\eta)J_N(\xi,\eta)d\xi d\eta,$$

$$I^{(12)}_{NijIk}(\mathbf{x}_0)=\int_{-1}^{1}\int_{-1}^{1} Q_{Ik}\left(\mathbf{x}(\xi,\eta),\mathbf{x}_0\right)\phi_i(\xi)\phi_j(\eta)J_N(\xi,\eta)d\xi d\eta,$$

where $J_N(\xi,\eta)=\left|\dfrac{\partial\mathbf{x}}{\partial\xi}\times\dfrac{\partial\mathbf{x}}{\partial\eta}\right|$ is a Jacobian of variable change on the boundary element Γ_N.

Since the shape functions $\phi_i(\xi)$, $\phi_j(\eta)$ can be selected in the form (34) or (35) for elements, which model the crack front, customary Gaussian quadrature can produce high error, even if the collocation point $\mathbf{x}_0$ does not belong to the boundary element Γ_N. Therefore, in the present boundary element formulation the following polynomial mapping is used

$$\xi=\frac{1}{2}\left(3-\xi_1^2\right)\xi_1,\quad \eta=\frac{1}{2}\left(3-\eta_1^2\right)\eta_1,\quad d\xi d\eta=\frac{9}{4}\left(1-\xi_1^2\right)\left(1-\eta_1^2\right)d\xi_1 d\eta_1, \tag{36}$$

which maps the domain $(-1;1)\times(-1;1)$ onto itself and smoothens the integrand at $\xi_1=\pm1$; $\eta_1=\pm1$. After (36) is applied, the regular integrals are evaluated numerically with Gaussian quadrature (20 nodes are used).

Special attention should be paid to the case, when $\mathbf{x}_0=\mathbf{x}\left(\xi^0,\eta^0\right)$ belongs to the boundary element Γ_N. From Eqs (14)–(16), (21)–(23) it follows that in this case integrals $I^{(1)}$, $I^{(5)}$, $I^{(10)}$, $I^{(11)}$ are weakly singular, $I^{(2)}$, $I^{(3)}$, $I^{(6)}$, $I^{(7)}$, $I^{(12)}$ are strongly singular, and $I^{(4)}$, $I^{(8)}$ are hypersingular. Integral $I^{(9)}$ is always regular; therefore, it is evaluated numerically within the Gaussian quadrature. All other integrals are evaluated in the polar coordinate system, which yield

$$I=\frac{9}{4}\sum_{q=1}^{4}\int_{\theta_q}^{\theta_{q+1}}\int_{0}^{R_q(\theta)} F\left(\mathbf{x}(\xi,\eta),\mathbf{x}_0\right)\phi_i(\xi)\phi_j(\xi)J_N(\xi,\eta)\left(1-\xi_1^2\right)\left(1-\eta_1^2\right)r dr d\theta, \tag{37}$$

where $F\left(\mathbf{x}(\xi,\eta)-\mathbf{x}_0\right)$ is a corresponding kernel; $\xi=\xi\left(\xi_1^0+r\cos\theta\right)$, $\eta=\eta\left(\eta_1^0+r\sin\theta\right)$; $\mathbf{x}_0=\mathbf{x}\left(\xi^0,\eta^0\right)$ $\left(\xi^0=\xi\left(\xi_1^0\right),\ \eta^0=\eta\left(\eta_1^0\right)\right)$ is a collocation point at the boundary element Γ_N; $\theta_1=\arctan\left(-1-\eta_1^0,1-\xi_1^0\right)$, $\theta_2=\arctan\left(1-\eta_1^0,1-\xi_1^0\right)$, $\theta_3=\arctan\left(1-\eta_1^0,-1-\xi_1^0\right)$; $\theta_4=2\pi+\arctan\left(-1-\eta_1^0,-1-\xi_0\right)$; $\theta_5=2\pi+\theta_1$; $R_1(\theta)=\left(1-\xi_1^0\right)/\cos\theta$; $R_2(\theta)=\left(1-\eta_1^0\right)/\sin\theta$; $R_3(\theta)=\left(-1-\xi_1^0\right)/\cos\theta$; $R_4(\theta)=\left(-1-\eta_1^0\right)/\sin\theta$.

It is readily seen from Eq (37) that if the kernel $F(\mathbf{x},\mathbf{x}_0)$ is weakly singular $(F\sim 1/r)$ integral (37) is regular, since the polar transformation Jacobian cancels this singularity. Therefore, convenient Gaussian quadrature rule can be applied to evaluate this integral numerically.

For numerical evaluation of singular $(F\sim 1/r^2)$ and hypersingular $(F\sim 1/r^3)$ integrals Pan and Yuan [6] proposed to use the finite part Kutt's numerical quadrature [31, 32] for inner integral with respect to r and Gaussian quadrature for the outer regular integral with respect to θ. The same procedure is proposed here, however, Kutt's quadrature is modified to be more accurate (see Appendix A). With respect to this, inner finite part integrals are evaluated via Eq (A.1) assuming that

$$f(r)=F\left(\mathbf{x}(\xi,\eta),\mathbf{x}_0\right)\phi_i(\xi)\phi_j(\xi)J_N(\xi,\eta)\left(1-\xi_1^2\right)\left(1-\eta_1^2\right)r^{\lambda+1},$$

where $\lambda+1$ is the strength of singularity of the kernel $F(\mathbf{x},\mathbf{x}_0)$. Since Chebyshev nodes (A.3) used in the quadrature (A.1) do not require to evaluate $f(0)$, no other special treatment of singular terms is required.

One of important tasks in the computation of general 3D geometries with the collocation BEM is an accurate treatment of quasi-singular integrals, which arise due to presence of thin shapes etc. In this case other nonlinear mappings, in particular sinh transform [33], can be applied for accurate evaluation of 2D quasi-singular integrals.

4.4.4. Determination of field intensity factors

Consider a local coordinate system at a point A of the crack front (Fig. 2). The axes of this system are defined by three unit orthogonal vectors $\mathbf{n}$, $\mathbf{m}$, $\boldsymbol{\tau}$, where $\mathbf{n}$ is a normal to crack face; $\mathbf{m}$ is a tangent to the crack front curve at A, and $\boldsymbol{\tau}=\mathbf{n}\times\mathbf{m}$. Without loss in generality consider that the boundary element, which the point A belongs to, models the crack front line with its side $\xi=1$ (Fig. 2).

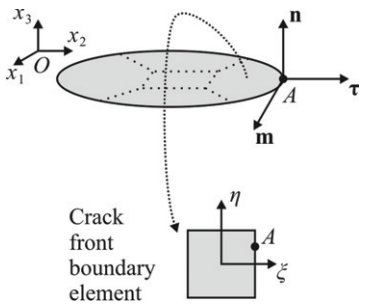

Fig. 2. Local coordinate system at crack front

Normal and tangent vectors are defined as

$$\mathbf{n}=\left(\frac{\partial\mathbf{x}}{\partial\xi}\times\frac{\partial\mathbf{x}}{\partial\eta}\right)\Big/\left|\frac{\partial\mathbf{x}}{\partial\xi}\times\frac{\partial\mathbf{x}}{\partial\eta}\right|;\quad \mathbf{m}=-\frac{\partial\mathbf{x}}{\partial\eta}\Big/\left|\frac{\partial\mathbf{x}}{\partial\eta}\right|, \tag{38}$$

where $\mathbf{x}(\xi,\eta)$ is a position vector, which defines the surface of the boundary element. Then according to Eq (32) the extended displacement discontinuity function $\Delta\tilde{\mathbf{u}}^*(\mathbf{x})$ in the local coordinate system on the considered boundary element is equal to

$$\Delta\tilde{\mathbf{u}}^*(\mathbf{x}) = \boldsymbol{\Omega}\sum_{i=1}^{3}\sum_{j=1}^{3}\Delta\tilde{\mathbf{u}}^{(i,j)}\phi_i^{\Delta}(\xi)\phi_j(\eta), \tag{39}$$

where $\Delta\tilde{\mathbf{u}}^{(i,j)}$ are the nodal values of the extended displacement discontinuity function, and $\boldsymbol{\Omega}$ is the rotation matrix, which is defined as

$$\boldsymbol{\Omega} = \begin{bmatrix} \tau_1 & n_1 & m_1 & 0 & 0 \\ \tau_2 & n_2 & m_2 & 0 & 0 \\ \tau_3 & n_3 & m_3 & 0 & 0 \\ 0 & 0 & 0 & 1 & 0 \\ 0 & 0 & 0 & 0 & 1 \end{bmatrix}. \tag{40}$$

According to [28, 29, 30] the field intensity factors vector at the point A of the crack front is defined as

$$\tilde{\mathbf{k}}^{(1)} = \lim_{\mathbf{x}\to\mathbf{x}(A)}\sqrt{\frac{\pi}{8s(\mathbf{x})}}\mathbf{L}\cdot\Delta\tilde{\mathbf{u}}^*(\mathbf{x}), \tag{41}$$

where $\tilde{\mathbf{k}}^{(1)} = [K_{\mathrm{II}}, K_{\mathrm{I}}, K_{\mathrm{III}}, K_D, K_B]^{\mathrm{T}}$; K_{I}, K_{II}, K_{III} are the stress intensity factors; K_D, K_B are electric displacement and magnetic induction intensity factors; $\mathbf{L}$ is a Barnett – Lothe tensor evaluated in the local coordinate system; and $s(\mathbf{x})$ is an arc length evaluated from $\mathbf{x}$ to A along the cross section of the crack with the plane $(\mathbf{n},\boldsymbol{\tau})$.

Expanding $s(\mathbf{x})$ into Taylor series at the vicinity of A one obtains

$$s = (1-\xi)\rho(\eta_A) + O\left((1-\xi)^2;(\eta_A-\eta)^2\right), \tag{42}$$

where

$$\rho(\eta_A) = \boldsymbol{\tau}\cdot\left.\frac{\partial\mathbf{x}}{\partial\xi}\right|_{\xi=1,\eta=\eta_A}. \tag{43}$$

Substituting (34) and (42) into (41) and evaluating the limit one obtains

$$\tilde{\mathbf{k}}^{(1)} = \sqrt{\frac{\pi}{8\rho(\eta_A)}}\mathbf{L}\cdot\boldsymbol{\Omega}\sum_{i=1}^{3}\sum_{j=1}^{3}\Delta\tilde{\mathbf{u}}^{(i,j)}\Phi_{i1}^{\Delta}\phi_j(\eta_A), \tag{44}$$

which is the formula implemented in the present BEM for precise evaluation of the field intensity factors.

According to [28] the Barnett – Lothe tensor in the local coordinate system can be evaluated with the following integral

$$\mathbf{L} = -\frac{1}{\pi}\int_0^{\pi}\boldsymbol{\Omega}\mathbf{N}_3(\theta)\boldsymbol{\Omega}^{\mathrm{T}}d\theta, \tag{45}$$

where $\mathbf{N}_3(\theta) = -\mathbf{R}(\theta)\mathbf{T}^{-1}(\theta)\mathbf{R}^{\mathrm{T}}(\theta) - \mathbf{Q}(\theta)$; $Q_{LJ}(\theta) = \tilde{C}_{IkJm}\omega_k\omega_m$, $T_{LJ}(\theta) = \tilde{C}_{IkJm}\vartheta_k\vartheta_m$, $R_{LJ}(\theta) = \tilde{C}_{IkJm}\omega_k\vartheta_m$; $\boldsymbol{\omega} = \boldsymbol{\tau}\cos\theta + \mathbf{n}\sin\theta$, $\boldsymbol{\vartheta} = -\boldsymbol{\tau}\sin\theta + \mathbf{n}\cos\theta$.

The same way the generalized heat flux intensity factors can be determined, which are defined as

$$K_{h1} = -\lim_{\mathbf{x}\to\mathbf{x}(A)} \sqrt{\frac{\pi}{8s(\mathbf{x})}} k_t \Delta\theta(\mathbf{x}), \quad K_{h2} = -\lim_{\mathbf{x}\to\mathbf{x}(A)} \sqrt{\frac{\pi s(\mathbf{x})}{2}} \Sigma h_n(\mathbf{x}). \tag{46}$$

Here $k_t = \sqrt{k_{\tau\tau}k_{nn} - k_{\tau n}^2}$; $k_{\tau\tau} = k_{ij}\tau_i\tau_j$, $k_{nn} = k_{ij}n_i n_j$, $k_{\tau n} = k_{ij}\tau_i n_j$.

Based on the analysis presented above the numerical formulae for accurate evaluation of the heat flux intensity factors are as follows

$$K_{h1} = -\sqrt{\frac{\pi}{8\rho(\eta_A)}} k_t \sum_{i=1}^{3}\sum_{j=1}^{3} \Delta\theta^{(i,j)} \Phi_{i1}^{\Lambda} \phi_j(\eta_A), \quad K_{h2} = -\sqrt{\frac{\pi\rho(\eta_A)}{2}} \sum_{i=1}^{3}\sum_{j=1}^{3} \Sigma h_n^{(i,j)} \Phi_{i1}^{\Sigma} \phi_j(\eta_A). \tag{47}$$

4.5. Numerical examples

4.5.1. Fast convergence of the trapezoid rule in evaluation of anisotropic kernels

Since at first glance it is not obvious that the trapezoid rule can efficiently handle evaluation of anisotropic kernels, consider an example of Xie et al. [20] of numerical evaluation of the second derivative $U_{IJ,km}$ of elastic Green's function. The results are obtained for Mg material with the following elastic properties [20]:

$C_{11} = C_{22} = 59.7$ GPa, $C_{33} = 61.7$ GPa, $C_{13} = C_{23} = 21.7$ GPa,

$C_{12} = 26.2$ GPa, $C_{44} = C_{55} = 16.4$ GPa, $C_{66} = 16.75$ GPa.

Second derivative of the Green's function is evaluated at the point $\mathbf{x} - \mathbf{x}_0 = (1,2,3)^{\mathrm{T}}$. Four methods are compared. They are the Numerical Integration Method (NIM) [20], the Residue Calculus Method (RCM) [20], the improved Residue Calculus Method (iRCM) [20], and the proposed numerical integration with the Trapezoid Rule (TR). Since the worst convergence is possessed by $U_{22,11}$ [20], only its value is presented in Table 1. The exact solution is taken from Pan and Chou [34]. Numerical calculations are held with the developed C++ program, which uses IEEE 64-bit double precision floating point number format (with 15–17 significant decimal digits).

One can see from Table 1 that the trapezoid rule converges very fast. Only 16 nodes of the trapezoid rule is enough to obtain the same accuracy as the Gaussian quadrature with 25 nodes or the improved RCM. The 8-point trapezoid rule has the accuracy comparable with the RCM.

Comparison of the results for different number of the trapezoid rule nodes allows to state that the number of true significant decimal digits is proportional to the number of nodal points in the trapezoid rule. However, the number of true decimal digits is also limited with the length of the mantissa used in floating-point computations.

Table 1. $U_{22,11}$ evaluated by different approaches at the given point of Mg anisotropic medium

Exact [34]	$-\mathbf{6.2581146860784102}\times10^{-5}$	$\times10^{9}$ m^{-1}/N
NIM with 25 Gaussian points [20]	$-\mathbf{6.2581146860783}276\times10^{-5}$	
RCM [20]	$-\mathbf{6.258114}7470664643\times10^{-5}$	
iRCM [20]	$-\mathbf{6.2581146860783}736\times10^{-5}$	
TR with 4 points	$-\mathbf{6.2}67696062871067\times10^{-5}$	
TR with 8 points	$-\mathbf{6.25811}2576749089\times10^{-5}$	
TR with 12 points	$-\mathbf{6.258114686}298868\times10^{-5}$	
TR with 16 points	$-\mathbf{6.258114686078}395\times10^{-5}$	
TR with 20 points	$-\mathbf{6.258114686078408}\times10^{-5}$	

The same exponential convergence of the trapezoid rule is observed in evaluation of anisotropic magnetoelectroelastic kernels compared to the numerical data of Buroni and Sáez [24].

Exponential convergence of the trapezoid rule is also observed in the numerical evaluation of the kernels Θ^{*} and $V_{I,j}$ and their derivatives. Therefore, in further numerical computations the kernels are evaluated with the 8-point trapezoid rule, which allows programming of fast and accurate BEM code.

The only kernel, which should be evaluated in the other way, is V_I. However, for crack problems in the infinite medium only extended stress integral equation can be used, which does not contain this kernel.

4.5.2. Numerical verification. Penny-shaped crack in an infinite isotropic thermoelastic medium

In order to verify the developed BEM consider the thermoelastic problem for a penny-shaped crack of radius R. The crack is meshed with only 12 quadrilateral discontinuous boundary elements (Fig. 3).

Four central boundary elements Nos. 1–4 use general quadratic shape functions (33), while other elements (Nos. 5–12) utilize special shape functions (34) to account for the square root singularity of stress and heat flux at the crack front. Special shape functions (35) are used if the temperature boundary conditions are set at crack surfaces to ensure the account of heat flux discontinuity function square root singularity at the crack front.

Two types of boundary conditions are set at crack faces

- type A: $\theta^{+}=\theta^{-}=-\theta_0$; $\tilde{\mathbf{t}}^{+}=\tilde{\mathbf{t}}^{-}=0$;
- type B: $h_n^{+}=-h_n^{-}=-h_0$; $\tilde{\mathbf{t}}^{+}=\tilde{\mathbf{t}}^{-}=0$.

According to [29, 35] nonzero field intensity factors for these two types of boundary conditions at crack faces are as follows,

- type A: $K_{\mathrm{I}}^{A}=\dfrac{2\mu(1+\nu)}{(1-\nu)}\alpha\theta_0\sqrt{\dfrac{R}{\pi}}$; $K_{h2}^{A}=-\dfrac{2k_t\theta_0}{\sqrt{\pi R}}$;

- type B: $K_{\mathrm{II}}^{B}=\dfrac{2\mu\alpha(1+\nu)h_0}{3(1-\nu)k_t}R\sqrt{\dfrac{R}{\pi}}$; $K_{h1}^{B}=-2h_0\sqrt{\dfrac{R}{\pi}}$.

where μ is a shear modulus; ν is a Poisson ratio; k_t is a heat conduction coefficient; α is a linear thermal expansion coefficient.

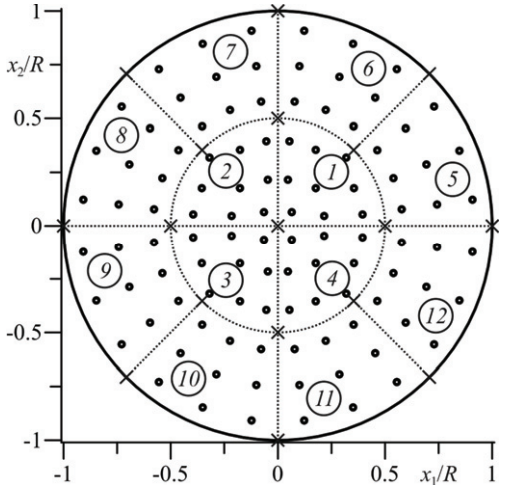

Fig. 3. Boundary element mesh of the penny-shaped crack

Numerical calculations were held for $\nu=0.3$. Normalized values of stress and heat flux intensity factors along the crack front for considered types of boundary conditions are presented in Fig. 4. Superscripts *NA* and *NB* corresponds to the intensity factors obtained based on the BEM numerical solution under corresponding type (A or B) of the boundary conditions. The plot is polar one, and φ is a polar angle. Crosses mark the points at which the values of the field intensity factors are evaluated.

The four curves presented in the plot cannot be visually distinguished. The highest relative error of heat flux intensity factors determination is 0.23 % for Type A boundary conditions, and 0.87 % for Type B conditions. The highest relative error of stress intensity factors determination is 0.87 % and 0.98 %, respectively. This proves high accuracy of the present 3D BEM and validates the proposed methods for precise evaluation of the field intensity factors.

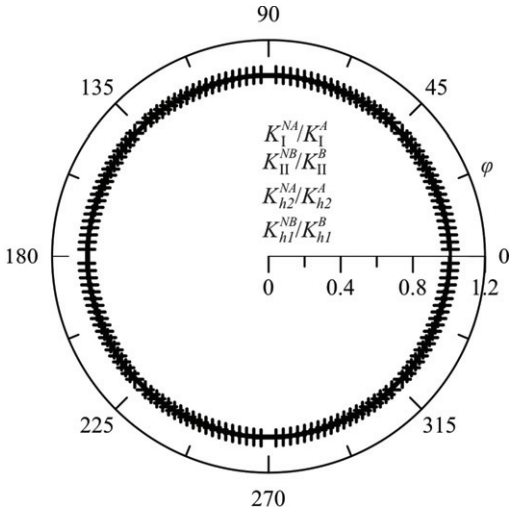

Fig. 4. Normalized field intensity factors along the front line of a penny-shaped crack in the isotropic medium

4.5.3. A penny-shaped crack in a thermoelectroelastic medium

Consider a transversely isotropic pyroelectric barium titanate ($BaTiO_3$), which has the following properties [36]:

- elastic moduli (GPa): $C_{11} = C_{22} = 150$; $C_{33} = 146$; $C_{12} = C_{13} = C_{23} = 66$; $C_{44} = C_{55} = 44$; $C_{66} = (C_{11} - C_{12})/2 = 42$;
- piezoelectric constants (C/m^2): $e_{31} = e_{32} = -4.35$; $e_{33} = 17.5$; $e_{15} = e_{24} = 11.4$;
- dielectric constants (nF/m): $\kappa_{11} = \kappa_{22} = 9.86775$; $\kappa_{33} = 11.151$;
- heat conduction coefficients (W/(m·K)): $k_{11} = k_{22} = k_{33} = 2.5$;
- thermal expansion coefficients (K^{-1}): $\alpha_{11} = \alpha_{22} = 8.53 \cdot 10^{-6}$; $\alpha_{33} = 1.99 \cdot 10^{-6}$;
- pyroelectric constants (GV/(m·K)): $\lambda_3 = 13.3 \cdot 10^{-6}$.

Here the Voigt notation [28, 29, 30] is used in the indices of elastic moduli and piezoelectric constants, which changes the index pairs in (3) with a single index as $11 \leftrightarrow 1$; $22 \leftrightarrow 2$; $33 \leftrightarrow 3$; $23,32 \leftrightarrow 4$; $13,31 \leftrightarrow 5$; $12,21 \leftrightarrow 6$.

Assume that this barium titanate medium contains a penny-shaped crack. Two types of thermal boundary conditions at crack faces are given the same as in the previous example. Consider the influence of crack orientation towards the orthotropy axes of the material on the field intensity factors. For this purpose the crack, which is parallel to the isotropy plane Ox_1x_2, and the inclined crack are studied. The normalization factors are equal to $K_\sigma^A = \theta_0 \beta_{11} \sqrt{\pi R}$, $K_\chi^A = \theta_0 \chi_2 \sqrt{\pi R}$ for Type A boundary conditions, and $K_\sigma^B = h_0 \beta_{11} R \sqrt{\pi R} / k_{11}$, $K_\chi^B = h_0 \chi_2 R \sqrt{\pi R} / k_{11}$ for Type B ones.

Fig. 5 depicts the normalized field intensity factors obtained for Type A (subfigures a, c) and Type B (subfigures b, d) thermal boundary conditions for a

penny-shaped crack parallel to the isotropy plane Ox_1x_2 (subfigure a, b) and the same one rotated about the Ox_1 axis at 45º (subfigures c, d).

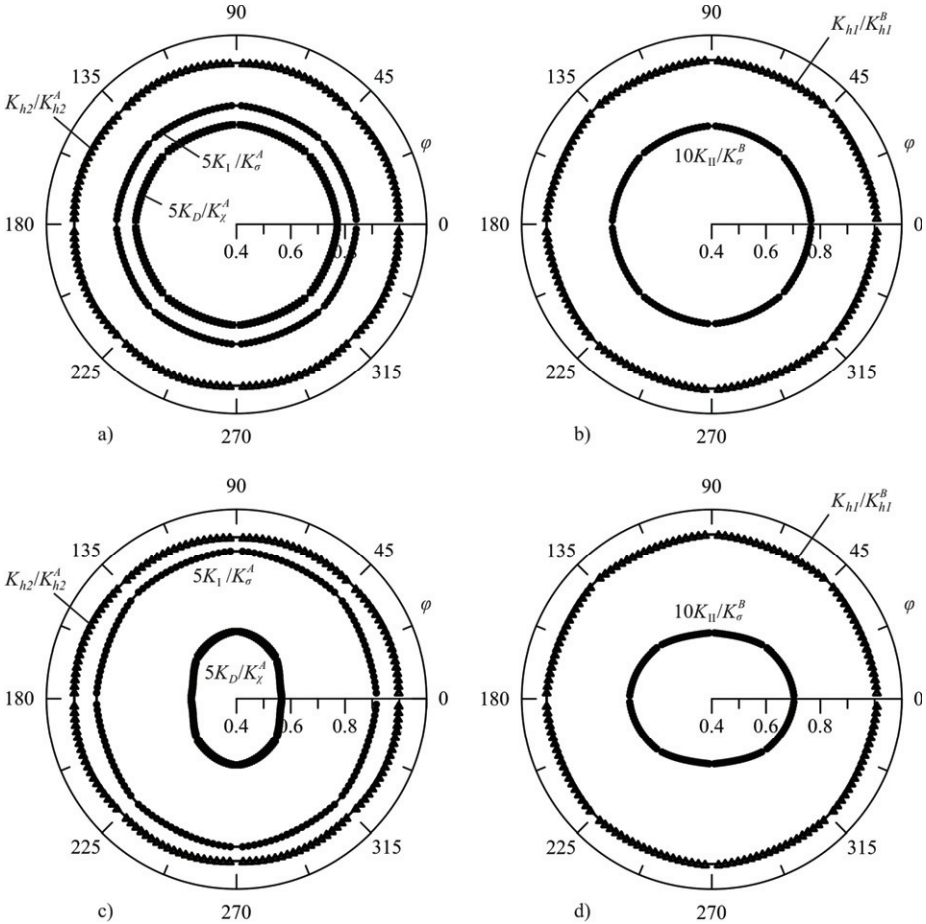

Fig. 5. Normalized field intensity factors of a penny-shaped crack in a barium titanate medium
(a, c – Type A boundary conditions; b, d – Type B boundary conditions;
a, b – crack parallel to the isotropy plane; c, d – crack rotated about the Ox_1 axis at 45º)

Since barium titanate is isotropic in heat conduction the heat flux intensity factors are the same as for the isotropic material both for the crack parallel to the isotropy plane and the inclined one. The field intensity factors of the penny-shaped crack lying in the isotropy plane are constant along its front. Obtained numerical

values of stress and electric displacement intensity factors are in good agreement with analytical solutions [17, 18, 19]. The error is less than 1 %.

In the case when the crack is inclined to the isotropy plane, stress and electric displacement intensity factors vary along its front. In the polar plots these values draw ellipses, which is consistent with the results of Pan and Yuan [6] obtained for elastic anisotropic solids. For Type A boundary conditions mode I stress intensity factor increases and electric displacement intensity factor decreases with crack inclination. For Type B boundary conditions mode II stress intensity factor decreases with crack inclination.

Conclusion

The chapter presents a comprehensive study on the boundary element analysis of thermomagnetoelectroelastic anisotropic solids. Several novelties are introduced, which allow derivation of the efficient boundary element approach.

The first of them is the usage of new boundary integral equations of 3D anisotropic thermomagnetoelectroelasticity. These integral equations do not contain temperature volume integral terms, which is advantageous comparing to existing boundary element formulations for anisotropic thermoelastic solids. Thermal effects are accounted for through the boundary integrals containing temperature and heat flux functions (or discontinuity functions).

The second one is application of the trapezoid rule to evaluation of anisotropic kernels. Due to its simplicity and exponential convergence for integrals over a periodic interval it allows accurate and fast evaluation of the kernels, which is essentially important in the derivation of fast BEM.

The third is the usage of polynomial mappings and modified Kutt's quadratures for finite part integrals, which allows accurate numerical integration of singular and hypersingular integrals. Introduction of special shape functions for the displacement, temperature and heat flux discontinuities at the crack allows accurate determination of the field intensity factors.

These novelties allowed derivation of the efficient 3D BEM, which allows studying both isotropic and anisotropic thermomagnetoelectroelastic materials with cracks of arbitrary shape. The numerical examples presented prove high accuracy of the present boundary element formulation.

Appendix 4.A. Modified Kutt's quadrature for finite part integrals

Kutt [31, 32] proposed the following quadrature rule for finite part integrals with algebraic singularity

$$\mathrm{HFP}\int_0^R \frac{f(x)}{x^\lambda}dx \approx R^{1-\lambda}\sum_{i=1}^{N}\left[w_i^{(\lambda)} + c_i^{(\lambda)}\frac{\ln R}{(\lambda-1)!}\right]f(Rt_i), \tag{A.1}$$

where $t_i \in [0;1]$ are quadrature nodes; λ is a positive integer, which indicates the strength of singularity; $R>0$; $w_i^{(\lambda)}$ and $c_i^{(\lambda)}$ are weights for the selected λ and t_i

$(i=1,...,N)$. The latter are determined from the following system of linear algebraic equations

$$\sum_{j=1}^{N} w_j^{(\lambda)} t_j^{(i-1)} = \begin{cases} \dfrac{1}{i-\lambda}, & i \neq \lambda, \\ 0, \quad \text{otherwise}; \end{cases}, \quad \sum_{j=1}^{N} c_j^{(\lambda)} t_j^{(i-1)} = \begin{cases} (\lambda-1)!, & i=\lambda, \\ 0, \quad \text{otherwise}; \end{cases} \quad (i=1,...,N). \qquad (A.2)$$

Due to its polynomial interpolation nature, Kutt's quadrature is exact for polynomials of degree $N-1$.

Kutt has selected the equidistant node set $t_i = (i-1)/N$ [31]. The same nodes were used by Pan and Yuan [6] for numerical evaluation of hypersingular integrals in their 3D BEM. However, this set of quadrature nodes has two inconveniencies, when implemented in BEM. The first one is that one has to know $f(0)$. Since in the BEM it is not given explicitly, one should consider the integrand behavior at a singular point separately. The second is that for high numbers N of quadrature nodes Runge's phenomenon can be observed, which can lead to sufficient errors, when integrating certain functions. These inconveniences can be overcome if one select Chebyshev nodes as the nodes of Kutt's quadrature

$$t_i = \frac{1}{2}\left(1 - \cos\frac{(2i-1)\pi}{2N}\right) \quad (i=1,...,N). \qquad (A.3)$$

Numerical tests on polynomials of degree higher than $N-1$ have shown that the error of the modified Kutt's quadrature with Chebyshev nodes is much less than those of the convenient Kutt's quadrature with equidistant nodes.

References

[1] Fang D, Liu J. Fracture mechanics of piezoelectric and ferroelectric solids. London: Springer, 2013.

[2] Aliabadi MH. Boundary element formulations in fracture mechanics. Applied Mechanics Review 1997; 50: 83–96.

[3] Mi Y, Aliabadi MH. Dual boundary element method for three-dimensional fracture mechanics analysis. Engineering Analysis with Boundary Elements 1992; 10: 161–171.

[4] Cruse TA. Boundary Element Analysis in Computational Fracture Mechanics, Dordrecht: Kluwer, 1988.

[5] Saez A, Ariza MP, Dominguez J. Three-dimensional fracture analysis in transversely isotropic solids. Engineering Analysis with Boundary Elements 1997; 20: 287–298.

[6] Pan E, Yuan FG. Boundary element analysis of three-dimensional cracks in anisotropic solids. Int. J. Numer. Meth. Engng. 2000; 48:211–237.

[7] Rungamornrat J, Mear ME. A weakly-singular SGBEM for analysis of cracks in 3D anisotropic media, Comput. Methods Appl. Mech. Eng. 2008; 197: 4319–4332.

[8] Phan AV, Gray LJ, Kaplan T. Residue approach for evaluating the 3D anisotropic elastic Green's function: multiple roots. Eng Anal Bound Elem 2005; 29: 570–576.

[9] Shiah YC, Tan CL, Lee VG. Evaluation of explicit-form fundamental solution for displacements and stresses in 3D anisotropic elastic solids. Comput Model Eng Sci 2008; 34(3): 205-226.

[10] Tan CL, Shiah YC, Wang CY. Boundary element elastic stress analysis of 3D generally anisotropic solids using fundamental solutions based on Fourier series. Int J Sol Struct 2013; 50: 2701–2711.

[11] Dell'erba DN, Aliabadi MH, Rooke DP. Dual boundary element method for three-dimensional thermoelastic crack problems. International Journal of Fracture 1998; 94: 89–101.

[12] Mukherjee YX, Shah K, Mukherjee S. Thermoelastic fracture mechanics with regularized hypersingular boundary integral equations. Eng Anal Bound Elem 1999; 23: 89–96.

[13] Rungamornrat J, Mear ME. Analysis of fractures in 3D piezoelectric media by a weakly singular integral equation method. Int J Fract 2008; 151:1–27.

[14] Rungamornrat J, Phongtinnaboot W, Wijeyewickrema AC. Analysis of cracks in 3D piezoelectric media with various electrical boundary conditions. International Journal of Fracture 2015; 192: 133–153.

[15] Zhao MH, Guo ZH, Fan CY, Zhang RL, Pan E. Three-dimensional vertical cracks in magnetoelectroelastic media via the extended displacement discontinuity boundary integral equation method. Journal of Intelligent Material Systems and Structures 2013; 24:1969–1984.

[16] Muñoz-Reja MM, Buroni FC, Sáez A, García-Sánchez F. 3D explicit-BEM fracture analysis for materials with anisotropic multifield coupling. Applied Mathematical Modelling 2016;40: 2897–2912.

[17] Shang F, Wang Z, Li Z. Thermal stresses analysis of a threedimensional crack in a thermopiezoelectric solid. Engineering Fracture Mechanics 1996; 55:737-750.

[18] Shang F, Kuna M, Scherzer M. Analytical solutions for two penny-shaped crack problems in thermo-piezoelectric materials and their finite element comparisons. International Journal of Fracture 2002; 117: 113–128.

[19] Kirilyuk VS. Thermostressed state of a piezoceramic body with a plane crack in a symmetric heat flow from its surfaces. International Applied Mechanics 2010; 46: 753–762.

[20] Xie L, Zhang C, Hwu C, Sladek J, Sladek V. A comparison of three evaluation methods for Green's function and its derivatives for 3D generally anisotropic solids, European Journal of Computational Mechanics 2016. http://dx.doi.org/10.1080/17797179.2016.1181039

[21] Xie L, Zhang C, Hwu C, Sladek J, Sladek V. On two accurate methods for computing 3D Green's function and its first and second derivatives in piezoelectricity. Engineering Analysis with Boundary Elements 2015; 61: 183–193.

[22] Pasternak I, Pasternak R, Sulym H. A comprehensive study on Green's functions and boundary integral equations for 3D anisotropic thermomagnetoelectroelasticity. Eng Anal Bound Elem 2016; 64: 222–229.

[23] Chen JT, Hong HK. Review of dual boundary element methods with emphasis on hypersingular integrals and divergent series. Appl Mech Rev 1999; 52, No. 1: 17–33.

[24] Buroni FC, Sáez A. Three-dimensional Green's function and its derivative for materials with general anisotropic magneto-electro-elastic coupling. Proc R Soc A 2010; 466: 515–537.

[25] Wang CY, Achenbach JD. Three-dimensional time-harmonic elastodynamic Green's functions for anisotropic solids. Proc R Soc Lond 1995; A 449: 441–458.

[26] Weideman JAC. Numerical integration of periodic functions: a few examples. The American Mathematical Monthly 2002; 109: 21-36.

[27] Trefethen LN, Weideman JAC. The exponentially convergent trapezoidal rule. SIAM Review 2014; 56: 385–458.

[28] Ting TCT. Anisotropic elasticity: theory and applications. Oxford University Press: Oxford, 1996.

[29] Barber JR. Elasticity. Springer: London, 2010.

[30] Qin QH. Green's function and boundary elements of multifield materials. Elsevier: Oxford, 2007.

[31] Kutt HR. On the numerical evaluation of finite-part integrals involving an algebraic singularity. PhD thesis, University of Stellenbosch, 1975.

[32] Kutt HR. The numerical evaluation of principal value integrals by finite-part integration. Numer. Math. 1975; 24: 205-210.

[33] Johnston BM, Johnston PR, Elliott D. A sinh transformation for evaluating two-dimensional nearly singular boundary element integrals. Int J Num Meth Eng 2007; 69: 1460–1479.

[34] Pan YC, Chou TW. Point force solution for an infinite transversely isotropic solid. Journal of Applied Mechanics 1976; 43: 608–612.

[35] Murakami Y. (ed.) Stress Intensity Factors Handbook. In 2 Volumes. Oxford: Pergamon press, 1987.

[36] Dunn ML. Micromechanics of coupled electroelastic composites: effective thermal expansion and pyroelectric coefficients. J Appl Phys 1993; 73: 5131–5140.